A qualitative study of solutions to partial differential equations based on dynamical systems theory and geometric approaches

メタデータ	言語: en 出版者: 公開日: 2023-05-31 キーワード (Ja): キーワード (En): 作成者: ICHIDA, YU メールアドレス: 所属:
URL	http://hdl.handle.net/10291/00023142

Meiji University
Graduate School of Science and Technology

Academic Year 2022

Doctoral Dissertation

A qualitative study of solutions to partial differential equations based on dynamical systems theory and geometric approaches

Mathematics Program

Yu ICHIDA

“A qualitative study of solutions to partial differential equations based on dynamical systems theory and geometric approaches”

Yu Ichida

Graduate School of Science and Technology, Meiji University
Supervisor: Shigetoshi Yazaki

February 13, 2023

Contents

Preface **9**

Acknowledgments **15**

List of Corresponding Papers **17**

1 Preliminaries **19**
1.1 Poincaré type compactification 19
1.2 Blow-up technique 23

2 Quasi traveling waves with quenching in a reaction-diffusion equation in the presence of negative powers nonlinearity **27**
2.1 Introduction 27
2.2 Dynamics on the Poincaré disk of (2.1.3) 30
2.2.1 Dynamics on the chart $\overline{U}_2$ 30
2.2.2 Dynamics on the chart $\overline{V}_2$ 33
2.2.3 Dynamics on the chart $\overline{U}_1$ 33
2.2.4 Dynamics on the chart $\overline{V}_1$ 34
2.3 Proof of Theorem 2.1.2 34
2.4 Conclusions and Remarks 36

3 Traveling waves with singularities in a damped hyperbolic MEMS type equation in the presence of negative powers nonlinearity **37**
3.1 Introduction 37
3.2 Known and Main results 39
3.3 Dynamics on the Poincaré disk of (3.1.5) 45
3.3.1 Dynamics on the chart $\overline{U}_2$ 46
3.3.2 Dynamics on the chart $\overline{V}_2$ 48
3.3.3 Dynamics on the chart $\overline{U}_1$ 50
3.3.4 Dynamics on the chart $\overline{V}_1$ 50
3.3.5 Dynamics and connecting orbits on the Poincaré disk 51
3.4 Proof of Theorems 52
3.4.1 Proof of Theorem 3.2.1 52
3.4.2 Proof of Theorem 3.2.2 54
3.4.3 Proof of Theorem 3.2.3 55
3.4.4 Proof of Theorem 3.2.4 55
3.5 Concluding remarks 55

4 Radial symmetric stationary solutions for a MEMS type reaction-diffusion equation with spatially dependent nonlinearity 57
4.1 Introduction . . . 57
4.2 Dynamics near finite equilibria of (4.1.8) . . . 62
4.3 Dynamics on the Poincaré disk of (4.1.8) : p is even . . . 62
4.3.1 Dynamics on the chart $\overline{U}_2$ . . . 63
4.3.2 Dynamics on the chart $\overline{V}_2$ . . . 66
4.3.3 Dynamics on the chart $\overline{U}_1$ . . . 66
4.3.4 Dynamics on the chart $\overline{V}_1$ . . . 68
4.3.5 Dynamics and connecting orbits on the Poincaré disk . . . 68
4.4 Dynamics on the Poincaré disk of (4.1.8) : p is odd . . . 71
4.5 Proof of the Theorems . . . 72
4.5.1 Proof of Theorem 4.1.1 . . . 72
4.5.2 Proof of Theorem 4.1.2 . . . 72
4.5.3 Proof of Theorem 4.1.3 . . . 75
4.6 Conclusions and Remarks . . . 76

5 Stationary solutions for a 1D pde problem with gradient term and negative powers nonlinearity 77
5.1 Introduction . . . 77
5.2 Main results . . . 79
5.3 Dynamics on the Poincaré-Lyapunov disk (5.1.4) . . . 85
5.3.1 Dynamics on the chart $\overline{U}_2$ . . . 86
5.3.2 Dynamics on the chart $\overline{V}_2$ . . . 87
5.3.3 Dynamics on the chart $\overline{U}_1$ . . . 88
5.3.4 Dynamics on the chart $\overline{V}_1$ . . . 89
5.3.5 Dynamics on the Poincaré-Lyapunov disk . . . 92
5.4 Proof of the Theorems . . . 94
5.4.1 Proof of Theorem 5.2.1 . . . 94
5.4.2 Proof of Theorem 5.2.2 . . . 96
5.4.3 Proof of Theorem 5.2.3 . . . 97
5.4.4 Proof of Theorem 5.2.4 . . . 97
5.4.5 Proof of Corollary 5.2.1 . . . 99
5.4.6 Proof of Theorem 5.2.5 . . . 100
5.5 Conclusions and Remarks . . . 101

6 Radially symmetric stationary solutions for a MEMS type reaction-diffusion equation with fringing field 103
6.1 Introduction . . . 103
6.1.1 Known results and motivation . . . 103
6.1.2 Preliminaries . . . 105
6.2 Main results . . . 108
6.3 Dynamics of (6.1.14) to infinity . . . 112
6.3.1 Dynamics on the chart $\overline{U}_2$ . . . 113
6.3.2 Dynamics on the chart $\overline{V}_2$ . . . 116
6.3.3 Dynamics on the chart $\overline{U}_1$ . . . 116
6.3.4 Dynamics on the chart $\overline{V}_1$ . . . 117
6.3.5 Dynamics and connecting orbits on the Poincaré disk . . . 117
6.3.6 Dynamics on the Poincaré disk in the case that p is odd . . . 118
6.4 Dynamics of (6.1.16) to infinity . . . 119

6.4.1 Dynamics of (6.4.2) near $(0,0)$ . . . 120
6.4.2 Asymptotically quasi-homogeneous vector field . . . 123
6.4.3 Dynamics on the chart $\overline{U}_2$ . . . 124
6.4.4 Dynamics on the chart $\overline{V}_2$ . . . 125
6.4.5 Dynamics on the chart $\overline{U}_1$ . . . 125
6.4.6 Dynamics and connecting orbits on the Poincaré-Lyapunov disk . . . 126
6.5 Dynamics of (6.1.18) to infinity . . . 127
6.5.1 Dynamics on the chart $\overline{U}_2$ . . . 128
6.5.2 Dynamics on the chart $\overline{V}_2$ . . . 129
6.5.3 Dynamics on the chart $\overline{U}_1$ . . . 129
6.5.4 Dynamics near finite equilibria . . . 129
6.5.5 Dynamics and connecting orbits on the Poincaré-Lyapunov disk . . . 132
6.6 Proof of Theorem . . . 133
6.6.1 Proof of Theorem 6.2.1 . . . 133
6.6.2 Proof of Theorem 6.2.2 . . . 136
6.6.3 Proof of Theorem 6.2.3 . . . 137
6.6.4 Proof of Theorem 6.2.4 . . . 138
6.6.5 Proof of Theorem 6.2.6 . . . 138
6.6.6 Proof of Theorem 6.2.7 . . . 138
6.7 Concluding remarks . . . 139

7 Traveling wave solutions for degenerate nonlinear parabolic equations 141
7.1 Introduction . . . 141
7.2 Dynamics on the Poincaré disk of (7.1.9) with $p \in 2\mathbb{N}$ . . . 145
7.2.1 Dynamics of (7.2.2) near $(0,0)$: the case $\delta = 0$ . . . 146
7.2.2 Dynamics of (7.2.2) near $(0,0)$: the case $\delta = 1$ . . . 146
7.2.3 Dynamics on the chart $\overline{U}_2$ . . . 148
7.2.4 Dynamics on the chart $\overline{V}_2$ . . . 149
7.2.5 Dynamics on the chart $\overline{U}_1$ . . . 149
7.2.6 Dynamics on the chart $\overline{V}_1$ . . . 150
7.2.7 Dynamics on the Poincaré disk . . . 150
7.3 Proof of the Theorems . . . 151
7.4 Dynamics on the Poincaré disk of (7.1.9) : p is odd . . . 156
7.4.1 Dynamics of (7.4.1) near $(0,0)$: the case $\delta = 0$ . . . 157
7.4.2 Dynamics of (7.4.1) near $(0,0)$: the case $\delta = 1$ . . . 159
7.4.3 Dynamics on the chart $\overline{U}_2$ . . . 162
7.4.4 Dynamics on the chart $\overline{V}_2$ . . . 164
7.4.5 Dynamics on the chart $\overline{U}_1$ . . . 165
7.4.6 Dynamics on the chart $\overline{V}_1$ . . . 165
7.4.7 Classification of the connecting orbits in odd case . . . 166
7.5 Conclusions and Remarks . . . 171

8 A refined asymptotic behavior of traveling wave solutions for degenerate nonlinear parabolic equations 173
8.1 Introduction . . . 173
8.2 Preliminaries . . . 175
8.3 Proof of Theorem 8.1.2 . . . 177
8.4 Conclusion . . . 181

9 Classification of nonnegative traveling wave solutions for the 1D degenerate parabolic equations 183
9.1 Introduction . . . 183
9.2 Main results . . . 186
9.3 Dynamics on the Poincaré disk of (9.1.4) . . . 191
9.3.1 Dynamics near finite equilibria . . . 191
9.3.2 Dynamics on the chart $\overline{U}_2$ . . . 193
9.3.3 Dynamics on the chart $\overline{V}_2$ . . . 193
9.3.4 Dynamics on the chart $\overline{U}_1$ . . . 194
9.3.5 Dynamics and connecting orbits on the Poincaré disk . . . 194
9.4 Proof of theorems . . . 195
9.4.1 Proof of Theorem 9.2.1 . . . 195
9.4.2 Proof of Theorem 9.2.2 . . . 197
9.4.3 Proof of Theorem 9.2.3 . . . 197
9.5 Concluding remarks . . . 199

10 Radially symmetric stationary solutions for certain chemotaxis systems in higher dimensions: a geometric approach 201
10.1 Introduction . . . 201
10.2 Main results . . . 206
10.3 Dynamics on the Poincaré-Lyapunov disk of (10.1.16) . . . 208
10.3.1 Dynamics near finite equilibria of (10.1.16) . . . 208
10.3.2 Asymptotically quasi-homogeneous vector field . . . 209
10.3.3 Dynamics on the chart $\overline{U}_2$ . . . 210
10.3.4 Dynamics on the chart $\overline{V}_2$ . . . 210
10.3.5 Dynamics on the chart $\overline{U}_1$ . . . 211
10.3.6 Dynamics on the chart $\overline{V}_1$ . . . 212
10.3.7 Dynamics and connecting orbits on the Poincaré-Lyapunov disk . . . 212
10.3.8 Dynamics on the Poincaré-Lyapunov disk of (10.1.16) in the case that $\alpha < \beta$ . . . 216
10.4 Proof of theorems . . . 218
10.4.1 Proof of Theorem 10.2.1 . . . 219
10.4.2 Proof of Proposition 10.2.1 . . . 221
10.4.3 Proof of Theorem 10.2.2 . . . 222
10.5 Discussion . . . 223
10.5.1 A connecting orbit between E_1 and E_6 in the case $\alpha = 1$ and $\beta = 0$ 223
10.5.2 A connecting orbit between E_0 and E_6 in the case $\alpha < \beta$ . . . 224
10.5.3 Connecting orbits between E_2 and E_9 in the case $\alpha < \beta$ . . . 224

11 On global behavior of a some SIR epidemic model based on the Poincaré compactification 227
11.1 Introduction . . . 227
11.2 The model as a test case . . . 228
11.2.1 The model . . . 229
11.2.2 Known results . . . 229
11.2.3 The case $\mathcal{R}_0 = 1$: Application of the center manifold theory . . . 230
11.3 Application of the Poincaré compactification . . . 231
11.3.1 Dynamics on the local charts . . . 231
11.3.2 Dynamics on the Poincaré disk . . . 232
11.4 Asymptotic behavior . . . 232

11.5 Concluding remarks 233

Preface

The main objective of this thesis is to investigate the properties of special solutions of various partial differential equations based on dynamical systems theory and geometric approaches. In particular, we use a unified method of clarifying the dynamics of systems of ordinary differential equations satisfied by special solutions of partial differential equations, including those at infinity, by means of Poincaré-type compactification. The result is a qualitative structure of solutions to partial differential equations with different backgrounds, which has not been revealed before.

According to [45], originally, the term "dynamical system" meant only mechanical systems whose motion is described by differential equations derived from classical mechanics. Basic results on such dynamical systems were obtained by Lyapunov and Poincaré at the end of the nineteenth century. Later on, it became clear that a dynamical systems theory is useful for the analysis of various evolutionary processes studied in different branches of science and described by ordinary differential equations (for short, ODEs), partial differential equations (for short, PDEs), or explicitly defined iterated maps. Today, there are many studies on dynamical systems theory and its related topics.

The PDEs treated in this thesis are developed as the model of chemical reactions, competition for survival among species, solar flares and other astrophysical phenomena, and the motion of elastic membranes in the micro-electro mechanical systems. These phenomena have been formulated by extracting the essence from the complexity, and the universality of the numerical formula has led to a new understanding of the phenomena, predictions, hypotheses, and derived mathematical problems, and has also given rise to new research. However, in general, it is not expected that exact solutions of nonlinear PDEs can be obtained.

Then, for instance, studying the following problems is important;

(i) well-posedness, solvability, and regularity (including local existence of solutions).

(ii) the existence of special solutions (stationary solutions, traveling wave solutions, self-similar solutions, etc.) and their profiles.

(iii) to develop the numerical schemes to visualize the solutions (including computer-assisted proof for (i) and (ii) and so on).

There are many problems such as the following, and various studies have been conducted so far. All of them are complementary and important problems. However, most of them are derived from the characteristics of individual equations, and it is difficult to clarify their structures and develop analytical methods from a unified viewpoint. To understand the mechanism of phenomena, results for (ii) and (iii) could be required. Now analytical methods and results that lead to the existence of special solutions and various properties, which are the first step to understanding the phenomena from the mathematical point of view have been presented in various models. However, we have not yet developed a

method that can be applied to different equations or classification of special solutions (i.e., a list of all those that exist), and the development of analytical methods to solve these problems is an important and promising development. Therefore, the author aims to obtain rich results by a unified method by first focusing on special solutions. Then, they aim to provide new perspectives for extensions to the general theory, pure mathematical research, and applications to phenomena.

According to [50], compactification is an embedding of the original phase space ($\mathbb{R}^n$ in the present argument) into a compact manifold or its tangent space such that the infinity corresponds to a point or the boundary of the manifold. In particular, the infinity is mapped to additional points or the boundary of compactified manifolds. The most familiar ones are Bendixson's compactification (embedding of $\mathbb{R}^n$ into the unit n-sphere $\mathbb{S}^n \subset \mathbb{R}^{n+1}$) and Poincaré's one (embedding of $\mathbb{R}^n$ into the unit upper hemisphere $\{(x_1, \ldots, x_{n+1}) \mid x_{n+1} > 0, \sum_{i=1}^{n+1} x_i^2 = 1\}$). Compactifications play key roles in understanding various natures of objects involving infinity. Nevertheless, compactification should be chosen so that it is compactible with the scale invariance of vector fields and that the scaling information of dynamical systems is kept through associated transformation. Quasi-homogeneous type compactifications are therefore applied to studying the structure of dynamics from the viewpoint of dynamical systems at infinity (e.g., [13]).

In this thesis, the aim is to propose the methods and applications of the Poincaré type compactification and blow-up technique that is based on [49, 50] and revealed the existence, profile, and asymptotic behavior of the characteristic solutions for PDEs such as a MEMS type reaction-diffusion equation, 1D degenerate nonlinear parabolic equations, and certain chemotaxis systems. Here, the Poincaré type compactification includes the Poincaré compactification in the case that the vector field is homogeneous and the Directional compactification (especially Poincaré-Lyapunov compactification) in the case that the vector field is quasi-homogeneous. Furthermore, the results obtained in this paper give us an abundance of information on typical solutions with detailed asymptotic behavior by using the technique of compactifications which maps infinity to bounded regions and time-scale desingularization. To the author's knowledge, there have been no studies of these equations with the dynamical system approach, therefore, our results will give the first step for the studies of these from the viewpoint of the geometric (dynamical system) approach. Moreover, we believe that our works contribute to new insights into these equations.

The contents of this paper are summarized as follows. In Chapter 1, the author explains the Poincaré type compactification and blow-up technique. They play important roles in this paper, based on [1, 8, 14, 49, 50]. This chapter cites [1, 8, 14, 31, 32, 33, 34, 49, 50] and summarizes the necessary parts of this study to understand it. In particular, the author introduces the explanation of the Poincaré compactification, the definition of an asymptotic quasi-homogeneous vector field at infinity for the Poincaré-Lyapunov compactification, and the explanation of the quasi-homogeneous type blow-up that includes polar it and directional it, based on a method of the Newton diagram (Section 1.2).

The following chapters describe the results of applying the above methods to understand the structure of special solutions to various partial differential equations. Chapters 2, 4, 7, and 8 are duplicates of the authors' master's thesis [40]. Chapter 5 is also described in [40], but was added and revised after the writing of [40].

Chapter 2 is devoted to studying the quasi traveling waves with quenching of a reaction-diffusion equation in the presence of negative powers nonlinearity. This chapter is based

on the published paper [31]. Namely, we consider the following equation:

$$u_t = u_{xx} + \frac{1}{(1-u)^\alpha}, \quad t > 0, \quad x \in \mathbb{R}, \quad \alpha \in \mathbb{N}. \tag{A}$$

It is revealed that its equation possesses a family of "quasi traveling waves with quenching on a finite interval". We also give quenching rates and their profile. Note that the proof of its existence is considering the restricted case of $\alpha \in 2\mathbb{N}$. In the case that $\alpha \in \mathbb{N}$, Matsue [50] gave the proof by assuming the existence of the traveling wave solution and showing the same quenching rates as our works.

Chapter 3 consider the traveling waves with singularities in a damped hyperbolic MEMS type equation in the presence of negative powers nonlinearity. This equation arises in the study of the Micro-Electro Mechanical System (MEMS) devices. We investigate how the behavior (shapes and asymptotic behavior) of traveling waves change depending on whether an inertial term $\varepsilon^2 u_{tt}$ is present or absent in the left-hand side of [31] (see Chapter 2). In this chapter, we classify all traveling waves in this equation and report their shapes and asymptotic behavior. These are studied by applying the Poincaré compactification and basic theory of dynamical systems. In author knowledge, there has been no studies of this equation with dynamical system approach, therefore, out results will give first step for the studies of it from the viewpoint of geometric (dynamical system) approach. This chapter is based on the published paper [37].

In Chapter 4, we consider the radial symmetric stationary solutions of the following equation:

$$u_t = \Delta u - |x|^q u^{-p}, \quad t > 0, \quad x \in \mathbb{R}^n, \tag{B}$$

with $3 \leq n \in \mathbb{N}$, $p \in \mathbb{N}$ and $q \in \mathbb{R}$. This equation arises in the study of the dynamic deflection of an elastic membrane inside a micro-electro mechanical system (MEMS). Above equation (A) is a special case of (B). This chapter is devoted to studying the radial symmetric stationary solution of (B). That is, we study the following equation (the radial symmetric stationary problem):

$$u'' + \frac{n-1}{r}u' - r^q u^{-p} = 0, \quad ' = \frac{d}{dr}, \tag{C}$$

where $r = |x| > 0$.

We first give a result on the existence of the negative value functions that satisfy the radial symmetric stationary problem on a finite interval for $p \in 2\mathbb{N}$, $q \in \mathbb{R}$. Moreover, we give the asymptotic behavior of $u(r)$ and $u'(r)$ at both ends of the finite interval. Second, we obtain the existence of the positive radial symmetric stationary solutions with the singularity at $r = 0$ for $p \in \mathbb{N}$ and $q \geq -2$. In fact, the behavior of solutions for $q > -2$ and $q = -2$ are different. In each case of $q = -2$ and $q > -2$, we derive the asymptotic behavior for $r \to 0$ and $r \to \infty$. This chapter is based on the published paper [33].

In Chapter 5, we consider the singular stationary solutions of following spatial one-dimensional partial differential equation

$$u_t = u_{xx} + \mu \frac{1 + \delta u_x^\beta}{(1-u)^\alpha}, \quad t > 0, \quad x \in \mathbb{R} \tag{D}$$

with $\alpha \in 2\mathbb{N}$, $4 < \beta \in 2\mathbb{N}$, $\mu > 0$, and $\delta \geq 0$. This chapter is based on the published paper [35]. This equation arises in the study of the Micro-Electro Mechanical System (MEMS) devices. In (A), this corresponds to the case where $\mu = 1$ and $\delta = 0$. One of the main purposes of this chapter is to prove the existence of (singular) stationary solutions of (D)

and to give the asymptotic behavior. Here, the stationary solution with singularity here means a solution that allows infinity or a solution with an infinite differential coefficient. In this chapter, we obtain a whole phase portrait on $\mathbb{R}^2$ with including infinity about a two-dimensional ordinary differential equation that introduced the change of coordinates: $1-u(x)=\phi(\xi),\ \xi=x$. In addition, we focus on the connecting orbits on it and give a result on the existence of the singular stationary solutions and detailed information about the asymptotic behavior. However, there are some problems that could not be completely solved.

Chapter 6 is based on the published paper [36]. This chapter is devoted to the study of the following problem:

$$U''+\frac{N-1}{r}U'+\frac{\mu+\delta(U')^2}{1-U}=0, \quad \left(\ '=\frac{d}{dr} \quad \text{and} \quad ''=\frac{d^2}{dr^2}\right) \tag{E}$$

with $U=U(r)$, $r=|x|>0$, $3\leq N\in\mathbb{N}$, $\mu>0$ and $\delta>0$. (E) corresponds to a radial symmetric stationary problem with the following equation:

$$U_t=\Delta U+\frac{\mu+\delta|\nabla U|^2}{1-U}, \quad t>0, \quad x\in\mathbb{R}^N, \quad U=U(t,x) \tag{F}$$

(F) is derived from the study of the Micro-Electro Mechanical System (for short, MEMS). Motivated by the previous study [21], this manuscript considers the question of how far we can investigate the structure of solutions in a unified way by applying the framework framework that combines Poincaré type compactification, classical dynamical systems theory, and geometric methods for desingularization of vector fields (blow-up technique). Then, our framework allowed us to obtain results that were not obtained in this previous work that is information about the shape and the asymptotic behavior and results that were partially included in the results it. It is expected that these will lead to a deeper understanding of the behavior of typical solutions to the MEMS equations. In authors knowledge, there is no study that clarifies the structure of the typical and characteristic solutions of (E) by the dynamical systems approach.

In Chapter 7, we consider the traveling wave solutions of the following degenerate nonlinear parabolic equation:

$$u_t=u^p(u_{xx}+u), \tag{G}$$

where p is a positive integer. This equation is derived from a model that reproduces a number of phenomena. We also deal with the equation

$$v_\tau=v^p(v_{xx}+v-v^{-p+1}) \tag{H}$$

related to it. We first give a result on the whole dynamics on the phase space $\mathbb{R}^2$ with including infinity about a two-dimensional ordinary differential equation that introduced the traveling wave coordinates: $\xi=x-ct$. Second, we focus on the connecting orbits on it and give a result on the existence of the weak traveling wave solutions with quenching for $c>0$ and $p\in 2\mathbb{N}$. Moreover, we give the detailed information about the asymptotic behavior of $u(\xi)$, $u'(\xi)$, $v(\xi)$ and $v'(\xi)$ for $p\in 2\mathbb{N}$. In the case that $p\in 2\mathbb{N}+1$, some singularities appear. However, we classify the connecting orbits and corresponding traveling wave solutions and obtain their asymptotic behavior. This chapter is based on the published paper [32].

In Chapter 8, we consider the asymptotic behavior of traveling wave solutions of the following degenerate nonlinear parabolic equation:

$$u_t=u^p(u_{xx}+u)-\delta u, \quad (\delta=0 \text{ or } 1) \tag{I}$$

for $\xi \equiv x - ct \to -\infty$ with $c > 0$. We give a refined one of them, which was not obtained in the previous chapter 7 (preceding work [32]), by an appropriate asymptotic study. During our proof of the main theorem, we see that the Lambert W function plays a key role in describing the asymptotic behavior. Evaluation of integrals including the Lambert W function is necessary to obtain the asymptotic behavior in the present form. Our argument here is based on an asymptotic study of solutions in a different form from that provided in e.g. [32, 50], which can be applied to asymptotic analysis towards further applications in various phenomena including their numerical calculations. We expect that our approach can be applied to the asymptotic behavior of typical solutions as well as that of singular solutions. This chapter is based on the published paper [30].

Chapter 9 discusses a classification (existence of (including a weak sense of meaning) solutions, information about the shape, and asymptotic behavior) of nonnegative traveling wave solutions of the space one-dimensional degenerate parabolic equations that derive from many phenomena. This chapter is based on the published paper [38]. In this chapter, the equations (G) and (H) treated in Chapter 7 and 8 (corresponding papers [32, 30]) are summarized and generalized to the following equation:

$$U_t = U^p(U_{xx} + \mu U) - \delta U, \quad t > 0, \quad x \in \mathbb{R}, \quad (\delta = 0 \text{ or } 1) \tag{J}$$

with $\mu > 0$. In chapter 7 and 8 above, the use of blow-up technique forced us to restrict the parameter p in the equation to a natural number greater than 1. Therefore, in this chapter we consider the following equation obtained by transformation $u = U^p$ for (J):

$$u_t = uu_{xx} - \gamma(u_x)^2 + ku^2 - \delta pu, \quad t > 0, \quad x \in \mathbb{R}. \tag{K}$$

Since the equation obtained by this transformation can be discussed without using the blow-up technique, it can be discussed in the same way as in the above chapter 7 and 8 without the assumption of natural numbers in the previous studies. In other words, in (K), we can obtain the classification of nonnegative traveling wave solutions for a real number$p$ greater than 1. Then, by reflecting these results in the original problem with the transformation $U = u^{1/p}$, we obtained results that generalize the result of the above two chapters ([32, 30]), which is a major achievement.

Chapter 10 considers the radially symmetric stationary solutions of the following systems:

$$\begin{cases} u_t = \Delta u - \nabla \cdot (u \nabla v), & x \in \mathbb{R}^N, \quad t > 0, \\ 0 = \Delta v + u, & x \in \mathbb{R}^N, \quad t > 0 \end{cases}$$

and

$$\begin{cases} u_t = \Delta u - \alpha \nabla \cdot (u \nabla p) + \beta \nabla \cdot (u \nabla q), & x \in \mathbb{R}^N, \quad t > 0, \\ 0 = \Delta p + u, & x \in \mathbb{R}^N, \quad t > 0, \\ 0 = \Delta q + u, & x \in \mathbb{R}^N, \quad t > 0, \end{cases}$$

where α and β are positive constants. In addition, let N be $N \geq 3$. Assume that $\alpha < \beta$ below. This chapter is based on the published paper [39].

The purpose of this chapter is to focus on the radially symmetric stationary solutions of the above systems and to investigate what kind of the radially symmetric stationary solutions exist, information about their shapes, and their asymptotic behavior. In particular, the construction of functions satisfying equations that diverge at the endpoints of finite intervals is an interesting result. The key to the discussion is to derive a scalar equation by using a transformation on the averaged mass for the equation satisfied by the radially symmetric stationary solution and to investigate the infinity dynamics as geometric information for the two-dimensional ordinary differential equations derived from it. To

achieve this, we use a method that combines classical results from the continuous dynamical systems theory and Poincaré-Lyapunov compactification. In addition, the results for singular solutions are discussed in light of the results of previous studies.

It is important to study the global behavior of solutions to systems of ordinary differential equations describing the transmission dynamics of infectious diseases. In chapter 11, we present a different approach from the Lyapunov function used in most of the study. This approach is based on the Poincaré compactification. We then apply the method to an SIR endemic model as a test case and discuss its effectiveness and the potential applications of this approach. In addition, we refine the discussion of dynamics near the equilibrium, derive the asymptotic behavior, and mention its relation to the basic reproduction number. This chapter follows the same method used to investigate various properties of special solutions of partial differential equations. However, it also reveals the global behavior of solutions to ordinary differential equations, providing a new perspective on the analysis of mathematical models of infectious diseases. This result demonstrates the broader potential of the author's research. This chapter is based on the published paper [34].

Acknowledgments

I would like to express my gratitude to Professor Shigetoshi Yazaki (Meiji University), who is my supervisor, for his valuable suggestion and encouragement throughout my Doctor's course at Meiji University. He gave me much valuable advice in the early stages of each work. He also gave me opportunities to give talks and various experiences over the past two years.

I am deeply grateful to Professor Takashi Sakamoto (Meiji University), who is my essential supervisor and supervisor throughout my Bachelor's and Master's course at Meiji University. He led me to the field of dynamical systems. His advice and suggestions generated the core of my research. Through discussions with him, I was able to write six papers. I cannot thank him enough.

Professor Kaname Matsue (Kyushu University) provides me with various valuable pieces of advice. I would like to thank him for the discussion on applying the Poincaré type compactification and finite-time singularities for differential equations. In particular, discussions among the three of us, including Professor Takashi Sakamoto mentioned above, resulted in the paper in [30].

Professor Yūki Naito (Hiroshima University) provided me with various useful advice in my research of the chemotaxis model. After discussions with him, I was able to submit the paper in [39].

I owe my deepest gratitude to Professor Hayato Nawa (Meiji University), Professor Hiroshi Konno (Meiji University), Professor Hiroshi Watanabe, Professor Munemitsu Hirose (Meiji University) and Professor Yuichi Nohara (Meiji University) for their valuable comments, suggestions, and encouragement throughout my Bachelor's, Master's and Doctor's course in Meiji University.

I would like to express my gratitude to Professor Mamoru Aizawa (Meiji University). He specializes in biomaterials. From the end of my second-year master's program, he participated in discussions on the research toward the construction of a mathematical model of injectable calcium-phosphate cement (CPC) pastes that are used in bone grafting. In addition, he made great efforts to promote interdisciplinary research with mathematics. I would like to thank Ms. Rika Yamada, a graduate of his laboratory, and laboratory members Ms. Shiori Kato and Ms. Yuki Kamaya for various discussions as important members of this study.

I would also like to express my gratitude to the many researchers who advised me on this work. I owe my deepest gratitude to Professor Yasuhito Miyamoto (The University of Tokyo), Professor Tetsuya Ishiwata (Shibaura Institute of Technology), Professor Akitoshi Takayasu (University of Tsukuba), Professor Koichi Anada (Waseda University Senior High School), Professor Ken-ichi Nakamura (Kanazawa University), Professor Hirokazu Ninomiya (Meiji University) Professor Kazuyuki Yagasaki (Kyoto University), Professor Yoshihisa Morita (Ryukoku University), Professor Tatsuki Kawakami (Ryukoku University), Professor Hirofumi Izuhara (Miyazaki University), Professor Yuk-

ihiko Nakata (Aoyama Gakuin University), Professor Hiroshi Wakui (Tokyo University of Science), Professor Koya Sakakibara (Okayama University of Science) and Professor Shunsuke Kobayashi (Kyoto University) for their valuable comments and suggestions.

During the two years of the doctor's course, I was partially supported by JSPS KAKENHI Grant Number JP21J20035. In addition, I was partially supported by the Research Fellowships of Japan Society for the Promotion of Science for Young Scientists.

I also would like to thank the members of Sakamoto laboratory (Meiji University) and Yazaki laboratory (Meiji University) for their kindness and support.

I would like to express their sincere gratitude to all staff of the mathematics reference room of Meiji University. I also wishes to express their sincerely all members and staff of the Department of Science and Technology, Meiji University.

Finally, I would also like to express the deepest appreciation to my family for their support and warm encouragement.

List of Corresponding Papers

Chapter 2

[31] Ichida, Y., Sakamoto, T.O.: Quasi traveling waves with quenching in a reaction-diffusion equation in the presence of negative powers nonlinearity, Proc. Japan Acad. Ser. A Math. Sci. **96** (2020), no. 1, 1–6.

Chapter 3

[37] Ichida, Y.: Traveling waves with singularities in a damped hyperbolic MEMS type equation in the presence of negative powers nonlinearity, Electron. J. Differ. Equ, **2023** (2023), no. 5, 1–20.

Chapter 4

[33] Ichida, Y., Sakamoto, T.O.: Radial symmetric stationary solutions for a MEMS type reaction-diffusion equation with spatially dependent nonlinearity, Jpn. J. Ind. Appl. Math. **38** (2021), no. 1, 297–322.

Chapter 5

[35] Ichida Y., Sakamoto, T.O.: Stationary solutions for a 1D pde problem with gradient term and negative powers nonlinearity, J . Elliptic Parabol. Equ, **8** (2022), no. 2, 885–918.

Chapter 6

[36] Ichida, Y., Sakamoto, T.O.: Radially symmetric stationary solutions for a MEMS type reaction-diffusion equation with fringing field, Nonlinearity, **36** (2023), no. 1, 71–109.

Chapter 7

[32] Ichida, Y., Sakamoto, T.O.: Traveling wave solutions for degenerate nonlinear parabolic equations, J. Elliptic Parabol. Equ. **6** (2020), no. 2, 795–832.

Chapter 8

[30] Ichida, Y., Matsue, K., Sakamoto, T.O.: A refined asymptotic behavior of traveling wave solutions for degenerate nonlinear parabolic equations, JSIAM Lett. **12** (2020), 65–68.

Chapter 9

[38] Ichida, Y: Classification of nonnegative traveling wave solutions for the 1D degenerate parabolic equations, Discrete Contin. Dyn. Syst., Ser. B, **28** (2023), no. 2, 1116–1132.

Chapter 10

[39] Ichida, Y.: Radially symmetric stationary solutions for certain chemotaxis systems in higher dimensions: a geometric approach, Discrete Contin. Dyn. Syst., **43** (2023), no. 5, 1975–2001.

Chapter 11

[34] Ichida, Y: On global behavior of a some SIR epidemic model based on the Poincaré compactification, JSIAM Lett., **14** (2022), 65–68.

Chapter 1

Preliminaries

Abstract

In this chapter, we briefly introduce the Poincaré type compactification (Poincaré compactification and Poincaré-Lyapunov compactification), asymptotically quasi-homogeneous vector fields at infinity, and blow-up technique in order to use our works. This chapeter cites [1, 8, 14, 31, 32, 33, 34, 49, 50] and summarizes the necessary parts of this study to understand it. It should be noted that we refer [14] for more details of Poincaré compactification and Newton diagram that find the coefficient (α, β) to use in a quasi-homogineous blow-up, [8] for the definition of quasi-homogeneous vector field of type $(\alpha_1, \alpha_2, \dots \alpha_n)$ and degree k and the Newton polyhedron method, [49] [50] for the definition of asymptotically quasi-homogeneous vector fields and the Poincaré-Lyapunov compactification (directional compactification). Further, we refer [1] for more details of blow-up technique.

1.1 Poincaré type compactification

In order to study the behavior of the trajectories of a planar differential system near infinity it is possible to use a compactifiction. One of the possible constructions relies on stereographic projection of the sphere onto the plane, in which case a single "point at infinity" is adjoined to the plane. It is called the Bendixson compactification (i.e., one-point compactification, see [14] and references therein). A better approach for studying the behavior of trajectories near infinity is to use the so called Poincaré sphere, introduced by Poincaré [60]. It has the advantage that the singular points at infinity are spread out along the equator of the sphere and are therefore of a simpler nature than the singular points of the Bendixson sphere. We call the compactification derived from this idea the Poincaré type compactification. The Poincaré type compactification is one of the compactifications of the original phase space (the embedding of $\mathbb{R}^n$ into the unit upper hemisphere of $\mathbb{R}^{n+1}$). In the following, the Poincaré type compactification includes both the Poincaré compactification and the Poincaré-Lyapunov compactification. The difference between the two is that the vector field is either homogeneous or quasi-homogeneous, respectively. In this section, we briefly introduce the Poincaré compactification and the Poincaré-Lyapunov compactification (especially the directional compactification).

First, we present an overview of the Poincaré compactification applied to homogeneous vector fields. It should be noted that we refer [14, 31, 32, 33, 60] for more details.

Let

$$X = P(a, b)\frac{\partial}{\partial a} + Q(a, b)\frac{\partial}{\partial b}$$

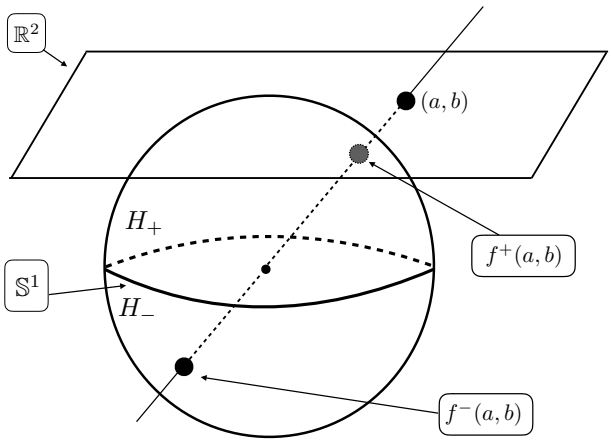

Figure 1.1.1: Position of the points $(a,b) \in \mathbb{R}^2$ and $f^{\pm}(a,b)$ on the Poincaré sphere $\mathbb{S}^2$.

be a polynomial vector field on $\mathbb{R}^2$, or in other words

$$\begin{cases} \dot{a} = P(a,b), \\ \dot{b} = Q(a,b), \end{cases}$$

where $\dot{}$ denotes d/dt, and P, Q are polynomials of arbitrary degree in the variables a and b.

First, we consider $\mathbb{R}^2$ as the plane in $\mathbb{R}^3$ defined by

$$(y_1, y_2, y_3) = (a, b, 1).$$

We consider the sphere

$$\mathbb{S}^2 = \{y \in \mathbb{R}^3 \,|\, y_1^2 + y_2^2 + y_3^2 = 1\}$$

which we call the Poincaré sphere. We divide the sphere into

$$H_+ = \{y \in \mathbb{S}^2 \,|\, y_3 > 0\},$$
$$H_- = \{y \in \mathbb{S}^2 \,|\, y_3 < 0\}$$

and

$$\mathbb{S}^1 = \{y \in \mathbb{S}^2 \,|\, y_3 = 0\}.$$

Let us consider the embedding of vector field X from $\mathbb{R}^2$ to $\mathbb{S}^2$ given by

$$f^+ : \mathbb{R}^2 \to \mathbb{S}^2 \quad \text{and} \quad f^- : \mathbb{R}^2 \to \mathbb{S}^2,$$

where

$$f^{\pm}(a,b) := \pm \left(\frac{a}{\Delta(a,b)}, \frac{b}{\Delta(a,b)}, \frac{1}{\Delta(a,b)} \right)$$

with $\Delta(a,b) = \sqrt{a^2 + b^2 + 1}$. This implies that $f^+(a,b)$ (resp. $f^-(a,b)$) is the intersection of the straight line passing through the point y and the origin with the northern (resp. southern) hemisphere of $\mathbb{S}^2$ (see also Figure 1.1.1).

Then, we consider six local charts on $\mathbb{S}^2$ given by

$$U_k = \{y \in \mathbb{S}^2 \,|\, y_k > 0\} \quad \text{and} \quad V_k = \{y \in \mathbb{S}^2 \,|\, y_k < 0\}$$

for $k = 1, 2, 3$. Consider the local projection

$$g_k^+ : U_k \to \mathbb{R}^2 \quad \text{and} \quad g_k^- : V_k \to \mathbb{R}^2$$

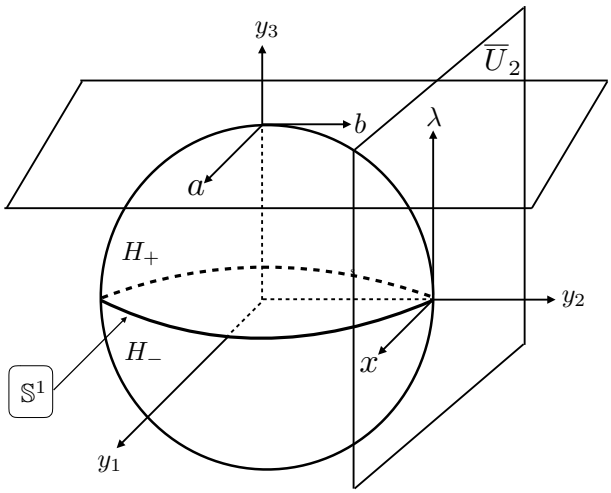

Figure 1.1.2: Locations of the Poincaré sphere and chart $\overline{U}_2$.

defined as

$$g_k^+(y_1, y_2, y_3) = -g_k^-(y_1, y_2, y_3) = \left(\frac{y_m}{y_k}, \frac{y_n}{y_k}\right)$$

for $m < n$ and $m, n \neq k$. The projected vector fields are obtained as the vector fields on the planes

$$\overline{U}_k = \{y \in \mathbb{R}^3 \,|\, y_k = 1\}$$

and

$$\overline{V}_k = \{y \in \mathbb{R}^3 \,|\, y_k = -1\}$$

for each local chart U_k and V_k. We denote by (x, λ) the value of $g_k^{\pm}(y)$ for any k.

For instance, it follows that

$$(g_2^+ \circ f^+)(a, b) = \left(\frac{a}{b}, \frac{1}{b}\right) = (x, \lambda),$$

therefore, we can obtain the dynamics on the local chart $\overline{U}_2$ by the change of variables $a = x/\lambda$ and $b = 1/\lambda$. The locations of the Poincaré sphere, (a, b)-plane, and $\overline{U}_2$ are expressed as Figure 1.1.2.

Throughout this master thesis, we follow the notations used here for the Poincaré compactification. It is sufficient to consider the dynamics on $H_+ \cup \mathbb{S}^1$, which is called Poincaré disk, to obtain our main results.

Second, we consider the case that a vector field is quasi-homogeneous. In this case, it should be noted that we choose appropriate compactifications to consider the information about dynamics at infinity. That is, when the vector field is quasi-homogeneous, the information at infinity may not be reflected correctly in the Poincaré compactification. Then, we introduce the Poincaré-Lyapunov compactification (the directional compactification) that is based on asymptotically quasi-homogeneous vector fields. Then we define a class of vector fields that are quasi-homogeneous near infinity, which is determined by types and orders. In the following, we reproduce the definitions given in [49] as an aid to understanding the methods used in this thesis. See [49, 50] for details.

Definition 1.1.1 ([49], Definition 2.1)
Let $f : \mathbb{R}^n \to \mathbb{R}$ be a smooth function. Let $\alpha_1, \alpha_2, \ldots, \alpha_n \geq 0$ with $(\alpha_1, \alpha_2, \ldots \alpha_n) \neq (0, 0, \ldots, 0)$ be integers and $k \geq 1$. We say that f is a quasi-homogeneous function of type

$(\alpha_1, \alpha_2, \ldots, \alpha_n)$ and order k if

$$f(R^{\alpha_1}x_1, R^{\alpha_2}x_2, \ldots, R^{\alpha_n}x_n) = R^k f(x_1, x_2, \ldots, x_n), \quad \forall x \in \mathbb{R}^n, \quad R \in \mathbb{R}.$$

Next, let

$$X = \sum_{j=1}^{n} f_j(x)\frac{\partial}{\partial x_j} \iff X : \begin{pmatrix} f_1(x_1, x_2, \ldots, x_n) \\ f_2(x_1, x_2, \ldots, x_n) \\ \vdots \\ f_n(x_1, x_2, \ldots, x_n) \end{pmatrix}$$

be a smooth vector field. We say that X, or $f = (f_1, f_2, \ldots, f_n)$ is a quasi-homogeneous vector field of type $(\alpha_1, \alpha_2, \ldots, \alpha_n)$ and order $k+1$ if each component f_j is a quasi-homogeneous function of type $(\alpha_1, \alpha_2, \ldots, \alpha_n)$ and order $k + \alpha_j$.

For applications to general vector fields, we define the following notion.

Definition 1.1.2 ([49], Definition 2.2)
Let $\alpha = (\alpha_1, \alpha_2, \ldots, \alpha_n)$ be a set of nonnegative integers. Let the index set I_α as

$$I_\alpha := \{i \in \{1, 2, \ldots, n\} \mid \alpha_i > 0\},$$

which we shall call the set of homogeneity indices associated with $\alpha = (\alpha_1, \alpha_2, \ldots, \alpha_n)$. Let $U \subset \mathbb{R}^n$. We say the domain $U \subset \mathbb{R}^n$ is admissible with respect to the sequence α if

$$U := \{x = (x_1, x_2, \ldots, x_n) \in \mathbb{R}^n \mid x_i \in \mathbb{R}, \text{ if } i \in I_\alpha, (x_{j_1}, x_{j_2}, \ldots, x_{j_{n-l}}) \in \tilde{U}\},$$

where $\{j_1, j_2, \ldots, j_{n-l}\} = \{1, 2, \ldots, n\} \backslash I_\alpha$ and $\tilde{U}$ is an $(n-l)$-dimensional open set.

Assumptions in Definition 1.1.1 indicate $I_\alpha \neq \emptyset$. The notion of asymptotic quasi-homogeneity defined below provides a systematic validity of scalings at infinity in many practical applications.

Definition 1.1.3 ([49], Definition 2.3)
Let $f = (f_1, f_2, \ldots, f_n) : U \to \mathbb{R}^n$ be a smooth function with an admissible domain $U \subset \mathbb{R}^n$ with respect to α such that f is uniformly bounded for each x_i with $i \in I_\alpha$, where I_α is the set of homogeneity indices associated with α. We say that

$$X = \sum_{j=1}^{n} f_j(x)\frac{\partial}{\partial x_j} \iff X : \begin{pmatrix} f_1(x_1, x_2, \ldots, x_n) \\ f_2(x_1, x_2, \ldots, x_n) \\ \vdots \\ f_n(x_1, x_2, \ldots, x_n) \end{pmatrix}$$

or simply f is an asymptotically quasi-homogeneous vector field of type $(\alpha_1, \alpha_2, \ldots, \alpha_n)$ and order $k+1$ at infinity if

$$\lim_{R \to +\infty} R^{-(k+\alpha_j)} \big\{ f_j(R^{\alpha_1}x_1, R^{\alpha_2}x_2, \ldots, R^{\alpha_n}x_n) - R^{k+\alpha_j}(f_{\alpha,k})_j(x_1, x_2, \ldots x_n) \big\} = 0$$

holds for any $(x_1, x_2, \ldots, x_n) \in U_1$, where $f_{\alpha,k} = ((f_{\alpha,k})_1, (f_{\alpha,k})_2, \ldots, (f_{\alpha,k})_n) : U \to \mathbb{R}^n$ is a quasi-homogeneous vector field of type $(\alpha_1, \alpha_2, \ldots, \alpha_n)$ and order $k+1$, and

$$U_1 := \{x = (x_1, x_2, \ldots, x_n) \in \mathbb{R}^n \mid (x_{i_1}, x_{i_2}, \ldots, x_{i_l}) \in \mathbb{S}^{l-1}, (x_{j_1}, x_{j_2}, \ldots, x_{j_{n-l}}) \in \tilde{U}\},$$

where $\{i_1, i_2, \ldots, i_l\} = I_\alpha$.

The geometric image of the locational relationship between the Poincaré-Lyapunov sphere corresponding to the Poincaré sphere and the local coordinate $\overline{U}_2$ is the same as in Figure 1.1.2. Using the type defined in Definition 1.1.3 in the case that $n = 2$, we consider the dynamics on the local chart $\overline{U}_2$ by the change of variables $\phi = x/\lambda^{\alpha_1}$, $\psi = 1/\lambda^{\alpha_2}$.

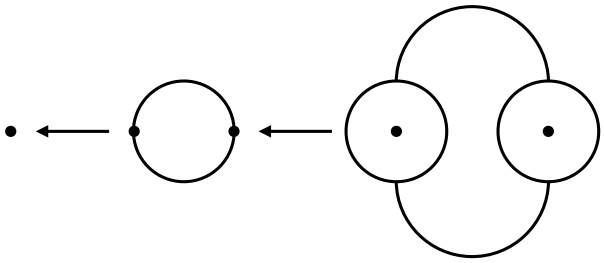

Figure 1.2.1: Schematic picture of the succession of blow-up (see [14] Fig. 3.3.).

1.2 Blow-up technique

In this chapter, we introduce the basic tool for studying nonelementary singularities of a differential system in the plane. This tool is based on changes of variables called blow-ups. We use this technique for classifying the singularities having both eigenvalues zero but whose linear part is not identically zero. We refer the reader to [1], [8], [14] for more detailed information.

According to [1], roughly speaking the idea behind the blow-up technique is to explode, through a change of variables that is not a diffeomorphism, the singularity to a line or circle. Then, for studying the original singular point one studies the new singular points that appear on this line or circle and that will be, probably, simpler. If some of these new singular points are degenerate the process is repeated. The succession of blow-up is schematized in Figure 1.2.1 by [14].

Let

$$X = P(a,b)\frac{\partial}{\partial a} + Q(a,b)\frac{\partial}{\partial b} \tag{1.2.1}$$

be a polynomial vector field on $\mathbb{R}^2$, or in other words

$$\begin{cases} \dot{a} = P(a,b), \\ \dot{b} = Q(a,b), \end{cases}$$

where $\dot{}$ denotes d/dt, and P, Q are polynomials of arbitrary degree in the variables a and b again. We consider the case where the vector field is quasi-homogeneous vector field of type $(\alpha_1, \alpha_2, \ldots, \alpha_n)$ and degree k (see Definition 1.1.1). Here, note that type $(\alpha_1, \alpha_2, \ldots, \alpha_n)$ is restricted to $(\alpha_1, \alpha_2, \ldots, \alpha_n) \in \mathbb{N}_+^n$ (see [8]). Of course, we remark that the homogeneous vector fields are included the quasi-homogeneous vector field.

The *quasi-homogeneous polar blow-up* (or the (α, β)-polar blow-up) is the mapping $(r, \theta) \mapsto (r^\alpha \cos\theta, r^\beta \sin\theta) = (a, b)$ with $r \in \mathbb{R}$ and $\theta \in [0, 2\pi)$, for some convenient $\alpha, \beta \in \mathbb{N}$. The case $\alpha = \beta = 1$ is called the homogeneous polar blow-up. On the other hand, the *quasi-homogeneous directional blow-up in the positive (*resp. negative*) a direction* is the mapping $(r, \bar{x}) \mapsto (r^\alpha, r^\beta \bar{b}) = (a, b)$ (resp. $(r, \bar{b}) \mapsto (-r^\alpha, r^\beta \bar{b}) = (a, b)$), where r, $\bar{b}$ are new variables. The *quasi-homogeneous directional blow-up in the positive (*resp. negative*) b direction* is the mapping $(r, \bar{a}) \mapsto (r^\alpha \bar{a}, r^\beta) = (a, b)$ (resp. $(r, \bar{a}) \mapsto (-r^\alpha \bar{a}, r^\beta) = (a, b)$), where r, $\bar{a}$ are new variables. The parameters $\alpha, \beta \in \mathbb{N}$ are chosen conveniently. If $\alpha = \beta = 1$, then we recover the (homogeneous) directional blow-up.

A question one might ask is how to effectively find the coefficient (α, β) to use in a quasi-homogenous blow-up. Of course we can use Definition 1.1.1 to determine (α, β), but we will show how to find it more easily. This can be obtained by using the so called Newton diagram. We first define the Newton diagram (see [1], [14] and references therein).

This method is effective only for polynomial vector field on $\mathbb{R}^2$. Otherwise, Definition 1.1.1 will be used.

Let (1.2.1) be a polynomial vector field with an isolated singularity at the origin.

Let

$$P(a,b)=\sum_{i+j\geq 1} p_{ij}a^ib^j, \quad Q(a,b)=\sum_{i+j\geq 1} q_{ij}a^ib^j.$$

The *support* of X is defined to be

$$S=\{(i-1,j)\mid p_{ij}\neq 0\}\cup\{(i,j-1)\mid q_{ij}\neq 0\}\subset\mathbb{R}^2,$$

and the *Newton polygon* of X is the convex hull Γ of the set

$$P=\bigcup_{(r,s)\in S}\{(r',s')\mid r'\geq r, s'\geq s\}.$$

The *Newton diagram* of X is the union γ of the compact faces γ_k of the Newton polygon Γ, which we enumerate from the left to the right. If there exists a face γ_k which lies completely on the half-plane $\{r\leq 0\}$, then we start the enumeration with $k=0$, otherwise we start with $k=1$. Since the origin is an isolated singularity we have that at least one of the points $(-1,s)$ or $(0,s)$ is an element of S for some s, and also at least one of the points $(r,0)$ or $(r,-1)$ is an element of S for some r. Hence there always exists a face γ_1 in the Newton diagram.

Suppose that γ_1 has equation $\alpha r+\beta s=d$, with $\gcd(\alpha,\beta)=1$. As a first step in the desingularization process we use a quasi-homogeneous blow-up of degree (α,β).

Example 1.2.1 ([14], Example 3.2)
As an example we calculate the Newton diagram of the following vector field:

$$b\frac{\partial}{\partial a}+(a^2+ab)\frac{\partial}{\partial b}+O(\|(a,b)\|^3), \tag{1.2.2}$$

providing the best choice of coefficients (α,β).

The support of (1.2.2) *surely contains* $(-1,1)$, $(2,-1)$, *and* $(1,0)$ *coming, respectively, from* $b\frac{\partial}{\partial a}$, $a^2\frac{\partial}{\partial b}$, *and* $ab\frac{\partial}{\partial b}$. *Besides these three points it can contain many other points, which are in fact not essential since they all lie in the convex hull* Q *of* $Q_1\cup Q_2\cup Q_3$ *with* $Q_1=\{(r,s)\mid r\geq -1, s\geq 1\}$, $Q_2=\{(r,s)\mid r\geq 2, s\geq -1\}$, *and* $Q_3=\{(r,s)\mid r\geq 1, s\geq 0\}$. *In Figure1.2.2 we represent* Q_i *for* $i=1,2,3$ *in (a) as well as* $P=Q$ *in (b).*

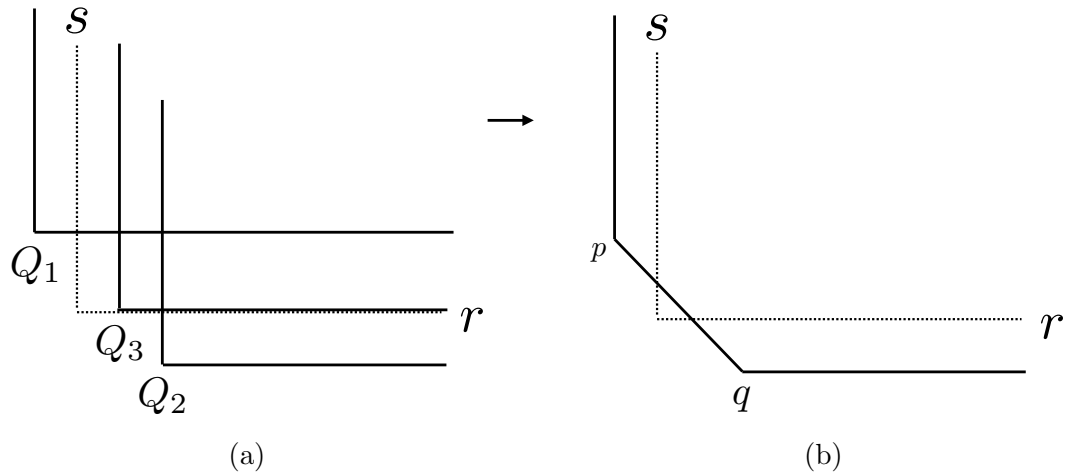

(a) (b)

Figure 1.2.2: Calculating the Newton polygon (see [14] Fig. 3.12.).

We see that the Newton diagram consists of one compact face, that we denote by γ_1 *and which is the line segment joining the points* $p = (-1, 1)$ *to* $q = (2, -1)$*. The line segment lies on the line of equation* $2r + 3s = 1$ *including the choice* $(\alpha, \beta) = (2, 3)$*.*

Chapter 2

Quasi traveling waves with quenching in a reaction-diffusion equation in the presence of negative powers nonlinearity

Abstract

The quasi traveling waves with quenching of $u_t = u_{xx} + (1-u)^{-\alpha}$ for $\alpha \in 2\mathbb{N}$ are considered. The existence of quasi traveling waves with quenching and their quenching rates are studied by applying the Poincaré compactification. This chapter is based on the following published paper ([31]):

> Ichida, Y., Sakamoto, T.O.: Quasi traveling waves with quenching in a reaction-diffusion equation in the presence of negative powers nonlinearity, Proc. Japan Acad. Ser. A Math Sci. **96**, 1–6 (2020).

2.1 Introduction

In this chapter, we consider the quasi traveling waves with quenching (see Definition 2.1.3) of the following equation

$$u_t = u_{xx} + \frac{1}{(1-u)^{\alpha}}, \quad t > 0, \quad x \in \mathbb{R}, \quad \alpha \in \mathbb{N}. \tag{2.1.1}$$

First, we state the definition of "quenching" for the solution of (2.1.1).

Definition 2.1.1 ([50], Definition 4.19)
We say that a solution $u(t,x)$ of (2.1.1) quenches at point (T, x_0) if

$$\lim_{t \uparrow T} u(t, x_0) = 1, \quad \lim_{t \uparrow T} \left| \frac{\partial u}{\partial t}(t, x_0) \right| = \infty.$$

In order to consider the traveling waves of (2.1.1), we introduce the following change of variables:

$$\phi(\xi) = 1 - u(t,x), \quad \xi = x - ct, \quad c > 0.$$

We then seek the solution $\phi(\xi)$ of the following equation:

$$c\phi' = -\phi'' + \phi^{-\alpha}, \quad \xi \in \mathbb{R}, \quad ' = \frac{d}{d\xi}, \tag{2.1.2}$$

or

$$\begin{cases} \phi' = \psi, \\ \psi' = -c\psi + \phi^{-\alpha}. \end{cases} \tag{2.1.3}$$

Second, we state the definition of quasi traveling waves and quasi traveling waves with quenching as follows.

Definition 2.1.2
We say that a function $u(t,x) \equiv 1-\phi(\xi)$ is a quasi traveling wave of (2.1.1) if the function $\phi(\xi)$ is a solution of (2.1.2) on a finite interval or semi-infinite interval.

Definition 2.1.3
We say that a function $u(t,x) \equiv 1-\phi(\xi)$ is a quasi traveling wave with quenching of (2.1.1) if the function $u(t,x)$ is a quasi traveling wave of (2.1.1) on a finite interval (resp. semi-infinite interval) such that $|\phi'|$ becomes infinite (namely, ϕ reaches 0) at both ends of the interval (resp. finite end point of the semi-infinite interval). More precisely, we have the following three cases:

(I) the function $\phi(\xi)$ is a solution of (2.1.2) on a semi-infinite interval $(-\infty, \xi_*)$ ($\phi(\xi) \in C^2(-\infty,\xi_*) \cap C^0(-\infty,\xi_*]$, $|\xi_*| < \infty$), and satisfies

$$\lim_{\xi\to\xi_*-0} \phi(\xi) = 0 \quad \text{and} \quad \lim_{\xi\to\xi_*-0} |\psi(\xi)| = \infty.$$

(II) the function $\phi(\xi)$ is a solution of (2.1.2) on a semi-infinite interval $(\xi_*, +\infty)$ ($\phi(\xi) \in C^2(\xi_*,+\infty) \cap C^0[\xi_*,+\infty)$, $|\xi_*| < \infty$), and satisfies

$$\lim_{\xi\to\xi_*+0} \phi(\xi) = 0 \quad \text{and} \quad \lim_{\xi\to\xi_*+0} |\psi(\xi)| = \infty.$$

(III) the function $\phi(\xi)$ is a solution of (2.1.2) on a finite interval (ξ_-, ξ_+) ($\phi(\xi) \in C^2(\xi_-,\xi_+) \cap C^0[\xi_-,\xi_+]$, $-\infty < \xi_- < \xi_+ < +\infty$), and satisfies the followings

$$\begin{aligned} &\lim_{\xi\to\xi_+-0} \phi(\xi) = 0, \quad &&\lim_{\xi\to\xi_-+0} \phi(\xi) = 0, \\ &\lim_{\xi\to\xi_+-0} |\psi(\xi)| = \infty, \quad &&\lim_{\xi\to\xi_-+0} |\psi(\xi)| = \infty. \end{aligned}$$

Remark 2.1.1
The definition of quasi traveling wave (with quenching) implies that it satisfies (2.1.1) only on semi-infinite interval or finite interval. In this chapter, we do not discuss the behavior of the solutions of (2.1.3) after ψ becomes infinity. It is necessary that more detailed (and hard) analysis in order to study the solutions after quenching (outside of the interval on that $\phi(\xi)$ satisfies (2.1.2)), and so we leave it open here.

In this setting, Matsue [50] proved the following theorem.

Theorem 2.1.1 ([50], Theorem 4.21)
Assume that $\alpha > 1$ with $\alpha \in \mathbb{N}$. Then, the quasi traveling waves with quenching for (2.1.1) are, if exist, characterized by trajectories whose initial data are on the stable manifold of

an equilibrium at infinity $(\phi, \psi) = (0, +\infty)$ *of* (2.1.3)*. The quenching rates, namely, the extinction rate of* ϕ *and blow-up rate of* ψ*, are*

$$\begin{cases} \phi(\xi) \sim C(\xi_* - \xi)^{\frac{2\alpha}{2\alpha^2-\alpha+1}} \\ \psi(\xi) \sim C(\xi_* - \xi)^{\frac{1-\alpha}{2\alpha^2-\alpha+1}} \end{cases} \quad \text{as} \quad \xi \to \xi_*$$

with $|\xi_*| < \infty$ *and* $C \neq 0$*.*

The proof is given in [50].

Remark 2.1.2
We can obtain the equilibria at infinity (of (2.1.3)*) not only* $(\phi, \psi) = (0, +\infty)$ *but also other equilibria by applying the Poincaré compactification (see [50] and Sec. 2.2 for the details).*

We note that the existence of the quasi traveling waves has not been proved yet. In this chapter, we give the proof of the existence of them by considering the restricted case of $\alpha \in 2\mathbb{N}$. The proof is based on Poincaré compactification (that is also used to prove Theorem 2.1.1 in [50]) and basic theory of dynamical systems. We then state the main theorem of this chapter (see also Figure 2.1.1).

Theorem 2.1.2
Assume that $\alpha \in 2\mathbb{N}$*. Then, the equation* (2.1.1) *possesses a family of "quasi traveling waves with quenching on a finite interval". Moreover, each quasi traveling wave with quenching* $u(t, x) = 1 - \phi(\xi)$ *(which satisfies* (2.1.2) *on a finite interval* (ξ_-, ξ_+)*) satisfies the followings:*

- $$\begin{cases} \lim\limits_{\xi \to \xi_+ - 0} \phi(\xi) = 0, & \lim\limits_{\xi \to \xi_- + 0} \phi(\xi) = 0, \\ \lim\limits_{\xi \to \xi_+ - 0} \psi(\xi) = \infty, & \lim\limits_{\xi \to \xi_- + 0} \psi(\xi) = -\infty. \end{cases}$$
- $\phi(\xi) < 0$ *holds for* $\xi \in (\xi_-, \xi_+)$*.*
- *There exists a constant* $\xi_* \in (\xi_-, \xi_+)$ *such that the following holds:* $\psi(\xi) < 0$ *for* $\xi \in (\xi_-, \xi_*)$*,* $\psi(\xi_*) = 0$ *and* $\psi(\xi) > 0$ *for* $\xi \in (\xi_*, \xi_+)$*.*

In addition, quenching rates are

$$\begin{cases} \phi(\xi) \sim -C(\xi_+ - \xi)^{\frac{2}{\alpha+1}} \\ \psi(\xi) \sim C\,(\xi_+ - \xi)^{-\frac{\alpha-1}{\alpha+1}} \end{cases} \quad \text{as} \quad \xi \to \xi_+ - 0$$

and

$$\begin{cases} \phi(\xi) \sim -C(\xi - \xi_-)^{\frac{2}{\alpha+1}} \\ \psi(\xi) \sim -C\,(\xi - \xi_-)^{-\frac{\alpha-1}{\alpha+1}} \end{cases} \quad \text{as} \quad \xi \to \xi_- + 0 \tag{2.1.4}$$

with $C > 0$*.*

In order to prove Theorem 2.1.2, it is necessary to seek a family of orbits that connect $(\phi, \psi) = (0, -\infty)$ and $(0, +\infty)$ of (2.1.3) (see Sec. 2.3 for the details). As shown in [14], [50], the Poincaré compactification is useful, and applicable for this problem. Asymptotic behaviors for both $\phi(\xi)$ and $\psi(\xi)$ that are more accurate than in [31] were obtained after publication of the paper. Note that this was obtained by refining the asymptotic form, as will be discussed later in the proof.

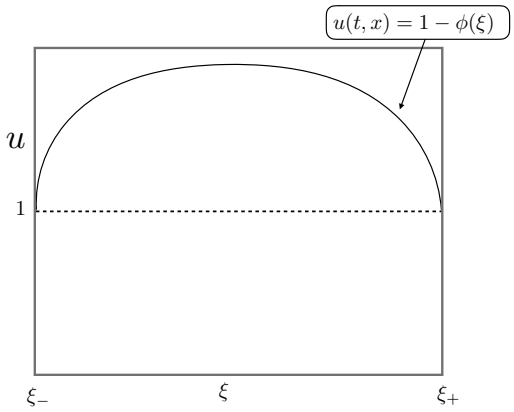

Figure 2.1.1: Schematic picture of the quasi traveling wave with quenching on $\xi \in [\xi_-, \xi_+]$ obtained in Theorem 2.1.2.

2.2 Dynamics on the Poincaré disk of (2.1.3)

In order to study the dynamics of (2.1.3) on the Poincaré disk, we desingularize it by the time-scale desingularization

$$ds/d\xi = \{\phi(\xi)\}^{-\alpha} \quad \text{for} \quad \alpha \in 2\mathbb{N}. \tag{2.2.1}$$

Since we assume that α is even, the direction of the time does not change via this desingularization. Then we have

$$\left\{ \begin{array}{l} \dot{\phi} = \phi^\alpha \psi, \\ \dot{\psi} = -c\phi^\alpha \psi + 1. \end{array} \right. \qquad \left(\cdot = \frac{d}{ds} \right). \tag{2.2.2}$$

It should be noted that the time scale desingularization (2.2.1) is simply multiplying the vector field by ϕ^α. Then, with excepting the singularity $\{\phi = 0\}$, the solution curves of the system (vector field) remain the same but are parameterized differently. Still, we refer to Section 7.7 of [44] and references therein for the analytical treatments of desingularization with the time rescaling. In what follows, we use the similar time rescaling (re-parameterization of the solution curves) repeatedly to desingularize the vector fields.

Now we can consider the dynamics of (2.2.2) on the charts $\overline{U}_j$ and $\overline{V}_j$.

2.2.1 Dynamics on the chart $\overline{U}_2$

To obtain the dynamics on the chart $\overline{U}_2$, we introduce coordinates (λ, x) by the formulas

$$\phi(s) = x(s)/\lambda(s), \quad \psi(s) = 1/\lambda(s).$$

Then we have

$$\left\{ \begin{array}{l} \dot{\lambda} = cx^\alpha \lambda^{1-\alpha} - \lambda^2, \\ \dot{x} = x(cx^\alpha \lambda^{-\alpha} - \lambda) + x^\alpha \lambda^{-\alpha}. \end{array} \right.$$

Time-scale desingularization $d\tau/ds = \lambda(s)^{-\alpha}$ yields

$$\left\{ \begin{array}{l} \lambda_\tau = cx^\alpha \lambda - \lambda^{2+\alpha}, \\ x_\tau = cx^{\alpha+1} - \lambda^{1+\alpha} x + x^\alpha, \end{array} \right. \tag{2.2.3}$$

where $\lambda_\tau = d\lambda/d\tau$ and $x_\tau = dx/d\tau$. The system (2.2.3) has the equilibria

$$p_0^+ : (\lambda, x) = (0, 0) \quad \text{and} \quad p_c : (\lambda, x) = (0, -1/c).$$

The Jacobian matrices at these equilibria are

$$p_0^+ : \begin{pmatrix} 0 & 0 \\ 0 & 0 \end{pmatrix} \quad \text{and} \quad p_c : \begin{pmatrix} c^{1-\alpha} & 0 \\ 0 & c^{1-\alpha} \end{pmatrix}.$$

Therefore, p_c is a source, and p_0^+ is not hyperbolic. In order to determine the dynamics near p_0^+, we desingularize p_0^+ by introducing the following blow-up coordinates:

$$\lambda = r^{\alpha-1}\bar{\lambda}, \quad x = r^{\alpha+1}\bar{x}$$

(see Section 1.2 of this thesis and Section 3 of [14] for the desingularizations of vector fields by the blow-up). Since we are interested in the dynamics on the Poincaré disk, we consider the dynamics of blow-up vector fields on the charts $\{\bar{\lambda} = 1\}$ and $\{\bar{x} = \pm 1\}$.

Dynamics on the chart $\{\bar{\lambda} = 1\}$

By the change of coordinates $\lambda = r^{\alpha-1}$, $x = r^{\alpha+1}\bar{x}$, we have

$$\begin{cases} r_\tau = \dfrac{r}{\alpha - 1}\left(c\bar{x}^\alpha r^{\alpha(\alpha+1)} - r^{\alpha^2-1}\right), \\ \bar{x}_\tau = \dfrac{2}{\alpha - 1}\left(\bar{x} r^{\alpha^2-1} - c\bar{x}^{\alpha+1} r^{\alpha(\alpha+1)}\right) + \bar{x}^\alpha r^{\alpha^2-1}. \end{cases}$$

The time-rescaling $d\eta/d\tau = r(\tau)^{\alpha^2-1}$ yields

$$\begin{cases} r_\eta = (\alpha - 1)^{-1}\left(-r + c\bar{x}^\alpha r^{2+\alpha}\right), \\ \bar{x}_\eta = 2(\alpha - 1)^{-1}\left(\bar{x} - c\bar{x}^{\alpha+1} r^{\alpha+1}\right) + \bar{x}^\alpha. \end{cases} \tag{2.2.4}$$

The equilibria of (2.2.4) on $\{r = 0\}$ are

$$\bar{p}_0^+ : (r, \bar{x}) = (0, 0), \quad \bar{p}_\alpha^+ : (r, \bar{x}) = \left(0, \left(\frac{-2}{\alpha - 1}\right)^{\frac{1}{\alpha-1}}\right).$$

The Jacobian matrices at these equilibria are

$$\bar{p}_0^+ : \begin{pmatrix} -\dfrac{1}{\alpha - 1} & 0 \\ 0 & \dfrac{2}{\alpha - 1} \end{pmatrix} \quad \text{and} \quad \bar{p}_\alpha^+ : \begin{pmatrix} -\dfrac{1}{\alpha - 1} & 0 \\ 0 & -2 \end{pmatrix}.$$

Moreover, since $|1/(\alpha - 1)| < 2$ holds, trajectories near $\bar{p}_\alpha^+$ are tangent to $\{\bar{x} = [-2/(\alpha - 1)]^{\frac{1}{\alpha-1}}, r \geq 0\}$ as $\eta \to +\infty$. The solutions are approximated as

$$\begin{cases} r(\eta) \sim C_1 e^{-\frac{1}{\alpha-1}\eta}(1 + o(1)), \\ \bar{x}(\eta) - A \sim C_2 e^{-2\eta}(1 + o(1)), \end{cases} \qquad A := \left(-\frac{2}{\alpha - 1}\right)^{\frac{1}{\alpha-1}}.$$

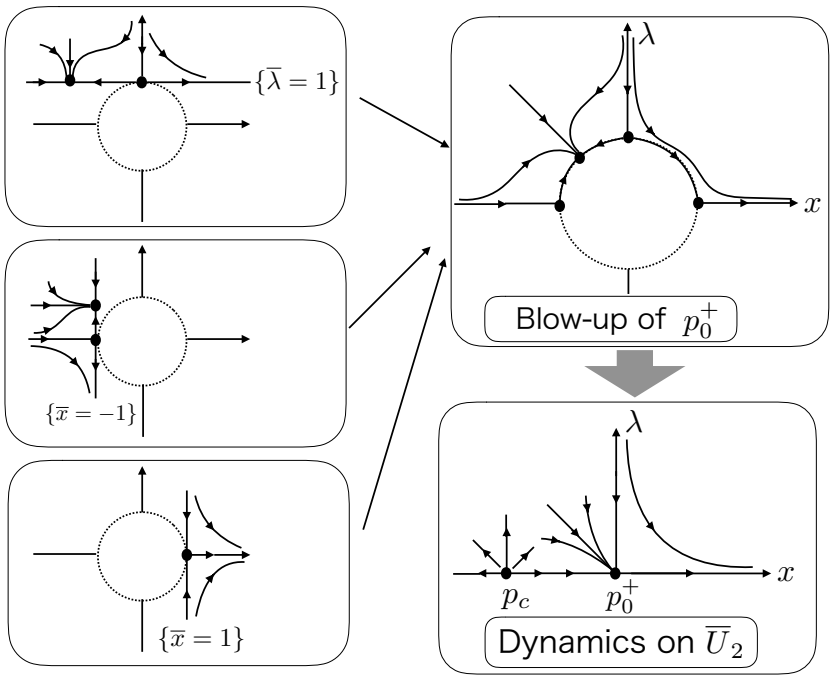

Figure 2.2.1: Schematic pictures of the dynamics of the blow-up vector fields and $\overline{U}_2$.

Dynamics on the chart $\{\bar{x}=-1\}$

By the change of coordinates $\lambda = r^{\alpha-1}\bar{\lambda}$, $x = -r^{\alpha+1}$, and time-rescaling $d\eta/d\tau = r(\tau)^{\alpha^2-1}$, we have

$$\begin{cases} r_\eta = (\alpha+1)^{-1}\left(cr^{\alpha+2} - r\bar{\lambda}^{1+\alpha} - r\right), \\ \bar{\lambda}_\eta = -(\alpha+1)^{-1}\left(2\bar{\lambda}^{2+\alpha} - (\alpha-1)\bar{\lambda} - 2cr^{\alpha+1}\bar{\lambda}\right). \end{cases}$$

The equilibria on $\{r=0\}$ are

$$(r,\bar{\lambda}) = (0,0), \quad (r,\bar{\lambda}) = \left(0, [(\alpha-1)/2]^{\frac{1}{\alpha+1}}\right).$$

By the further computations, we can see that $(0,0)$ is a saddle, and $(0,[(\alpha-1)/2]^{\frac{1}{\alpha+1}})$ is a sink.

Dynamics on the chart $\{\bar{x}=1\}$

The change of coordinates $\lambda = r^{\alpha-1}\bar{\lambda}$, $\quad x = r^{\alpha+1}$, and time-rescaling $d\eta/d\tau = r(\tau)^{\alpha^2-1}$ yield

$$\begin{cases} r_\eta = (\alpha+1)^{-1}\left(cr^{\alpha+2} - r\bar{\lambda}^{1+\alpha} + r\right), \\ \bar{\lambda}_\eta = -(\alpha+1)^{-1}\left(2\bar{\lambda}^{2+\alpha} + (\alpha-1)\bar{\lambda} - 2cr^{\alpha+1}\bar{\lambda}\right). \end{cases}$$

The equilibrium on $\{r=0, \bar{\lambda}\geq 0\}$ is $(0,0)$. The linearized eigenvalues are $(\alpha+1)^{-1}$ and $-(\alpha-1)/(\alpha+1)$ with corresponding eigenvectors $(1,0)$ and $(0,1)$, respectively. Therefore, $(r,\bar{\lambda}) = (0,0)$ on the chart $\{\bar{x}=1\}$ is a saddle.

Combining the dynamics on the charts $\{\bar{\lambda}=1\}$ and $\{\bar{x}=\pm 1\}$, we obtain the dynamics on $\overline{U}_2$ (see Figure 2.2.1).

Still, we continue to study the dynamics on other charts in order to obtain the whole dynamics on the Poincaré disk.

2.2.2 Dynamics on the chart $\overline{V}_2$

The change of coordinates

$$\phi(s) = -x(s)/\lambda(s), \quad \psi(s) = -1/\lambda(s)$$

give the projected dynamics of (2.1.3) on the chart $\overline{V}_2$:

$$\begin{cases} \lambda_\tau = cx^\alpha\lambda + \lambda^{2+\alpha}, \\ x_\tau = x^\alpha + cx^{\alpha+1} + \lambda^{1+\alpha}x, \end{cases} \tag{2.2.5}$$

where τ is the new time introduced by $d\tau/ds = \lambda(s)^{-\alpha}$. The system (2.2.5) can be transformed into (2.2.3) by the change of coordinates $(\lambda, x) \mapsto (-\lambda, x)$. Therefore, it is sufficient to consider the blow-up of singularity $p_0^- : (\lambda, x) = (0, 0)$ by the formulas

$$\lambda = r^{\alpha-1}\bar{\lambda}, \quad x = r^{\alpha+1}\bar{x} \quad \text{with} \quad \bar{\lambda} = 1.$$

Then we have

$$\begin{cases} r_\eta = (\alpha-1)^{-1}\left(r + c\bar{x}^\alpha r^{\alpha+2}\right), \\ \bar{x}_\eta = \bar{x}^\alpha - 2(\alpha-1)^{-1}\left(\bar{x} + c\bar{x}^{\alpha+1}r^{\alpha+1}\right), \end{cases} \tag{2.2.6}$$

where η satisfies $d\eta/d\tau = \{r(\tau)\}^{\alpha^2-1}$. The equilibria of (2.2.6) on $\{r = 0\}$ are

$$\bar{p}_0^- : (r, \bar{x}) = (0, 0), \quad \bar{p}_\alpha^- : (r, \bar{x}) = \left(0, \left(\frac{2}{\alpha-1}\right)^{\frac{1}{\alpha-1}}\right).$$

The equilibrium $\bar{p}_0^-$ is a saddle with the eigenvalues $(\alpha-1)^{-1}$ and $-2(\alpha-1)^{-1}$ whose corresponding eigenvectors are $(1, 0)$ and $(0, 1)$, respectively. Further, $\bar{p}_\alpha^-$ is a source with the eigenvalues $(\alpha-1)^{-1}$ and 2 whose corresponding eigenvectors are $(1, 0)$ and $(0, 1)$, respectively.

2.2.3 Dynamics on the chart $\overline{U}_1$

Let us study the dynamics on the chart $\overline{U}_1$. The transformations

$$\phi(s) = 1/\lambda(s), \quad \psi(s) = x(s)/\lambda(s)$$

yield

$$\begin{cases} \lambda_\tau = -x\lambda, \\ x_\tau = -cx + \lambda^{1+\alpha} - x^2 \end{cases} \tag{2.2.7}$$

via time-rescaling $d\tau/ds = \{\lambda(s)\}^{-\alpha}$. The equilibria of (2.2.7) are $(0, 0)$ and $(0, -c)$ whose Jacobian matrices are

$$\begin{pmatrix} 0 & 0 \\ 0 & -c \end{pmatrix} \quad \text{and} \quad \begin{pmatrix} c & 0 \\ 0 & c \end{pmatrix},$$

respectively. Then the center manifold theory is applicable to study the dynamics near $(0, 0)$ (for instance, see [9]). It implies that there exists a function $h(\lambda)$ satisfying

$$h(0) = \frac{dh}{d\lambda}(0) = 0$$

such that the center manifold of (2.2.7) is represented as $\{(\lambda, x) \,|\, x = h(\lambda)\}$ near $(0, 0)$. Differentiating it with respect to τ, we have

$$-\lambda h(\lambda)\frac{dh}{d\lambda}(\lambda) = -ch(\lambda) + \lambda^{1+\alpha} - \{h(\lambda)\}^2.$$

Then we can obtain the approximation of the (graph of) center manifold as follows:

$$\left\{(\lambda, x) \,|\, x = \lambda^{\alpha+1}/c + O\left(\lambda^{2\alpha+2}\right)\right\}.$$

Therefore, the dynamics of (2.2.7) near $(0,0)$ is topologically equivalent to the dynamics of the following equation:

$$\lambda_\tau = -\lambda^{\alpha+2}/c + O(\lambda^{2\alpha+3}).$$

These results give us the dynamics on the chart $\overline{U}_1$.

2.2.4 Dynamics on the chart $\overline{V}_1$

The transformations

$$\phi(s) = -1/\lambda(s), \quad \psi(s) = -x(s)/\lambda(s)$$

yield

$$\begin{cases} \lambda_\tau = -x\lambda, \\ x_\tau = -cx - \lambda^{1+\alpha} - x^2 \end{cases} \tag{2.2.8}$$

via time-rescaling $d\tau/ds = \{\lambda(s)\}^{-\alpha}$. We can see that the system (2.2.8) can be transformed into the system (2.2.7) by the change of variables: $(\lambda, x) \mapsto (-\lambda, x)$. Therefore, the dynamics of (2.2.8) is equivalent to the reflected one of (2.2.7) with respect to $\{\lambda = 0\}$.

2.3 Proof of Theorem 2.1.2

Since the point $(y_1, y_2, y_3) = (0, 1, 0)$ on the Poincaré disk corresponds to p_0^+, we denote it by p_0^+ as well. Similarly, we denote by p_0^- the point $(y_1, y_2, y_3) = (0, -1, 0)$. In order to prove Theorem 2.1.2, it is necessary to find the orbits that connect p_0^- and p_0^+ on the Poincaré disk. The phase portrait on the Poincaré disk of (2.1.3) is shown in Figure 2.3.1 for the convenience of readers.

Proof. (I) : For a given compact subset $W \subset H_+$, there are no equilibria or closed orbits in W. Therefore, by the Poincaré-Bendixson theorem, any trajectories starting from the points in W can not stay in W with increasing s. This implies that the trajectories in H_+ go to $\mathbb{S}^1$, which corresponds to $\{\|(\phi, \psi)\| = \infty\}$.
(II): The line $\{\phi = 0\}$ is invariant under the flow of (2.2.2). Therefore, any trajectories start from the points in $\{y \in H_+ \,|\, y_1 < 0\}$ can not go to $\{y \in H_+ \,|\, y_1 > 0\}$.
(III): Let $\overline{\mathcal{W}}^s_{\bar{p}^+_\alpha}$ be a stable manifold of $\bar{p}^+_\alpha$ (which is the equilibrium of the system (2.2.4)). We denote by $\mathcal{W}^s(\bar{p}^+_\alpha)$ the stable set, which corresponds to $\overline{\mathcal{W}}^s_{\bar{p}^+_\alpha}$ on the blow-up vector filed (2.2.4), of the equilibrium p_0^+ of (2.2.3). Similarly, we denote by $\mathcal{W}^u(\bar{p}^-_\alpha)$ the unstable set of p_0^-, corresponding to the unstable manifold of $\bar{p}^-_\alpha$ on the blow-up vector field (2.2.6). Consider the trajectories start from the points on $\mathcal{W}^u(\bar{p}^-_\alpha) \subset \{y \in H_+ \,|\, y_1 < 0\}$. The trajectories can not stay in any compact subset on H_+, and can not go to $\{y \in H_+ \,|\, y_1 > 0\}$, therefore, they go to p_0^+ with lying on $\mathcal{W}^s(\bar{p}^+_\alpha)$. This implies that the system (2.2.2) possesses the orbits that connect p_0^- and p_0^+ on the Poincaré disk. It is easy to see that $d\phi/d\psi$ takes the same values on the vector fields defined by (2.2.2) and (2.1.3) by excepting the singularity $\{\phi = 0\}$. Thus, there are orbits connecting $(\phi, \psi) = (0, -\infty)$ and $(0, +\infty)$ on the original vector field (2.1.3).

(IV): As shown in [50], we can obtain the quenching rates of $\phi(\xi)$ and $\psi(\xi)$. Indeed,

$$\begin{aligned}
\frac{d\eta}{d\xi} &= \frac{ds}{d\xi}\cdot\frac{d\tau}{ds}\cdot\frac{d\eta}{d\tau}\\
&= \phi^{-\alpha}\cdot\lambda^{-\alpha}\cdot r^{\alpha^2-1}\\
&= r^{-\alpha-1}\cdot\bar{x}^{-\alpha}\\
&\sim \left\{C_1e^{-\frac{1}{\alpha-1}\eta}(1+o(1))\right\}^{-\alpha-1}\cdot\left\{C_2e^{-2\eta}(1+o(1))+A\right\}^{-\alpha}\\
&\sim C_3e^{\frac{\alpha+1}{\alpha-1}\eta}\cdot\left\{C_2e^{-2\eta}(1+o(1))+A\right\}^{-\alpha}\\
&= C_3e^{\frac{\alpha+1}{\alpha-1}\eta}\cdot\frac{1}{\{C_2e^{-2\eta}(1+o(1))+A\}^{\alpha}}\\
&= C_3e^{\frac{\alpha+1}{\alpha-1}\eta}\cdot\frac{1}{\{C_2e^{-2\eta}(1+o(1))\}^{\alpha}+\alpha\{C_2e^{-2\eta}(1+o(1))\}^{\alpha-1}\cdot A+\cdots+A^{\alpha}}\\
&\sim Ce^{\frac{\alpha+1}{\alpha-1}\eta}\quad\text{as}\quad\eta\to+\infty
\end{aligned}$$

holds with constants C and C_j. Note that this argument is a refinement of [31]. Here, " $f(x)\sim g(x)$ as $x\to a$" means that $f(x)-g(x)=o(g(x))$ as $x\to a$, equivalently,

$$\lim_{x\to a}\left|\frac{f(x)}{g(x)}\right|=1.$$

This yields

$$\xi(\eta)=Ce^{-\frac{\alpha+1}{\alpha-1}\eta}+\tilde{C},\quad(\tilde{C}\in\mathbb{R}).$$

Set $\xi_+=\lim_{\eta\to+\infty}\xi(\eta)$, then we have

$$\xi_+=C\int_0^{+\infty}e^{-\frac{\alpha+1}{\alpha-1}\eta}\,d\eta<\infty.$$

Therefore,

$$\xi_+-\xi\sim C\,e^{-\frac{\alpha+1}{\alpha-1}\eta}$$

holds. Finally, we obtain

$$\begin{aligned}
\phi(\xi)=\frac{x}{\lambda}&=\frac{r^{\alpha+1}}{r^{\alpha-1}}\overline{x}=r^2\overline{x}\\
&\sim\left\{C_1e^{-\frac{1}{\alpha-1}\eta}(1+o(1))\right\}^{2}\cdot\left\{C_2e^{-2\eta}(1+o(1))+A\right\}\\
&\sim C_4e^{-\frac{2}{\alpha-1}\eta}\cdot\left\{C_2e^{-2\eta}(1+o(1))+A\right\}\\
&= C_5e^{-\frac{2}{\alpha-1}\eta}e^{-2\eta}+C_4\cdot A\cdot e^{-\frac{2}{\alpha-1}\eta}\\
&= C_5e^{-\frac{2\alpha}{\alpha-1}\eta}+C_4\cdot A\cdot e^{-\frac{2}{\alpha-1}\eta}\\
&\sim -Ce^{-\frac{2}{\alpha-1}\eta}.
\end{aligned}$$

Here, in last relation, since $e^{-\frac{2\alpha}{\alpha-1}\eta}<e^{-\frac{2}{\alpha-1}\eta}$ $(\eta>0)$ is satisfied by $-2\alpha/(\alpha-1)<-2/(\alpha-1)$, we choose the term with the greater influence when $\eta\to+\infty$. Therefore, we have

$$\phi(\xi)\sim -Ce^{-\frac{2}{\alpha-1}\eta}\sim -C(\xi_+-\xi)^{\frac{2}{\alpha+1}}\quad(\xi\to\xi_+-0).$$

Since the trajectories are lying on $\{a<0\}$, it holds that $C>0$. Similarly, we can obtain the quenching rates for $\psi(\xi)$ as $\xi\to\xi_+$ and (2.1.4).

This completes the proof. □

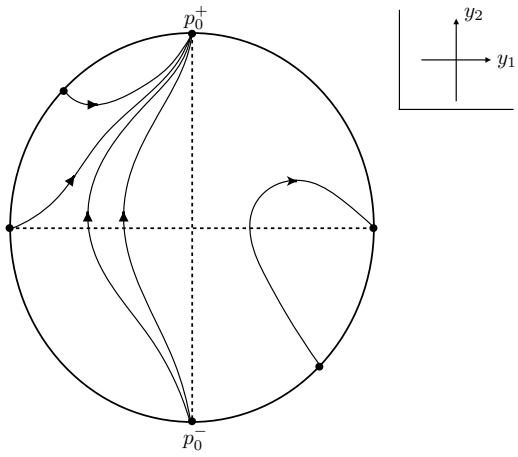

Figure 2.3.1: Compactification of the system (2.1.3).

2.4 Conclusions and Remarks

In this chapter, we studied whole dynamics of (2.1.3) on the phase space $\mathbb{R}^2 \cup \{(\phi, \psi) \mid \|(\phi, \psi)\| = +\infty\}$, the existence of quasi traveling waves with quenching, and their quenching rates on a finite interval (ξ_-, ξ_+) $(-\infty < \xi_- < \xi_+ < +\infty)$ of (2.1.1) by applying the Poincaré compactification and dynamical system approach.

From the viewpoint of theory of partial differential equations, it should be considered that how can we formulate the solutions of (2.1.1) obtained in Theorem 2.1.2. Namely, it is necessary to construct the entire solution. As discussed previously, we do not discuss the behavior of the solutions of (2.1.3) after ψ becomes infinity since our interest in this chapter is to study the solutions of (2.1.1) from the dynamical system view point. It is necessary that more detailed (and hard) analysis in order to study the solutions after quenching (outside of the interval on that $\phi(\xi)$ satisfies (2.1.2)), and so we leave it open here. Further, It should be noted that the mathematical formulation of the solution (in weak sense) could be obtained by considering a suitable function space as shown in [51] (it will be addressed in future works as well).

In addition, since the theory of blow-up (desingularization of the vector field) is not applicable for the non-polynomial vector fields, we cannot deal with the general case that $\alpha \in \mathbb{R}$. Hence, we leave it open here.

Chapter 3

Traveling waves with singularities in a damped hyperbolic MEMS type equation in the presence of negative powers nonlinearity

Abstract

Traveling waves with singularities in a damped hyperbolic MEMS type equation in the presence of negative powers nonlinearity are considered. The purpose of this chapter is to investigate how the existence of the traveling waves, their shapes, and asymptotic behavior change with the presence or absence of an inertial term. These are studied by applying the framework that combines Poincaré compactification, classical dynamical systems theory, and geometric methods for the desingularization of vector fields. These allow us to classify all traveling waves and their properties since we know all the solution trajectories of the equations they satisfy, including those to infinity. We report that the presence of this term causes the shapes to change significantly for sufficiently large wave speeds. This chapter is based on the following published paper ([37]):

> Ichida, Y.: Traveling waves with singularities in a damped hyperbolic MEMS type equation in the presence of negative powers nonlinearity, Electron. J. Differ. Equ., **2023**, 1–20 (2023).

3.1 Introduction

In this chapter, we consider the following damped hyperbolic MEMS type equation with negative powers nonlinearity

$$\varepsilon^2 u_{tt} + u_t = u_{xx} + (1-u)^{-\alpha}, \quad t > 0, \quad x \in \mathbb{R}, \tag{3.1.1}$$

where $\alpha \in 2\mathbb{N}$ and $\varepsilon > 0$. Here, ε is a small constant and the ratio of the interaction due to the inertial and damped terms (see [15, 23, 24, 25] and references therein).

The equation (3.1.1) is based on the equation

$$u_t = u_{xx} + (1-u)^{-\alpha}, \quad t > 0, \quad x \in \mathbb{R}, \quad \alpha \in \mathbb{N} \tag{3.1.2}$$

treated in [31, 50], with the term $\varepsilon^2 u_{tt}$ added to the left-hand side. (3.1.1) is a type of partial differential equation commonly referred to as a damped hyperbolic equation. Since

(3.1.1) has aspects of both parabolic and hyperbolic types, it has recently attracted attention from the viewpoint of partial differential equation theory (see [23, 18]). Guo [23] considers both parabolic and hyperbolic type problem about MEMS, and provides some quenching criteria. For MEMS, see below. In addition, it discusses the global existence of solutions. The previous work [18] is concerned with the behavior of the solutions to the nonlinear damped hyperbolic Allen-Cahn equation with appropriate boundary conditions and initial data in a bounded domain. They argue that reaction-diffusion equations have the lack of inertial and others. There are many ways to overcome these unphysical properties; one of them is to consider hyperbolic reaction-diffusion equations.

Furthermore, (3.1.1) and (3.1.2) are special cases of the generalized MEMS type partial differential equation (see [15, 24, 35] and references therein). The MEMS model is the Micro-Electro Mechanical System devices and used in many machines around us (for instance, see [68]). In general, the MEMS model is known to induce the touchdown phenomenon (mathematically, quenching). Clarification of the structure of singularity formation, such as quench, is one of the most important issues in MEMS type equations, and there have been a lot of studies recently. However, since the nonlinear terms of MEMS equations are not simple, then they have both hyperbolic and parabolic aspects, it is not fully understood what kind of typical solutions exist.

In this chapter, we investigate how the behavior (shapes and asymptotic behavior) of traveling waves change depending on whether the $\varepsilon^2 u_{tt}$ term is present or absent in the left-hand side of [31]. More precisely, in the traveling wave framework, we compare the family of functions satisfying (3.1.1) with the family of functions satisfying (3.1.2) revealed in [31] in terms of the asymptotic behavior and shapes. The reason why we refer to the traveling waves as families of functions satisfying the equations is that they cause singularities at the endpoints of finite intervals despite the equations being defined over the whole domain, which makes subsequent analysis difficult (see [31]). In addition, we are interested in whether the asymptotic behavior obtained from (3.1.1) and that from (3.1.2) coincide as $\varepsilon \to 0$. Although it appears to be nothing more than adding $\varepsilon^2 u_{tt}$ to the left-hand side of (3.1.2), this extension allows us to obtain conclusions from the perspective of traveling waves that cannot be obtained in [31]. To the best of the author's knowledge, there has been no analysis of the existence, shapes and asymptotic behavior of traveling waves in such a type of equation with both hyperbolic and parabolic forms. We believe that this chapter will provide this abundant information through a dynamical systems approach and give a new perspective on these types of equations.

In order to consider the traveling waves of (3.1.1), we introduce the following change of variables:

$$\phi(\xi) = 1 - u(t,x), \quad \xi = x - ct, \quad 0 < c \in \mathbb{R}.$$

The equation of $\phi(\xi)$ solving (3.1.1) is then reduced to

$$(1-\varepsilon^2 c^2)\phi'' = -c\phi' + \phi^{-\alpha}, \quad \left(' = \frac{d}{d\xi}\right). \tag{3.1.3}$$

The equation with $\varepsilon = 0$ in (3.1.3) is discussed in [31]. In (3.1.3), there is a case classification for $1-\varepsilon^2 c^2$ that did not appear in [31].

When $1-\varepsilon^2 c^2 = 0$, i.e., $c = 1/\varepsilon$, the following differential equation is obtained from (3.1.3):

$$0 = -c\phi' + \phi^{-\alpha}.$$

This can be solved as follows:

$$\phi(\xi) = \left(\frac{\alpha+1}{c}\xi + B\right)^{\frac{1}{\alpha+1}} \tag{3.1.4}$$

with a constant $B \in \mathbb{R}$. In other words, we can express $\phi(\xi)$ explicitly in this case. For a discussion of this case, see Remark 3.2.4.

Hereinafter referred to as $1 - \varepsilon^2 c^2 \neq 0$. Then, (3.1.3) is equivalent to

$$\begin{cases} \phi' = \psi, \\ \psi' = (1 - \varepsilon^2 c^2)^{-1}(-c\psi + \phi^{-\alpha}). \end{cases} \tag{3.1.5}$$

In (3.1.5), the dynamics to infinity in the equation with $\varepsilon = 0$ has been studied in [31, 33]. In [33], although the partial differential equations are different, the ordinary differential equations (ODEs for short) derived from them include the ODEs of [31]. As can be seen from these previous studies, (3.1.5) is not easy to analyze. However, as shown in [31, 33, 49, 50], it is possible to study the dynamics of this ODE to infinity in the framework that combines Poincaré compactification (for instance, see Section 1.1 in this thesis and [14, 49, 50] for the details of it), classical dynamical systems theory, and geometric methods for desingularization of vector fields (see Section 1.2 in this thesis and Section 3 of [14] and references therein). By using these methods, the whole dynamics on the phase space $\mathbb{R}^2$ including infinity (denoted by Poincaré disk) generated by the two-dimensional differential equation (3.1.5) is obtained. In other words, from these dynamics, we expect to categorize all traveling waves as in these previous studies. Furthermore, the strength of the analysis in this framework is that the existence of connecting orbits in dynamical systems including infinity not only proves the existence of these traveling waves, provides information about their shapes but allows us to study their asymptotic behavior.

This chapter is organized as follows. In the next section, we reproduce the terminology defined in [31] and the main results obtained, and state the main results of this chapter. In Section 3.3, we obtain the dynamics of (3.1.5) on the Poincaré disk via Poincaré compactification and basic theory of the dynamical systems. The proof of Theorems will be completed in Section 3.4. Section 3.5 is devoted to the concluding remarks.

3.2 Known and Main results

Before we state the main results of this chapter, we reproduce the following definitions of quasi traveling waves and quasi traveling waves with quenching. The reason for this is that the main result in this chapter will be compared later with that in [31] (see Proposition 3.2.1 and Theorem 3.2.1). Here, quenching in ODE (3.1.5) roughly means that the following holds

$$\phi(\xi) \to 0, \quad |\phi'(\xi)| \to +\infty, \quad \text{as} \quad \xi \to |\xi_*|$$

with $|\xi_*| < +\infty$.

Definition 3.2.1 (Definition 2.1.2 (Definition 2, [31]))
We say that a function $u(t,x) \equiv 1 - \phi(\xi)$ is a quasi traveling wave of (3.1.2) if the function $\phi(\xi)$ is a solution of (3.1.3) with $\varepsilon = 0$ on a finite interval or semi-infinite interval.

Definition 3.2.2 (Definition 2.1.3 (Definition 3, [31]))
We say that a function $u(t,x) \equiv 1 - \phi(\xi)$ is a quasi traveling wave with quenching of (3.1.2) if the function $u(t,x)$ is a quasi traveling wave of (3.1.2) on a finite interval (resp. semi-infinite interval) such that ϕ reaches 0 and $|\phi'|$ becomes infinite at both ends of the interval (resp. finite end point of the semi-infinite interval). More precisely, we have the following three cases:

(I) The function $\phi(\xi)$ is a solution of (3.1.3) *with $\varepsilon = 0$ on a semi-infinite interval $(-\infty, \xi_*)$ ($\phi(\xi) \in C^2(-\infty, \xi_*) \cap C^0(-\infty, \xi_*]$, $|\xi_*| < \infty$), and satisfies*

$$\lim_{\xi \to \xi_* - 0} \phi(\xi) = 0 \quad \text{and} \quad \lim_{\xi \to \xi_* - 0} |\psi(\xi)| = \infty.$$

(II) The function $\phi(\xi)$ is a solution of (3.1.3) *with $\varepsilon = 0$ on a semi-infinite interval $(\xi_*, +\infty)$ ($\phi(\xi) \in C^2(\xi_*, +\infty) \cap C^0[\xi_*, +\infty)$, $|\xi_*| < \infty$), and satisfies*

$$\lim_{\xi \to \xi_* + 0} \phi(\xi) = 0 \quad \text{and} \quad \lim_{\xi \to \xi_* + 0} |\psi(\xi)| = \infty.$$

(III) The function $\phi(\xi)$ is a solution of (3.1.3) *with $\varepsilon = 0$ on a finite interval (ξ_-, ξ_+) ($\phi(\xi) \in C^2(\xi_-, \xi_+) \cap C^0[\xi_-, \xi_+]$, $-\infty < \xi_- < \xi_+ < +\infty$), and satisfies the followings*

$$\begin{array}{ll} \lim_{\xi \to \xi_+ - 0} \phi(\xi) = 0, & \lim_{\xi \to \xi_- + 0} \phi(\xi) = 0, \\ \lim_{\xi \to \xi_+ - 0} |\psi(\xi)| = \infty, & \lim_{\xi \to \xi_- + 0} |\psi(\xi)| = \infty. \end{array}$$

With these definitions, we review the results obtained in [31]. Hereinafter, note that the meaning of the symbol $F(\eta) \sim G(\eta)$ as $\eta \to +\infty$ is as follows:

$$\lim_{\eta \to +\infty} \left| \frac{F(\eta)}{G(\eta)} \right| = 1.$$

Proposition 3.2.1 (Theorem 2.1.2 (Theorem 2, [31]))
Assume that $\alpha \in 2\mathbb{N}$. Then, the equation (3.1.2) *possesses a family of quasi traveling waves with quenching on a finite interval. Moreover, each quasi traveling wave with quenching $u(t, x) = 1 - \phi(\xi)$ satisfies the followings:*

- $\begin{cases} \lim_{\xi \to \xi_+ - 0} \phi(\xi) = 0, & \lim_{\xi \to \xi_- + 0} \phi(\xi) = 0, \\ \lim_{\xi \to \xi_+ - 0} \psi(\xi) = \infty, & \lim_{\xi \to \xi_- + 0} \psi(\xi) = -\infty. \end{cases}$
- *$\phi(\xi) < 0$ holds for $\xi \in (\xi_-, \xi_+)$.*
- *There exists a constant $\xi_* \in (\xi_-, \xi_+)$ such that the following holds: $\psi(\xi) < 0$ for $\xi \in (\xi_-, \xi_*)$, $\psi(\xi_*) = 0$ and $\psi(\xi) > 0$ for $\xi \in (\xi_*, \xi_+)$.*

In addition, the quenching rates are

$$\begin{cases} \phi(\xi) \sim -C(\xi_+ - \xi)^{\frac{2}{\alpha+1}} \\ \psi(\xi) \sim C\,(\xi_+ - \xi)^{-\frac{\alpha-1}{\alpha+1}} \end{cases} \quad \text{as} \quad \xi \to \xi_+ - 0 \tag{3.2.1}$$

and

$$\begin{cases} \phi(\xi) \sim -C(\xi - \xi_-)^{\frac{2}{\alpha+1}} \\ \psi(\xi) \sim -C\,(\xi - \xi_-)^{-\frac{\alpha-1}{\alpha+1}} \end{cases} \quad \text{as} \quad \xi \to \xi_- + 0 \tag{3.2.2}$$

with $C > 0$.

Remark 3.2.1
Note that the asymptotic behavior for (3.2.1) *and* (3.2.2) *in Proposition 3.2.1 differs in the exponential part from the asymptotic behavior obtained in Theorem 2 of [31] and Proposition 1 of [33]. The reason for this is that, after the publication of [31, 33], we chose more appropriate principal terms in the computational process of deriving the asymptotic*

behavior, which resulted in higher accuracy. This improvement is described in detail in Subsection 3.4.1. Furthermore, this improvement has already been introduced into [35], and the asymptotic behavior, which was previously difficult to derive, has been obtained. However, the underlying idea is similar to the previous ones.

Next, the main results of this chapter are described. Figure 3.2.1, Figure 3.2.2, and Figure 3.2.3 show the schematic pictures of traveling waves obtained by each theorem.

Theorem 3.2.1
Assume that $\alpha \in 2\mathbb{N}$, $\varepsilon > 0$, *and* $1 - \varepsilon^2 c^2 > 0$. *Then, for a given positive constant* $0 < c < 1/\varepsilon$, *there exists a family of the functions (which corresponds to a family of the orbits of* (3.1.5)*) defined on the finite intervals such that each function* $u(t, x)$ *satisfies equation* (3.1.1) *on a finite interval* (ξ_-, ξ_+) $(-\infty < \xi_- < \xi_+ < +\infty)$. *Moreover, each function* $u(t, x) \equiv 1 - \phi(\xi)$ *satisfies the following:*

- $\begin{cases} \lim\limits_{\xi \to \xi_+ - 0} \phi(\xi) = 0, & \lim\limits_{\xi \to \xi_- + 0} \phi(\xi) = 0, \\ \lim\limits_{\xi \to \xi_+ - 0} \psi(\xi) = \infty, & \lim\limits_{\xi \to \xi_- + 0} \psi(\xi) = -\infty. \end{cases}$
- $\phi(\xi) < 0$ *holds for* $\xi \in (\xi_-, \xi_+)$.
- *There exists a constant* $\xi_* \in (\xi_-, \xi_+)$ *such that the following holds:* $\psi(\xi) < 0$ *for* $\xi \in (\xi_-, \xi_*)$, $\psi(\xi_*) = 0$ *and* $\psi(\xi) > 0$ *for* $\xi \in (\xi_*, \xi_+)$.

In addition, the asymptotic behavior for $\xi \to \xi_+ - 0$ *and* $\xi \to \xi_- + 0$ *are same as* (3.2.1) *and* (3.2.2).

On the other hand, assume that $1 - \varepsilon^2 c^2 < 0$. *Then, for a given positive constant* $c > 1/\varepsilon$, *there exists a family of the functions (which corresponds to a family of the orbits of* (3.1.5)*) defined on the finite intervals such that each function* $u(t, x)$ *satisfies equation* (3.1.1) *on a finite interval* (ξ_-, ξ_+) $(-\infty < \xi_- < \xi_+ < +\infty)$. *Moreover, each function* $u(t, x) \equiv 1 - \phi(\xi)$ *satisfies the following:*

- $\begin{cases} \lim\limits_{\xi \to \xi_+ - 0} \phi(\xi) = 0, & \lim\limits_{\xi \to \xi_- + 0} \phi(\xi) = 0, \\ \lim\limits_{\xi \to \xi_+ - 0} \psi(\xi) = -\infty, & \lim\limits_{\xi \to \xi_- + 0} \psi(\xi) = +\infty. \end{cases}$
- $\phi(\xi) > 0$ *holds for* $\xi \in (\xi_-, \xi_+)$.
- *There exists a constant* $\xi_* \in (\xi_-, \xi_+)$ *such that the following holds:* $\psi(\xi) > 0$ *for* $\xi \in (\xi_-, \xi_*)$, $\psi(\xi_*) = 0$ *and* $\psi(\xi) < 0$ *for* $\xi \in (\xi_*, \xi_+)$.

In addition, the asymptotic behavior for $\xi \to \xi_+ - 0$ *and* $\xi \to \xi_- + 0$ *are*

$$\begin{cases} \phi(\xi) \sim C(\xi_+ - \xi)^{\frac{2}{\alpha+1}} \\ \psi(\xi) \sim -C\,(\xi_+ - \xi)^{-\frac{\alpha-1}{\alpha+1}} \end{cases} \quad \text{as} \quad \xi \to \xi_+ - 0 \tag{3.2.3}$$

and

$$\begin{cases} \phi(\xi) \sim C(\xi - \xi_-)^{\frac{2}{\alpha+1}} \\ \psi(\xi) \sim C\,(\xi - \xi_-)^{-\frac{\alpha-1}{\alpha+1}} \end{cases} \quad \text{as} \quad \xi \to \xi_- + 0 \tag{3.2.4}$$

with $C > 0$.

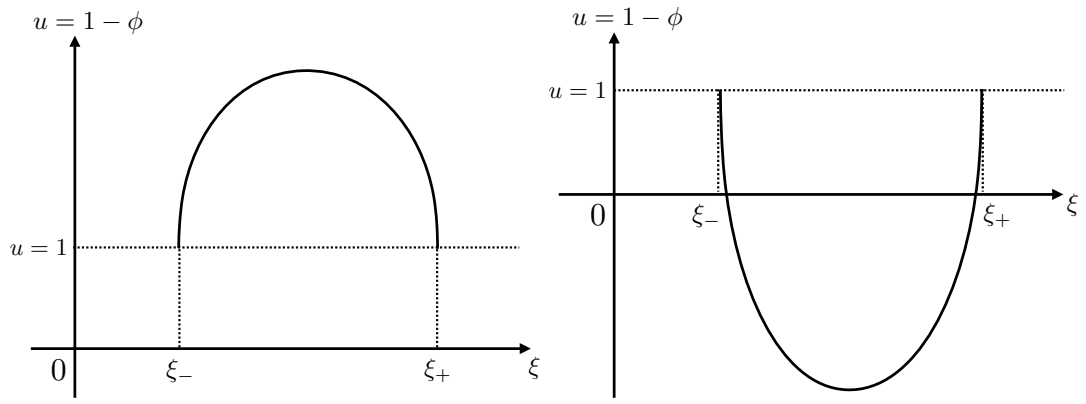

Figure 3.2.1: Schematic picture of the functions defined on the finite interval such that each function $u(t,x) \equiv 1 - \phi(\xi)$ satisfies equation (3.1.1) on a finite interval (ξ_-, ξ_+) in Theorem 3.2.1. Here it should be noted that the position of the singular points ξ_- and ξ_+ are not determined in our studies, however, they are shown in this figure for the convenience. [Left: In the case that $1 - \varepsilon^2 c^2 > 0$.] [Right: In the case that $1 - \varepsilon^2 c^2 < 0$.] Note that in the figure on the right, the trajectory in which the minimum of u is below the ξ-axis is chosen from among the infinitely many trajectories that correspond to Theorem 3.2.1.

Remark 3.2.2
In Theorem 3.2.1, the result for the case $1 - \varepsilon^2 c^2 > 0$ is almost the same as in Proposition 3.2.1. However, since (3.1.1) *is a hyperbolic equation and there is room for consideration in adopting Definition 3.2.2 as a rigorous discussion of the mathematical formulation of the solution, Theorem 3.2.1 is phrased as the existence of a family of functions satisfying the equation. Notable points in Theorem 3.2.1 are as follows:*

(i) In addition, the asymptotic behavior obtained in the above theorem is the same as Proposition 3.2.1, except for the difference in the sign of the coefficients. This means that the behavior of these as $\varepsilon \to 0$ does not change. This may be due to the fact that the principal part of the derived vector field (3.3.2) *does not change.*

(ii) The most important point to be emphasized in this result is that a condition on the wave speed that is not obtained in [31] appears, and when the wave speed exceeds $c = 1/\varepsilon$, that is, when the wave speed is sufficiently large, traveling waves that are not seen in [31] are observed (see Figure 3.2.1 and Figure 1 of [31]).

Theorem 3.2.2
Assume that $\alpha \in 2\mathbb{N}$, $\varepsilon > 0$, and $1 - \varepsilon^2 c^2 > 0$. Then, for a given positive constant $0 < c < 1/\varepsilon$, there exists a family of the functions (which corresponds to a family of the orbits of (3.1.5)*) defined on the semi-infinite intervals such that each function $u(t,x)$ satisfies equation* (3.1.1) *on a semi-infinite interval $(-\infty, \xi_+)$ $(-\infty < \xi_+ < +\infty)$. Moreover, each function $u(t,x) \equiv 1 - \phi(\xi)$ satisfies the following:*

- $\lim_{\xi \to \xi_+ - 0} \phi(\xi) = 0, \quad \lim_{\xi \to -\infty} \phi(\xi) = -\infty, \quad \lim_{\xi \to \xi_+ - 0} \psi(\xi) = \infty.$
- $\phi(\xi) < 0$ *holds for* $\xi \in (-\infty, \xi_+)$.

In addition, the asymptotic behavior for $\xi \to \xi_+ - 0$ and $\xi \to -\infty$ are (3.2.1) *and*

$$\phi(\xi) \sim -Ce^{-\frac{c}{1-\varepsilon^2 c^2}\xi} \quad \text{as} \quad \xi \to -\infty \tag{3.2.5}$$

with $C > 0$.

On the other hand, assume that $1 - \varepsilon^2 c^2 < 0$. *Then, for a given positive constant* $c > 1/\varepsilon$, *there exists a family of the functions (which corresponds to a family of the orbits of* (3.1.5)*) defined on the semi-infinite intervals such that each function* $u(t,x)$ *satisfies equation* (3.1.1) *on a semi-infinite interval* $(\xi_-, +\infty)$ $(-\infty < \xi_- < +\infty)$. *Moreover, each function* $u(t,x) \equiv 1 - \phi(\xi)$ *satisfies the following:*

- $\lim_{\xi \to \xi_- + 0} \phi(\xi) = 0, \quad \lim_{\xi \to \infty} \phi(\xi) = +\infty, \quad \lim_{\xi \to \xi_- + 0} \psi(\xi) = +\infty.$
- $\phi(\xi) > 0$ *holds for* $\xi \in (\xi_-, +\infty)$.

In addition, the asymptotic behavior for $\xi \to \xi_- + 0$ *and* $\xi \to +\infty$ *are* (3.2.4) *and*

$$\phi(\xi) \sim C e^{-\frac{c}{1-\varepsilon^2 c^2}\xi} \quad \text{as} \quad \xi \to +\infty \tag{3.2.6}$$

with $C > 0$.

Theorem 3.2.3
Assume that $\alpha \in 2\mathbb{N}$, $\varepsilon > 0$, *and* $1 - \varepsilon^2 c^2 > 0$. *Then, for a given positive constant* $0 < c < 1/\varepsilon$, *there exists a family of the functions (which corresponds to a family of the orbits of* (3.1.5)*) defined on the semi-infinite intervals such that each function* $u(t,x)$ *satisfies equation* (3.1.1) *on a semi-infinite interval* $(-\infty, \xi_+)$ $(-\infty < \xi_+ < +\infty)$. *Moreover, each function* $u(t,x) \equiv 1 - \phi(\xi)$ *satisfies the following:*

- $\lim_{\xi \to \xi_+ - 0} \phi(\xi) = 0, \quad \lim_{\xi \to -\infty} \phi(\xi) = -\infty, \quad \lim_{\xi \to \xi_+ - 0} \psi(\xi) = \infty.$
- $\phi(\xi) < 0$ *holds for* $\xi \in (-\infty, \xi_+)$.

In addition, the asymptotic behavior for $\xi \to \xi_+ - 0$ *and* $\xi \to -\infty$ *are* (3.2.1) *and*

$$\begin{cases} \phi(\xi) \sim O(\xi^{\frac{1}{\alpha+1}}), \\ \psi(\xi) \sim O((-\xi)^{-\frac{\alpha}{\alpha+1}}), \end{cases} \quad \text{as} \quad \xi \to -\infty. \tag{3.2.7}$$

On the other hand, assume that $1 - \varepsilon^2 c^2 < 0$. *Then, for a given positive constant* $c > 1/\varepsilon$, *there exists a family of the functions (which corresponds to a family of the orbits of* (3.1.5)*) defined on the semi-infinite intervals such that each function* $u(t,x)$ *satisfies equation* (3.1.1) *on a semi-infinite interval* $(\xi_-, +\infty)$ $(-\infty < \xi_- < +\infty)$. *Moreover, each function* $u(t,x) \equiv 1 - \phi(\xi)$ *satisfies the following:*

- $\lim_{\xi \to \xi_- + 0} \phi(\xi) = 0, \quad \lim_{\xi \to +\infty} \phi(\xi) = +\infty, \quad \lim_{\xi \to \xi_- + 0} \psi(\xi) = +\infty.$
- $\phi(\xi) > 0$ *holds for* $\xi \in (\xi_-, +\infty)$.

In addition, the asymptotic behavior for $\xi \to \xi_- + 0$ *and* $\xi \to +\infty$ *are* (3.2.4) *and*

$$\begin{cases} \phi(\xi) \sim O(\xi^{\frac{1}{\alpha+1}}), \\ \psi(\xi) \sim O((-\xi)^{-\frac{\alpha}{\alpha+1}}), \end{cases} \quad \text{as} \quad \xi \to +\infty. \tag{3.2.8}$$

Remark 3.2.3
Note that the families of functions satisfying the equations obtained in Theorem 3.2.2 and Theorem 3.2.3 are lumped together in a rough form in Figure 3.2.2, although their asymptotic behavior is strictly different.

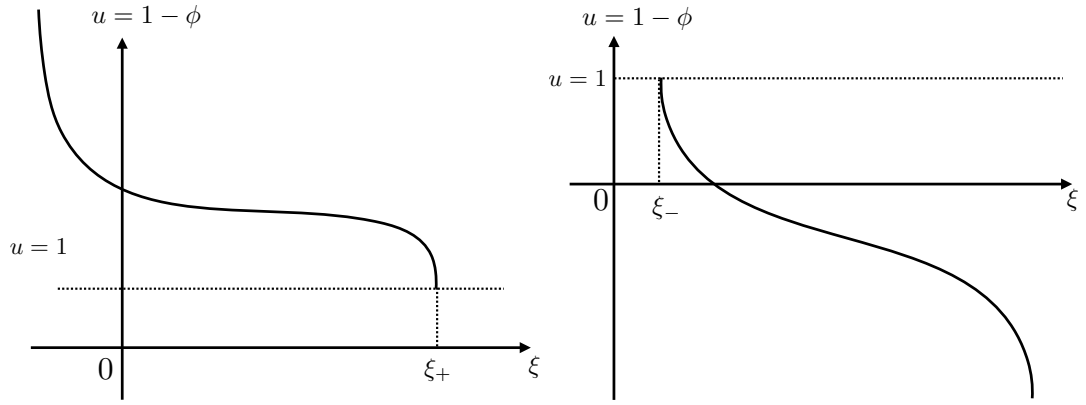

Figure 3.2.2: Schematic pictures of the functions defined on the semi-infinite interval such that each function $u(t,x) \equiv 1 - \phi(\xi)$ satisfies equation (3.1.1) on a semi-infinite interval in Theorem 3.2.2 and Theorem 3.2.3. Here it should be noted that the position of the singular point ξ_+ (or ξ_-) are not determined in our studies, however, they are shown in these figures for the convenience. [Left: In the case that $1 - \varepsilon^2 c^2 > 0$.] [Right: In the case that $1 - \varepsilon^2 c^2 < 0$.]

Theorem 3.2.4
Assume that $\alpha \in 2\mathbb{N}$, $\varepsilon > 0$, and $1 - \varepsilon^2 c^2 > 0$. Then, for a given positive constant $0 < c < 1/\varepsilon$, the equation (3.1.1) has a family of the traveling wave solutions (which corresponds to a family of the orbits of (3.1.5)) with singularities at $\xi \to -\infty$ and $\xi \to +\infty$. Moreover, its each function $u(t,x) \equiv 1 - \phi(\xi)$ satisfies the following:

- $\lim_{\xi \to +\infty} \phi(\xi) = +\infty, \quad \lim_{\xi \to -\infty} \phi(\xi) = +\infty.$
- *$\phi(\xi) > 0$ holds for $\xi \in \mathbb{R}$.*
- *There exists a constant $\xi_* \in \mathbb{R}$ such that the following holds: $\psi(\xi) < 0$ for $\xi \in (-\infty, \xi_*)$, $\psi(\xi_*) = 0$ and $\psi(\xi) > 0$ for $\xi \in (\xi_*, +\infty)$.*

In addition, the asymptotic behavior for $\xi \to +\infty$ and $\xi \to -\infty$ are

$$\begin{cases} \phi(\xi) \sim O(\xi^{\frac{1}{\alpha+1}}), \\ \psi(\xi) \sim O((-\xi)^{-\frac{\alpha}{\alpha+1}}), \end{cases} \qquad \text{as} \quad \xi \to +\infty \tag{3.2.9}$$

and

$$\phi(\xi) \sim C e^{-\frac{c}{1-\varepsilon^2 c^2}\xi} \quad \text{as} \quad \xi \to -\infty \tag{3.2.10}$$

with $C > 0$.

On the other hand, assume that $1 - \varepsilon^2 c^2 < 0$. Then, for a given positive constant $c > 1/\varepsilon$, the equation (3.1.1) has a family of the traveling wave solutions (which corresponds to a family of the orbits of (3.1.5)) with singularities at $\xi \to -\infty$ and $\xi \to +\infty$. Moreover, its each function $u(t,x) \equiv 1 - \phi(\xi)$ satisfies the following:

- $\lim_{\xi \to +\infty} \phi(\xi) = -\infty, \quad \lim_{\xi \to -\infty} \phi(\xi) = -\infty.$
- *$\phi(\xi) < 0$ holds for $\xi \in \mathbb{R}$.*
- *There exists a constant $\xi_* \in \mathbb{R}$ such that the following holds: $\psi(\xi) > 0$ for $\xi \in (-\infty, \xi_*)$, $\psi(\xi_*) = 0$ and $\psi(\xi) < 0$ for $\xi \in (\xi_*, +\infty)$.*

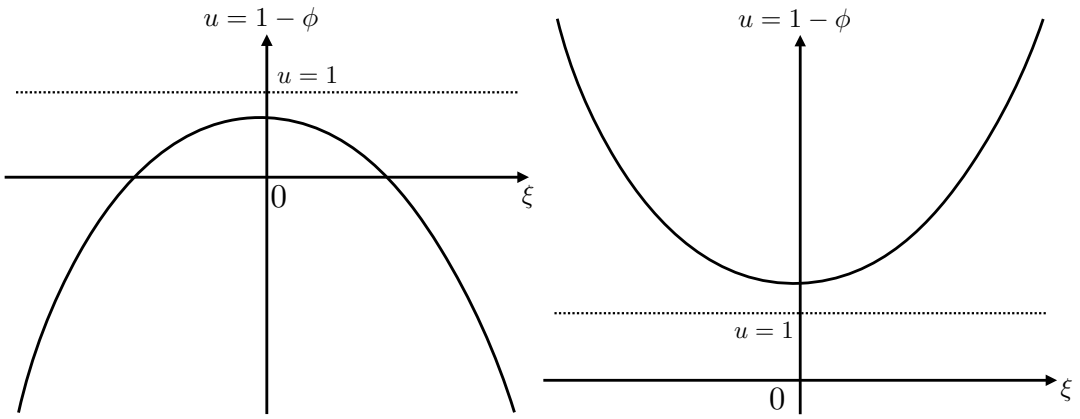

Figure 3.2.3: Schematic picture of the each traveling wave solutions with the singularities at $\xi \to -\infty$ and $\xi \to +\infty$ in obtained Theorem 3.2.4. [Left: In the case that $1-\varepsilon^2c^2 > 0$.] [Right: In the case that $1 - \varepsilon^2c^2 < 0$.] Note that in the figure on the right, the trajectory in which the maximum of u is above the ξ-axis is chosen from among the infinitely many trajectories that correspond to Theorem 3.2.4.

In addition, the asymptotic behavior for $\xi \to +\infty$ and $\xi \to -\infty$ are

$$\phi(\xi) \sim -Ce^{-\frac{c}{1-\varepsilon^2c^2}\xi} \quad \text{as} \quad \xi \to +\infty \tag{3.2.11}$$

with $C > 0$, and

$$\begin{cases} \phi(\xi) \sim O(\xi^{\frac{1}{\alpha+1}}), \\ \psi(\xi) \sim O((-\xi)^{-\frac{\alpha}{\alpha+1}}), \end{cases} \quad \text{as} \quad \xi \to -\infty. \tag{3.2.12}$$

Remark 3.2.4
We mentioned that when $1 - \varepsilon^2c^2 = 0$, $\phi(\xi)$ can be expressed explicitly as in (3.1.4)*. This is the same as the number of order of $\phi(\xi)$ in* (3.2.7), (3.2.8), (3.2.9), *and* (3.2.12)*. However, the detailed relationships and mathematical meanings of these are not known yet, and will be the subject of future work.*

Remark 3.2.5
Some functions obtained in the above Theorems satisfy the equation only on finite interval or semi-infinite interval. In this chapter, we do not discuss the behavior of the solutions of (3.1.5) *after $\psi(\xi)$ becomes infinity (outside of the interval on that $\phi(\xi)$ satisfies* (3.1.3)*). It is necessary that more detailed (and hard) analysis in order to study the solutions after $\psi(\xi)$ reaches the singularity. So we leave it open here. It should be noted that equation* (3.1.1) *is invariant under translation for spatial coordinates, so many of the same waves connected together should also satisfy the equation, except at the points where the derivatives diverge. However, since our interest in this chapter is to study the traveling waves of* (3.1.5) *from the viewpoint of dynamical systems, we do not discuss this chapter.*

3.3 Dynamics on the Poincaré disk of (3.1.5)

In this section, we study $\mathbb{R}^2 \cup \{(\phi, \psi) \mid \|(\phi, \psi)\| = +\infty\}$, i.e., the dynamics on the Poincaré disk, by the Poincaré compactification. In order to study the dynamics of (3.1.5) on the Poincaré disk, we desingularize it by the time-scale desingularization

$$ds/d\xi = \phi^{-\alpha} \quad \text{for} \quad \alpha \in 2\mathbb{N}. \tag{3.3.1}$$

Since that α is even, the direction of the time does not change via this desingularization. Then, we have

$$\begin{cases} \phi' = \phi^\alpha \psi, \\ \psi' = (1-\varepsilon^2 c^2)^{-1}(-c\phi^\alpha \psi + 1), \end{cases} \qquad \left({}' = \frac{d}{ds} \right) \tag{3.3.2}$$

with $1-\varepsilon^2 c^2 \neq 0$. This system (3.3.2) does not have equilibria.

It should be noted that the time scale desingularization (3.3.1) is simply multiplying the vector field by ϕ^α. Then, except the singularity $\{\phi = 0\}$, the solution curves of the system (vector field) remain the same but are parameterized differently. Still, we refer to Section 7.7 of [44] and references therein for the analytical treatments of desingularization with the time rescaling. In what follows, we use similar time rescaling (re-parameterization of the solution curves) repeatedly to desingularize the vector fields.

Now we can consider the dynamics of (3.3.2) on the charts $\overline{U}_j$ and $\overline{V}_j$ $(j = 1, 2)$. See [14, 31, 33] and their references for definitions of these local coordinates. Note that these results described below are consistent with the process shown in Theorem 2 of [31] and Proposition 1 of [33], assuming $\varepsilon = 0$. For the reader's convenience, the calculation process is described here considering the case where $\varepsilon > 0$.

3.3.1 Dynamics on the chart $\overline{U}_2$

To obtain the dynamics on the chart $\overline{U}_2$, we introduce coordinates (λ, x) by the formulas

$$\phi = x/\lambda, \quad \psi = 1/\lambda.$$

In this chart, it corresponds to $\phi \to 0$ and $\psi \to +\infty$ and the direction in which x is positive corresponds to the direction in which ϕ is positive. See Figure 2 in [31] for a geometric image. Then, these transformations yield

$$\begin{cases} \lambda' = (1-\varepsilon^2 c^2)^{-1}(c\lambda^{-\alpha+1}x^\alpha - \lambda^2), \\ x' = \lambda^{-\alpha}x^\alpha + (1-\varepsilon^2 c^2)^{-1}(c\lambda^{-\alpha}x^{\alpha+1} - \lambda x), \end{cases} \qquad \left({}' = \frac{d}{ds} \right).$$

By using the time-scale desingularization $d\tau/ds = \lambda^{-\alpha}$, we have

$$\begin{cases} \lambda_\tau = (1-\varepsilon^2 c^2)^{-1}(c\lambda x^\alpha - \lambda^{\alpha+2}), \\ x_\tau = x^\alpha + (1-\varepsilon^2 c^2)^{-1}(cx^{\alpha+1} - \lambda^{\alpha+1}x), \end{cases} \tag{3.3.3}$$

where $\lambda_\tau = d\lambda/d\tau$ and $x_\tau = dx/d\tau$. The system (3.3.3) has the equilibria

$$E_0^+ : (\lambda, x) = (0, 0), \quad E_c : (\lambda, x) = (0, M_1), \quad M_1 = -(1-\varepsilon^2 c^2)c^{-1}.$$

The Jacobian matrices of the vector field (3.3.3) at these equilibria are

$$E_0^+ : \begin{pmatrix} 0 & 0 \\ 0 & 0 \end{pmatrix}, \quad E_c : \begin{pmatrix} M_2 & 0 \\ 0 & M_2 \end{pmatrix}, \quad M_2 = \frac{(1-\varepsilon^2 c^2)^{\alpha-1}}{c^{\alpha-1}}.$$

Therefore, E_c is a source when $1-\varepsilon^2 c^2 > 0$, and a sink when $1-\varepsilon^2 c^2 < 0$. The equilibrium E_0^+ is not hyperbolic. Thus, to determine the dynamics near E_0^+, we desingularize it by introducing the following blow-up coordinates:

$$\lambda = r^{\alpha-1}\bar{\lambda}, \quad x = r^{\alpha+1}\bar{x}$$

(see [14]). Since we are interested in the dynamics on the Poincaré disk, we consider the dynamics of blow-up vector fields on the charts $\{\bar{\lambda} = 1\}$ and $\{\bar{x} = \pm 1\}$ (see also [31, 33]).

Dynamics on the chart $\{\bar{\lambda}=1\}$

By the change of coordinates $\lambda = r^{\alpha-1}$, $x = r^{\alpha+1}\bar{x}$, we have

$$\begin{cases} r_\tau = r(\alpha-1)^{-1}(1-\varepsilon^2c^2)^{-1}(cr^{\alpha(\alpha+1)}\bar{x}^\alpha - r^{\alpha^2-1}), \\ \bar{x}_\tau = 2(\alpha-1)^{-1}(1-\varepsilon^2c^2)^{-1}(r^{\alpha^2-1}\bar{x} - cr^{\alpha(\alpha+1)}\bar{x}^{\alpha+1}) + r^{\alpha^2-1}\bar{x}^\alpha. \end{cases}$$

The time-rescaling $d\eta/d\tau = r^{\alpha^2-1}$ yields

$$\begin{cases} r_\eta = (\alpha-1)^{-1}(1-\varepsilon^2c^2)^{-1}(cr^{\alpha+2}\bar{x}^\alpha - r), \\ \bar{x}_\eta = 2(\alpha-1)^{-1}(1-\varepsilon^2c^2)^{-1}(\bar{x} - cr^{\alpha+1}\bar{x}^{\alpha+1}) + \bar{x}^\alpha, \end{cases} \tag{3.3.4}$$

where $r_\eta = dr/d\eta$ and $\bar{x}_\eta = d\bar{x}/d\eta$. The equilibria of (3.3.4) on $\{r=0\}$ are

$$\overline{E}_0^+ : (r,\bar{x}) = (0,0), \quad \overline{E}_\alpha^+ : (r,\bar{x}) = (0,M_3), \quad M_3 = [-2(\alpha-1)^{-1}(1-\varepsilon^2c^2)^{-1}]^{\frac{1}{\alpha-1}}.$$

Note that $M_3 < 0$ when $1-\varepsilon^2c^2 > 0$ and $M_3 > 0$ when $1-\varepsilon^2c^2 < 0$. The Jacobian matrices of the vector field (3.3.4) at these equilibria are

$$\overline{E}_0^+ : \begin{pmatrix} -\frac{1}{(\alpha-1)(1-\varepsilon^2c^2)} & 0 \\ 0 & \frac{2}{(\alpha-1)(1-\varepsilon^2c^2)} \end{pmatrix}, \quad \overline{E}_\alpha^+ : \begin{pmatrix} -\frac{1}{(\alpha-1)(1-\varepsilon^2c^2)} & 0 \\ 0 & -\frac{2}{1-\varepsilon^2c^2} \end{pmatrix}.$$

Therefore, $\overline{E}_0^+$ is a saddle, and $\overline{E}_\alpha^+$ is a sink in the case that $1-\varepsilon^2c^2 > 0$. In addition, $\overline{E}_0^+$ is a saddle, and $\overline{E}_\alpha^+$ is a source in the case that $1-\varepsilon^2c^2 < 0$.

Furthermore, since $|-(\alpha-1)^{-1}(1-\varepsilon^2c^2)^{-1}| < |-2(1-\varepsilon^2c^2)^{-1}|$ holds, trajectories near $\overline{E}_\alpha^+$ are tangent to $\{\bar{x}=M_3, r\geq 0\}$ as $\eta\to+\infty$. The solutions around $\overline{E}_\alpha^+$ are approximated as

$$\begin{cases} r(\eta) = C_1 e^{-\frac{1}{(\alpha-1)(1-\varepsilon^2c^2)}\eta}(1+o(1)), \\ \bar{x}(\eta) = C_2 e^{-\frac{2}{1-\varepsilon^2c^2}\eta} + M_3(1+o(1)), \end{cases} \quad \text{as} \quad \eta\to+\infty \tag{3.3.5}$$

with constants C_1 and C_2.

Dynamics on the chart $\{\bar{x}=1\}$

By the change of coordinates $\lambda = r^{\alpha-1}\bar{\lambda}$, $x = r^{\alpha+1}$, and time-rescaling $d\eta/d\tau = r^{\alpha^2-1}$, we have

$$\begin{cases} r_\eta = (\alpha+1)^{-1}r + (\alpha+1)^{-1}(1-\varepsilon^2c^2)^{-1}(cr^{\alpha+2} - r\bar{\lambda}^{\alpha+1}), \\ \bar{\lambda}_\eta = -(\alpha-1)(\alpha+1)^{-1}\bar{\lambda} + (\alpha+1)^{-1}(1-\varepsilon^2c^2)^{-1}(2cr^{\alpha+1}\bar{\lambda} - 2\bar{\lambda}^{\alpha+2}). \end{cases} \tag{3.3.6}$$

If $1-\varepsilon^2c^2 > 0$, then the equilibrium on $\{r=0, \bar{\lambda}\geq 0\}$ is $(r,\bar{\lambda}) = (0,0)$. The Jacobian matrix of the vector field (3.3.6) at this equilibrium is

$$(0,0) : \begin{pmatrix} \frac{1}{\alpha+1} & 0 \\ 0 & -\frac{\alpha-1}{\alpha+1} \end{pmatrix}.$$

Therefore, the equilibrium $(0,0)$ is a saddle.

If $1-\varepsilon^2c^2 < 0$, the system (3.3.6) has the equilibria on $\{r=0, \bar{\lambda}\geq 0\}$

$$(r,\bar{\lambda}) = (0,0), \quad (r,\bar{\lambda}) = (0,M_4), \quad M_4 = [-2^{-1}(\alpha-1)(1-\varepsilon^2c^2)]^{\frac{1}{\alpha+1}} > 0.$$

The Jacobian matrices of the vector field (3.3.6) at these equilibria are

$$(0,0): \begin{pmatrix} \frac{1}{\alpha+1} & 0 \\ 0 & -\frac{\alpha-1}{\alpha+1} \end{pmatrix}, \quad (0,M_4): \begin{pmatrix} \frac{1}{2} & 0 \\ 0 & \alpha-1 \end{pmatrix}.$$

Therefore, the equilibrium $(0,0)$ is a saddle, and $(0,M_4)$ is a source.

Dynamics on the chart $\{\bar{x}=-1\}$

The change of coordinates $\lambda = r^{\alpha-1}\bar{\lambda}$, $x = -r^{\alpha+1}$, and time-rescaling $d\eta/d\tau = r^{\alpha^2-1}$ yield

$$\begin{cases} r_\eta = -(\alpha+1)^{-1}r + (\alpha+1)^{-1}(1-\varepsilon^2c^2)^{-1}(cr^{\alpha+2} - r\bar{\lambda}^{\alpha+1}), \\ \bar{\lambda}_\eta = (\alpha-1)(\alpha+1)^{-1}\bar{\lambda} + (\alpha+1)^{-1}(1-\varepsilon^2c^2)^{-1}(2cr^{\alpha+1}\bar{\lambda} - 2\bar{\lambda}^{\alpha+2}). \end{cases} \tag{3.3.7}$$

If $1-\varepsilon^2c^2 > 0$, the system (3.3.7) has the equilibria on $\{r=0, \bar{\lambda} \geq 0\}$

$$(r,\bar{\lambda}) = (0,0), \quad (r,\bar{\lambda}) = (0,M_5), \quad M_5 = [2^{-1}(\alpha-1)(1-\varepsilon^2c^2)]^{\frac{1}{\alpha+1}} > 0.$$

The Jacobian matrices of the vector field (3.3.7) at these equilibria are

$$(0,0): \begin{pmatrix} -\frac{1}{\alpha+1} & 0 \\ 0 & \frac{\alpha-1}{\alpha+1} \end{pmatrix}, \quad (0,M_5): \begin{pmatrix} -\frac{1}{2} & 0 \\ 0 & -\alpha-1 \end{pmatrix}.$$

Therefore, the equilibrium $(0,0)$ is a saddle, and $(0,M_5)$ is a sink.

If $1-\varepsilon^2c^2 < 0$, then the equilibrium on $\{r=0, \bar{\lambda} \geq 0\}$ is $(r,\bar{\lambda}) = (0,0)$. Eigenvalues of the linearized matrix are $-(\alpha+1)^{-1}$ and $(\alpha-1)(\alpha+1)^{-1}$ with corresponding eigenvectors $(1,0)$ and $(0,1)$, respectively. Therefore, the equilibrium $(0,0)$ is a saddle.

Combining the dynamics on the charts $\{\bar{\lambda}=1\}$ and $\{\bar{x}=\pm 1\}$, we can obtain the dynamics on $\overline{U}_2$ (see Figure 3.3.1). The figure for the case $1-\varepsilon^2c^2 < 0$ can be drawn in the same way as for the case $1-\varepsilon^2c^2 > 0$.

3.3.2 Dynamics on the chart $\overline{V}_2$

In this chart, it corresponds to $\phi \to 0$ and $\psi \to -\infty$ and the direction in which x is negative corresponds to the direction in which ϕ is positive. The change of coordinates

$$\phi = -x/\lambda, \quad \psi = -1/\lambda$$

give the projected dynamics of (3.3.2) on the chart $\overline{V}_2$:

$$\begin{cases} \lambda_\tau = (1-\varepsilon^2c^2)^{-1}(c\lambda x^\alpha + \lambda^{2+\alpha}), \\ x_\tau = x^\alpha + (1-\varepsilon^2c^2)^{-1}(cx^{\alpha+1} + \lambda^{\alpha+1}x), \end{cases} \tag{3.3.8}$$

where τ is the new variable introduced by $d\tau/ds = \lambda(s)^{-\alpha}$. The system (3.3.8) has the equilibria

$$E_0^- : (\lambda,x) = (0,0), \quad E_{c'} : (\lambda,x) = (0,M_1), \quad M_1 = -(1-\varepsilon^2c^2)c^{-1}.$$

The Jacobian matrices of the vector field (3.3.8) at these equilibria are the same as that of $\overline{U}_2$.

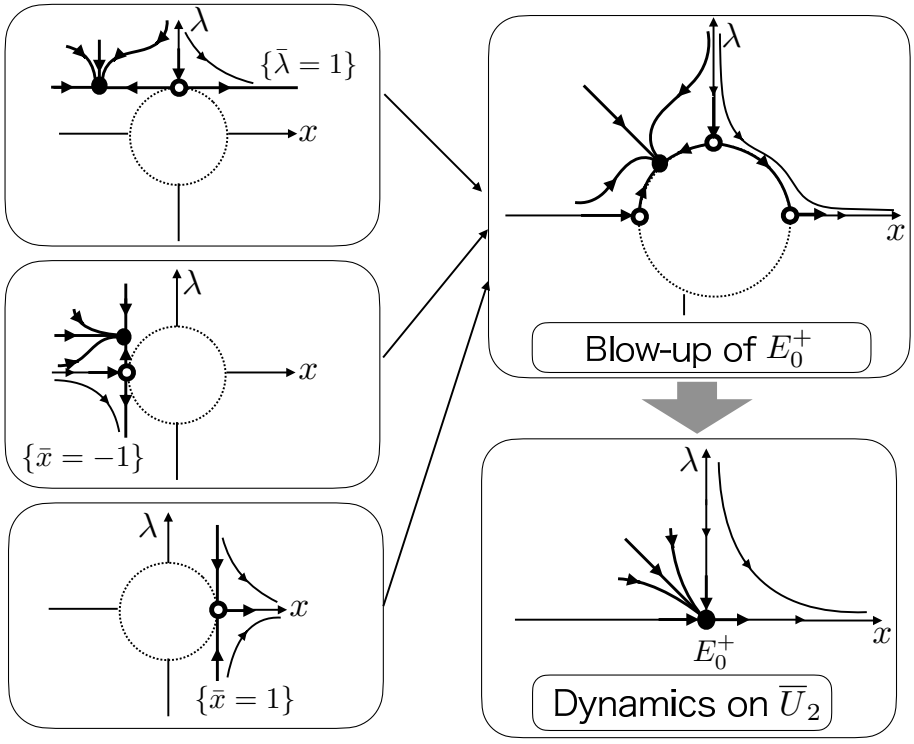

Figure 3.3.1: Schematic pictures of the dynamics of the blow-up vector fields and $\overline{U}_2$ in the case that $1-\varepsilon^2c^2>0$.

The system (3.3.8) can be transformed into (3.3.3) by the change of coordinates $(\lambda,x)\mapsto(-\lambda,x)$. Therefore, it is sufficient to consider the blow-up of singularity E_0^- : $(\lambda,x)=(0,0)$ by the formulas

$$\lambda=r^{\alpha-1},\quad x=r^{\alpha+1}\bar{x}\quad\text{with}\quad\bar{\lambda}=1.$$

Then, we have

$$\begin{cases} r_\eta=(\alpha-1)^{-1}(1-\varepsilon^2c^2)^{-1}(cr^{\alpha+2}\bar{x}^\alpha+r),\\ \bar{x}_\eta=2(\alpha-1)^{-1}(1-\varepsilon^2c^2)^{-1}(-\bar{x}-cr^{\alpha+1}\bar{x}^{\alpha+1})+\bar{x}^\alpha, \end{cases} \tag{3.3.9}$$

where η satisfies $d\eta/d\tau=r^{\alpha^2-1}$. The equilibria of (3.3.9) on $\{r=0\}$ are

$$\overline{E}_0^-:(r,\bar{x})=(0,0),\quad \overline{E}_\alpha^-:(r,\bar{x})=(0,M_6),\quad M_6=[2(\alpha-1)^{-1}(1-\varepsilon^2c^2)^{-1}]^{\frac{1}{\alpha-1}}.$$

Note that $M_6>0$ when $1-\varepsilon^2c^2>0$ and $M_6<0$ when $1-\varepsilon^2c^2<0$. The equilibrium $\overline{E}_0^-$ is a saddle with the eigenvalues $(\alpha-1)^{-1}(1-\varepsilon^2c^2)^{-1}$ and $-2(\alpha-1)^{-1}(1-\varepsilon^2c^2)^{-1}$ whose corresponding eigenvectors are $(1,0)$ and $(0,1)$, respectively for both $1-\varepsilon^2c^2>0$ and $1-\varepsilon^2c^2<0$.

When $1-\varepsilon^2c^2>0$ holds, $\overline{E}_\alpha^-$ is a source with the eigenvalues $(\alpha-1)^{-1}(1-\varepsilon^2c^2)^{-1}$ and $2(1-\varepsilon^2c^2)^{-1}$ whose corresponding eigenvectors are $(1,0)$ and $(0,1)$, respectively. Furthermore, $\overline{E}_\alpha^-$ is a sink in the case that $1-\varepsilon^2c^2<0$.

The solutions around $\overline{E}_\alpha^-$ are approximated as

$$\begin{cases} r(\eta)=C_1e^{\frac{1}{(\alpha-1)(1-\varepsilon^2c^2)}\eta}(1+o(1)),\\ \bar{x}(\eta)=C_2e^{\frac{2}{1-\varepsilon^2c^2}\eta}+M_6(1+o(1)), \end{cases}\qquad\text{as}\quad\eta\to-\infty$$

with constants C_1 and C_2. This equation will be used later in Subsection 3.4.1 to derive the asymptotic behavior for $\xi \to \xi_- + 0$.

3.3.3 Dynamics on the chart $\overline{U}_1$

Let us study the dynamics on the chart $\overline{U}_1$. In this chart, it corresponds to $\phi \to +\infty$ and $\psi \to 0$. The transformations

$$\phi = 1/\lambda, \quad \psi = x/\lambda$$

yield

$$\begin{cases} \lambda_\tau = -\lambda x, \\ x_\tau = (1-\varepsilon^2 c^2)^{-1}(-cx + \lambda^{\alpha+1}) - x^2, \end{cases} \tag{3.3.10}$$

via time-rescaling $d\tau/ds = \lambda^{-\alpha}$. This system has the equilibria

$$e_0^+ : (\lambda, x) = (0,0), \quad e_c : (\lambda, x) = (0, M_7), \quad M_7 = -c(1-\varepsilon^2 c^2)^{-1}.$$

Note that $M_7 > 0$ when $1 - \varepsilon^2 c^2 < 0$ and $M_7 < 0$ when $1 - \varepsilon^2 c^2 > 0$. The Jacobian matrices of the vector field (3.3.10) at these equilibria are

$$e_0^+ : \begin{pmatrix} 0 & 0 \\ 0 & M_7 \end{pmatrix}, \quad e_c : \begin{pmatrix} -M_7 & 0 \\ 0 & -M_7 \end{pmatrix}.$$

Therefore, e_c is a source when $1 - \varepsilon^2 c^2 > 0$, and should matches $E_{c'}$. When $1 - \varepsilon^2 c^2 < 0$, e_c is sink and should matches E_c.

In a similar way to [31, 33], the dynamics near e_0^+ can be determined by the center manifold theorem (for instance, see [9] for the details of it). The approximation of the (graph of) center manifold can be obtained as follows:

$$\{(\lambda, x) \mid x = \lambda^{\alpha+1}/c + O(\lambda^{2\alpha+2})\}.$$

Further, we can see that the dynamics of (3.3.10) near $(0,0)$ is topologically equivalent to the dynamics of the following equation:

$$\lambda_\tau = -\lambda^{\alpha+2}/c + O(\lambda^{2\alpha+3}).$$

These results were also obtained in [31, 33]. However, we reproduce them since they will be used in the proof of Theorem 3.2.4 later.

3.3.4 Dynamics on the chart $\overline{V}_1$

In this chart, it corresponds to $\phi \to -\infty$ and $\psi \to 0$. The transformations

$$\phi = -1/\lambda, \quad \psi = -x/\lambda$$

yield

$$\begin{cases} \lambda_\tau = -\lambda x, \\ x_\tau = (1-\varepsilon^2 c^2)^{-1}(-cx - \lambda^{\alpha+1}) - x^2 \end{cases} \tag{3.3.11}$$

via time-rescaling $d\tau/ds = \lambda^{-\alpha}$. We can see that the system (3.3.11) can be transformed into the system (3.3.10) by the change of variables: $(\lambda, x) \mapsto (-\lambda, x)$. Thus, with the exception of $\{\lambda = 0\}$, the dynamics of (3.3.11) is immediately obvious from the dynamics of (3.3.10), however, we summarize the results for the derivation of the asymptotic behavior (as it is necessary for the proof of Theorem 3.2.3).

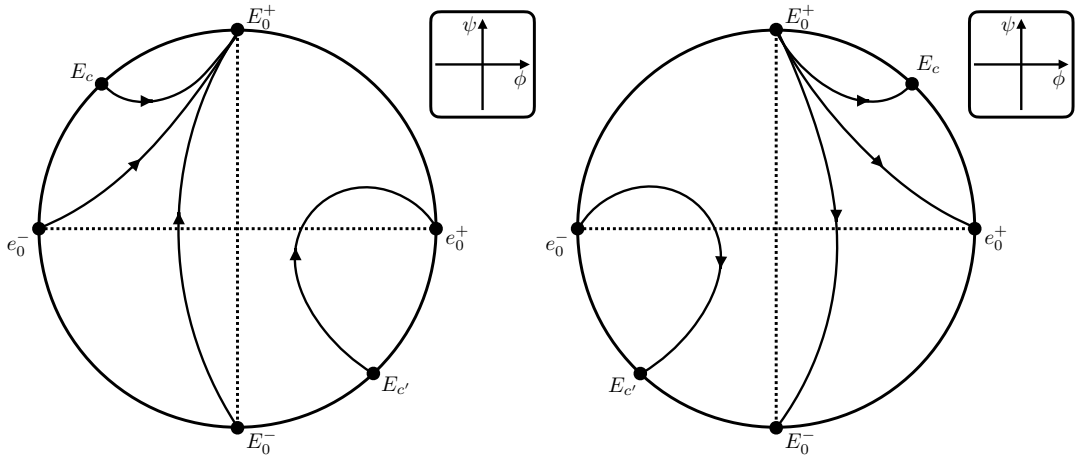

Figure 3.3.2: Schematic pictures of the dynamics on the Poincaré disk for (3.1.5) in the case that $\alpha \in 2\mathbb{N}$ and $\varepsilon > 0$. [Left: Case $1 - \varepsilon^2 c^2 > 0$.] [Right: Case $1 - \varepsilon^2 c^2 < 0$.] See also Fig. 3.3.1 for the dynamics around E_0^+ for $1 - \varepsilon^2 c^2 > 0$.

This system has the equilibria

$$e_0^- : (\lambda, x) = (0, 0), \quad e_{c'} : (\lambda, x) = (0, M_7), \quad M_7 = -c(1 - \varepsilon^2 c^2)^{-1}.$$

The Jacobian matrices of the vector field (3.3.11) at these equilibria are

$$e_0^- : \begin{pmatrix} 0 & 0 \\ 0 & M_7 \end{pmatrix}, \quad e_{c'} : \begin{pmatrix} -M_7 & 0 \\ 0 & -M_7 \end{pmatrix}.$$

Therefore, $e_{c'}$ is a source when $1 - \varepsilon^2 c^2 > 0$, and should matches E_c. When $1 - \varepsilon^2 c^2 < 0$, $e_{c'}$ is sink and should matches $E_{c'}$. The dynamics near e_0^- can be determined by the center manifold theorem. In the same way as above, the approximation of the (graph of) center manifold can be obtained as follows:

$$\{(\lambda, x) \mid x = -\lambda^{\alpha+1}/c + O(\lambda^{2\alpha+2})\}. \tag{3.3.12}$$

Further, we can see that the dynamics of (3.3.11) near $(0, 0)$ is topologically equivalent to the dynamics of the following equation:

$$\lambda_\tau = \lambda^{\alpha+2}/c + O(\lambda^{2\alpha+3}). \tag{3.3.13}$$

3.3.5 Dynamics and connecting orbits on the Poincaré disk

Combining the dynamics on the charts $\overline{U}_j$ and $\overline{V}_j$ $(j = 1, 2)$, we obtain the dynamics on the Poincaré disk that is equivalent to the dynamics of (3.1.5) (or (3.3.2)) in the case that α is even as the following Proposition (see also Figure 3.3.2). We set the phase space Φ as follows:

$$\Phi = \{(\phi, \psi) \mid (\phi, \psi) \in \mathbb{R}^2 \cup \{\|(\phi, \psi)\| = +\infty\}\}.$$

Note that in Figure 3.3.2, the circumference corresponds to $\{\|(\phi, \psi)\| = +\infty\}$.

Proposition 3.3.1
Assume that $\alpha \in 2\mathbb{N}$ and $\varepsilon > 0$. Then, the dynamics on the Poincaré disk of the system (3.1.5) *is expressed as Figure 3.3.2 in both cases $1 - \varepsilon^2 c^2 > 0$ and $1 - \varepsilon^2 c^2 < 0$.*

Proof. First, the dynamics on the Poincaré disk for the case $1-\varepsilon^2c^2>0$ is immediately shown by the results of [31, 33]. In exactly the same way as [31, 33], it is proved that there exists connecting orbits between E_0^- and E_0^+. Therefore, we can conclude the existence of orbits that connect e_0^- and E_0^+, E_c and E_0^+, and $E_{c'}$ and e_0^+.

Next, we prove it for the case where $1-\varepsilon^2c^2<0$. In (3.1.5), the transformation of reversing the positive and negative values of $1-\varepsilon^2c^2$ is equivalent to applying the following transformation:

$$\phi\mapsto-\phi,\quad \psi\mapsto\psi,\quad \xi\mapsto-\xi. \tag{3.3.14}$$

In fact, (3.1.5) becomes

$$\begin{cases}\phi'=\psi,\\ \psi'=-(1-\varepsilon^2c^2)^{-1}(-c\psi+\phi^{-\alpha})\end{cases}$$

by the transformation in (3.3.14). This equation corresponds to the reversal of the sign of $1-\varepsilon^2c^2$ in (3.1.5). Thus, the dynamics on the Poincaré disk for $1-\varepsilon^2c^2<0$ is a symmetry transformation of (3.3.14) over that for $1-\varepsilon^2c^2>0$. This completes the proof. □

3.4 Proof of Theorems

In this section, we prove the main theorems. If the initial data are located on $\Phi\backslash\{\phi=0\}$, the existence of the solutions follows from the standard theory for the ordinary differential equations. Therefore, we consider the existence of the trajectories that connect equilibria and the detailed dynamics near the equilibria on the Poincaré disk and their asymptotic behavior. The table 3.1 shows the correspondence between each connecting orbit obtained by the proposition and the traveling wave described in the theorem proved below.

Table 3.1: The correspondence between each connecting orbit obtained by the proposition and the traveling wave described in the theorem proved below.

Theorem	Connecting orbits
Theorem 3.2.1	between E_0^- and E_0^+
Theorem 3.2.2	between E_c and E_0^+
Theorem 3.2.3	between e_0^- and E_0^+ for $1-\varepsilon^2c^2>0$
	between E_0^+ and e_0^+ for $1-\varepsilon^2c^2<0$.
Theorem 3.2.4	between $E_c^{'}$ and e_0^+ for $1-\varepsilon^2c^2>0$
	between e_0^- and $E_c^{'}$ for $1-\varepsilon^2c^2<0$.

3.4.1 Proof of Theorem 3.2.1

The proof of existence of the connecting orbits between E_0^- and E_0^+ in both cases $1-\varepsilon^2c^2>0$ and $1-\varepsilon^2c^2<0$ is obtained in [31], [33], and Proposition 3.3.1. Therefore, there exists a family of the functions which corresponds to a family of the orbits of (3.1.5).

Next, we prove the existence of a constant $\xi_*\in(\xi_-,\xi_+)$. It is sufficient to show the connecting orbits pass through the line $\{\psi=0\}$. This is evident from the existence of connecting orbits in both cases $1-\varepsilon^2c^2>0$ and $1-\varepsilon^2c^2<0$. Furthermore, this means that we are giving information about the increase or decrease of ψ.

Finally, we compute the asymptotic behavior of the trajectories near the equilibria E_0^- and E_0^+ as follows. This derivation is a refinement of the discussion in [31, 33]. Note that

the basic idea is the same as the previous ones. However, the detailed principal part is chosen as carefully as in [35] (see Remark 3.2.1).

Assume that $1-\varepsilon^2c^2>0$. Using (3.3.5), we then have

$$\begin{aligned}
\frac{d\eta}{d\xi} &= \frac{ds}{d\xi}\cdot\frac{d\tau}{ds}\cdot\frac{d\eta}{d\tau} = \phi^{-\alpha}\cdot\lambda^{-\alpha}\cdot r^{\alpha^2-1}\\
&= r^{-\alpha-1}\cdot\bar{x}^{-\alpha}\\
&= \left\{C_1e^{-\frac{1}{(\alpha-1)(1-\varepsilon^2c^2)}\eta}(1+o(1))\right\}^{-\alpha-1}\cdot\left\{C_2e^{-\frac{2}{1-\varepsilon^2c^2}\eta}(1+o(1))+M_3\right\}^{-\alpha}\\
&\sim C_3e^{\frac{\alpha+1}{(\alpha-1)(1-\varepsilon^2c^2)}\eta}\cdot\left\{C_2e^{-\frac{2}{1-\varepsilon^2c^2}\eta}(1+o(1))+M_3\right\}^{-\alpha} \quad \text{as} \quad \eta\to+\infty\\
&= \frac{C_3e^{\frac{\alpha+1}{(\alpha-1)(1-\varepsilon^2c^2)}\eta}}{\left\{C_2e^{-\frac{2}{1-\varepsilon^2c^2}\eta}(1+o(1))\right\}^{\alpha}+\alpha\left\{C_2e^{-\frac{2}{1-\varepsilon^2c^2}\eta}(1+o(1))\right\}^{\alpha-1}\cdot M_3+\cdots+(M_3)^{\alpha}}\\
&\sim C_4e^{\frac{\alpha+1}{(\alpha-1)(1-\varepsilon^2c^2)}\eta} \quad \text{as} \quad \eta\to+\infty
\end{aligned}$$

with constants C_j. As a note, we emphasize that the last part "$\sim$" corresponds to an improvement from [31, 33] (see Remark 3.2.1).

From this result, we can obtain

$$\frac{d\xi}{d\eta} = C_5e^{-\frac{\alpha+1}{(\alpha-1)(1-\varepsilon^2c^2)}\eta}(1+o(1)) \quad \text{as} \quad \eta\to+\infty.$$

This yields

$$\xi(\eta)\sim C_6e^{-\frac{\alpha+1}{(\alpha-1)(1-\varepsilon^2c^2)}\eta}+C_7, \quad C_7\in\mathbb{R}.$$

Set

$$\xi_+ := \lim_{\eta\to+\infty}\xi(\eta),$$

then we have

$$\xi_+ = \int_0^{+\infty}\frac{d\xi}{d\eta}d\eta = C_5\int_0^{+\infty}e^{-\frac{\alpha+1}{(\alpha-1)(1-\varepsilon^2c^2)}\eta}d\eta < +\infty.$$

Therefore,

$$\xi_+-\xi\sim Ce^{-\frac{\alpha+1}{(\alpha-1)(1-\varepsilon^2c^2)}\eta} \quad \text{as} \quad \eta\to+\infty$$

holds. Finally, we obtain

$$\begin{aligned}
\phi(\xi) = \frac{x}{\lambda} &= \frac{r^{\alpha+1}\bar{x}}{r^{\alpha-1}} = r^2\overline{x}\\
&= \left\{C_1e^{-\frac{1}{(\alpha-1)(1-\varepsilon^2c^2)}\eta}(1+o(1))\right\}^{2}\cdot\left\{C_2e^{-\frac{2}{1-\varepsilon^2c^2}\eta}(1+o(1))+M_3\right\}\\
&\sim C_8e^{-\frac{2}{(\alpha-1)(1-\varepsilon^2c^2)}\eta}\cdot\left\{C_2e^{-\frac{2}{1-\varepsilon^2c^2}\eta}(1+o(1))+M_3\right\} \quad \text{as} \quad \eta\to+\infty\\
&= C_9e^{-\frac{2\alpha}{(\alpha-1)(1-\varepsilon^2c^2)}\eta}+C_8\cdot M_3\cdot e^{-\frac{2}{(\alpha-1)(1-\varepsilon^2c^2)}\eta}\\
&\sim -Ce^{-\frac{2}{(\alpha-1)(1-\varepsilon^2c^2)}\eta} \quad \text{as} \quad \eta\to+\infty.
\end{aligned}$$

Note that the process here is also different from the process in [31, 33], as we have chosen a more appropriate principal term. Here, in the last relation, since

$$e^{-\frac{2\alpha}{(\alpha-1)(1-\varepsilon^2c^2)}\eta} < e^{-\frac{2}{(\alpha-1)(1-\varepsilon^2c^2)}\eta}$$

is satisfied by $\eta > 0$, we choose the term $e^{-\frac{2}{(\alpha-1)(1-\varepsilon^2c^2)}\eta}$ as $\eta \to +\infty$.

From the above results, we obtain

$$\phi(\xi) \sim -Ce^{-\frac{2}{(\alpha-1)(1-\varepsilon^2c^2)}\eta} \sim -C(\xi_+ - \xi)^{\frac{2}{\alpha+1}} \quad \text{as} \quad \xi \to \xi_+ - 0.$$

Since the trajectories are lying on $\{\phi < 0\}$, it holds that $C > 0$. Similarly, the asymptotic behavior of $\psi(\xi)$ as $\xi \to \xi_+ - 0$ for $1 - \varepsilon^2c^2 > 0$ is also derived. Therefore, we can derive (3.2.1) and (3.2.2). Furthermore, (3.2.3) and (3.2.4) for $1-\varepsilon^2c^2 < 0$ are derived in exactly the same way. This completes the proof. □

Remark 3.4.1
Rewriting the process of deriving the asymptotic behavior in the proof above, we can see that

$$\phi'(\xi) \sim \psi(\xi) \quad \text{as} \quad \xi \to \xi_+ - 0$$

holds. This implies that the first equation in (3.1.5) *also holds in the sense of asymptotic behavior. Since this relation does not hold in the results for Theorem 2 of [31] and Proposition 1 of [33], we believe that this improvement may have improved the accuracy of the asymptotic behavior.*

3.4.2 Proof of Theorem 3.2.2

The proof of existence of the connecting orbits between E_c and E_0^+ in both cases $1-\varepsilon^2c^2 > 0$ and $1 - \varepsilon^2c^2 < 0$ is obtained in Proposition 3.3.1. That is, in the same way as in the proof of Theorem 3.2.1, a family of the functions which corresponds to a family of the orbits of (3.1.5) is shown.

Assume that $1 - \varepsilon^2c^2 > 0$. In this case, all that remains to be shown is to derive (3.2.5). The solutions at the around $e_{c'}$ on the chart $\overline{V}_1$ (matches E_c) have the form

$$\begin{cases} \lambda_\tau \sim C_1e^{-M_7\tau}(1 + o(1)), \\ x_\tau \sim C_2e^{-M_7\tau}(1 + o(1)) + M_7, \end{cases} \qquad M_7 = -\frac{c}{1 - \varepsilon^2c^2},$$

where C_1 and C_2 are constants. Then,

$$\frac{d\tau}{d\xi} = \frac{d\tau}{ds}\frac{ds}{d\xi} = \lambda^{-\alpha}\phi^{-\alpha} = 1$$

holds. This yields

$$\xi(\tau) = \tau + C_3, \quad (C_3 \in \mathbb{R}).$$

We can see $\xi \to -\infty$ as $\tau \to -\infty$. This relationship shows that

$$\tau(\xi) = \xi + C_4, \quad (C_3 \in \mathbb{R})$$

holds. Therefore, we have

$$\begin{aligned} \phi(\xi) &= -\frac{1}{\lambda} \\ &\sim -\left\{ C_1e^{\frac{c}{1-\varepsilon^2c^2}\tau}(1 + o(1)) \right\}^{-1} \\ &\sim -C_5e^{-\frac{c}{1-\varepsilon^2c^2}\tau} \\ &= -Ce^{-\frac{c}{1-\varepsilon^2c^2}\xi} \quad \text{as} \quad \xi \to -\infty \end{aligned}$$

with constants $C_5 > 0$ and $C > 0$. The reason why $C > 0$ ($C_5 > 0$) is the trajectories are lying on $\{\phi < 0\}$. Therefore, (3.2.5) can be derived.

Furthermore, (3.2.6) for $1 - \varepsilon^2c^2 < 0$ are derived in exactly the same way. This completes the proof. □

3.4.3 Proof of Theorem 3.2.3

Assume that $1-\varepsilon^2c^2 > 0$. The existence of the orbits connecting e_0^- and E_0^+ is as described in Proposition 3.3.1 above. Note that the same is true for $1-\varepsilon^2c^2 < 0$. That is, the existence of the orbits connecting E_0^+ and e_0^+ is as described in Proposition 3.3.1 above. As in the previous proofs of the Theorems, this implies the existence of a family of the functions which corresponds to a family of the orbits of (3.1.5).

In this case, all that remains to be shown is to derive (3.2.7). The proof is almost identical to the proof of Theorem 3 in [33]. However, there are some symbols and parts that are different. We briefly reproduce the proof and describe it below for the reader's convenience.

If the initial value is on the center manifold, the solution at around e_0^- on the chart $\overline{V}_1$ has the form

$$\begin{cases} \lambda(\tau) = \sqrt[\alpha+1]{\dfrac{1}{-\dfrac{\alpha+1}{c}\tau - (\alpha+1)\cdot A_0}} = O(\tau^{-\frac{1}{\alpha+1}}), \\ x(\tau) = \dfrac{1}{(\alpha+1)\tau + c(\alpha+1)A_0} + O(\lambda^{2\alpha+2}) = O(\tau^{-1}) \end{cases} \quad \text{as} \quad \tau \to -\infty$$

with a constant A_0. These results are derived (3.3.12) and (3.3.13). We then have

$$\frac{d\tau}{d\xi} = \frac{d\tau}{ds}\frac{ds}{d\xi} = \lambda^{-\alpha}\phi^{-\alpha} = 1.$$

This yields $\tau(\xi) = \xi + \tilde{C}$ with a constant $\tilde{C}$.

If $\tilde{\phi}(\xi)$ is a solution of (3.1.3) (or (3.1.5)), then $\tilde{\phi}(\xi+\theta)$ is also solution for any $\theta \in \mathbb{R}$. Therefore, there exists a solution $\phi(\xi)$ such that the following holds:

$$\phi(\xi) = -\lambda^{-1} \sim O(\tau^{\frac{1}{\alpha+1}}) \sim O(\xi^{\frac{1}{\alpha+1}}) \quad \text{as} \quad \xi \to -\infty.$$

In addition, we can obtain

$$\psi(\xi) = -x\lambda^{-1} \sim -O(\xi^{\frac{1}{\alpha+1}}) \cdot O(\xi^{-1}) = O(\xi^{-\frac{\alpha}{\alpha+1}}) \quad \text{as} \quad \xi \to -\infty.$$

Therefore, (3.2.7) can be derived.

Furthermore, (3.2.8) for $1-\varepsilon^2c^2 < 0$ are derived in exactly the same way. This completes the proof. □

3.4.4 Proof of Theorem 3.2.4

The existence of the orbits connecting $E_{c'}$ and e_0^+ (resp. e_0^-) in the case that $1-\varepsilon^2c^2 > 0$ (resp. $1-\varepsilon^2c^2 < 0$) is as described in Proposition 3.3.1 above. By focusing on $E_{c'}$, (3.2.10) and (3.2.11) can be proved in the same way as Theorem 3.2.2. Furthermore, we assume that $1-\varepsilon^2c^2 > 0$. By focusing on e_0^+, (3.2.9) can be proved in the same way as Theorem 3.2.3. Similarly, by focusing on e_0^- when $1-\varepsilon^2c^2 < 0$, we obtain (3.2.12). This completes the proof. □

3.5 Concluding remarks

The general MEMS type equation is a combination of hyperbolic and parabolic equations as shown in (3.1.1). In addition, the reaction-diffusion equation with $\varepsilon = 0$ is often

considered for convenience of analysis and comparison. In this chapter, we studied the existence, information about the shapes, and the asymptotic behavior of traveling waves with the singularity of equation (3.1.1) by adding $\varepsilon^2 u_{tt}$ to the left-hand side of the equation treated in [31]. Furthermore, by reviewing the process of deriving the asymptotic behavior obtained in Theorem 2 of [31] and Proposition 1 of [33], and by carefully selecting the principal terms, we were able to obtain a better asymptotic behavior than these results (see Remark 3.4.1). Even if we add $\varepsilon^2 u_{tt}$, the asymptotic behavior obtained by improving the derivation process does not change, and the condition for the wave speed with respect to the shape, which did not appear in [31], is obtained. In other words, the existence of this term and its coefficients have a significant effect on the wave speed and the shapes of the traveling waves. These are studied by applying the framework that combines Poincaré compactification, classical dynamical systems theory, and geometric methods for the desingularization of vector fields.

Since the addition of this term changes the type of the equation from parabolic to hyperbolic, a rigorous discussion of the mathematical formulation of the solution is necessary. As previously mentioned, since the emphasis of this chapter is on discussing how the behavior of traveling waves changes from the viewpoint of dynamical systems, we do not discuss it here and leave it for future work.

Chapter 4

Radial symmetric stationary solutions for a MEMS type reaction-diffusion equation with spatially dependent nonlinearity

Abstract

We consider the radial symmetric stationary solutions of $u_t = \Delta u - |x|^q u^{-p}$. We first give a result on the existence of the negative value functions that satisfy the radial symmetric stationary problem on a finite interval for $p \in 2\mathbb{N}$, $q \in \mathbb{R}$. Moreover, we give the asymptotic behavior of $u(r)$ and $u'(r)$ at both ends of the finite interval. Second, we obtain the existence of the positive radial symmetric stationary solutions with the singularity at $r = 0$ for $p \in \mathbb{N}$ and $q \geq -2$. In fact, the behavior of solutions for $q > -2$ and $q = -2$ are different. In each case of $q = -2$ and $q > -2$, we derive the asymptotic behavior for $r \to 0$ and $r \to \infty$. These facts are studied by applying the Poincaré compactification and basic theory of dynamical systems. This chapter is based on the following published paper ([33]):

> Ichida, Y., Sakamoto, T.O.: Radial symmetric stationary solutions for a MEMS type reaction-diffusion equation with spatially dependent nonlinearity, Jpn. J. Ind. Appl. Math. **38**, no. 1, 297–322 (2021).

4.1 Introduction

In this chapter, we consider the following MEMS type reaction-diffusion equation

$$u_t = \Delta u - |x|^q u^{-p}, \quad t > 0, \quad x \in \mathbb{R}^n, \tag{4.1.1}$$

with $3 \leq n \in \mathbb{N}$, $p \in \mathbb{N}$ and $q \in \mathbb{R}$. This equation arises in the study of the dynamic deflection of an elastic membrane inside a micro-electro mechanical system (MEMS).

In the case of one-dimensional space, the function u represents the distance between the membrane and the fixed bottom plate. The function $|x|^q$ is a particular choice of the permittivity profile (the dielectric property of the membrane) (for instance see [27] and references therein). Guo-Morita-Yotsutani [27] studied the self-similar solutions for one-dimensional case of (4.1.1). It was proved the existence of backward solutions and given a detailed analysis of the behavior of global solutions at the origin.

There have been a lot of research in the MEMS equation recently, especially, touchdown (quenching) phenomena (see [15, 16] and references therein). Further, we refer the readers to works [17, 59] and references therein for more details on the background and derivation of the MEMS model.

We study the stationary solutions of (4.1.1), namely we consider the following equation:

$$\Delta u - |x|^q u^{-p} = 0, \quad x \in \mathbb{R}^n.$$

This chapter is devoted to the study of the radial symmetric stationary solution of (4.1.1). That is, we study the following equation (the radial symmetric stationary problem):

$$u'' + \frac{n-1}{r}u' - r^q u^{-p} = 0, \quad ' = \frac{d}{dr}, \tag{4.1.2}$$

where $r = |x| > 0$.

From the results in [41], asymptotic behavior of the radial solutions and uniqueness of singular ground states for a reaction-diffusion equation with spatially dependent nonlinearity are proved by applying the invariant manifold theory of dynamical systems. More precisely, it was devoted to the study of positive solutions of semilinear elliptic equation

$$\Delta u + K(|x|)u^\ell = 0, \quad x \in \mathbb{R}^n \tag{4.1.3}$$

for $\dfrac{n+2}{n-2} < \ell \in \mathbb{R}$, $n \geq 3$, where $K(|x|)$ satisfies some conditions. They studied the existence of the radial symmetric stationary solutions of (4.1.3) and detailed information about the asymptotic behavior of them. Further, we note that our problem corresponds to (4.1.3) in the case that $K(|x|) = -|x|^q$ and $0 > \ell\,(= -p) \in \mathbb{Z}$.

As in [41], we introduce the following change of variables:

$$t = \log r, \quad a(t) = r^{-\alpha}u(r), \quad \alpha := (q+2)/(p+1). \tag{4.1.4}$$

Then, (4.1.2) is transformed into the following:

$$\ddot{a} + (2\alpha + n - 2)\dot{a} + \alpha(\alpha + n - 2)a - a^{-p} = 0, \quad \left(\dot{} = \frac{d}{dt} \text{ and } \ddot{} = \frac{d^2}{dt^2} \right). \tag{4.1.5}$$

Since $r \to \infty$ as $t = \log r \to \infty$, to discuss the asymptotic behavior of the solutions for (4.1.2) as $r \to \infty$, we study that of the solutions for (4.1.5) as $t \to \infty$. Similarly, to discuss the asymptotic behavior for $r \to 0$, we consider the following change of variables:

$$t = -\log r, \quad a(t) = r^{-\alpha}u(r), \quad \alpha := (q+2)/(p+1). \tag{4.1.6}$$

Then, we have

$$\ddot{a} - (2\alpha + n - 2)\dot{a} + \alpha(\alpha + n - 2)a - a^{-p} = 0. \tag{4.1.7}$$

In order to study the solutions for (4.1.5) and (4.1.7), we consider the dynamics of the following ordinary differential equation

$$\ddot{a} + A\dot{a} + Ba - a^{-p} = 0$$

or equivalently,

$$\begin{cases} \dot{a} = b, \\ \dot{b} = -Ab - Ba + a^{-p}, \end{cases} \tag{4.1.8}$$

where

$$A = \delta(2\alpha + n - 2), \quad B = \alpha(\alpha + n - 2) \quad \text{and} \quad \delta = \pm 1.$$

We set

$$p^* := -2 - (n-2)(p+1) \quad \text{and} \quad p_* := -2 - \frac{1}{2}(n-2)(p+1).$$

Then, the sign of the constants A and B depend on the parameters q and δ as shown in Table 4.1.

δ	A or B	$q < p^*$	$q = p^*$	$p^* < q < p_*$	$p_* < q < -2$	$q = -2$	$q > -2$
1	A	$-$	$-$	$-$	$+$	$+$	$+$
1	B	$+$	0	$-$	$-$	0	$+$
-1	A	$+$	$+$	$+$	$-$	$-$	$-$
-1	B	$+$	0	$-$	$-$	0	$+$

Table 4.1: The sign of A and B.

We can see that there are the ranges of parameter q such that A and B attain the same sign on both of them. For instance, $\mathrm{sign}(A, B) = (+, +)$ holds for $q > -2, \delta = 1$ and $q < p^*$, $\delta = -1$.

The dynamical system approach works well to the equation (4.1.3) as shown in [41]. Similarly, we expect that it works well for our problem (4.1.8). However, the negative powers nonlinear term a^{-p} could induce the singularity in finite time (see [49, 50]). Therefore, we apply the Poincaré compactification (see Section 1.1) to the dynamical system of (4.1.8) to obtain the detailed information of the solutions for (4.1.2). Then, the following three theorems are main results of this chapter:

Theorem 4.1.1
Assume that $n \geq 3$, $p \in 2\mathbb{N}$ and $q \in \mathbb{R}$. Then, there exists a family of the functions (which corresponds to a family of the orbits of (4.1.8)) defined on the finite intervals such that each function $u(r)$ satisfies equation (4.1.2) on a finite interval (r_-, r_+) $(0 < r_- < r_+ < +\infty)$. Moreover, for each function $u(r)$, the followings hold:

- $\begin{cases} \lim\limits_{r \to r_+ - 0} u(r) = 0, & \lim\limits_{r \to r_- + 0} u(r) = 0, \\ \lim\limits_{r \to r_+ - 0} u'(r) = \infty, & \lim\limits_{r \to r_- + 0} u'(r) = -\infty. \end{cases}$
- *$u(r) < 0$ holds for $r \in (r_-, r_+)$.*
- *There exists a constant $r_* \in (r_-, r_+)$ such that the following holds: $u'(r) < 0$ for $r \in (r_-, r_*)$, $u'(r_*) = 0$ and $u'(r) > 0$ for $r \in (r_*, r_+)$.*

In addition, asymptotic behavior for $r \to r_- + 0$ and $r \to r_+ - 0$ are

$$\begin{cases} u(r) \sim -Cr^\alpha (\log r_+ - \log r)^{\frac{2}{p+1}}, \\ u'(r) \sim -C\alpha r^{\alpha-1} (\log r_+ - \log r)^{\frac{2}{p+1}} + Cr^\alpha \left(\log r_+ - \log r\right)^{-\frac{p-1}{p+1}}, \end{cases} \quad \text{as} \quad r \to r_+ - 0 \tag{4.1.9}$$

and

$$\begin{cases} u(r) \sim -Cr^\alpha (-\log r_- + \log r)^{\frac{2}{p+1}}, \\ u'(r) \sim -C\alpha r^{\alpha-1} (-\log r_- + \log r)^{\frac{2}{p+1}} - Cr^\alpha \left(-\log r_- + \log r\right)^{-\frac{p-1}{p+1}}, \end{cases} \quad \text{as} \quad r \to r_- + 0 \tag{4.1.10}$$

with $C > 0$.

Remark 4.1.1
In Theorem 4.1.1, each function $u(r)$ satisfies (4.1.2) only on the finite interval. In this chapter, we do not discuss the behavior of the functions of (4.1.2) after $u'(r)$ becomes infinity. It is necessary that more detailed (and hard) analysis in order to study the functions after $u'(r)$ blows up, and so we leave it open here. Asymptotic behaviors for both $u(r)$ and $u'(r)$ that are more accurate than in [33] were obtained after publication of the paper. Note that this was obtained by refining the asymptotic form, as will be discussed later in the proof.

Theorem 4.1.2
Assume that $n \geq 3$, $p \in \mathbb{N}$ and $q > -2$. Then the equation (4.1.2) has a family of positive radial symmetric stationary solutions (which corresponds to a family of the orbits of (4.1.8)) with the singularity at $r = 0$. Moreover, each solution $u(r)$ satisfies the followings:

- $\lim_{r\to 0} u(r) = +\infty, \quad \lim_{r\to+\infty} u(r) = +\infty.$
- *$u(r) > 0$ holds for $r \in (0, +\infty)$.*

In addition, asymptotic behavior of $u(r)$ are

$$u(r) \sim Cr^{2-n} \quad \text{as} \quad r \to 0$$

with $C > 0$ and for $r \to +\infty$, the following holds:

$$u(r) \sim \begin{cases} C_1 r^{\alpha+\sigma_1} + C_2 r^{\alpha+\sigma_2} + r^{\alpha} B^{\frac{-1}{p+1}}, & (F > 0), \\ C_1 r^{\alpha+\sigma} \log r + (C_2 + C_3) r^{\alpha+\sigma} + r^{\alpha} B^{\frac{-1}{p+1}}, & (F = 0), \\ r^{\alpha} B^{\frac{-1}{p+1}} + r^{\frac{2-n}{2}} \left(C_4 \cdot [\sin \frac{\sqrt{|D|}}{2} \log r] + C_5 \cdot [\cos \frac{\sqrt{|D|}}{2} \log r] \right), & (F < 0), \end{cases}$$

where C_j are constants, and

$$\sigma_1 = \frac{-A + \sqrt{D}}{2}, \quad \sigma_2 = \frac{-A - \sqrt{D}}{2}, \quad \sigma = -\frac{A}{2}, \quad D = \frac{F}{(p+1)^2},$$

with

$$F = (n-2)^2(p+1)^2 + 4p(q+2)\{-q - 2 - (n-2)(p+1)\}.$$

Here it should be noted that for $F < 0$, we can observe that $u(r)$ go to infinity with damping oscillatory terms.

Theorem 4.1.3
Assume that $n \geq 3$, $p \in \mathbb{N}$ and $q = -2$. Then the equation (4.1.2) has a family of positive radial symmetric stationary solutions (which corresponds to a family of the orbits of (4.1.8)) with the singularity at $r = 0$. Moreover, each solution $u(r)$ satisfies the followings:

- $\lim_{r\to 0} u(r) = +\infty, \quad \lim_{r\to+\infty} u(r) = +\infty.$
- *$u(r) > 0$ holds for $r \in (0, +\infty)$.*

In addition, asymptotic behavior for $r \to +\infty$ and $r \to 0$ are

$$\begin{aligned} u(r) &\sim O(\{\log r\}^{\frac{1}{p+1}}) \quad \text{as} \quad r \to +\infty, \\ u(r) &\sim Cr^{2-n} \quad \text{as} \quad r \to 0 \end{aligned}$$

with $C > 0$.

For the case that $q = -2$, we refer to [31] for the proof of Theorem 4.1.1 except the asymptotic behavior (they will be discussed in Section5).

We note that the equation dealt with in the chapter [31] is actually a special case of the MEMS type equation (4.1.1). More precisely, we studied the following equation:

$$u_t = u_{xx} + (1-u)^{-p}, \quad t > 0, \quad x \in \mathbb{R}, \quad p \in \mathbb{N}. \tag{4.1.11}$$

Here we see the relationship between (4.1.8) and (4.1.11) as follows. Substituting $v(t,x) = 1 - u(t,x)$ into (4.1.11), we have

$$v_t = v_{xx} - v^{-p}$$

and it gives (4.1.1) with $n = 1$ and $q = 0$. We then consider the quasi traveling waves with quenching (see [31] for the definition) of the above equation by introducing the following change of variables:

$$a(\xi) = v(t,x), \quad \xi = x - ct, \quad c > 0.$$

The function $a(\xi)$ satisfies the following equation:

$$a'' + ca' - a^{-p} = 0, \quad \xi \in \mathbb{R}, \quad ' = \frac{d}{d\xi},$$

or

$$\begin{cases} a' = b, \\ b' = -cb + a^{-p}. \end{cases} \tag{4.1.12}$$

This equation agrees with (4.1.8) ($A = c$ and $B = 0$). We then note that results in [31] are included in Theorem 4.1.1.

Further, let us consider the radial symmetric problem of the multi-dimensional version of (4.1.11) with spatially dependent nonlinearity:

$$w_t = \Delta w + \frac{|x|^q}{(1-w)^p}, \quad t > 0, \quad x \in \mathbb{R}^n, \tag{4.1.13}$$

that is,

$$w'' + \frac{n-1}{r} w' + \frac{r^q}{(1-w)^p} = 0, \quad r > 0. \tag{4.1.14}$$

In the case that $q = 0$ of (4.1.13) is strictly corresponding to the multi-dimensional version of (4.1.11). Then, we can see that the equation (4.1.14) is equivalent to (4.1.2) with $u(r) = 1 - w(r)$. Therefore, the function $u(r)$ obtained in Theorem 4.1.1 gives a positive function $w(r) = 1 - u(r) \geq 1$ that satisfies (4.1.14) on a finite interval and $|w'(r)|$ goes to infinity at both ends of the interval.

It should be noted again that (4.1.12) has a singularity in finite time, that is, $a'(\xi)$ blows up in finite time. From the viewpoint of the dynamical system approach, as shown in [31], such solution corresponds to an orbit which goes to $(\pm\infty, 0)$ on $\mathbb{R}^2 \ni (a,b)$ in finite time. In this chapter, we show that the similar approach works well and give the information for the radial symmetric stationary solutions of (4.1.1) as stated in main Theorems.

Indeed, we obtain whole phase portrait of (4.1.8) on $\mathbb{R}^2 \cup \{\|(a,b)\| = \infty\}$ in the latter section. Then each orbit should correspond to a function satisfying (4.1.2) on an interval ($r \in$)$I \subseteq [0,\infty)$. Therefore, if it is possible to classify all orbits and compute the asymptotic behavior for each class of orbits, we can classify all solutions for (4.1.2).

As we will note in Section 4.6, there are orbits for that we cannot obtain the asymptotic behavior in this chapter. However, in authors knowledge, there has been no studies of

(4.1.2) with dynamical system approach, therefore, our results will give first step for the studies of (4.1.2) from the viewpoint of geometric (dynamical system) approach.

This chapter is organized as follows. In the next section, we study the dynamics near the finite equilibria of (4.1.8). In Section 4.3, we obtain the dynamics of (4.1.8) with $p \in 2\mathbb{N}$ on the Poincaré disk via Poincaré compactification and basic theory of the dynamical systems. Section 4.4 is devoted to showing the phase portraits of (4.1.8) on the Poincaré disk in the case that p is odd. In Section 4.5, the asymptotic behavior of the trajectories that corresponding to the function satisfying (4.1.2) on the finite interval or $(0, \infty)$ and the proofs of Theorems will be completed. Section 4.6 is devoted to the conclusions and remarks.

4.2 Dynamics near finite equilibria of (4.1.8)

Before starting the detailed analysis, we study the dynamics near finite equilibrium of (4.1.8). This gives a demonstration to see the relationship between the dynamics of (4.1.8) and asymptotic behavior of the solutions for (4.1.2). If $B \neq 0$ and p is even (resp. p is odd), then (4.1.8) has an equilibrium $E_B : (a, b) = (B^{\frac{-1}{p+1}}, 0)$ (resp. have the equilibria $\pm E_B : (a, b) = (\pm B^{\frac{-1}{p+1}}, 0)$).

Let J be the Jacobian matrix of the vector field (4.1.8) at E_B. Then, the behavior of the solution around E_B is different by the sign of F (which is defined in Theorem 4.1.2). For instance, the matrix J has the real distinct eigenvalues if $F > 0$ and other cases can be concluded similarly. In addition, if $n \geq 3$, $q > -2$ and $\delta = 1$, then the real part of all eigenvalues of J are negative. Even in cases other than $q > -2$, we can similarly determine the stability of the equilibrium E_B. Then, the stabilities of the equilibrium E_B are obtained as in Table 4.2.

E_B	$q < p^*$	$q = p^*$	$p^* < q < -2$	$q = -2$	$q > -2$
$\delta = 1$	source	–	saddle	–	sink
$\delta = -1$	sink	–	saddle	–	source

Table 4.2: The stabilities of the equilibrium E_B.

Remark 4.2.1
The equilibrium E_B does not exist in the case that $q = -2$ and $q = p^*$.

Therefore, we can obtain the asymptotic behavior of $u(r)$ for $r \to +\infty$ in Theorem 4.1.2 by considering the asymptotic dynamics near E_B via (4.1.4) or (4.1.6) (see Section 4.5 for more details).

4.3 Dynamics on the Poincaré disk of (4.1.8) : p is even

In order to study the dynamics of (4.1.8) on the Poincaré disk, we desingularize it by the time-scale desingularization

$$ds/dt = \{a(t)\}^{-p} \quad \text{for} \quad p \in 2\mathbb{N}. \tag{4.3.1}$$

Since we assume that p is even, the direction of the time does not change via this desingularization. Then, we have

$$\begin{cases} a' = a^p b, \\ b' = -Aa^p b - Ba^{p+1} + 1, \end{cases} \qquad \left(' = \frac{d}{ds}\right). \tag{4.3.2}$$

In this section, we only discuss the case that p is even. The odd case is discussed in the next section.

It should be noted that the time scale desingularization (4.3.1) is simply multiplying the vector field by a^p. Then, except the singularity $\{a = 0\}$, the solution curves of the system (vector field) remain the same but are parameterized differently. Still, we refer to Section 7.7 of [44] and references therein for the analytical treatments of desingularization with the time rescaling. In what follows, we use the similar time rescaling (re-parameterization of the solution curves) repeatedly to desingularize the vector fields.

Now we can consider the dynamics of (4.3.2) on the charts $\overline{U}_j$ and $\overline{V}_j$.

4.3.1 Dynamics on the chart $\overline{U}_2$

To obtain the dynamics on the chart $\overline{U}_2$, we introduce coordinates (λ, x) by the formulas

$$a(s) = x(s)/\lambda(s), \quad b(s) = 1/\lambda(s).$$

Then, we have

$$\begin{cases} \lambda' = Ax^p\lambda^{1-p} + Bx^{p+1}\lambda^{1-p} - \lambda^2, \\ x' = x^p\lambda^{-p} + Ax^{p+1}\lambda^{-p} + Bx^{p+2}\lambda^{-p} - x\lambda. \end{cases}$$

Time-scale desingularization $d\tau/ds = \lambda(s)^{-p}$ yields

$$\begin{cases} \lambda_\tau = Ax^p\lambda + Bx^{p+1}\lambda - \lambda^{p+2}, \\ x_\tau = x^p + Ax^{p+1} + Bx^{p+2} - x\lambda^{p+1}, \end{cases} \tag{4.3.3}$$

where $\lambda_\tau = d\lambda/d\tau$ and $x_\tau = dx/d\tau$. When the parameter q is other than $q = p^*$, $q = -2$, the system (4.3.3) has the equilibria

$$E_0^+ : (\lambda, x) = (0, 0),$$

$$E_1 : (\lambda, x) = \left(0, \frac{-A - (n-2)}{2B}\right) \quad \text{and} \quad E_2 : (\lambda, x) = \left(0, \frac{-A + (n-2)}{2B}\right).$$

The Jacobian matrices of the vector field (4.3.3) at these equilibria are

$$E_0^+ : \begin{pmatrix} 0 & 0 \\ 0 & 0 \end{pmatrix}, \quad E_1 : \begin{pmatrix} \left(\frac{-A-(n-2)}{2B}\right)^p \frac{A-(n-2)}{2} & 0 \\ 0 & \left(\frac{-A-(n-2)}{2B}\right)^{p-1} \frac{(n-2)(n-2+A)}{2B} \end{pmatrix},$$

$$E_2 : \begin{pmatrix} \left(\frac{-A+(n-2)}{2B}\right)^p \frac{A+(n-2)}{2} & 0 \\ 0 & \left(\frac{-A+(n-2)}{2B}\right)^{p-1} \frac{(n-2)(n-2-A)}{2B} \end{pmatrix}.$$

Therefore, the stabilities of the equilibria E_1 and E_2 are determined as shown in Table 4.3.

E_1	$q < p^*$	$p^* < q < -2$	$q > -2$
$\delta = 1$	sink	sink	saddle
$\delta = -1$	saddle	sink	sink
E_2	$q < p^*$	$p^* < q < -2$	$q > -2$
$\delta = 1$	saddle	source	source
$\delta = -1$	source	source	saddle

Table 4.3: The stabilities of the equilibria E_1 and E_2.

If $q = p^*$ and $q = -2$, then the system (4.3.3) has the equilibria

$$E_0^+ : (\lambda, x) = (0, 0) \quad \text{and} \quad E_c : (\lambda, x) = (0, -[1/\delta(n-2)]).$$

The Jacobian matrices of the vector field (4.3.3) at these equilibria are

$$E_0^+ : \begin{pmatrix} 0 & 0 \\ 0 & 0 \end{pmatrix} \quad \text{and} \quad E_c : \begin{pmatrix} \delta(n-2)^{1-p} & 0 \\ 0 & \delta(n-2)^{1-p} \end{pmatrix}.$$

In the case that $q = -2$, if $\delta = 1$ (resp. $\delta = -1$), then E_c is a source (resp. sink). We note that $A < 0$ and $B = 0$ hold in both cases of $q = -2$ and $q = p^*$ (see Table 4.1).

The equilibrium E_0^+ is not hyperbolic for $q \in \mathbb{R}$. Therefore, to determine the dynamics near E_0^+, we desingularize E_0^+ by introducing the following blow-up coordinates:

$$\lambda = \varepsilon^{p-1}\bar{\lambda}, \quad x = \varepsilon^{p+1}\bar{x}$$

(see Section 1.2 of this thesis and Section 3 of [14] for the desingularizations of vector fields by the blow-up). Since we are interested in the dynamics on the Poincaré disk, we consider the dynamics of blow-up vector fields on the charts $\{\bar{\lambda} = 1\}$ and $\{\bar{x} = \pm 1\}$. We note that they are independent of $q \in \mathbb{R}$.

Dynamics on the chart $\{\bar{\lambda} = 1\}$

By the change of coordinates $\lambda = \varepsilon^{p-1}$, $x = \varepsilon^{p+1}\bar{x}$, we have

$$\begin{cases} \varepsilon_\tau = (p-1)^{-1}(A\varepsilon^{p^2+p+1}\bar{x}^p + B\varepsilon^{p^2+2p+2}\bar{x}^{p+1} - \varepsilon^{p^2}), \\ \bar{x}_\tau = 2(p-1)^{-1}(-A\varepsilon^{p^2+p}\bar{x}^{p+1} - B\varepsilon^{p^2+2p+1}\bar{x}^{p+2} + \varepsilon^{p^2-1}\bar{x}) + \varepsilon^{p^2-1}\bar{x}^p. \end{cases}$$

The time-rescaling $d\eta/d\tau = \varepsilon(\tau)^{p^2-1}$ yields

$$\begin{cases} \varepsilon_\eta = (p-1)^{-1}(A\varepsilon^{p+2}\bar{x}^p + B\varepsilon^{2p+3}\bar{x}^{p+1} - \varepsilon), \\ \bar{x}_\eta = 2(p-1)^{-1}(-A\varepsilon^{p+1}\bar{x}^{p+1} - B\varepsilon^{2p+2}\bar{x}^{p+2} + \bar{x}) + \bar{x}^p. \end{cases} \tag{4.3.4}$$

The equilibria of (4.3.4) on $\{\varepsilon = 0\}$ are

$$\overline{E}_0^+ : (\varepsilon, \bar{x}) = (0, 0), \quad \overline{E}_p^+ : (\varepsilon, \bar{x}) = \left(0, [-2/(p-1)]^{\frac{1}{p-1}}\right).$$

Here it should be noted that since $\overline{x}(\eta)$ is real valued, $[-2/(p-1)]^{\frac{1}{p-1}}$ denotes the real solution of the equation: $2(p-1)^{-1} + \overline{x}^{p-1} = 0$. The Jacobian matrices of the vector fields (4.3.4) at these equilibria are

$$\overline{E}_0^+ : \begin{pmatrix} -\dfrac{1}{p-1} & 0 \\ 0 & \dfrac{2}{p-1} \end{pmatrix} \quad \text{and} \quad \overline{E}_p^+ : \begin{pmatrix} -\dfrac{1}{p-1} & 0 \\ 0 & -2 \end{pmatrix}.$$

Therefore, $\overline{E}_0^+$ is a saddle, and $\overline{E}_p^+$ is a sink.

Moreover, since $|1/(p-1)| < 2$ holds, trajectories near $\overline{E}_p^+$ are tangent to $\{\bar{x} = [-2/(p-1)]^{\frac{1}{p-1}}, \varepsilon \geq 0\}$ as $\eta \to +\infty$. The solutions are approximated as

$$\varepsilon(\eta) \sim C_1 e^{-\frac{1}{p-1}\eta}(1 + o(1)), \tag{4.3.5}$$

$$\bar{x}(\eta) \sim C_2 e^{-2\eta}(1 + o(1)) + A, \quad A = \left(-\frac{2}{p-1}\right)^{\frac{1}{p-1}}. \tag{4.3.6}$$

Dynamics on the chart $\{\bar{x} = -1\}$

By the change of coordinates $\lambda = \varepsilon^{p-1}\bar{\lambda}$, $x = -\varepsilon^{p+1}$, and time-rescaling $d\eta/d\tau = \varepsilon(\tau)^{p^2-1}$, we have

$$\begin{cases} \varepsilon_\eta = -(p+1)^{-1}(\varepsilon - A\varepsilon^{p+2} + B\varepsilon^{2p+3} + \varepsilon\bar{\lambda}^{p+1}), \\ \bar{\lambda}_\eta = (p-1)(p+1)^{-1}\bar{\lambda} + 2(p+1)^{-1}(A\varepsilon^{p+1}\bar{\lambda} - B\varepsilon^{2p+2}\bar{\lambda} - \bar{\lambda}^{p+2}). \end{cases}$$

The equilibria on $\{\varepsilon = 0\}$ are

$$(\varepsilon, \bar{\lambda}) = (0,0), \quad (\varepsilon, \bar{\lambda}) = \left(0, [(p-1)/2]^{\frac{1}{p+1}}\right).$$

By the further computations, we can see that $(0,0)$ is a saddle, and $(0, [(p-1)/2]^{\frac{1}{p+1}})$ is a sink.

Dynamics on the chart $\{\bar{x} = 1\}$

The change of coordinates $\lambda = \varepsilon^{p-1}\bar{\lambda}$, $\quad x = \varepsilon^{p+1}$, and time-rescaling $d\eta/d\tau = \varepsilon(\tau)^{p^2-1}$ yield

$$\begin{cases} \varepsilon_\eta = (p+1)^{-1}(\varepsilon + A\varepsilon^{p+2} + B\varepsilon^{2p+3} - \varepsilon\bar{\lambda}^{p+1}), \\ \bar{\lambda}_\eta = -(p-1)(p+1)^{-1}\bar{\lambda} + 2(p+1)^{-1}(A\varepsilon^{p+1}\bar{\lambda} + B\varepsilon^{2p+2}\bar{\lambda} - \bar{\lambda}^{p+2}). \end{cases}$$

The equilibrium on $\{\varepsilon = 0, \bar{\lambda} \geq 0\}$ is $(0,0)$. Eigenvalues of the linearized matrix are $(p+1)^{-1}$ and $-(p-1)/(p+1)$ with corresponding eigenvectors $(1,0)$ and $(0,1)$, respectively. Therefore, $(\varepsilon, \bar{\lambda}) = (0,0)$ on the chart $\{\bar{x} = 1\}$ is a saddle.

Combining the dynamics on the charts $\{\bar{\lambda} = 1\}$ and $\{\bar{x} = \pm 1\}$, we obtain the dynamics on $\overline{U}_2$ (see Figure 4.3.1).

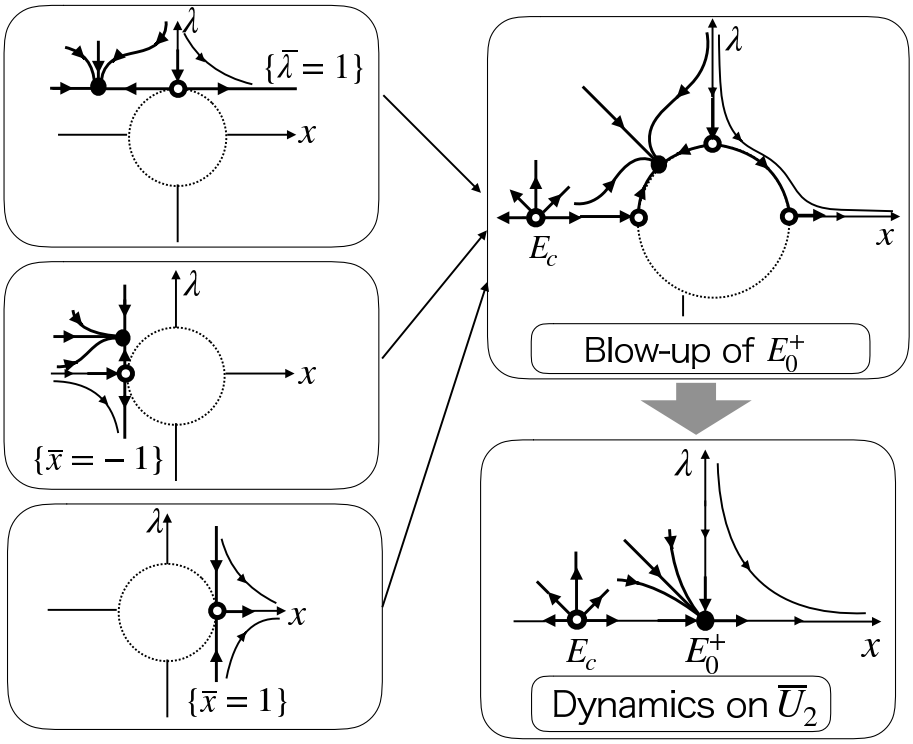

Figure 4.3.1: Schematic pictures of the dynamics of the blow-up vector fields and $\overline{U}_2$ in the case that $n \geq 3$, $p \in 2\mathbb{N}$, $q = -2$ and $\delta = 1$.

4.3.2 Dynamics on the chart $\overline{V}_2$

The change of coordinates

$$a(s) = -x(s)/\lambda(s), \quad b(s) = -1/\lambda(s)$$

give the projected dynamics of (4.3.2) on the chart $\overline{V}_2$:

$$\begin{cases} \lambda_\tau = Ax^p\lambda + Bx^{p+1}\lambda + \lambda^{p+2}, \\ x_\tau = x^p + Ax^{p+1} + Bx^{p+2} + x\lambda^{p+1}, \end{cases} \tag{4.3.7}$$

where τ is the new time introduced by $d\tau/ds = \lambda(s)^{-p}$. The system (4.3.7) can be transformed into (4.3.3) by the change of coordinates $(\lambda, x) \mapsto (-\lambda, x)$. Therefore, it is sufficient to consider the blow-up of singularity $E_0^- : (\lambda, x) = (0, 0)$ by the formulas

$$\lambda = \varepsilon^{p-1}\bar{\lambda}, \quad x = \varepsilon^{p+1}\bar{x} \quad \text{with} \quad \bar{\lambda} = 1.$$

Then, we have

$$\begin{cases} \varepsilon_\eta = (p-1)^{-1}(A\varepsilon^{p+2}\bar{x}^p + B\varepsilon^{2p+3}\bar{x}^{p+1} + \varepsilon), \\ \bar{x}_\eta = 2(p-1)^{-1}(-A\varepsilon^{p+1}\bar{x}^{p+1} - B\varepsilon^{2p+2}\bar{x}^{p+2} - \bar{x}) + \bar{x}^p. \end{cases} \tag{4.3.8}$$

where η satisfies $d\eta/d\tau = \{\varepsilon(\tau)\}^{p^2-1}$. The equilibria of (4.3.8) on $\{\varepsilon = 0\}$ are

$$\overline{E}_0^- : (\varepsilon, \bar{x}) = (0, 0), \quad \overline{E}_p^- : (\varepsilon, \bar{x}) = \left(0, [2/(p-1)]^{\frac{1}{p-1}}\right).$$

The equilibrium $\overline{E}_0^-$ is a saddle with the eigenvalues $(p-1)^{-1}$ and $-2(p-1)^{-1}$ whose corresponding eigenvectors are $(1, 0)$ and $(0, 1)$, respectively. Further, $\overline{E}_p^-$ is a source with the eigenvalues $(p-1)^{-1}$ and 2 whose corresponding eigenvectors are $(1, 0)$ and $(0, 1)$, respectively.

4.3.3 Dynamics on the chart $\overline{U}_1$

Let us study the dynamics on the chart $\overline{U}_1$. The transformations

$$a(s) = 1/\lambda(s), \quad b(s) = x(s)/\lambda(s)$$

yield

$$\begin{cases} \lambda_\tau = -x\lambda, \\ x_\tau = -Ax - B + \lambda^{p+1} - x^2, \end{cases} \tag{4.3.9}$$

via time-rescaling $d\tau/ds = \{\lambda(s)\}^{-p}$. If $q < p^*$ and $q > -2$ hold, then the system (4.3.9) has the equilibria

$$E_B : (\lambda, x) = (B^{\frac{-1}{p+1}}, 0),$$

$$E_3 : (\lambda, x) = \left(0, \frac{-A-(n-2)}{2}\right) \quad \text{and} \quad E_4 : (\lambda, x) = \left(0, \frac{-A+(n-2)}{2}\right).$$

The stabilities of the equilibrium E_B are same as Table 4.2. If $p^* < q < -2$, then the system (4.3.9) has only the equilibria E_3 and E_4.

The Jacobian matrices of the vector field (4.3.9) at these equilibria are

$$E_3 : \begin{pmatrix} \frac{A+(n-2)}{2} & 0 \\ 0 & n-2 \end{pmatrix}, \quad \text{and} \quad E_4 : \begin{pmatrix} \frac{A-(n-2)}{2} & 0 \\ 0 & -(n-2) \end{pmatrix}.$$

Therefore, the stabilities of the equilibria E_3 and E_4 are determined as shown in Table 4.4 with corresponding the equilibria E_2 and E_1, respectively.

E_3	$q < p^*$	$p^* < q < -2$	$q > -2$
$\delta = 1$	saddle	source	source
$\delta = -1$	source	source	saddle
E_4	$q < p^*$	$p^* < q < -2$	$q > -2$
$\delta = 1$	sink	sink	saddle
$\delta = -1$	saddle	sink	sink

Table 4.4: The stabilities of the equilibrium E_3 and E_4.

The solutions at E_4 are approximated as

$$\begin{cases} \lambda(\tau) \sim Ce^{\frac{A-(n-2)}{2}\tau}(1+o(1)), \\ x(\tau) \sim Ce^{-(n-2)\tau}(1+o(1)) + \dfrac{-A+(n-2)}{2}. \end{cases}$$

These results will be used to prove Theorem 4.1.2.

If $q = p^*$ or $q = -2$, then the system (4.3.9) has the equilibria

$$E_0 : (\lambda, x) = (0,0) \quad \text{and} \quad E_c : (\lambda, x) = (0, -\delta(n-2)).$$

The Jacobian matrices of the vector field (4.3.9) at these equilibria are

$$E_0 : \begin{pmatrix} 0 & 0 \\ 0 & -\delta(n-2) \end{pmatrix}, \quad E_c : \begin{pmatrix} \delta(n-2) & 0 \\ 0 & \delta(n-2) \end{pmatrix}.$$

In the case that $q = -2$, if $\delta = 1$ (resp. $\delta = -1$), then E_c is a source (resp. sink). Note that if $q = -2$ (resp. $q = p^*$), then $\mathrm{sign}(A, B) = (\pm, 0)$ holds for $\delta = \pm 1$ (resp. $\delta = \mp 1$) (see Table 4.1).

The solutions at E_c are approximated as

$$\begin{cases} \lambda(\tau) \sim Ce^{(2-n)\tau}(1+o(1)), \\ x(\tau) \sim Ce^{(2-n)\tau}(1+o(1)) + (n-2). \end{cases}$$

These results will be used to prove Theorem 4.1.3.

Then, the center manifold theory is applicable to study the dynamics near $(0,0)$ (for instance, see [9]). It implies that there exists a function $h(\lambda)$ satisfying

$$h(0) = \frac{dh}{d\lambda}(0) = 0$$

such that the center manifold of (4.3.9) is represented as $\{(\lambda, x) \,|\, x = h(\lambda)\}$ near $(0,0)$. We shall recall $B = 0$ holds in both cases of $q = -2$ and $q = p^*$. Differentiating it with respect to τ, we have

$$-\lambda h(\lambda)\frac{dh}{d\lambda}(\lambda) = -\delta(n-2)h(\lambda) + \lambda^{1+p} - \{h(\lambda)\}^2.$$

Then, we can obtain the approximation of the (graph of) center manifold as follows:

$$\left\{(\lambda, x) \,|\, x = \lambda^{p+1}/[\delta(n-2)] + O\left(\lambda^{2p+2}\right)\right\}. \tag{4.3.10}$$

Therefore, the dynamics of (4.3.9) near $(0,0)$ is topologically equivalent to the dynamics of the following equation:

$$\lambda_\tau = -\lambda^{p+2}/[\delta(n-2)] + O(\lambda^{2p+3}). \tag{4.3.11}$$

These results give us the dynamics on the chart $\overline{U}_1$.

4.3.4 Dynamics on the chart $\overline{V}_1$

The transformations

$$a(s) = -1/\lambda(s), \quad b(s) = -x(s)/\lambda(s)$$

yield

$$\begin{cases} \lambda_\tau = -x\lambda, \\ x_\tau = -Ax - B - \lambda^{p+1} - x^2, \end{cases} \tag{4.3.12}$$

via time-rescaling $d\tau/ds = \{\lambda(s)\}^{-p}$. We can see that the system (4.3.12) can be transformed into the system (4.3.9) by the change of variables: $(\lambda, x) \mapsto (-\lambda, x)$. Therefore, the dynamics of (4.3.12) is equivalent to the reflected one of (4.3.9) with respect to $\{\lambda = 0\}$.

4.3.5 Dynamics and connecting orbits on the Poincaré disk

Combining the dynamics on the chart $\overline{U}_j$ and $\overline{V}_j$, we obtain the dynamics on the Poincaré disk in the case that p is even (see Figure 4.3.2). If E_B is asymptotically stable, then E_B is stable node for $F \geq 0$ and is a stable focus (spiral sink) for $F < 0$.

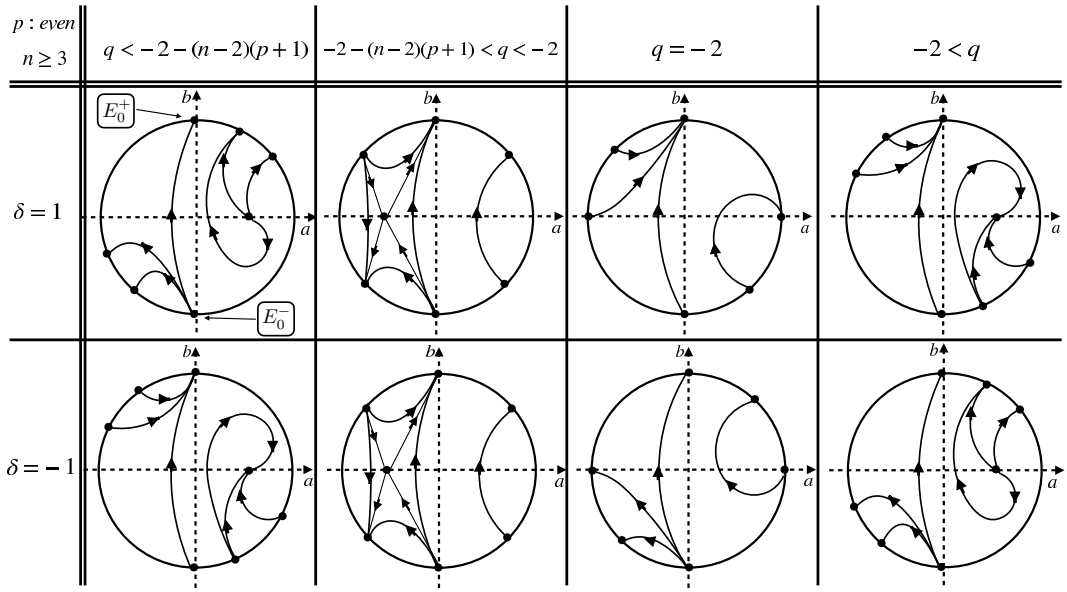

Figure 4.3.2: Schematic pictures of the dynamics on the Poincaré disk in the case that p is even and $F > 0$.

We note that $t \to \infty$ of $\delta = 1$ is corresponding to $t \to -\infty$ of $\delta = -1$.

If there exist the connecting orbits between the equilibria at infinity, then they correspond to the functions that satisfy (4.1.2) on a finite interval or $(0, \infty)$. In particular, if $q = -2$, then there exits a family of the connecting orbits corresponding to a family of the functions such that each function $a(t)$ satisfies (4.1.8) on a finite interval and $\dot{a}(t)$ go to infinity in finite time (see [31]). Indeed, these connecting orbits can be parameterized by position of the intersection of the each connecting orbit and a-axis i.e., let $(a^*, 0)$ be an intersection of the each connecting orbit and a-axis, then the connecting orbits between E_0^- and E_0^+ are parameterized by $a^* < 0$. Figure 4.3.3 (which is similar one shown in [31]) shows a family of the connecting orbits in the case that $q = -2$.

Similarly, for $q \in \mathbb{R}$, there exists a family of functions that corresponds to a family of connecting orbits from $(a, b) = (0, -\infty)$ to $(0, +\infty)$. More precisely, we have the following Proposition.

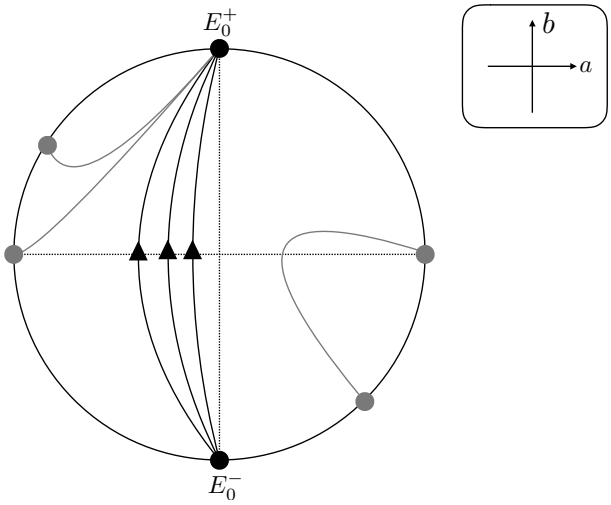

Figure 4.3.3: Schematic picture of the dynamics on the Poincaré disk in the case that p is even and $q = -2$. The orbits drawn in the black curves correspond to a family of connecting orbits between E_0^+ and E_0^-. The other orbits and equilibria are drawn in grayscale.

Proposition 4.3.1
Assume that $n \geq 3$, $p \in 2\mathbb{N}$ and $q \in \mathbb{R}$. Then, there exists a family of the functions such that the each function $a(t)$ satisfies the followings:

(I) $a(t)$ is a continuous function on a finite interval $[t_-, t_+]$ and it satisfies the equation (4.1.8) on (t_-, t_+) ($a(t) \in C^2(t_-, t_+) \cap C^0[t_-, t_+]$, $-\infty < t_- < t_+ < +\infty$).

(II) $a(t)$ has $a(t) < 0$ ($t_- < t < t_+$) and satisfies the following:

$$\lim_{t \to t_+ - 0} a(t) = 0, \quad \lim_{t \to t_+ - 0} \dot{a}(t) = +\infty,$$
$$\lim_{t \to t_- + 0} a(t) = 0, \quad \lim_{t \to t_- + 0} \dot{a}(t) = -\infty.$$

(III) $a(t)$ satisfies the following with constant $C > 0$:

$$\begin{cases} a(t) \sim -C(t_+ - t)^{\frac{2}{p+1}} \\ \dot{a}(t) \sim C\,(t_+ - t)^{-\frac{p-1}{p+1}} \end{cases} \quad \text{as} \quad t \to t_+ - 0,$$

$$\begin{cases} a(t) \sim -C(t - t_-)^{\frac{2}{p+1}} \\ \dot{a}(t) \sim -C\,(t - t_-)^{-\frac{p-1}{p+1}} \end{cases} \quad \text{as} \quad t \to t_- + 0.$$

Proof. Since the point $(y_1, y_2, y_3) = (0, 1, 0)$ on the Poincaré disk corresponds to E_0^+, we denote it by E_0^+ as well. Similarly, we denote by E_0^- the point $(y_1, y_2, y_3) = (0, -1, 0)$ (see also Figure 4.3.2). In order to prove Proposition 4.3.1, it is necessary to find the orbits that connect E_0^- and E_0^+ on the Poincaré disks (see Figure 4.3.2). Moreover, they are symmetric in $\delta = 1$ and $\delta = -1$. For instance, the one in $\delta = 1$ and $q < -2-(n-2)(p+1)$ and the one in $\delta = -1$ and $q > -2$ are the same. Therefore, we need to prove the case of the four disk in $\delta = 1$.
(I) Except for $-2 - (n-2)(p+1) < q < -2$, the proof of the existence of the connecting orbits is given in [31]. In the case that $-2 - (n-2)(p+1) < q < -2$, the flow on

$\{(a,b) \in H_+ \cup \mathbb{S}^2 \,|\, a > 0\}$ and $\{(a,b) \in H_+ \cup \mathbb{S}^2 \,|\, a < 0\}$ are separated by the line $\{a = 0\}$ that is invariant under the flow of (4.3.2), and da/db takes the same values except $\{a = 0\}$ (see [31]).

Let $\mathcal{W}^s(E_B)$ and $\mathcal{W}^u(E_B)$ be the stable and unstable manifolds of E_B, respectively. Then, there exists a connecting orbit from E_0^- to the stable manifold of E_B (E_B is a saddle). Similarly, there exists an orbit that connects $\mathcal{W}^u(E_B)$ and E_0^+. In the region surrounded by these orbits and the line $\{a = 0\}$, there are trajectories connecting E_0^- and E_0^+.

(II) As shown in [31], we can obtain the asymptotic behavior of $a(t)$ at $\overline{E}_p^+$ and E_0^- as follows. We have

$$\begin{aligned}
\frac{d\eta}{dt} &= \frac{ds}{dt} \cdot \frac{d\tau}{ds} \cdot \frac{d\eta}{d\tau} = a^{-p} \cdot \lambda^{-p} \cdot \varepsilon^{p^2-1} = \varepsilon^{p^2-1} \cdot \lambda^{-p} \cdot \left(\frac{x}{\lambda}\right)^{-p} \\
&= \varepsilon^{p^2-1} \cdot x^{-p} = \varepsilon^{p^2-1} \cdot (r^{p+1}\bar{x})^{-p} \\
&= \varepsilon^{-p-1} \cdot \bar{x}^{-p} \\
&\sim \left\{C_1 e^{-\frac{1}{p-1}\eta}(1 + o(1))\right\}^{-p-1} \cdot \left\{C_2 e^{-2\eta}(1 + o(1)) + A\right\}^{-p} \\
&\sim C_3 e^{\frac{p+1}{p-1}\eta} \cdot \left\{C_2 e^{-2\eta}(1 + o(1)) + A\right\}^{-p} \quad \text{as} \quad \eta \to +\infty \\
&= C_3 e^{\frac{p+1}{p-1}\eta} \cdot \frac{1}{\{C_2 e^{-2\eta}(1 + o(1)) + A\}^p} \\
&= C_3 e^{\frac{p+1}{p-1}\eta} \cdot \frac{1}{\{C_2 e^{-2\eta}(1 + o(1))\}^p + p\{C_2 e^{-2\eta}(1 + o(1))\}^{p-1} \cdot A + \cdots + A^p} \\
&\sim C e^{\frac{p+1}{p-1}\eta} \quad \text{as} \quad \eta \to +\infty
\end{aligned}$$

holds with constants C and C_j. Note that this argument is a refinement of [33]. Here, " $f(x) \sim g(x)$ as $x \to a$" means that $f(x) - g(x) = o(g(x))$ as $x \to a$, equivalently,

$$\lim_{x \to a} \left| \frac{f(x)}{g(x)} \right| = 1.$$

This yields

$$t(\eta) = C e^{-\frac{p+1}{p-1}\eta} + \tilde{C} \quad (\tilde{C} \in \mathbb{R}).$$

Set $t_+ = \lim_{\eta \to +\infty} t(\eta)$, then we have

$$t_+ = \int_0^{+\infty} \frac{dt}{d\eta} d\eta = C \int_0^{+\infty} e^{-\frac{p+1}{p-1}\eta} d\eta < +\infty.$$

Therefore,

$$t_+ - t \sim C e^{-\frac{p+1}{p-1}\eta} \quad (\eta \to +\infty)$$

holds. Finally, we obtain

$$\begin{aligned}
a(t) = \frac{x}{\lambda} &= \frac{\varepsilon^{p+1}}{\varepsilon^{p-1}} \overline{x} = \varepsilon^2 \overline{x} \\
&\sim \left\{C_1 e^{-\frac{1}{p-1}\eta}(1 + o(1))\right\}^2 \cdot \left\{C_2 e^{-2\eta}(1 + o(1)) + A\right\} \\
&\sim C_4 e^{-\frac{2}{p-1}\eta} \cdot \left\{C_2 e^{-2\eta}(1 + o(1)) + A\right\} \\
&= C_5 e^{-\frac{2}{p-1}\eta} e^{-2\eta} + C_4 \cdot A \cdot e^{-\frac{2}{p-1}\eta} \\
&= C_5 e^{-\frac{2p}{p-1}\eta} + C_4 \cdot A \cdot e^{-\frac{2}{p-1}\eta} \\
&\sim -C e^{-\frac{2}{p-1}\eta}.
\end{aligned}$$

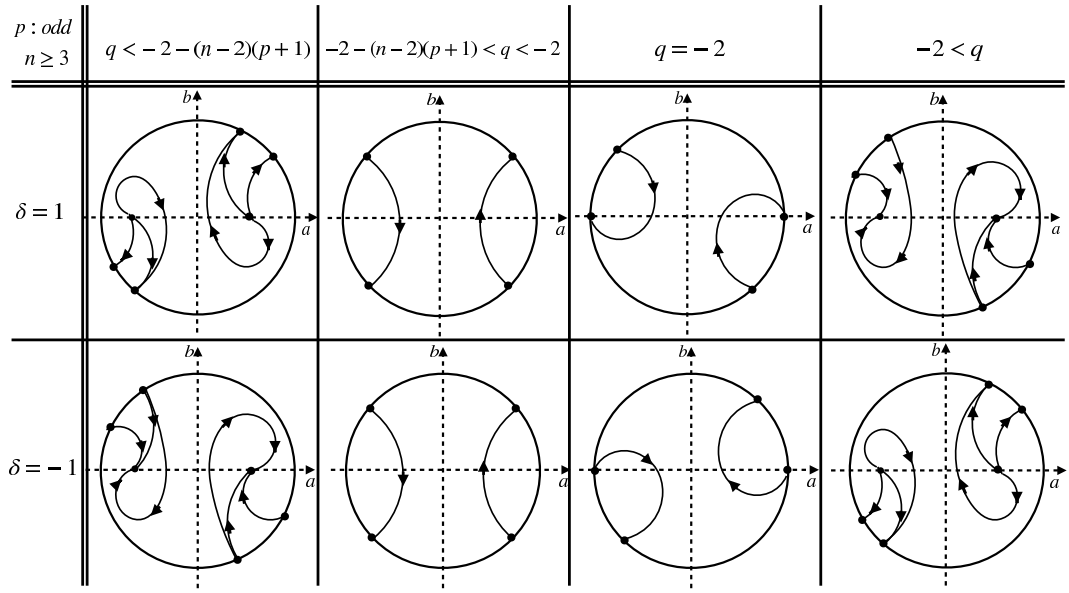

Figure 4.4.1: Schematic pictures of the dynamics on the Poincaré disk when the parameter p is odd and $F > 0$.

Here, in last relation, since $e^{-\frac{2p}{p-1}\eta} < e^{-\frac{2}{p-1}\eta}$ $(\eta > 0)$ is satisfied by $-2p/(p-1) < -2/(p-1)$, we choose the term with the greater influence when $\eta \to +\infty$. Therefore, we have

$$a(t) \sim -Ce^{-\frac{2}{p-1}\eta} \sim -C(t_+ - t)^{\frac{2}{p+1}} \quad (t \to t_+ - 0).$$

Since the trajectories are lying on $\{a < 0\}$, it holds that $C > 0$. Similarly, we can obtain the rates for $a(t)$ as $t \to t_-$ and $\dot{a}(t) = b(t)$ as $t \to t_\pm$. This completes the proof of Proposition 4.3.1. □

4.4 Dynamics on the Poincaré disk of (4.1.8) : p is odd

In this section, we consider the dynamics (4.1.8) on the Poincaré disk in the case that p is odd. We desingularize it by the time-scale desingularization

$$ds/dt = \{a(t)\}^{-p-1}.$$

Then, we have

$$\begin{cases} a' = a^{p+1}b, \\ b' = -Aa^{p+1}b - Ba^{p+2} + a, \end{cases} \qquad \left(' = \frac{d}{ds}\right). \tag{4.4.1}$$

As in the previous section, we can consider the dynamics of (4.4.1) on the charts $\overline{U}_j$ and $\overline{V}_j$. Since the direction of the time does not change via (4.3.1) on $H_{(+,a>0)} := \{(a,b) \in H_+ \cup \mathbb{S}^1 \mid a > 0\}$ for both even and odd cases, the flow of (4.4.1) on $H_{(+,a>0)}$ for $p \in 2\mathbb{N}-1$ is similar to that of (4.3.2) on $H_{(+,a>0)}$ for $p \in 2\mathbb{N}$. Moreover, (4.4.1) is invariant under the mapping:$(a,b) \mapsto -(a,b)$. Therefore, we can draw the phase portraits on the Poincaré disk of (4.1.8) when p is odd as shown in Figure 4.4.1 (cf. the flow on $\{a > 0\}$ of Figure 4.3.2).

The trajectories that connect equilibria on the Poincaré disk correspond to the solutions (which includes the functions satisfying the equation on the finite intervals) to (4.1.2).

Hence, it is possible to compute the asymptotic behavior of them as in the even case. The detailed dynamics of (4.1.8) around the equilibria, which gives asymptotic behavior, on the Poincaré disk is discussed in the next section.

4.5 Proof of the Theorems

In this section, we prove our main results. If the initial data are located on $H_+ \setminus \{a = 0\}$, the existence of the solutions follows from the standard theory of ordinary differential equations. Therefore, we only consider the existence of the trajectories that connect equilibria and the detailed dynamics near the equilibria on the Poincaré disk.

4.5.1 Proof of Theorem 4.1.1

We first give the proof of Theorem 4.1.1 as follows.

Proof. The results are immediately follows by Proposition 4.3.1 and [31]. Still, we note that

$$u'(r) = \frac{d}{dr}\{r^\alpha a(\delta \log r)\} = r^{\alpha-1}(\alpha a \pm b) \quad \text{for} \quad \delta = \pm 1$$

holds and the computations of asymptotic behavior for $r \to r_- + 0$ and $r \to r_+ - 0$ as follows. Using $u(r) = r^\alpha a(t)$, $t = \pm \log r$, we have

$$u(r) \sim -Cr^\alpha (\log r_+ - \log r)^{\frac{2}{p+1}} \quad \text{as} \quad r \to r_+ - 0$$

and

$$u(r) \sim -Cr^\alpha (-\log r_- + \log r)^{\frac{2}{p+1}} \quad \text{as} \quad r \to r_- + 0.$$

Similarly, we can obtain the rates for $b(t)$ as $t \to t_+$ and asymptotic behavior (4.1.9) and (4.1.10). This completes the proof. □

4.5.2 Proof of Theorem 4.1.2

Next, we give the proof of Theorem 4.1.2 as follows.

Proof. Suppose that $q > -2$ and $p \in \mathbb{N}$. First, we note that the flow on $\{(a, b) \in H_+ \cup \mathbb{S}^2 \,|\, a > 0\}$ and $\{(a, b) \in H_+ \cup \mathbb{S}^2 \,|\, a < 0\}$ are separated by the line $\{a = 0\}$. In other words, any trajectories start from the point on the unstable manifold $\mathcal{W}^u(E_4)$ of E_4 cannot go to $\{(a, b) \in H_+ \cup \mathbb{S}^2 \,|\, a < 0\}$ in the case that $\delta = 1$ (see Figures 4.3.2, 4.4.1). We can observe that any trajectories that start from the point on $\mathcal{W}^u(E_4)$ must go to the equilibrium E_B by considering the dimension numbers of the stable and unstable manifolds. Then it holds that there exist the connecting orbits from E_4 to E_B.

Similarly, we obtain the connecting orbits from E_B to E_4 in the case that $\delta = -1$. Therefore, we conclude the existence of the positive radial symmetric stationary solutions.

Second, we derive the asymptotic behavior for $r \to \infty$. We focus our attention on the dynamics around E_B. It is divided into three cases by the value of F. We define

$$\tilde{a} := a - B^{-\frac{1}{p+1}} \quad \text{and} \quad \tilde{b} := b.$$

Then, there are three cases to consider:

(I) Let us consider the case that $F > 0$, namely, the matrix J has the real distinct eigenvalues

$$\sigma_1 = \frac{-A + \sqrt{D}}{2}, \quad \sigma_2 = \frac{-A - \sqrt{D}}{2}.$$

The eigenvectors corresponding to each eigenvalue are

$$\mathbf{v}_1 = \begin{pmatrix} 1 \\ \sigma_1 \end{pmatrix}, \quad \mathbf{v}_2 = \begin{pmatrix} 1 \\ \sigma_2 \end{pmatrix}.$$

We then obtain the following asymptotic behavior:

$$\begin{pmatrix} \tilde{a}(t) \\ \tilde{b}(t) \end{pmatrix} = C_1 \begin{pmatrix} 1 \\ \sigma_1 \end{pmatrix} e^{\sigma_1 t} + C_2 \begin{pmatrix} 1 \\ \sigma_2 \end{pmatrix} e^{\sigma_2 t}$$

with any constants C_1 and C_2. Therefore, the solution around the equilibrium E_B is

$$\begin{cases} a(t) \sim C_1 e^{\sigma_1 t} + C_2 e^{\sigma_2 t} + B^{\frac{-1}{p+1}}, \\ b(t) \sim C_1 \sigma_1 e^{\sigma_1 t} + C_2 \sigma_2 e^{\sigma_2 t}. \end{cases}$$

Using (4.1.4), we can derive the following:

$$\begin{aligned} u(r) &\sim C_1 r^\alpha e^{\sigma_1 t} + C_2 r^\alpha e^{\sigma_2 t} + r^\alpha B^{\frac{-1}{p+1}} \\ &\sim C_1 r^{\alpha+\sigma_1} + C_2 r^{\alpha+\sigma_2} + r^\alpha B^{\frac{-1}{p+1}} \quad \text{as} \quad r \to \infty. \end{aligned}$$

Since $q > -2$, it hold that

$$\alpha + \sigma_1 < 0, \quad \text{and} \quad \alpha + \sigma_2 = \frac{2 - n - \sqrt{D}}{2} < 0.$$

(II) Consider the case that $F = 0$, namely, the matrix J has a multiple real eigenvalue $\sigma = -\dfrac{A}{2}$. The eigenvector and generalized eigenvector corresponding to the eigenvalue are

$$\mathbf{v}_1 = \begin{pmatrix} 1 \\ \dfrac{-A}{2} \end{pmatrix}, \quad \mathbf{v}_2 = \begin{pmatrix} c \\ 1 - \dfrac{A}{2}c \end{pmatrix},$$

with c is arbitrary constant. Therefore, the solution around the equilibrium E_B is

$$\begin{cases} a(t) \sim (C_1 t + C_2 + cC_1) e^{\sigma t} + B^{\frac{-1}{p+1}}, \\ b(t) \sim -\dfrac{A}{2}(C_1 t + C_2) e^{\sigma t} + C_1 \left(1 - \dfrac{A}{2}\right) e^{\sigma t}. \end{cases}$$

Then, we can derive the following:

$$\begin{aligned} u(r) &\sim C_1 t \cdot r^\alpha e^{\sigma t} + (C_2 + cC_1) r^\alpha e^{\sigma t} + r^\alpha B^{\frac{-1}{p+1}} \\ &= C_1 \cdot r^{\alpha+\sigma} \log r + (C_2 + cC_1) r^{\alpha+\sigma} + r^\alpha B^{\frac{-1}{p+1}} \quad \text{as} \quad r \to \infty. \end{aligned}$$

Note that we can determine $\alpha + \sigma = \dfrac{2 - n}{2} < 0$ and

$$\lim_{r\to\infty} (r^{\alpha+\sigma} \log r) = \lim_{r\to\infty} \frac{\log r}{r^{-\alpha-\sigma}} = 0$$

by the L'Hôpital's Rule.

(III) Consider the case that $F < 0$, namely, the matrix J has the complex eigenvalues $\sigma = \mu \pm i\nu = \frac{-A}{2} \pm i\frac{1}{2}\sqrt{|D|}$. The eigenvectors corresponding to each eigenvalue are

$$\mathbf{v} = \begin{pmatrix} 1 \\ -\frac{A}{2} \end{pmatrix} \pm i \begin{pmatrix} 0 \\ \frac{1}{2}\sqrt{|D|} \end{pmatrix}.$$

The function $\tilde{a}(t)$ and $\tilde{b}(t)$ are expressed as following:

$$\begin{pmatrix} \tilde{a}(t) \\ \tilde{b}(t) \end{pmatrix} = z(t) \begin{pmatrix} 0 \\ \frac{1}{2}\sqrt{|D|} \end{pmatrix} + w(t) \begin{pmatrix} 1 \\ -\frac{A}{2} \end{pmatrix},$$

where

$$\begin{pmatrix} z(t) \\ w(t) \end{pmatrix} := e^{\mu t} \begin{pmatrix} \cos\nu t & -\sin\nu t \\ \sin\nu t & \cos\nu t \end{pmatrix} \begin{pmatrix} z(0) \\ w(0) \end{pmatrix}.$$

Therefore, the solution $a(t)$ around the equilibrium E_B is

$$a(t) = e^{-\frac{A}{2}t} \left(z(0) \sin \frac{\sqrt{|D|}}{2} t + w(0) \cos \frac{\sqrt{|D|}}{2} t \right) + B^{\frac{-1}{p+1}}.$$

Using (4.1.4), we can derive the following:

$$\begin{aligned} u(r) &= r^{\alpha} e^{-\frac{A}{2}t} \left(z(0) \cdot \sin \frac{\sqrt{|D|}}{2} t + w(0) \cdot \cos \frac{\sqrt{|D|}}{2} t \right) + r^{\alpha} B^{\frac{-1}{p+1}} \\ &= r^{\frac{2-n}{2}} \left(z(0) \cdot [\sin \frac{\sqrt{|D|}}{2} \log r] + w(0) \cdot [\cos \frac{\sqrt{|D|}}{2} \log r] \right) \\ &\quad + r^{\alpha} B^{\frac{-1}{p+1}} \quad \text{as} \quad r \to \infty. \end{aligned}$$

Last, we can derive the asymptotic behavior for $r \to 0$. Indeed,

$$\frac{d\tau}{dt} = \frac{d\tau}{ds}\frac{ds}{dt} = \lambda^{-p} a^{-p} = \lambda^{-p}\lambda^{p} = 1.$$

This yields $\tau = t + C$ with a constant C. Therefore, using the approximation of the solution at E_4, we have

$$\begin{aligned} a(t) = \frac{1}{\lambda} &\sim C e^{\frac{-A+(n-2)}{2}\tau} = C e^{(\alpha+n-2)\tau} \\ &= C e^{(\alpha+n-2)(t+C)} = C e^{(\alpha+n-2)t}. \end{aligned}$$

Since the trajectories are lying on $\{a > 0\}$, it follows that $C > 0$. Using (4.1.6), we can obtain as following :

$$u(r) \sim r^{\alpha} \cdot C e^{(\alpha+n-2)t} = C r^{2-n} \quad \text{as} \quad r \to 0.$$

This completes the proof of Theorem 4.1.2. □

Remark 4.5.1
It is possible to take the parameters n, p and q so that $F = 0$ holds. For instance, $F = 0$ holds if $n = 3$, $p = 2$ and $q = (3\sqrt{6} - 14)/4$. Similarly, there are sets of the parameters such that $F < 0$ and $F > 0$ holds, respectively.

4.5.3 Proof of Theorem 4.1.3

Last, we give the proof of Theorem 4.1.3 as follows.

Proof. Suppose that $q = -2$ and $p \in \mathbb{N}$. The proof of existence of the connecting orbits between E_c and E_0 at chart $\overline{U}_1$ is obtained in [31] with using the Poincaré-Bendixson theorem. Therefore, we conclude the existence of the singular positive radial symmetric stationary solutions.

To do this, we compute the asymptotic behavior for $r \to \infty$ and $r \to 0$ as follows.

(i) If the initial value is on the center manifold, the solution at the around E_0 on chart $\overline{U}_1$ has the form

$$\begin{cases} \lambda(\tau) = \sqrt[p+1]{\dfrac{1}{\dfrac{p+1}{n-2}\tau - (p+1)\cdot M_1}} = (M_2 + M_3\tau)^{-\frac{1}{p+1}}, \\ x(\tau) = \dfrac{1}{n-2}\lambda^{p+1} + O(\lambda^{2p+2}) \end{cases}$$

for $\delta = 1$. These results are derived (4.3.10) and (4.3.11). We then obtain the following:

$$x(\tau) = \frac{1}{(n-2)M_2 + (n-2)M_3\tau} + O(\tau^{-2}) \sim (M_4 + M_5\tau)^{-1}$$

with the constants M_j $(1 \le j \le 5)$. We then have

$$\frac{d\tau}{dt} = \frac{d\tau}{ds}\frac{ds}{dt} = \lambda^{-p}a^{-p} = \lambda^{-p}\left(\frac{1}{\lambda}\right)^{-p} = 1.$$

This yields $\tau(t) = t + C$ with a constant C.

If $\overline{a}(t)$ is a solution of (4.1.8), then $\overline{a}(t+\theta)$ is also solution for any $\theta \in \mathbb{R}$. Therefore, there exists a solution $a(t)$ such that the following holds

$$a(t) = \lambda^{-1} \sim O(t^{\frac{1}{p+1}}) \quad \text{as} \quad t \to \infty.$$

Since it hold that $t = \log r$ and $u(r) = a(t)$ for $q = -2$, we have

$$u(r) = a(t) \sim O(t^{\frac{1}{p+1}}) = O(\{\log r\}^{\frac{1}{p+1}}) \quad \text{as} \quad r \to \infty.$$

This completes the derivation of rate for $r \to \infty$.

(ii) It follows that

$$\frac{d\tau}{dt} = \frac{d\tau}{ds}\frac{ds}{dt} = \lambda^{-p}a^{-p} = \lambda^{-p}\left(\frac{1}{\lambda}\right)^{-p} = 1.$$

This yields $\tau(t) = t + \tilde{C}$ with a constant $\tilde{C}$. Therefore, we use the approximation of the solution at E_c,

$$a(t) = \frac{1}{\lambda} \sim Ce^{(n-2)\tau} = Ce^{(n-2)(t+\tilde{C})} = C'e^{(n-2)t}.$$

with $C' > 0$. The sign of the constant C' can be determined by considering the geometric situations on the Poincaré disk (the orbits starting from the point on $\{a > 0\}$ cannot go to the set $\{a < 0\}$). We then have

$$u(r) = a(t) \sim Ce^{(n-2)t} = Cr^{2-n} \quad \text{as} \quad r \to 0.$$

We obtain the derivation of rate for $r \to 0$.

Finally, we can complete the proof of Theorem 4.1.3. □

4.6 Conclusions and Remarks

In this chapter, we studied whole dynamics of (4.1.8) on the phase space $\mathbb{R}^2 \cup \{(a,b)\,;\, \|(a,b)\| = +\infty\}$ and asymptotic behavior of the solutions on an interval $I \subseteq (0,\infty)$ of (4.1.2) by applying the Poincaré compactification and dynamical system approach. However, there are connecting orbits whose asymptotic behavior are not discussed (for instance, the orbits on $\{(a,b) \,|\, a > 0\}$ for $q < -2$ are not discussed). The reason for that is more detailed analysis is necessary to obtain the asymptotic behavior, therefore, they will be addressed in future works.

From the viewpoint of theory of partial differential equations, it should be considered that how can we formulate the solutions of (4.1.2) on $r \in [0,\infty)$ (or $(0,\infty)$) with the functions $u(r)$ obtained in Theorem 4.1.1. However, since our interest in this chapter is to study the solutions of (4.1.2) from the dynamical system view point, we did not discuss it. It should be noted that the mathematical formulation of the solution (in weak sense) could be obtained by considering a suitable function space as shown in [51] (it will be addressed in future works as well).

In addition, since the theory of blow-up (desingularization of the vector fields) is not applicable for the non-polynomial vector fields, we cannot deal with the general case that $p \in \mathbb{R}$. Hence, we leave it open here.

Chapter 5

Stationary solutions for a 1D pde problem with gradient term and negative powers nonlinearity

Abstract

Stationary solutions for the one-dimensional partial differential equation with gradient term and negative powers nonlinearity are considered. This equation is a kind of MEMS equation that has the phenomena of MEMS (Micro-Electro Mechanical System) devices as its background. However, it is not easy to understand the behavior of the solution from the effect of the nonlinear term. Therefore, the purpose of this chapter is to investigate the properties of a stationary solution that is a typical solution. That is, we prove the existence of stationary solutions including singularities, and give information about their shapes and the asymptotic behavior. Here, the stationary solution with singularity here means a solution that allows infinity or a solution with an infinite differential coefficient. These are studied by applying the framework that combines the Poincaré-Lyapunov compactification and classical dynamical systems theory. The key to use these methods is to reveal the dynamics including infinity of an ordinary differential equation satisfied by stationary solutions. This chapter is based on the following published paper ([35]):

> Ichida Y., Sakamoto, T.O.: Stationary solutions for a 1D pde problem with gradient term and negative powers nonlinearity, J . Elliptic Parabol. Equ, **8** (2022) , 885–918.

5.1 Introduction

In this chapter, we consider the following spatial one-dimensional partial differential equation:

$$u_t = u_{xx} + \mu \frac{1 + \delta u_x^\beta}{(1-u)^\alpha}, \quad t > 0, \quad x \in \mathbb{R}, \tag{5.1.1}$$

where $\alpha \in 2\mathbb{N}$, $4 < \beta \in 2\mathbb{N}$, $\mu > 0$, and $\delta \geq 0$. The equation (5.1.1) arises from the work of the Micro-Electro Mechanical System (for short, MEMS) model, which has been studied extensively in recent years, but we generalize the nonlinear terms for mathematical interest (see [17, 19, 26, 54, 69, 68] and references therein). From the viewpoint of the phenomena in MEMS devices, the Dirichlet boundary condition is imposed. In general, the MEMS model is known to induce a touchdown phenomenon (mathematically, quenching). Thus,

clarifying the structure of singularity formation is one of the key problems in this type of equation. However, the equation (5.1.1) is not easy to analyze since it has gradient term and negative powers nonlinearity. Since it is not fully understood what kind of solutions the equation has in the first place, it is also important to clarify this point.

The authors have used a kind of compactification of phase space called the Poincaré type compactification to investigate the structure of characteristic solutions (e.g. the stationary solution, the traveling wave solution) of partial differential equations with negative powers nonlinearity and degenerate parabolic equation ([31, 32, 33]). The Poincaré type compactification is one of the compactifications of the original phase space (the embedding of $\mathbb{R}^n$ into the unit upper hemisphere of $\mathbb{R}^{n+1}$). See [14, 31, 32, 33, 49, 50] and its references for details. A brief overview is given in Section 1.1 in this thesis. As noted in [49, 50], via these compactifications, the infinity for the original phase space corresponds to the boundary of compact manifolds. For the ordinary differential equations derived from these partial differential equations, the most important feature of this method is that it can reveal the dynamics including infinity. Here, we split the boundary and project each of them to some local charts, and study the dynamics. By combining this information from some local charts, we can obtain the dynamics including infinity. In the following, the Poincaré type compactification includes both the Poincaré compactification and the Poincaré-Lyapunov compactification. The difference between the two is that the vector field is either homogeneous or quasi-homogeneous, respectively. For the quasi-homogeneity of a vector field, see Section 1.1 and [49, 50]. In addition, the dynamics including infinity, obtained by Poincaré-Lyapunov's one is hereafter referred to as Poincaré-Lyapunov disk. Here, the Poincaré-Lyapunov compactification is also employed in [13], and corresponds to the directional compactification in [49, 50].

We note that the equation dealt with in [31] is actually a special case of this equation (5.1.1). In (5.1.1), this corresponds to the case where $\mu = 1$ and $\delta = 0$. In [31], we study the quasi traveling waves with quenching of a reaction-diffusion equation in the presence of negative powers nonlinearity. These are studied by applying the Poincaré compactification. From the viewpoint of the dynamical system approach, as shown in [31], such a solution corresponds to an orbit which goes to $(0, \pm\infty)$ on $\mathbb{R}^2$ in finite time. This approach should also be applicable to (5.1.1).

A stationary solution is a typical and characteristic solution in dynamical systems theory. However, there are limited results on the structure of such solutions for this type of equation. For instance, in [26], they studied the structure of stationary solutions of (5.1.1) with zero Dirichlet boundary condition in the case that $\beta = 2$. It was discussed the existence of exactly two solutions and the stability of the smaller stationary solutions for $\mu \in (0, \mu^*)$, where μ^* is a positive finite critical value. In [26], the equation is transformed using the key transformation proposed in [69] and they have investigated mainly using the comparison principle.

In this chapter, the purpose is to prove the existence of stationary solutions of (5.1.1) and to give information about their shapes and the asymptotic behavior. Note that the stationary solutions include those with singularity. Here, the stationary solution with singularity here means a solution that allows infinity or a solution with an infinite differential coefficient. Although this chapter is an extension of [26] in terms of the equation, the emphasis is on investigating the shape and asymptotic behavior of stationary solutions from the viewpoint of dynamical systems theory. Furthermore, by using the Poincaré-Lyapunov compactification, if it is possible to list the connecting orbits on the Poincaré-Lyapunov disk corresponding to all the stationary solutions, it will lead to a deeper understanding of the structure of the stationary solutions. As we will see later (see Subsection 5.3.5,

Remark 5.3.2, Section 5.5), we did not reach a complete classification of the connecting orbits, but it is true that they provide many suggestions. With this motivation, we first consider the problem without any additional boundary conditions. It should be noted that this method is not used in [26] and is essentially a different approach from it.

We study the stationary solutions of (5.1.1), namely we consider the following equation:

$$0 = u_{xx} + \mu \frac{1 + \delta u_x^{\beta}}{(1-u)^{\alpha}}, \quad x \in \mathbb{R}. \tag{5.1.2}$$

Further, we introduce the following change of variables:

$$\phi(\xi) = 1 - u(x), \quad \xi = x.$$

We then seek the solution $\phi(\xi)$ of the following equation:

$$\phi'' = \mu\{1 + \delta(\phi')^{\beta}\} \cdot \phi^{-\alpha}, \quad \xi \in \mathbb{R}, \quad ' = \frac{d}{d\xi}, \tag{5.1.3}$$

equivalently

$$\begin{cases} \phi' = \psi, \\ \psi' = \mu(1 + \delta\psi^{\beta})\phi^{-\alpha}. \end{cases} \tag{5.1.4}$$

Note that for any $\phi(\xi)$ except $\phi = 0$, $\psi'(\xi)$ satisfies the following:

$$\psi' > 0. \tag{5.1.5}$$

The equation (5.1.4) is not easy to analyze since it contains the negative powers nonlinear term $\phi^{-\alpha}$ that yields singularity at $\phi = 0$. However, as shown in [31, 33, 32, 49, 50], it is possible to study the dynamics of (5.1.4) including infinity in a framework that combines the Poincaré-Lyapunov compactification (see Section 1.1), classical dynamical systems theory, and geometric methods for desingularization of vector fields (blow-up technique, see Section 1.2 in this thesis and [14] and references therein).

This chapter is organized as follows. In the next section, we state the main results of this chapter. In Section 5.3, we obtain the dynamics of (5.1.4) with $\alpha \in 2\mathbb{N}$ on the Poincaré-Lyapunov disk via Poincaré-Lyapunov compactification and basic theory of the dynamical systems. The proof of Theorems will be completed in Section 5.4. Section 5.5 is devoted to the conclusions and remarks.

5.2 Main results

Before explaining the main results, we first give some remarks on the whole. The main key to obtaining the main results is the availability of a phase portrait corresponding to the Poincaré-Lyapunov disk in (5.1.4), which will be explained in detail in a later section (see Section 5.3). Then each orbit should correspond to a solution of (5.1.2). This allows us to obtain the existence of stationary solutions, their shapes, and asymptotic behavior. However, some solutions obtained in the following theorems satisfy the equation only on the finite interval (ξ_-, ξ_+) $(-\infty < \xi_- < \xi_+ < +\infty)$ or semi-infinite interval. That is, even though we are considering the equation in the whole domain, we are constructing solutions that cause singularity at the endpoints of a finite (or semi-infinite) interval. This has also been reported in [31]. In this chapter, we do not discuss the behavior of the solutions of (5.1.4) after $\psi(\xi)$ becomes infinity (outside of the interval on which $\phi(\xi)$ satisfies (5.1.3)).

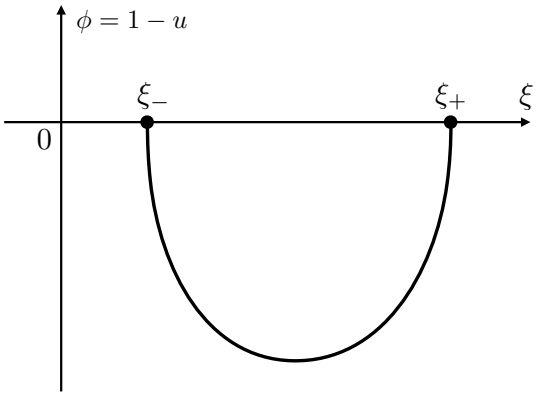

Figure 5.2.1: Schematic picture of the functions defined on the finite interval such that each function $u(x)$ satisfies equation (5.1.2) on a finite interval (ξ_-, ξ_+) in Theorem 5.2.1.

It is necessary that a more detailed (and hard) analysis in order to study the solutions after $\psi(\xi)$ reaches singularity, and so we leave it open here.

From the above discussion, the following theorems were obtained. Hereinafter, note that the meaning of the symbol $f(\xi) \sim g(\xi)$ as $\xi \to a$ is as follows:

$$\lim_{\xi \to a} \left| \frac{f(\xi)}{g(\xi)} \right| = 1.$$

Theorem 5.2.1
Assume that $\alpha \in 2\mathbb{N}$ and $4 < \beta \in 2\mathbb{N}$. Then, there exists a family of the functions (which corresponds to a family of the orbits of (5.1.4)) defined on the finite interval such that each function $u(x)$ satisfies equation (5.1.2) on a finite interval (ξ_-, ξ_+) $(-\infty < \xi_- < \xi_+ < +\infty)$. Moreover, for each function $u(x) = 1 - \phi(\xi)$, the following holds:

- $\begin{cases} \lim\limits_{\xi \to \xi_+ - 0} \phi(\xi) = 0, & \lim\limits_{\xi \to \xi_- + 0} \phi(\xi) = 0, \\ \lim\limits_{\xi \to \xi_+ - 0} \phi'(\xi) = +\infty, & \lim\limits_{\xi \to \xi_- + 0} \phi'(\xi) = -\infty. \end{cases}$
- *$\phi(\xi) < 0$ holds for $\xi \in (\xi_-, \xi_+)$.*
- *There exists a constant $\xi_* \in (\xi_-, \xi_+)$ such that the following holds: $\phi'(\xi) < 0$ for $\xi \in (\xi_-, \xi_*)$, $\phi'(\xi_*) = 0$ and $\phi'(\xi) > 0$ for $\xi \in (\xi_*, \xi_+)$.*

In addition, asymptotic behaviors for $\xi \to \xi_+ - 0$ and $\xi \to \xi_- + 0$ are

$$\begin{cases} \phi(\xi) \sim -A_1(\xi_+ - \xi)^{\frac{\beta-2}{\beta-1}} \\ \phi'(\xi) \sim A_2(\xi_+ - \xi)^{-\frac{1}{\beta-1}} \end{cases} \quad \text{as} \quad \xi \to \xi_+ - 0 \tag{5.2.1}$$

and

$$\begin{cases} \phi(\xi) \sim -A_3(\xi - \xi_-)^{\frac{\beta-2}{\beta-1}} \\ \phi'(\xi) \sim -A_4(\xi - \xi_-)^{-\frac{1}{\beta-1}} \end{cases} \quad \text{as} \quad \xi \to \xi_- + 0, \tag{5.2.2}$$

where $A_j > 0$ $(1 \le j \le 4)$ is a constant.

Remark 5.2.1
Some notes on Theorem 5.2.1 are given. We impose $\alpha \in 2\mathbb{N}$ and $4 < \beta \in 2\mathbb{N}$ for the convenience of the analysis described below. The schematic picture of the function constructed

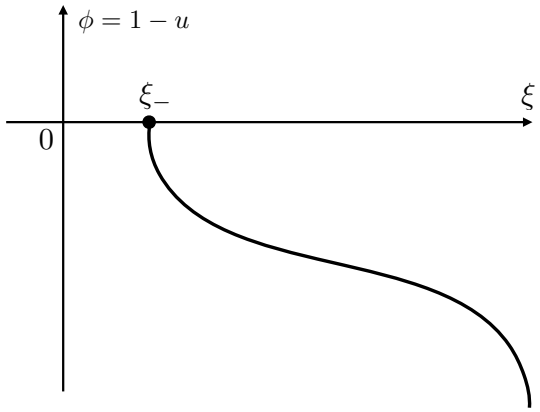

Figure 5.2.2: Schematic pictures of the functions defined on the semi-infinite interval such that each function $u(x)$ satisfies equation (5.1.2) on a semi-infinite interval $(\xi_-, +\infty)$ in Theorem 5.2.2.

in Theorem 5.2.1 is shown in Figure 5.2.1. No specific evaluation has been obtained for the endpoints ξ_- and ξ_+ of this finite interval. However, they are shown in this figure for convenience.

Theorem 5.2.2
Assume that $\alpha \in 2\mathbb{N}$ and $4 < \beta \in 2\mathbb{N}$. Then, there exists a family of the functions (which corresponds to a family of the orbits of (5.1.4)) defined on the semi-infinite intervals such that each function $u(x)$ satisfies equation (5.1.2) on a semi-infinite interval $(\xi_-, +\infty)$ $(-\infty < \xi_- < +\infty)$. Moreover, for each function $u(x) = 1 - \phi(\xi)$, the following holds:

- $\begin{cases} \lim\limits_{\xi \to +\infty} \phi(\xi) = -\infty, \quad \lim\limits_{\xi \to \xi_- + 0} \phi(\xi) = 0, \\ \lim\limits_{\xi \to \xi_- + 0} \phi'(\xi) = -\infty. \end{cases}$
- *$\phi(\xi) < 0$ holds for $\xi \in (\xi_-, +\infty)$.*

In addition, asymptotic behaviors are (5.2.2) and

$$\phi(\xi) \sim -A_3 \left(\frac{\xi - A_2}{A_1} \right)^{\frac{2}{\alpha+1}} \quad \text{as} \quad \xi \to +\infty, \tag{5.2.3}$$

in the case that trajectory whose initial data are on a stable manifold of equilibrium at infinity $(\phi, \psi) = (-\infty, 0)$ of (5.1.4), and

$$\phi(\xi) \sim -A_6 \left(\frac{\xi - A_5}{A_4} \right) \quad \text{as} \quad \xi \to +\infty, \tag{5.2.4}$$

in the case that initial data are not on a stable manifold of equilibrium at infinity $(\phi, \psi) = (-\infty, 0)$ of (5.1.4) and the trajectories enter $(\phi, \psi) = (-\infty, 0)$. Here, $A_j \in \mathbb{R}$ are constants and $A_1, A_3, A_4, A_6 > 0$.

The schematic picture of the function constructed in Theorem 5.2.2 is shown in Figure 5.2.2. Here it should be noted that the position of the singular point ξ_- is not determined in our studies, however, it is shown in these figures for convenience.

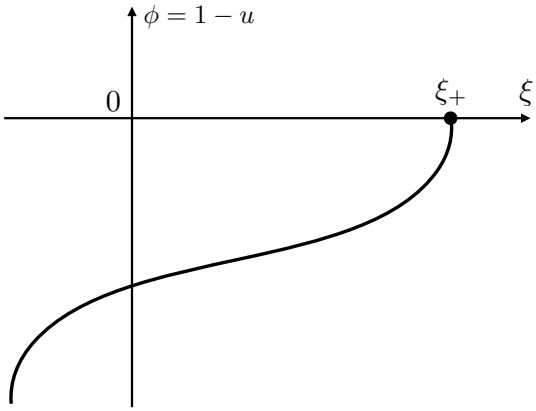

Figure 5.2.3: Schematic pictures of the functions defined on the semi-infinite interval such that each function $u(x)$ satisfies equation (5.1.2) on a semi-infinite interval $(-\infty, \xi_+)$ in Theorem 5.2.3.

Theorem 5.2.3
Assume that $\alpha \in 2\mathbb{N}$ and $4 < \beta \in 2\mathbb{N}$. Then, there exists a family of the functions (which corresponds to a family of the orbits of (5.1.4)) defined on the semi-infinite intervals such that each function $u(x)$ satisfies equation (5.1.2) on a semi-infinite interval $(-\infty, \xi_+)$ $(-\infty < \xi_+ < +\infty)$. Moreover, for each function $u(x) = 1 - \phi(\xi)$, the following holds:

- $\begin{cases} \lim\limits_{\xi \to \xi_+ - 0} \phi(\xi) = 0, & \lim\limits_{\xi \to -\infty} \phi(\xi) = -\infty, \\ \lim\limits_{\xi \to \xi_+ - 0} \phi'(\xi) = +\infty. \end{cases}$
- *$\phi(\xi) < 0$ holds for $\xi \in (-\infty, \xi_+)$.*

In addition, asymptotic behaviors are (5.2.1) and

$$\phi(\xi) \sim -A_3 \left(-\frac{\xi - A_2}{A_1} \right)^{\frac{2}{\alpha+1}} \quad \text{as} \quad \xi \to -\infty, \tag{5.2.5}$$

in the case that trajectory whose initial data are on an unstable manifold of equilibrium at infinity $(\phi, \psi) = (-\infty, 0)$ of (5.1.4), and

$$\phi(\xi) \sim -A_6 \left(-\frac{\xi - A_5}{A_4} \right) \quad \text{as} \quad \xi \to -\infty, \tag{5.2.6}$$

in the case that initial data are not on an unstable manifold of equilibrium at infinity $(\phi, \psi) = (-\infty, 0)$ of (5.1.4) and the trajectories exit $(\phi, \psi) = (-\infty, 0)$. Here, $A_j \in \mathbb{R}$ are constants and $A_1, A_3, A_4, A_6 > 0$.

The schematic picture of the function constructed in Theorem 5.2.3 is shown in Figure 5.2.3. Here it should be noted that the position of the singular point ξ_+ is not determined in our studies, however, it is shown in these figures for convenience.

Theorem 5.2.4
Assume that $\alpha \in 2\mathbb{N}$ and $4 < \beta \in 2\mathbb{N}$. In the case that $\alpha > \beta - 1$, there exists the function (which corresponds to the orbit of (5.1.4)) defined on the finite interval such that each function $u(x)$ satisfies equation (5.1.2) on a finite interval (ξ_-, ξ_+) $(-\infty < \xi_- < \xi_+ < +\infty)$. Moreover, for each function $u(x) = 1 - \phi(\xi)$, the following holds:

- $\lim_{\xi\to\xi_+-0}\phi(\xi)=+\infty, \quad \lim_{\xi\to\xi_-+0}\phi(\xi)=+\infty.$
- $\phi(\xi)>0$ *holds for* $\xi\in(\xi_-,\xi_+)$.
- *There exists a constant* $\xi_*\in(\xi_-,\xi_+)$ *such that the following holds:* $\phi'(\xi)<0$ *for* $\xi\in(\xi_-,\xi_*)$, $\phi'(\xi_*)=0$ *and* $\phi'(\xi)>0$ *for* $\xi\in(\xi_*,\xi_+)$.

In addition, asymptotic behaviors for $\xi\to\xi_+-0$ *and* $\xi\to\xi_-+0$ *are*

$$\phi(\xi)\sim A_1(\xi_+-\xi)^{-\frac{\beta-2}{\alpha-\beta+1}} \quad \text{as} \quad \xi\to\xi_+-0 \tag{5.2.7}$$

and

$$\phi(\xi)\sim A_2(\xi-\xi_-)^{-\frac{\beta-2}{\alpha-\beta+1}} \quad \text{as} \quad \xi\to\xi_-+0 \tag{5.2.8}$$

with a constant $A_j>0$.

On the other hand, in the case that $\alpha<\beta-1$, *the equation* (5.1.1) *has a stationary solution (which corresponds to the orbit of* (5.1.4)*) with the singularities at* $\xi\to-\infty$ *and* $\xi\to+\infty$. *Moreover, its solution* $u(x)=1-\phi(\xi)$, *the following holds:*

- $\lim_{\xi\to+\infty}\phi(\xi)=+\infty, \quad \lim_{\xi\to-\infty}\phi(\xi)=+\infty.$
- $\phi(\xi)>0$ *holds for* $\xi\in\mathbb{R}$.
- *There exists a constant* $\xi_*\in\mathbb{R}$ *such that the following holds:* $\phi'(\xi)<0$ *for* $\xi\in(-\infty,\xi_*)$, $\phi'(\xi_*)=0$ *and* $\phi'(\xi)>0$ *for* $\xi\in(\xi_*,+\infty)$.

In addition, asymptotic behaviors for $\xi\to+\infty$ *and* $\xi\to-\infty$ *are*

$$\phi(\xi)\sim C\left(\frac{\xi-A}{B}\right)^{M_3} \quad \text{as} \quad \xi\to+\infty \tag{5.2.9}$$

and

$$\phi(\xi)\sim C\left(-\frac{\xi-A}{B}\right)^{M_3} \quad \text{as} \quad \xi\to-\infty \tag{5.2.10}$$

with $A\in\mathbb{R}$, $B>0$, $C>0$, $M_3>0$, *and we set*

$$M_3=\frac{M_1}{M_2}=-\frac{\beta-2}{\alpha-\beta+1}, \quad M_2=-\frac{\alpha-\beta+1}{\beta-2}M_1, \quad M_1=\left(\frac{\alpha-1}{(\beta-2)\mu\delta}\right)^{\frac{1}{\beta-2}}.$$

The schematic picture of the function constructed in Theorem 5.2.4 is shown in Figure 5.2.4. Here it should be noted that the positions of the singular points ξ_- and ξ_+ are not determined in our studies, however, they are shown in these figures for convenience.

Corollary 5.2.1
The asymptotic behaviors of $\phi'(\xi)=\psi(\xi)$ *obtained in Theorem 5.2.4 are*

$$\psi(\xi)\sim A_3(\xi_+-\xi)^{-\frac{\alpha-1}{\alpha-\beta+1}} \quad \text{as} \quad \xi\to\xi_+-0,$$

and

$$\psi(\xi)\sim -A_4(\xi-\xi_-)^{-\frac{\alpha-1}{\alpha-\beta+1}} \quad \text{as} \quad \xi\to\xi_--0, \tag{5.2.11}$$

with $A_j>0$ *and* $\alpha>\beta-1$.

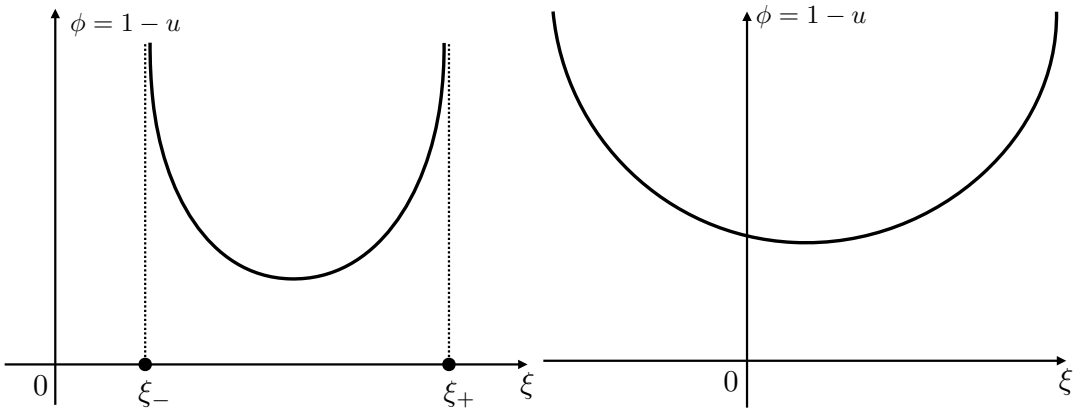

Figure 5.2.4: Schematic pictures of the functions defined on the finite interval (resp. infinite interval) such that each function $u(x)$ satisfies equation (5.1.2) on a finite (resp. infinite) interval (ξ_-, ξ_+) (resp. $(-\infty, +\infty)$) in Theorem 5.2.4. [Left: In the case that $\alpha > \beta - 1$.] [Right: In the case that $\alpha < \beta - 1$.]

On the other hand,

$$\psi(\xi) \sim C \left(\frac{\xi - A}{B} \right)^{M_4} \quad \text{as} \quad \xi \to +\infty,$$

and

$$\psi(\xi) \sim -C \left(-\frac{\xi - A}{B} \right)^{M_4} \quad \text{as} \quad \xi \to -\infty, \tag{5.2.12}$$

with $A \in \mathbb{R}$, $B > 0$, $C > 0$, $\alpha < \beta - 1$, *and* $M_4 = \dfrac{\alpha - 1}{\beta - 2} M_3 = -\dfrac{\alpha - 1}{\alpha - \beta + 1}$.

In addition, let $\overline{\mathcal{W}}^s(e_2^+)$ be a stable manifold of e_2^+ (which is the equilibrium of the system (5.3.11)). We denote by $\mathcal{W}^s(e_2^+)$ the stable set, which corresponds to $\overline{\mathcal{W}}^s(e_2^+)$ on the blow-up vector field (5.3.11), of the equilibrium e_0^+ of (5.3.7). Similarly, we denote by $\mathcal{W}^u(e_1^+)$ the unstable set of e_1^+, corresponding to the unstable manifold of e_1^+ on the blow-up vector field (5.3.10), of the equilibrium e_0^+ of (5.3.7).

Theorem 5.2.5
Assume that $\alpha \in 2\mathbb{N}$ *and* $4 < \beta \in 2\mathbb{N}$. *If there exists a connecting orbit that connects* $\mathcal{W}^u(e_1^+)$ *and* $\mathcal{W}^s(e_2^+)$, *then the equation* (5.1.1) *has a stationary solution (which corresponds to the orbit of* (5.1.4)*) with the singularities at* $\xi \to -\infty$ *and* $\xi \to +\infty$. *Moreover, its solution* $u(x) = 1 - \phi(\xi)$, *the following holds:*

- $\lim_{\xi \to +\infty} \phi(\xi) = +\infty$, $\lim_{\xi \to -\infty} \phi(\xi) = +\infty$.
- $\phi(\xi) > 0$ *holds for* $\xi \in \mathbb{R}$.
- *There exists a constant* $\xi_* \in \mathbb{R}$ *such that the following holds:* $\phi'(\xi) < 0$ *for* $\xi \in (-\infty, \xi_*)$, $\phi'(\xi_*) = 0$ *and* $\phi'(\xi) > 0$ *for* $\xi \in (\xi_*, +\infty)$.

In addition, asymptotic behaviors for $\xi \to +\infty$ *and* $\xi \to -\infty$ *are*

$$\phi(\xi) \sim C \left(\frac{\xi - A}{B} \right) \quad \text{as} \quad \xi \to +\infty, \tag{5.2.13}$$

$$\phi(\xi) \sim C \left(-\frac{\xi - A}{B} \right) \quad \text{as} \quad \xi \to -\infty, \tag{5.2.14}$$

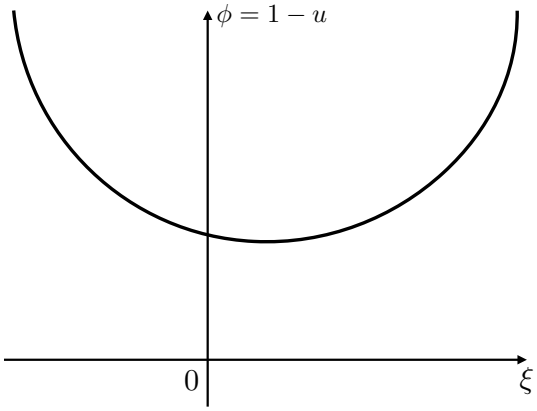

Figure 5.2.5: Schematic picture of the stationary solution with the singularities at $\xi \to -\infty$ and $\xi \to +\infty$ in obtained Theorem 5.2.5.

where $A \in \mathbb{R}$, $B > 0$, and $C > 0$ are constants.

The schematic picture of the stationary solution with the singularities at $\xi \to -\infty$ and $\xi \to +\infty$ in obtained Theorem 5.2.5 is shown in Figure 5.2.5. Here it should be noted that the positions of the singular points ξ_- and ξ_+ are not determined in our studies, however, they are shown in these figures for convenience.

5.3 Dynamics on the Poincaré-Lyapunov disk (5.1.4)

In order to study the dynamics of (5.1.4) on the Poincaré-Lyapunov disk, we desingularize it by the time-scale desingularization

$$ds/d\xi = \{\phi(\xi)\}^{-\alpha} \quad \text{for} \quad \alpha \in 2\mathbb{N}. \tag{5.3.1}$$

Since we assume that α is even, the direction of the time does not change via this desingularization. As we will discuss in Section 5.5, we do not discuss the case of $\alpha \in 2\mathbb{N}+1$ in this chapter, since it is difficult to capture the dynamics near the singularity. Then we have

$$\begin{cases} \phi'(s) = \phi^{\alpha}\psi, \\ \psi'(s) = \mu + \mu\delta\psi^{\beta}, \end{cases} \qquad \left(' = \frac{d}{ds}\right). \tag{5.3.2}$$

It should be noted that the time scale desingularization (5.3.1) is simply multiplying the vector field by ϕ^{α}. Then, except for the singularity $\{\phi = 0\}$, the solution curves of the system (vector field) remain the same but are parameterized differently. Still, we refer to Section 7.7 of [44] and references therein for the analytical treatments of desingularization with the time rescaling. In what follows, we use a similar time rescaling (re-parameterization of the solution curves) repeatedly to desingularize the vector fields. Also, we note that the system (5.3.2) has no equilibrium.

Before we consider the dynamics of (5.3.2) on the charts $\overline{U}_j$ and $\overline{V}_j$, we state the type and order of this vector field (5.3.2). See Appendix for the definition of local charts. Let $f(\phi,\psi) = (f_1(\phi,\psi), f_2(\phi,\psi))$ be $f_1(\phi,\psi) = \phi^{\alpha}\psi$ and $f_2(\phi,\psi) = \mu + \mu\delta\psi^{\beta}$. Then we have the following observation (see Section 1.2 and [49, 50] for more details).

Lemma 5.3.1
The vector field f is asymptotically quasi-homogeneous of type $(\beta-2, \alpha-1)$ and order $(\beta-1)(\alpha-1)+1$ at infinity. See Definition 1.1.3 in Section 1.2 for a definition of this term.

Proof. Let a type be (α_1, α_2), $R \in \mathbb{R}$ and an order be $k+1$ with $k \geq 1$. For all $(\phi, \psi) \in \mathbb{R}^2$, the following holds:

$$f_1(R^{\alpha_1}\phi, R^{\alpha_2}\psi) = R^{k+\alpha_1} f_1(\phi, \psi),$$
$$f_2(R^{\alpha_1}\phi, R^{\alpha_2}\psi) = R^{k+\alpha_2} f_2(\phi, \psi).$$

The left hand side above is calculated as:

$$f_1(R^{\alpha_1}\phi, R^{\alpha_2}\psi) = R^{\alpha\alpha_1+\alpha_2}\phi^\alpha\psi,$$
$$f_2(R^{\alpha_1}\phi, R^{\alpha_2}\psi) = \mu + \mu\delta R^{\beta\alpha_2}\psi^\beta.$$

By comparing the order parts, we get

$$\begin{cases} \alpha\alpha_1 + \alpha_2 = k + \alpha_1, \\ 0 = k + \alpha_2, \\ \beta\alpha_2 = k + \alpha_2. \end{cases}$$

Therefore, we can see that $\alpha_1 = \beta - 2$, $\alpha_2 = \alpha - 1$, and $k = (\beta-1)(\alpha-1)$ hold by ignoring the second equation. The reason for ignoring the second equation is that it is smaller than the third equation. Furthermore, they satisfy the following:

$$\lim_{R\to+\infty} R^{-(k+\alpha_1)}\big\{ f_1(R^{\alpha_1}\phi, R^{\alpha_2}\psi) - R^{k+\alpha_1}(f_{\alpha,k})_1(\phi,\psi) \big\} \equiv 0,$$
$$\lim_{R\to+\infty} R^{-(k+\alpha_2)}\big\{ f_2(R^{\alpha_1}y_1, R^{\alpha_2}y_2) - R^{k+\alpha_2}(f_{\alpha,k})_2(y_1,y_2) \big\} = 0,$$

where $(f_{\alpha,k})_1$ and $(f_{\alpha,k})_2$ are $(f_{\alpha,k})_1 := \phi^\alpha\psi$ and $(f_{\alpha,k})_2 = \mu\delta\psi^\beta$. From the above results, we can see that the vector field f is asymptotically quasi-homogeneous of type $(\beta-2, \alpha-1)$ and order $(\beta-1)(\alpha-1)+1$ at infinity. □

Therefore, we should consider the Poincaré-Lyapunov compactification (the directional compactification) rather than Poincaré compactification that corresponds to homogeneous vector fields. Furthermore, from Lemma 5.3.1, we can see that we need to exclude $\beta = 2$ in this case. Since the solution structure for the case $\beta = 2$ has been studied in [26], we only need to study the case $4 < \beta \in 2\mathbb{N}$ in this chapter. The reasons for not considering $\beta = 4$ are discussed later in Remark 5.3.1.

Now, we can consider the dynamics of (5.3.2) on the charts $\overline{U}_j$ and $\overline{V}_j$.

5.3.1 Dynamics on the chart $\overline{U}_2$

To obtain the dynamics on the chart $\overline{U}_2$, we introduce coordinates (λ, x) by the formulas

$$\phi(s) = x(s)/\{\lambda(s)\}^{\beta-2}, \quad \psi(s) = 1/\{\lambda(s)\}^{\alpha-1}.$$

Here, note that the exponents of λ are derived from the type found in Lemma 5.3.1. The image of the geometric position of these local coordinates is almost the same as in Figure 1.1.2. Then we have

$$\begin{cases} \lambda' = -\mu(\alpha-1)^{-1}(\lambda^\alpha + \delta\lambda^{-\alpha\beta+\alpha+\beta}), \\ x' = \lambda^{-\alpha\beta+\alpha+\beta-1}x^\alpha - \mu(\beta-2)(\alpha-1)^{-1}(\lambda^{\alpha-1}x + \delta\lambda^{-\alpha\beta+\alpha+\beta-1}x). \end{cases}$$

Note that $-\alpha\beta+\alpha+\beta-1 = -(\alpha-1)(\beta-1) < 0$ holds. Time-scale desingularization $d\tau/ds = \lambda^{-\alpha\beta+\alpha+\beta-1}$ yields

$$\begin{cases} \lambda_\tau = -\mu(\alpha-1)^{-1}(\lambda^{\alpha\beta-\beta+1} + \delta\lambda), \\ x_\tau = x^\alpha - \mu(\beta-2)(\alpha-1)^{-1}(\lambda^{\alpha\beta-\beta}x + \delta x), \end{cases} \tag{5.3.3}$$

where $\lambda_\tau = d\lambda/d\tau$ and $x_\tau = dx/d\tau$. Here, we can solve for λ. λ satisfies

$$\lambda(\tau) = \left(C_1 e^{\mu\delta\beta\tau} - \frac{1}{\delta} \right)^{-\frac{1}{\alpha\beta-\beta}} \tag{5.3.4}$$

Since we are considering $\lambda(\tau) \geq 0$, C_1 is a sufficiently large positive constant.

Further, the system (5.3.3) has the equilibria

$$E_0^+ : (\lambda, x) = (0, 0), \quad E_\alpha^+ : (\lambda, x) = (0, [(\beta-2)\mu\delta/(\alpha-1)]^{\frac{1}{\alpha-1}}).$$

The Jacobian matrices of the vector field (5.3.3) at these equilibria are

$$E_0^+ : \begin{pmatrix} -\dfrac{\mu\delta}{\alpha-1} & 0 \\ 0 & -\dfrac{\beta-2}{\alpha-1}\mu\delta \end{pmatrix}, \quad E_\alpha^+ : \begin{pmatrix} -\dfrac{\mu\delta}{\alpha-1} & 0 \\ 0 & \mu\delta(\beta-2) \end{pmatrix}.$$

Therefore, E_0^+ is a sink and E_α^+ is a saddle. Moreover, since $|-(\alpha-1)^{-1}\mu\delta| < |-(\beta-2)(\alpha-1)^{-1}\mu\delta|$ holds, trajectories near E_0^+ are tangent to $\{x = 0, \lambda \geq 0\}$ as $\tau \to +\infty$.

The solution for x near E_0^+ is approximated as

$$x(\tau) = C_2 e^{-\frac{\beta-2}{\alpha-1}\mu\delta\tau}(1 + o(1)) \quad \text{as} \quad \tau \to +\infty \tag{5.3.5}$$

with a constant C_2.

5.3.2 Dynamics on the chart $\overline{V}_2$

The change of coordinates

$$\phi(s) = -x(s)/\{\lambda(s)\}^{\beta-2}, \quad \psi(s) = -1/\{\lambda(s)\}^{\alpha-1}$$

give the projected dynamics of (5.3.2) on the chart $\overline{V}_2$:

$$\begin{cases} \lambda_\tau = \mu(\alpha-1)^{-1}(\lambda^{\alpha\beta-\beta+1} + \delta\lambda), \\ x_\tau = x^\alpha + \mu(\beta-2)(\alpha-1)^{-1}(\lambda^{\alpha\beta-\beta}x + \delta x), \end{cases} \tag{5.3.6}$$

where τ is the new time introduced by $d\tau/ds = \lambda^{-\alpha\beta+\alpha+\beta-1}$. Here, we can solve for λ. λ satisfies

$$\lambda(\tau) = \left(C_1 e^{-\mu\delta\beta\tau} - \frac{1}{\delta} \right)^{-\frac{1}{\alpha\beta-\beta}}$$

with a sufficiently large positive constant C_1.

Further, the system (5.3.6) has the equilibria

$$E_0^- : (\lambda, x) = (0, 0), \quad E_\alpha^- : (\lambda, x) = (0, [-(\beta-2)\mu\delta/(\alpha-1)]^{\frac{1}{\alpha-1}}).$$

The Jacobian matrices of the vector field (5.3.6) at these equilibria are

$$E_0^- : \begin{pmatrix} \dfrac{\mu\delta}{\alpha-1} & 0 \\ 0 & \dfrac{\beta-2}{\alpha-1}\mu\delta \end{pmatrix}, \quad E_\alpha^- : \begin{pmatrix} \dfrac{\mu\delta}{\alpha-1} & 0 \\ 0 & -\mu\delta(\beta-2) \end{pmatrix}.$$

Therefore, E_0^- is a source and E_α^- is a saddle.

5.3.3 Dynamics on the chart $\overline{U}_1$

Let us study the dynamics on the chart $\overline{U}_1$. The transformations

$$\phi(s) = 1/\{\lambda(s)\}^{\beta-2}, \quad \psi(s) = x(s)/\{\lambda(s)\}^{\alpha-1}$$

yield

$$\begin{cases} \lambda_\tau = -(\beta-2)^{-1}\lambda x, \\ x_\tau = \mu\lambda^{\alpha\beta-\beta} + \mu\delta x^\beta - (\alpha-1)(\beta-2)^{-1}x^2, \end{cases} \tag{5.3.7}$$

via time-rescaling $d\tau/ds = \lambda^{-\alpha\beta+\alpha+\beta-1}$. The system (5.3.7) has the equilibria

$$e_0^+ : (\lambda, x) = (0,0), \quad E_\pm^\alpha : (\lambda, x) = (0, \pm M_1), \quad M_1 := [(\alpha-1)/\{(\beta-2)\mu\delta\}]^{\frac{1}{\beta-2}}.$$

The Jacobian matrices of the vector field (5.3.7) at these equilibria are

$$e_0^+ : \begin{pmatrix} 0 & 0 \\ 0 & 0 \end{pmatrix}, \quad E_\pm^\alpha : \begin{pmatrix} \mp\dfrac{1}{\beta-2}M_1 & 0 \\ 0 & \pm(\alpha-1)M_1 \end{pmatrix}.$$

Therefore, $E_\pm^\alpha$ is a saddle and e_0^+ is not hyperbolic. The solutions near E_+^α are approximated as

$$\begin{cases} \lambda(\tau) = C_1 e^{-\frac{1}{\beta-2}M_1\tau}(1+o(1)), \\ x(\tau) - M_1 = C_2 e^{(\alpha-1)M_1\tau}(1+o(1)), \end{cases} \quad \text{as} \quad \tau \to +\infty \tag{5.3.8}$$

with constants $C_1 > 0$ and C_2.

In order to determine the dynamics near e_0^+, we desingularize it by introducing the following blow-up coordinates:

$$\lambda = r\overline{\lambda}, \quad x = r^{(\alpha\beta-\beta)/2}\overline{x}$$

(see Section 1.2 in this thesis and Section 3 of [14] for the desingularizations of vector fields by the blow-up). Since we are interested in the dynamics on the Poincaré-Lyapunov disk, we consider the dynamics of blow-up vector fields on the charts $\{\overline{\lambda} = 1\}$ and $\{\overline{x} = \pm 1\}$.

Dynamics on the chart $\{\overline{\lambda} = 1\}$

By the change of coordinates $\lambda = r$, $x = r^{(\alpha\beta-\beta)/2}\overline{x}$, and time-rescaling $d\eta/d\tau = r^{(\alpha\beta-\beta)/2}$, we have

$$\begin{cases} r_\eta = -(\beta-2)^{-1}r\overline{x}, \\ \overline{x}_\eta = 2^{-1}(\alpha-1)\overline{x}^2 + \mu + \mu\delta r^{\beta(\alpha-1)(\beta-2)/2}\overline{x}^\beta. \end{cases} \tag{5.3.9}$$

The system (5.3.9) has not the equilibrium.

Dynamics on the chart $\{\overline{x} = -1\}$

By the change of coordinates $\lambda = r\overline{\lambda}$, $x = -r^{(\alpha\beta-\beta)/2}$, and time-rescaling $d\eta/d\tau = r^{(\alpha\beta-\beta)/2}$, we have

$$\begin{cases} r_\eta = -2\mu\beta^{-1}(\alpha-1)^{-1}r(\overline{\lambda}^{\alpha\beta-\beta} + \delta r^{\beta(\alpha-1)(\beta-2)/2}) + 2\beta^{-1}(\beta-2)^{-1}r, \\ \overline{\lambda}_\eta = 2\mu\beta^{-1}(\alpha-1)^{-1}(\overline{\lambda}^{\alpha\beta-\beta+1} + \delta r^{\beta(\alpha-1)(\beta-2)/2}\overline{\lambda}) + \beta^{-1}\overline{\lambda}. \end{cases} \tag{5.3.10}$$

The equilibrium on $\{r = 0\}$ is

$$e_1^+ : (r, \overline{\lambda}) = (0,0).$$

The Jacobian matrix of the vector field (5.3.10) at its equilibrium is

$$e_1^+ : \begin{pmatrix} \dfrac{2}{\beta(\beta-2)} & 0 \\ 0 & \dfrac{1}{\beta} \end{pmatrix}.$$

Therefore, we can see that e_1^+ is a source.

Dynamics on the chart $\{\overline{x}=1\}$

The change of coordinates $\lambda = r\overline{\lambda}$, $x = r^{(\alpha\beta-\beta)/2}$, and time-rescaling $d\eta/d\tau = r^{(\alpha\beta-\beta)/2}$ yield

$$\begin{cases} r_\eta = 2\mu\beta^{-1}(\alpha-1)^{-1}r(\overline{\lambda}^{\alpha\beta-\beta} + \delta r^{\beta(\alpha-1)(\beta-2)/2}) - 2\beta^{-1}(\beta-2)^{-1}r, \\ \overline{\lambda}_\eta = -2\mu\beta^{-1}(\alpha-1)^{-1}(\overline{\lambda}^{\alpha\beta-\beta+1} + \delta r^{\beta(\alpha-1)(\beta-2)/2}\overline{\lambda}) - \beta^{-1}\overline{\lambda}. \end{cases} \tag{5.3.11}$$

The equilibrium on $\{r=0\}$ is

$$e_2^+ : (r, \overline{\lambda}) = (0,0).$$

The Jacobian matrix of the vector field (5.3.11) at its equilibrium is

$$e_2^+ : \begin{pmatrix} -\dfrac{2}{\beta(\beta-2)} & 0 \\ 0 & -\dfrac{1}{\beta} \end{pmatrix}.$$

Therefore, e_2^+ is a sink. Moreover, since $|-\beta^{-1}| > |-2\beta^{-1}(\beta-2)^{-1}|$ holds, trajectories near e_2^+ are tangent to $\{\overline{\lambda}=0\}$ as $\eta \to +\infty$. The solutions near e_2^+ are approximated as

$$\begin{cases} r(\eta) = Ce^{-\frac{2}{\beta(\beta-2)}\eta}(1+o(1)), \\ \overline{\lambda}(\eta) = Ce^{-\frac{1}{\beta}\eta}(1+o(1)), \end{cases} \quad \text{as} \quad \eta \to +\infty \tag{5.3.12}$$

with constants $C_j > 0$.

Combining the dynamics on the charts $\{\overline{\lambda}=1\}$ and $\{\overline{x}=\pm 1\}$, we obtain the dynamics on $\overline{U}_1$ (see Figure 5.3.1).

Remark 5.3.1
Considering $\beta = 4$, $|-\beta^{-1}| = |-2\beta^{-1}(\beta-2)^{-1}|$ holds. Therefore, we assume $4 < \beta \in 2\mathbb{N}$.

5.3.4 Dynamics on the chart $\overline{V}_1$

The transformations

$$\phi(s) = -1/\{\lambda(s)\}^{\beta-2}, \quad \psi(s) = -x(s)/\{\lambda(s)\}^{\alpha-1}$$

yield

$$\begin{cases} \lambda_\tau = -(\beta-2)^{-1}\lambda x, \\ x_\tau = -\mu\lambda^{\alpha\beta-\beta} - \mu\delta x^\beta - (\alpha-1)(\beta-2)^{-1}x^2, \end{cases} \tag{5.3.13}$$

via time-rescaling $d\tau/ds = \lambda^{-\alpha\beta+\alpha+\beta-1}$. The system (5.3.13) has the equilibrium

$$e_0^- : (\lambda, x) = (0,0),$$

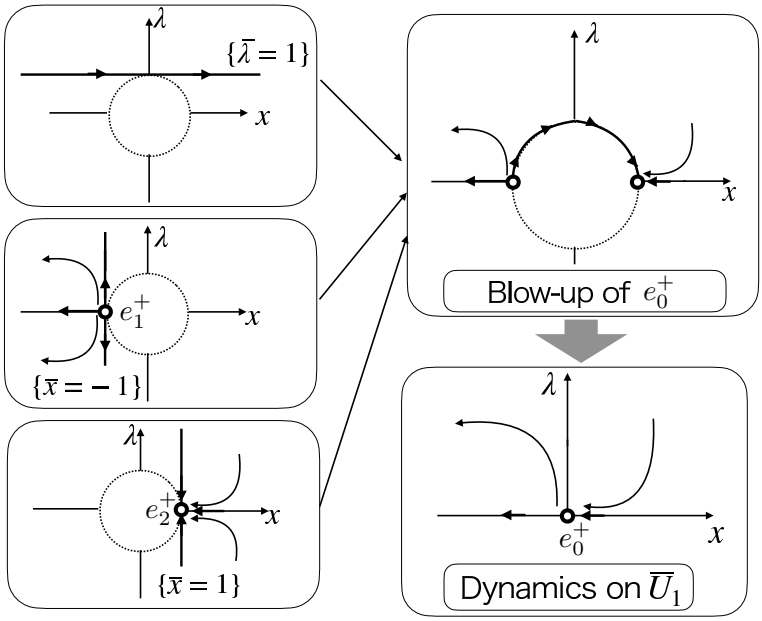

Figure 5.3.1: Schematic pictures of the dynamics of the blow-up vector fields and $\overline{U}_1$.

where we note that $4 < \beta \in 2\mathbb{N}$. The Jacobian matrix of the vector field (5.3.13) at its equilibrium is

$$e_0^- : \begin{pmatrix} 0 & 0 \\ 0 & 0 \end{pmatrix}.$$

Therefore, e_0^- is not hyperbolic. Similarly as $\overline{U}_1$, in order to determine the dynamics near e_0^-, we desingularize it by introducing the following blow-up coordinates:

$$\lambda = r\overline{\lambda}, \quad x = r^{(\alpha\beta-\beta)/2}\overline{x}.$$

Since we are interested in the dynamics on the Poincaré-Lyapunov disk, we consider the dynamics of blow-up vector fields on the charts $\{\bar{\lambda} = 1\}$ and $\{\bar{x} = \pm 1\}$.

Dynamics on the chart $\{\overline{\lambda} = 1\}$

By the change of coordinates $\lambda = r$, $x = r^{(\alpha\beta-\beta)/2}\overline{x}$, and time-rescaling $d\eta/d\tau = r^{(\alpha\beta-\beta)/2}$, we have

$$\begin{cases} r_\eta = -(\beta-2)^{-1} r\overline{x}, \\ \overline{x}_\eta = 2^{-1}(\alpha-1)\overline{x}^2 - \mu - \mu\delta r^{\beta(\alpha-1)(\beta-2)/2}\overline{x}^\beta. \end{cases} \tag{5.3.14}$$

The equilibria of (5.3.14) on $\{r = 0\}$ are

$$e_1^- : (r, \overline{x}) = (0, -K), \quad e_2^- : (r, \overline{x}) = (0, K), \quad K := [(2\mu)/(\alpha-1)]^{\frac{1}{2}}.$$

The Jacobian matrices of the vector fields (5.3.14) at these equilibria are

$$e_1^- : \begin{pmatrix} \dfrac{1}{\beta-2}K & 0 \\ 0 & -(\alpha-1)K \end{pmatrix}, \quad e_2^- : \begin{pmatrix} -\dfrac{1}{\beta-2}K & 0 \\ 0 & (\alpha-1)K \end{pmatrix}.$$

Therefore, both e_1^- and e_2^- are saddles. The solutions near e_2^- are approximated as

$$\begin{cases} r(\eta) = C_1 e^{-\frac{1}{\beta-2}K\eta}(1 + o(1)), \\ \overline{x}(\eta) - K = C_2 e^{(\alpha-1)K\eta}(1 + o(1)) \end{cases} \quad \text{as} \quad \eta \to +\infty \tag{5.3.15}$$

with constants $C_1 > 0$ and C_2.

Dynamics on the chart $\{\overline{x} = -1\}$

By the change of coordinates $\lambda = r\overline{\lambda}$, $x = -r^{(\alpha\beta-\beta)/2}$, and time-rescaling $d\eta/d\tau = r^{(\alpha\beta-\beta)/2}$, we have

$$\begin{cases} r_\eta = 2\mu\beta^{-1}(\alpha-1)^{-1}r(\overline{\lambda}^{\alpha\beta-\beta} + \delta r^{\beta(\alpha-1)(\beta-2)/2}) + 2\beta^{-1}(\beta-2)^{-1}r, \\ \overline{\lambda}_\eta = -2\mu\beta^{-1}(\alpha-1)^{-1}(\overline{\lambda}^{\alpha\beta-\beta+1} + \delta r^{\beta(\alpha-1)(\beta-2)/2}\overline{\lambda}) + \beta^{-1}\overline{\lambda}. \end{cases} \tag{5.3.16}$$

The equilibria of (5.3.16) on $\{r = 0\}$ are

$$e_3^- : (r, \overline{\lambda}) = (0, 0), \quad e_4^- : (r, \overline{\lambda}) = (0, [(\alpha-1)/(2\mu)]^{\frac{1}{\alpha\beta-\beta}}).$$

The Jacobian matrices of the vector fields (5.3.16) at these equilibria are

$$e_3^- : \begin{pmatrix} \dfrac{2}{\beta(\beta-2)} & 0 \\ 0 & \dfrac{1}{\beta} \end{pmatrix}, \quad e_4^- : \begin{pmatrix} \dfrac{1}{\beta-2} & 0 \\ 0 & -(\alpha-1) \end{pmatrix}.$$

Therefore, e_3^- is a source and e_4^- is a saddle.

Dynamics on the chart $\{\overline{x} = 1\}$

By the change of coordinates $\lambda = r\overline{\lambda}$, $x = r^{(\alpha\beta-\beta)/2}$, and time-rescaling $d\eta/d\tau = r^{(\alpha\beta-\beta)/2}$, we have

$$\begin{cases} r_\eta = -2\mu\beta^{-1}(\alpha-1)^{-1}r(\overline{\lambda}^{\alpha\beta-\beta} + \delta r^{\beta(\alpha-1)(\beta-2)/2}) - 2\beta^{-1}(\beta-2)^{-1}r, \\ \overline{\lambda}_\eta = 2\mu\beta^{-1}(\alpha-1)^{-1}(\overline{\lambda}^{\alpha\beta-\beta+1} + \delta r^{\beta(\alpha-1)(\beta-2)/2}\overline{\lambda}) - \beta^{-1}\overline{\lambda}. \end{cases} \tag{5.3.17}$$

The equilibria of (5.3.17) on $\{r = 0\}$ are

$$e_5^- : (r, \overline{\lambda}) = (0, 0), \quad e_6^-(r, \overline{\lambda}) = (0, [(\alpha-1)/(2\mu)]^{\frac{1}{\alpha\beta-\beta}}).$$

The Jacobian matrices of the vector fields (5.3.17) at these equilibria are

$$e_5^- : \begin{pmatrix} -\dfrac{2}{\beta(\beta-2)} & 0 \\ 0 & -\dfrac{1}{\beta} \end{pmatrix}, \quad e_6^- : \begin{pmatrix} -\dfrac{1}{\beta-2} & 0 \\ 0 & \alpha-1 \end{pmatrix}.$$

Therefore, e_5^- is a sink and e_6^- is a saddle. Moreover, since $|-2/\beta(\beta-2)| < |-1/\beta|$ holds, trajectories near e_5^- are tangent to $\{\overline{\lambda} = 0, r \geq 0\}$ as $\eta \to +\infty$. Considering $\beta = 4$, $|-2/\beta(\beta-2)| = |-1/\beta|$ holds. The solutions near e_5^- are approximated as

$$\begin{cases} r(\eta) = C_1 e^{-\frac{2}{\beta(\beta-2)}\eta}(1+o(1)), \\ \overline{\lambda}(\eta) = C_2 e^{-\frac{1}{\beta}\eta}(1+o(1)) \end{cases} \quad \text{as} \quad \eta \to +\infty \tag{5.3.18}$$

with positive constants C_j.

Combining the dynamics on the charts $\{\overline{\lambda} = 1\}$ and $\{\overline{x} = \pm 1\}$, we obtain the dynamics on $\overline{V}_1$ (see Figure 5.3.2).

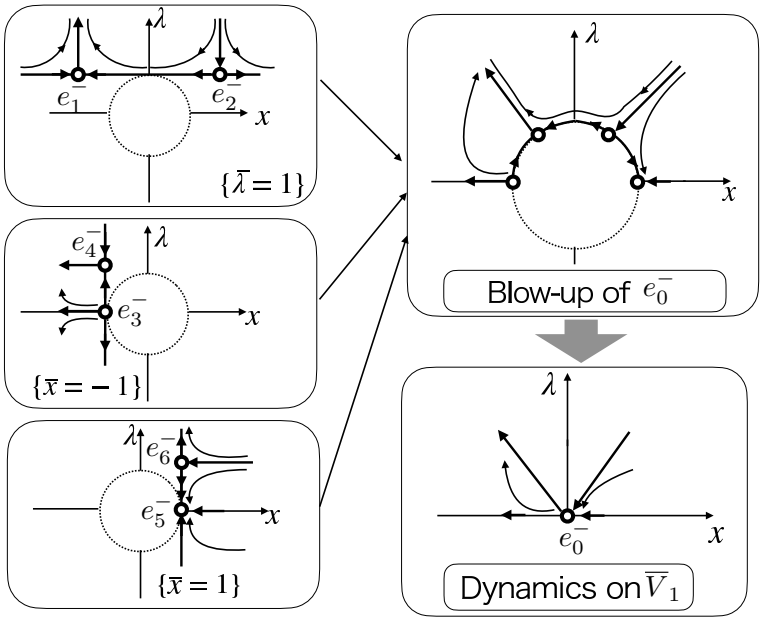

Figure 5.3.2: Schematic pictures of the dynamics of the blow-up vector fields and $\overline{V}_1$.

5.3.5 Dynamics on the Poincaré-Lyapunov disk

Combining dynamics on the charts $\overline{U}_j$ and $\overline{V}_j$, we obtain the dynamics on the Poincaré-Lyapunov disk of the system (5.1.4) in the case that α is even (see Figure 5.3.3).

We explain why the connecting orbits can be represented as shown in Figure 5.3.3.
(I): We set Φ as follows:

$$\Phi = \{(\phi,\psi) \mid (\phi,\psi) \in \mathbb{R}^2 \cup \{\|(\phi,\psi)\| = \infty\}\}.$$

For a given compact subset $W \subset \Phi$, there is no equilibrium or closed orbit in W. Therefore, by the Poincaré-Bendixson theorem, any trajectories starting from the points in W cannot stay in W with increasing s. This implies that the trajectories in Φ go to $\mathbb{S}^1$, which corresponds to $\{\|(\phi,\psi)\| = \infty\}$. Since the line $\{\phi = 0\}$ is invariant under the flow of (5.3.2), therefore, any trajectories start from the points in $\{(\phi,\psi) \in \Phi \mid \phi < 0\}$ cannot go to $\{(\phi,\psi) \in \Phi \mid \phi > 0\}$. Namely, we conclude that the flow on $\{(\phi,\psi) \in \Phi \mid \phi < 0\}$ and $\{(\phi,\psi) \in \Phi \mid \phi > 0\}$ are separated by the line $\{\phi = 0\}$.
(II): It is easy to see that $d\phi/d\psi$ takes the same values on the vector fields defined by (5.3.2) and (5.1.4) by excepting the singularity $\{\phi = 0\}$. Therefore, note that the solution curves in the variable s (vector field (5.3.2)) draw the same solution curves in the original vector field (5.1.4), the variable ξ.
(III): We determine the dynamics on $\{(\phi,\psi) \in \Phi \mid \phi < 0\}$. Note that we have the following:

$$\begin{aligned} &\phi' = 0 \quad \text{on} \quad \psi = 0, \\ &\psi' > 0 \quad \text{on} \quad \psi = 0,\ \phi < 0. \end{aligned}$$

Let $\mathcal{W}^s(E_0^+)$ be a stable manifold of E_0^+ (which is the equilibrium of the system (5.3.3)). Similarly, let $\mathcal{W}^u(E_0^-)$ be an unstable manifold of E_0^- (which is the equilibrium of the system (5.3.6)).

In addition, let $\overline{\mathcal{W}}^s(e_2^-)$, $\overline{\mathcal{W}}^s(e_5^-)$, and $\overline{\mathcal{W}}^s(e_6^-)$ be stable manifolds of e_2^- (which is the equilibrium of the system (5.3.14)), e_5^- and e_6^- (which are the equilibria of the system

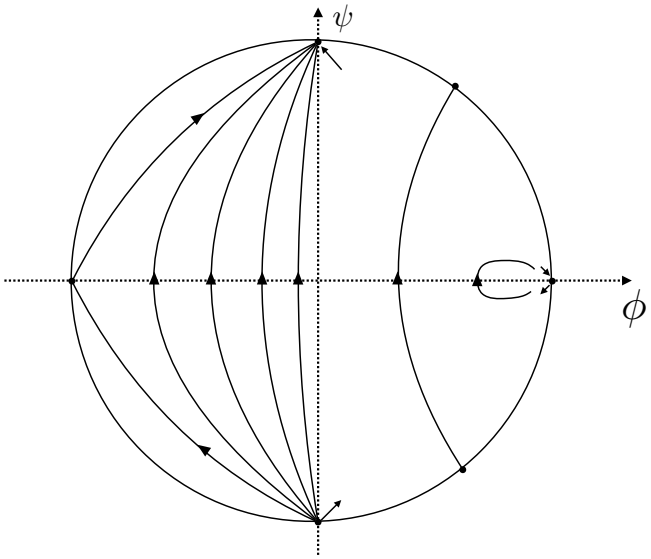

Figure 5.3.3: Schematic pictures of the dynamics on the Poincaré-Lyapunov disk in the case that α is even.

(5.3.17)), respectively. We denote by $\mathcal{W}^s(e_2^-)$, $\mathcal{W}^s(e_5^-)$, and $\mathcal{W}^s(e_6^-)$ the stable sets, which correspond to $\overline{\mathcal{W}}^s(e_2^-)$, $\overline{\mathcal{W}}^s(e_5^-)$, and $\overline{\mathcal{W}}^s(e_6^-)$ on the blow-up vector fields (5.3.14) and (5.3.17), of the equilibrium e_0^- of (5.3.13). Similarly, we denote by $\mathcal{W}^u(e_1^-)$, $\mathcal{W}^u(e_3^-)$, and $\mathcal{W}^u(e_4^-)$ the unstable sets of e_1^-, e_3^-, and e_4^-, corresponding to the unstable manifolds of e_1^-, e_3^-, and e_4^- on the blow-up vector fields (5.3.14) and (5.3.16), of the equilibrium e_0^- of (5.3.13).

Consider the trajectories start from the points on $\mathcal{W}^u(e_1^-)$, $\mathcal{W}^u(e_3^-)$ or $\mathcal{W}^u(e_4^-)$. These trajectories cannot stay in any compact subset on Φ, and cannot go to $\{(\phi,\psi)\in\Phi \mid \phi>0\}$ from the discussion in **(I)** and **(II)**. Furthermore, since these orbits cannot cross the ψ axis, they must go to the points on $\mathcal{W}^s(E_0^+)$.

Next, we consider the trajectories start from the points on $\mathcal{W}^u(E_0^-)\subset\{(\phi,\psi)\in\Phi \mid \phi<0\}$. Since the equilibrium E_0^- is source, these trajectories must go to the points on $\mathcal{W}^s(e_2^-)$, $\mathcal{W}^s(e_5^-)$ or $\mathcal{W}^s(e_6^-)$ and the points on $\mathcal{W}^s(E_0^+)\subset\{(\phi,\psi)\in\Phi \mid \phi<0\}$ by considering the dimension numbers of the stable and unstable manifolds, the discussion in **(I)** and **(II)**.

From the discussion so far, we can fully determine the dynamics on $\{(\phi,\psi)\in\Phi \mid \phi<0\}$.

(IV): We determine the dynamics on $\{(\phi,\psi)\in\Phi \mid \phi>0\}$. Note that (5.1.4) is invariant under the mapping: $\psi\mapsto-\psi$, $\xi\mapsto-\xi$ and we remember (5.1.5).

Let $\mathcal{W}^s(E_+^\alpha)$ be a stable manifold of E_+^α (which is the equilibrium of the system (5.3.7)). Similarly, let $\mathcal{W}^u(E_-^\alpha)$ be an unstable manifold of E_-^α (which is the equilibrium of the system (5.3.7)).

Consider the trajectory start from the points on $\mathcal{W}^u(E_-^\alpha)$. Since we have the discussion in **(I)(II)** and the invariant under $\psi\mapsto-\psi$, $\xi\mapsto-\xi$, and (5.1.5), this orbit must go to the points on $\mathcal{W}^s(E_+^\alpha)$. This implies that system (5.1.4) possesses the orbits that connect E_-^α and E_+^α on the Poincaré-Lyapunov disk.

Remark 5.3.2
Any trajectories that start from the point on $\mathcal{W}^u(e_1^+)$ *go to the region* $\{(\phi,\psi) \mid \phi>0,\psi<0\}$, *that is,* ψ *should decrease. On the other hand, since* (5.1.5) *holds, any trajectories*

that start from the point on $\{(\phi,\psi) \mid \phi > 0, \psi < 0\}$ *should satisfy that* ψ *increases. Additionally, we can see a similar situation on* $\mathcal{W}^s(e_2^+)$*. Therefore, the dynamics around* e_0^+ *(which corresponds to* $(\phi,\psi) = (+\infty, 0)$*) cannot be determined. Similarly, any trajectories that start from the point on* $\{(\phi,\psi) \mid \phi > 0, \psi > 0\}$ *should satisfy that* ϕ *increase, but, this does not match the dynamics near* E_0^+ *(which corresponds to* $(\phi,\psi) = (0, +\infty)$*) on the chart* $\overline{U}_2$*. Also, the dynamics near* $(\phi,\psi) = (0, -\infty)$ *cannot be determined. This is the reason why we only show the direction of the vector fields (arrows) in Figure 5.3.3 near* $(\phi,\psi) = (0, \pm\infty)$ *and* $(+\infty, 0)$*.*

5.4 Proof of the Theorems

In this section, we prove our main results. If the initial data are located on $\Phi \setminus \{\phi = 0\}$, the existence of the solutions follows from the standard theory for the ordinary differential equations. Therefore, we consider the existence of the trajectories that connect equilibria and the detailed dynamics near the equilibria on the Poincaré-Lyapunov disk and their asymptotic behavior.

5.4.1 Proof of Theorem 5.2.1

We first give the proof of Theorem 5.2.1 as follows.

Proof. The proof of the existence of the connecting orbits between E_0^- and E_0^+ for $\{(\phi,\psi) \in \Phi \mid \phi < 0\}$ is obtained in Subsection 5.3.5. Therefore, there exists a family of the functions which corresponds to a family of the orbits of (5.1.4).

Next, we prove the existence of a constant $\xi_* \in (\xi_-, \xi_+)$. It is sufficient to show the connecting orbits pass through the line $\{\psi = 0\}$. Considering (5.1.4),

$$\phi' = 0 \quad \text{on} \quad \psi = 0, \quad \psi' = \mu\phi^{-\alpha} > 0 \quad \text{on} \quad \psi = 0.$$

Therefore, when the orbits that connect E_0^- and E_0^+ passes through the ϕ axis, ξ is ξ_*. From the above discussion, we conclude that we prove the existence of a constant $\xi_* \in (\xi_-, \xi_+)$.

Finally, we compute the asymptotic behavior of the trajectories near the equilibria E_0^- and E_0^+ as follows. The solution around the E_0^+ on chart $\overline{U}_2$ has the form

$$\begin{cases} \lambda(\tau) = \left(C_1 e^{\mu\delta\beta\tau} - \dfrac{1}{\delta}\right)^{-\frac{1}{\alpha\beta-\beta}}, \\ x(\tau) = C_2 e^{-\frac{\beta-2}{\alpha-1}\mu\delta\tau}(1 + o(1)) \quad \text{as} \quad \tau \to +\infty, \end{cases}$$

where $C_1 > 0$ and C_2 are constants. These results are derived from (5.3.4) and (5.3.5). Then,

$$\begin{aligned} \frac{d\tau}{d\xi} &= \frac{d\tau}{ds} \cdot \frac{ds}{d\xi} = \lambda^{-\alpha\beta+\alpha+\beta-1} \cdot \phi^{-\alpha} = \lambda^{-\alpha+\beta-1} \cdot x^{-\alpha} \\ &= \left(C_1 e^{\mu\delta\beta\tau} - \frac{1}{\delta}\right)^{-\frac{-\alpha+\beta-1}{\beta(\alpha-1)}} \cdot \left(C_2 e^{-\frac{\beta-2}{\alpha-1}\mu\delta\tau}(1 + o(1))\right)^{-\alpha} \quad \text{as} \quad \tau \to +\infty \\ &\sim \left(C_1 e^{\mu\delta\beta\tau} - \frac{1}{\delta}\right)^{\frac{\alpha-\beta+1}{\beta(\alpha-1)}} \cdot C_3 e^{\frac{\alpha(\beta-2)}{\alpha-1}\mu\delta\tau} \qquad \text{as} \quad \tau \to +\infty \\ &= C_4 e^{\frac{\alpha(\beta-2)}{\alpha-1}\mu\delta\tau} e^{\frac{\alpha-\beta+1}{\alpha-1}\mu\delta\tau} \left\{1 + \left(-\frac{1}{C_1\delta} e^{-\mu\delta\beta\tau}\right)\right\}^{\frac{\alpha-\beta+1}{\beta(\alpha-1)}} \end{aligned}$$

holds. Since we are focusing on $\tau \to +\infty$, using the generalized binomial theorem under $[1/C_1\delta]e^{-\mu\delta\beta\tau} < 1$,

$$\begin{aligned}\frac{d\tau}{d\xi} &\sim C_4 e^{\frac{\alpha(\beta-2)}{\alpha-1}\mu\delta\tau} e^{\frac{\alpha-\beta+1}{\alpha-1}\mu\delta\tau} \left\{1 + \sum_{k=1}^{\infty} \binom{\frac{\alpha-\beta+1}{\beta(\alpha-1)}}{k} \left(-\frac{1}{C_1\delta} e^{-\mu\delta\beta\tau}\right)^k\right\} \\ &\sim C_4 e^{\frac{\alpha(\beta-2)}{\alpha-1}\mu\delta\tau} e^{\frac{\alpha-\beta+1}{\alpha-1}\mu\delta\tau} \quad \text{as} \quad \tau \to +\infty \\ &= C_4 e^{(\beta-1)\mu\delta\tau}\end{aligned}$$

holds. Note that C_4 is positive constant. Here, we have

$$\binom{\alpha}{k} := \frac{\alpha(\alpha-1)(\alpha-2)\cdots(\alpha-k+1)}{k!}, \quad \alpha \in \mathbb{R}.$$

Integrating $d\xi/d\tau \sim C_4^{-1} e^{-(\beta-1)\mu\delta\tau}$ on $[0, +\infty]$, we have

$$\xi_+ - \xi(0) = \int_0^{+\infty} C_4^{-1} e^{-(\beta-1)\mu\delta\tau}(1 + o(1))\, d\tau,$$

where $\xi_+ = \lim_{\tau\to+\infty} \xi(\tau)$. Without loss of generality, we may set $\xi(0) = 0$. This yields

$$\xi_+ = C_5 \int_0^{\infty} e^{-(\beta-1)\mu\delta\tau}(1 + o(1))\, d\tau < \infty$$

with $C_5 > 0$. Therefore,

$$\xi_+ - \xi \sim C_6 e^{-(\beta-1)\mu\delta\tau} \quad \text{as} \quad \tau \to +\infty$$

holds with positive constant C_6. Finally, we obtain

$$\begin{aligned}\phi'(\xi) = \psi(\xi) &= \frac{1}{\lambda^{\alpha-1}} = \lambda^{-\alpha+1} \\ &= \left\{\left(C_1 e^{\mu\delta\beta\tau} - \frac{1}{\delta}\right)^{-\frac{1}{\alpha\beta-\beta}}\right\}^{-\alpha+1} = \left(C_1 e^{\mu\delta\beta\tau} - \frac{1}{\delta}\right)^{\frac{1}{\beta}} \\ &= C_7 e^{\mu\delta\tau}\left\{1 + \left(-\frac{1}{C_1\delta} e^{-\mu\delta\beta\tau}\right)\right\}^{\frac{1}{\beta}} \\ &= C_7 e^{\mu\delta\tau}\left\{1 + \sum_{k=1}^{\infty} \binom{\frac{1}{\beta}}{k} \left(-\frac{1}{C_1\delta} e^{-\mu\delta\beta\tau}\right)^k\right\} \\ &\sim C_7 e^{\mu\delta\tau} \quad \text{as} \quad \tau \to +\infty \\ &\sim A_2(\xi_+ - \xi)^{-\frac{1}{\beta-1}} \quad \text{as} \quad \xi \to \xi_+ - 0.\end{aligned}$$

Since the trajectories are lying on $\{\psi > 0\}$, it holds that $A_2 > 0$. In addition, using $\phi'(\xi) \sim \psi(\xi)$, we can obtain

$$\phi(\xi) \sim -A_1(\xi_+ - \xi)^{\frac{\beta-2}{\beta-1}} \quad \text{as} \quad \xi \to \xi_+ - 0.$$

Since the trajectories are lying on $\{\phi < 0\}$, it holds that $A_1 > 0$.

Similarly, we can obtain (5.2.2). This completes the proof of Theorem 5.2.1. □

Remark 5.4.1

We note how to derive the asymptotic behavior of $\phi(\xi)$. In the above proof of Theorem 5.2.1, the asymptotic behavior of $\phi(\xi)$ was found by integrating the asymptotic behavior of $\psi(\xi)$ using the fact that $\phi'(\xi) \sim \psi(\xi)$ is satisfied. In order to derive the asymptotic behavior of $\phi(\xi)$ directly, we need information on the higher-order terms of $x(\tau)$ in the solution around E_0^+.

5.4.2 Proof of Theorem 5.2.2

Next, we give the proof of Theorem 5.2.2 as follows.

Proof. The proof of the existence of the connecting orbits between E_0^- and e_0^- for $\{(\phi,\psi) \in \Phi \mid \phi < 0\}$ is obtained in Subsection 5.3.5. Therefore, there exists a family of the functions which corresponds to a family of the orbits of (5.1.4) and it is sufficient for us to prove (5.2.3) and (5.2.4).

Next, we derive (5.2.3). Note that we consider the case that trajectory whose initial data are on a stable manifold of equilibrium at infinity $(\phi,\psi) = (-\infty, 0)$ of (5.1.4). Using (5.3.15), we then have

$$\begin{aligned}
\frac{d\eta}{d\xi} &= \frac{d\eta}{d\tau}\cdot\frac{d\tau}{ds}\cdot\frac{ds}{d\xi} = r^{\frac{\alpha\beta-\beta}{2}}\cdot\lambda^{-\alpha\beta+\alpha+\beta-1}\cdot\phi^{-\alpha} \\
&= r^{\frac{(\alpha+1)(\beta-2)}{2}} \\
&= \left\{C_1 e^{-\frac{1}{\beta-2}K\eta}(1+o(1))\right\}^{\frac{(\alpha+1)(\beta-2)}{2}} \quad \text{as} \quad \eta\to+\infty \\
&\sim Ce^{-\frac{\alpha+1}{2}K\eta} \quad \text{as} \quad \eta\to+\infty
\end{aligned}$$

with constant $C > 0$. This yields

$$\xi(\eta) \sim A_1 e^{\frac{\alpha+1}{2}K\eta} + A_2, \quad (K>0, A_1>0, A_2\in\mathbb{R}) \quad \text{as} \quad \eta\to+\infty$$

We can see $\xi(\eta)\to+\infty$ as $\eta\to\infty$ since we focus on the points on $\mathcal{W}^s(e_2^-)$. This relationship shows that

$$\eta(\xi) \sim \frac{2}{(\alpha+1)K}\log\left(\frac{\xi-A_2}{A_1}\right) \quad \text{as} \quad \xi\to+\infty$$

holds. Therefore, we have

$$\begin{aligned}
\phi(\xi) &= -\lambda^{-\beta+2} = -r^{-(\beta-2)} \\
&= -\left\{C_1 e^{-\frac{1}{\beta-2}K\eta}(1+o(1))\right\}^{-(\beta-2)} \quad \text{as} \quad \eta\to+\infty \\
&\sim -A_3 e^{K\eta} \quad \text{as} \quad \eta\to+\infty \\
&\sim -A_3\exp\left\{K\frac{2}{(\alpha+1)K}\log\left(\frac{\xi-A_2}{A_1}\right)\right\} \\
&= -A_3\left(\frac{\xi-A_2}{A_1}\right)^{\frac{2}{\alpha+1}} \quad \text{as} \quad \xi\to+\infty
\end{aligned}$$

with constants $A_1 > 0$, A_2, and $A_3 > 0$. The reason why $A_3 > 0$ is the trajectories are lying on $\{\phi < 0\}$.

Finally, we derive (5.2.4). Note that we consider the case that trajectory whose initial data are not on a stable manifold of equilibrium at infinity $(\phi,\psi) = (-\infty, 0)$ of (5.1.4).

Using (5.3.18), we then have

$$\begin{aligned}\frac{d\eta}{d\xi} &= \frac{d\eta}{d\tau}\cdot\frac{d\tau}{ds}\cdot\frac{ds}{d\xi} = r^{\frac{\alpha\beta-\beta}{2}}\cdot\lambda^{-\alpha\beta+\alpha+\beta-1}\cdot\phi^{-\alpha}\\ &= r^{\frac{(\alpha+1)(\beta-2)}{2}}\overline{\lambda}^{-\alpha+\beta-1}\\ &= \left\{C_1e^{-\frac{2}{\beta(\beta-2)}\eta}(1+o(1))\right\}^{\frac{(\alpha+1)(\beta-2)}{2}}\cdot\left\{C_2e^{-\frac{1}{\beta}\eta}(1+o(1))\right\}^{-\alpha+\beta-1}\\ &\sim C_3e^{-\frac{\alpha+1}{\beta}\eta}\cdot e^{-\frac{-\alpha+\beta-1}{\beta}\eta} \quad \text{as} \quad \eta\to+\infty\\ &= C_3e^{-\eta}\end{aligned}$$

with constant $C_3 > 0$. This yields

$$\xi(\eta) \sim A_4e^{\eta} + A_5 \quad \text{as} \quad \eta\to+\infty, \quad (A_4 > 0, \quad A_5 \in \mathbb{R}).$$

We can see $\xi(\eta) \to +\infty$ as $\eta \to \infty$ since we focus on the points on $\mathcal{W}^s(e_5^-)$. This relationship shows that

$$\eta(\xi) \sim \log\left(\frac{\xi - A_5}{A_4}\right) \quad \text{as} \quad \eta\to+\infty$$

holds. Therefore, we have

$$\begin{aligned}\phi(\xi) &= -\lambda^{-\beta+2} = -r^{-(\beta-2)}\overline{\lambda}^{-(\beta-2)}\\ &= -\left\{C_1e^{-\frac{2}{\beta(\beta-2)}\eta}(1+o(1))\right\}^{-(\beta-2)}\left\{C_2e^{-\frac{1}{\beta}\eta}(1+o(1))\right\}^{-(\beta-2)} \quad \text{as} \quad \eta\to+\infty\\ &\sim -A_6e^{\eta}\\ &\sim -A_6\left(\frac{\xi - A_5}{A_4}\right) \quad \text{as} \quad \xi\to+\infty\end{aligned}$$

with constants $A_4 > 0$, A_5, and $A_6 > 0$. The reason why $A_6 > 0$ is the trajectories are lying on $\{\phi < 0\}$.

Therefore, we can complete the proof of Theorem 5.2.2. □

5.4.3 Proof of Theorem 5.2.3

Next, we give the proof of Theorem 5.2.3 as follows.

Proof. The proof of existence of the connecting orbits between e_0^- and E_0^+ for $\{(\phi,\psi) \in \Phi \mid \phi < 0\}$ is obtained in Subsection 5.3.5. Furthermore, the asymptotic behavior (5.2.5) and (5.2.6) can be obtained by similar computations in the proof of Theorem 5.2.3. □

5.4.4 Proof of Theorem 5.2.4

Next, we give the proof of Theorem 5.2.4 as follows.

Proof. The proof of the existence of the connecting orbit between E_-^α and E_+^α for $\{(\phi,\psi) \in \Phi \mid \phi > 0\}$ is obtained in Subsection 5.3.5. In addition, this orbit passes through the line $\{\psi = 0\}$. Thus, there exists a function (which corresponds to the orbit of (5.1.4)) such that (5.1.2) is satisfied in a finite interval (or $\xi \in \mathbb{R}$) and we prove the existence of a constant ξ_*, and it is sufficient for us to prove (5.2.7), (5.2.8), (5.2.9), and (5.2.10).

Using (5.3.8), we then have

$$\begin{aligned}\frac{d\tau}{d\xi} &= \frac{d\tau}{ds}\cdot\frac{ds}{d\xi} = \lambda^{-\alpha\beta+\alpha+\beta-1}\cdot\phi^{-\alpha} = \lambda^{-\alpha+\beta-1}\\ &= \left\{C_1 e^{-\frac{1}{\beta-2}M_1\tau}(1+o(1))\right\}^{-\alpha+\beta-1}\\ &\sim B_1 e^{\frac{\alpha-\beta+1}{\beta-2}M_1\tau} \quad \text{as} \quad \tau\to+\infty,\end{aligned}$$

where B_1 and M_1 are positive constants. This yields

$$\xi(\tau) \sim B_2 e^{-\frac{\alpha-\beta+1}{\beta-2}M_1\tau} + A \quad \text{as} \quad \tau\to+\infty, \quad (B_2>0,\ A\in\mathbb{R}).$$

Since the sign of $\alpha-\beta+1$ cannot be determined, we consider the following cases. Here, α and β are even, so they can never be $\alpha=\beta-1$.

(i) Let us consider the case that $\alpha>\beta-1$. We can see $\xi(\tau)\to A$ as $\tau\to+\infty$. Then, setting $\xi_+ = \lim_{\tau\to+\infty}\xi(\tau)$, we have

$$\xi_+ = B_3\int_0^{+\infty} e^{-\frac{\alpha-\beta+1}{\beta-2}M_1\tau}(1+o(1))\,d\tau < \infty$$

(see also Subsection 5.4.1). Therefore,

$$\xi_+ - \xi \sim B_4 e^{-\frac{\alpha-\beta+1}{\beta-2}M_1\tau} \quad \text{as} \quad \tau\to+\infty$$

holds. Finally, we have

$$\phi(\xi) = \lambda^{-\beta+2} \sim Ce^{M_1\tau} \sim A_1(\xi_+-\xi)^{-\frac{\beta-2}{\alpha-\beta+1}} \quad \text{as} \quad \xi\to\xi_+-0$$

with a constant A_1. Since the trajectories are lying on $\{\phi>0\}$, it holds that $A_1>0$.

(ii) Consider the case that $\alpha<\beta-1$. We can see $\xi(\tau)\to+\infty$ as $\tau\to+\infty$ since we focus on the points on $\mathcal{W}^s(E_+^\alpha)$. This relationship shows that

$$\tau(\xi) \sim \frac{1}{M_2}\log\frac{\xi-A}{B} \quad \text{as} \quad \xi\to+\infty$$

holds. Here, we set

$$M_2 = -\frac{\alpha-\beta+1}{\beta-2}M_1 > 0.$$

Therefore, we have

$$\phi(\xi) = \lambda^{-\beta+2} \sim Ce^{M_1\tau} \sim C\exp\left(\frac{M_1}{M_2}\log\frac{\xi-A}{B}\right) = C\left(\frac{\xi-A}{B}\right)^{M_3},$$

where C is a constant and

$$M_3 = \frac{M_1}{M_2} = -\frac{\beta-2}{\alpha-\beta+1}.$$

Since the trajectories are lying on $\{\phi>0\}$, it holds that $C>0$. Similarly, we can obtain (5.2.8) and (5.2.10). This completes the proof of Theorem 5.2.4. □

Remark 5.4.2
E_α^+ and E_+^α are equilibria of different charts, $\overline{U}_2$ and $\overline{U}_1$ respectively, but they overlap on the Poincaré-Lyapunov disk. Similarly, E_α^- and E_-^α are the same point on this disk. In other words, the calculation of asymptotic behavior can also be done by focusing on the connecting orbits between E_α^+ and E_α^-. However, we adopt E_+^α and E_-^α since it provides better information, including the relationship between E_α^+ and E_α^-.

5.4.5 Proof of Corollary 5.2.1

Next, we give the proof of Corollary 5.2.1 as follows.

Proof. We recall from (5.3.8) that the solutions near a saddle point E_+^α are approximated as

$$\begin{cases} \lambda(\tau) = C_1 e^{-\frac{1}{\beta-2}M_1\tau}(1+o(1)), \\ x(\tau) - M_1 = C_2 e^{(\alpha-1)M_1\tau}(1+o(1)), \end{cases} \quad \text{as} \quad \tau \to +\infty,$$

where $M_1 = [(\alpha-1)/\{(\beta-2)\mu\delta\}]^{1/(\beta-2)}$. Note that we focus on the direction of stable manifold $\mathcal{W}^s(E_+^\alpha)$. We choose $C_1 e^{-(\beta-2)^{-1}M_1\tau}$ as "principal term".

From the results of Subsection 5.4.4, we consider the following cases.

(i) Let us consider the case that $\alpha > \beta - 1$. We have

$$\xi_+ - \xi \sim B e^{-\frac{\alpha-\beta+1}{\beta-2}M_1\tau} \quad \text{as} \quad \tau \to +\infty.$$

The asymptotic behavior of $\psi(\xi)$ can be calculated as follows:

$$\begin{aligned} \psi(\xi) &= \lambda^{-\alpha+1}x \\ &= \left\{C_1 e^{-\frac{1}{\beta-2}M_1\tau}(1+o(1))\right\}^{-\alpha+1}\left\{C_2 e^{(\alpha-1)M_1\tau}(1+o(1)) + M_1\right\} \\ &\sim C_3 e^{\frac{\alpha-1}{\beta-2}M_1\tau}\left\{C_2 e^{(\alpha-1)M_1\tau}(1+o(1)) + M_1\right\} \\ &\sim C e^{\frac{\alpha-1}{\beta-2}M_1\tau} \quad \text{as} \quad \tau \to +\infty. \end{aligned}$$

Note that the last "$\sim$" ignores the x term in order to extract the components in the stable manifold direction, as described above. Therefore, we obtain

$$\begin{aligned} \psi(\xi) &\sim C e^{\frac{\alpha-1}{\beta-2}M_1\tau} \\ &= C\left(e^{-\frac{\alpha-\beta+1}{\beta-2}M_1\tau}\right)^{-\frac{\alpha-1}{\alpha-\beta+1}} \\ &\sim A_3(\xi_+ - \xi)^{-\frac{\alpha-1}{\alpha-\beta+1}} \quad \text{as} \quad \xi \to \xi_+ - 0 \end{aligned}$$

with a constant A_3. Since the trajectories are lying on $\{\psi > 0\}$, it holds that $A_3 > 0$. Furthermore, together with (5.2.7), we find that $\phi'(\xi) \sim \psi(\xi)$ as $\xi \to \xi_+ - 0$ is satisfied.

Similarly, we can obtain (5.2.11).

(ii) Consider the case that $\alpha < \beta - 1$. We have

$$\tau(\xi) \sim \frac{1}{M_2}\log\frac{\xi - A}{B} \quad (\xi \to +\infty)$$

with $A \in \mathbb{R}$, $B > 0$, and $M_2 = -[(\alpha-\beta+1)/(\beta-2)]M_1 > 0$. Using the same

concept as in (i), the asymptotic behavior of $\psi(\xi)$ can be calculated as follows:

$$\begin{aligned}\psi(\xi) &= \lambda^{-\alpha+1}x \\ &= \left\{C_1 e^{-\frac{1}{\beta-2}M_1\tau}(1+o(1))\right\}^{-\alpha+1}\left\{C_2 e^{(\alpha-1)M_1\tau}(1+o(1))+M_1\right\} \\ &\sim Ce^{\frac{\alpha-1}{\beta-2}M_1\tau} \quad \text{as} \quad \tau\to+\infty \\ &= Ce^{\frac{\alpha-1}{\beta-2}M_1\cdot\frac{1}{M_2}\cdot\log\left(\frac{\xi-A}{B}\right)} \\ &= Ce^{\log\left(\frac{\xi-A}{B}\right)^{M_4}} \\ &= C\left(\frac{\xi-A}{B}\right)^{M_4} \quad \text{as} \quad \xi\to+\infty\end{aligned}$$

with a constant C and $M_4 := [(\alpha-1)M_1/(\beta-2)M_2] > 0$. Since the trajectories are lying on $\{\psi > 0\}$, it holds that $C > 0$. Furthermore, together with (5.2.9), we find that $\phi'(\xi) \sim \psi(\xi)$ as $\xi \to \infty$ is satisfied.

Similarly, we can obtain (5.2.12).

This completes the proof of Corollary 5.2.1. □

5.4.6 Proof of Theorem 5.2.5

Finally, we give the proof of Theorem 5.2.5 as follows.

Proof. We assume that there exists a connecting orbit that connect e_0^+ and e_0^+ for $\{(\phi,\psi) \in \Phi \mid \phi > 0\}$. This orbit passes through the line $\{\psi = 0\}$. Thus, there exists a stationary solution (which corresponds to the orbit of (5.1.4)) with the singularities at $\xi \to -\infty$ and $\xi \to +\infty$ and we prove the existence of a constant ξ_*, and it is sufficient for us to prove (5.2.13) and (5.2.14).

Using (5.3.12), we then have

$$\begin{aligned}\frac{d\eta}{d\xi} &= \frac{d\eta}{d\tau}\cdot\frac{d\tau}{ds}\cdot\frac{ds}{d\xi} = r^{\frac{\alpha\beta-\beta}{2}}\cdot\lambda^{-\alpha\beta+\alpha+\beta-1}\cdot\phi^{-\alpha} \\ &= r^{\frac{(\alpha+1)(\beta-2)}{2}}\overline{\lambda}^{-\alpha+\beta-1} \\ &= \left\{C_1 e^{-\frac{2}{\beta(\beta-2)}\eta}(1+o(1))\right\}^{\frac{(\alpha+1)(\beta-2)}{2}}\cdot\left\{C_2 e^{-\frac{1}{\beta}\eta}(1+o(1))\right\}^{-\alpha+\beta-1} \\ &\sim B_1 e^{-\frac{\alpha+1}{\beta}\eta}\cdot e^{-\frac{-\alpha+\beta-1}{\beta}\eta} = B_1 e^{-\eta} \quad \text{as} \quad \eta\to+\infty\end{aligned}$$

with a constant $B_1 > 0$. This yields

$$\xi(\eta) \sim B_2 e^{\eta} + A \quad \text{as} \quad \eta\to+\infty, \quad (B_2 > 0,\ A \in \mathbb{R}).$$

We can see $\xi(\eta) \to +\infty$ as $\eta \to +\infty$ since we focus on the points on $\mathcal{W}^s(e_2^+)$. This relationship shows that

$$\eta(\xi) \sim \log\frac{\xi-A}{B} \quad \text{as} \quad \xi\to+\infty$$

holds. Therefore, we have

$$\phi(\xi) = \lambda^{-\beta+2} = r^{-(\beta-2)}\overline{\lambda}^{-(\beta-2)} \sim Ce^{\eta} \sim C\left(\frac{\xi-A}{B}\right)$$

with a constant C. Since the trajectories are lying on $\{\phi > 0\}$, it holds that $C > 0$. Similarly, we can obtain (5.2.14). □

5.5 Conclusions and Remarks

In this chapter, we studied the stationary problem (5.1.2) on the bases of the theory of dynamical systems. The Poincaré-Lyapunov compactification gives the information on the dynamics around the equilibria at infinity, and then we obtain the existence and asymptotic behavior of the stationary solutions of (5.1.1).

From the viewpoint of the theory of partial differential equations, it should be considered how we can formulate the solutions of (5.1.2) on a finite-interval or semi-infinite interval or $\mathbb{R}$ with the functions obtained in Theorems. However, since our interest in this chapter is to study the solutions of (5.1.2) from the dynamical system viewpoint, we did not discuss it. It should be noted that the mathematical formulation of the solution (in a weak sense) could be obtained by considering a suitable function space as shown in [32] (it will be addressed in future works as well). Furthermore, in the MEMS equation, the solution u is meaningful in the range $0 \leq u < 1$, and the behavior at $u = 1$ is of interest. However, our results constitute solutions outside of this range. This chapter does not approach the aspect of singularity formation at $u = 1$ in (5.1.1) from the viewpoint of stationary problems. These suggest that further analysis is needed to clarify the behavior of (5.1.1) at $u = 1$.

In addition, since the theory of blow-up (desingularization of the vector fields) is not applicable for the non-polynomial vector fields, we cannot deal with the general case that $\alpha \in \mathbb{R}$. Furthermore, in the case that α, $\beta \in 2\mathbb{N}+1$, it is too complicated to determine the dynamics near the singularities on the Poincaré-Lyapunov disk. Hence, we leave it open here.

Furthermore, we discuss a property of (5.1.4) as follows. The function

$$H(\phi, \psi) = -\frac{1}{\alpha - 1}\phi^{-\alpha+1} - \int \frac{\psi}{\mu(1 + \delta\psi^{\beta})}\, d\psi$$

is a conserved quantity of (5.1.4). In fact,

$$\frac{d\phi}{d\psi} = \frac{d\phi/d\xi}{d\psi/d\xi} = \frac{\psi}{\mu(1 + \delta\psi^{\beta})}\phi^{\alpha}$$

holds. However, the integral part of this conserved quantity cannot be represented explicitly. The derivation of the conserved quantity for the general case is going to be a future work.

As mentioned in Remark 5.3.2, we only show the direction of vector fields (arrows) in Figure 5.3.3 and have not been able to give a mathematically rigorous explanation for the closed orbits from e_0^+ to e_0^+. We leave it open here as well.

We could raise the question of whether the results of classical dynamical systems hold in dynamical systems at infinity (we can see a similar situation in equation (5.13) of [14]).

Chapter 6

Radially symmetric stationary solutions for a MEMS type reaction-diffusion equation with fringing field

Abstract

Radially symmetric stationary solutions for a MEMS type reaction-diffusion equation with fringing field are considered. This equation arises in the study of the Micro-Electro-Mechanical System (MEMS) devices. This chapter is devoted to the study of the existence of these solutions, information about their shape, and their asymptotic behavior. These are studied by applying the framework that combines Poincaré type compactification, classical dynamical systems theory, and geometric methods for desingularization of vector fields called the blow-up technique. This chapter is based on the following published paper ([36]):

> Ichida, Y., Sakamoto, T.O.: Radially symmetric stationary solutions for a MEMS type reaction-diffusion equation with fringing field, Nonlinearity, **36**, 71–109 (2023).

6.1 Introduction

6.1.1 Known results and motivation

In this chapter, we consider the following MEMS type reaction-diffusion equation

$$U_t = \Delta U + \frac{\mu + \delta|\nabla U|^2}{1-U}, \quad t > 0, \quad x \in \mathbb{R}^N, \quad U = U(t,x) \tag{6.1.1}$$

with $3 \leq N \in \mathbb{N}$, $\mu > 0$, and $\delta > 0$. In addition, δ is not a continuous value, however, a discrete value that satisfies certain conditions for analytical convenience, as described later. (6.1.1) is derived from the study of the Micro-Electro-Mechanical System (for short, MEMS). Here, μ represents the applied voltage, and the nonlinear and gradient term $\delta|\nabla U|^2$ is due to an effect called the fringing field. There has been a lot of research on the MEMS equation. We refer the readers to works [17, 59] and references therein for more details on the background and derivation of the MEMS model. For instance, we also refer

[19, 21, 26, 35, 54, 68, 69] and references therein for a detailed description of the fringing field and equations of this type.

The spatial one-dimensional version of (6.1.1):

$$u_t = u_{xx} + \mu \frac{1+\delta u_x^\beta}{(1-u)^\alpha}, \quad t > 0, \quad x \in \mathbb{R}, \tag{6.1.2}$$

is studied in Chapter 5 ([35]). Here, $\alpha \in 2\mathbb{N}$, $2 \neq \beta \in 2\mathbb{N}$, $\mu > 0$, and $\delta \geq 0$. In Chapter 5 ([35]), the existence, profiles, and asymptotic behavior of the stationary solutions of (6.1.2) are studied by applying Poincaré-Lyapunov compactification and dynamical systems theory. Additionally, we note that the results follow from the analysis of the dynamics at infinity.

Not only these results but also studies in [21] have motivated us to study the multidimensional version of (6.1.2). Indeed, Ghergu-Miyamoto [21] considered the following problem

$$\begin{cases} -\Delta U = \dfrac{\lambda + \delta |\nabla U|^2}{1-U}, \quad U > 0 & \text{in} \quad B, \\ U = 0 & \text{on} \quad \partial B, \end{cases} \tag{6.1.3}$$

where $B \subset \mathbb{R}^N$ $(N \geq 2)$ denotes the open ball and $\lambda, \delta > 0$ are real numbers. This equation is an elliptic equation representing the steady-state of (6.1.1). The singularity at the origin and the bifurcation structure of the radial regular / rupture solution were discussed. According to [21], regular solution is to satisfy $0 < U < 1$ in B and rupture solution is to satisfy $U(0) = 1$. They showed a clear difference from the result in [69], considered the case separation by the value taken by δ ($0 < \delta < 1$, $\delta = 1$, and $\delta > 1$), discussed the solution structure. Also, Joseph-Lundgren [42] studied a related ODE:

$$(r^{n-1}u')' + \lambda r^{n-1} \mathcal{F}(u) = 0, \tag{6.1.4}$$

where

$$\mathcal{F}(u) = (1+\alpha u)^\beta, \quad \alpha\beta > 0 \tag{6.1.5}$$

or

$$\mathcal{F}(u) = e^u. \tag{6.1.6}$$

with the boundary conditions $u(1) = u'(0) = 0$. They discuss the uniqueness properties of the positive solutions for (6.1.4) (cf. [21]). The relation between (6.1.4) and (6.1.3) is shown in the next subsection.

In this chapter, we study the radially symmetric solutions for (6.1.1) using Poincaré type compactification and dynamical systems theory. Here, we refer to [31, 33, 32] for the details of the Poincaré type compactification.

Here we note that for the 1-dimensional case (6.1.2), the results stated in Chapter 5 ([35]) can not be obtained by applying the computations shown in the later sections of this chapter straightforwardly (see Chapter 5 ([35]) for the details). Moreover, for $N = 2$, the dynamics associated with the radially symmetric stationary problem of (6.1.1) is not topologically equivalent to the case with $N \geq 3$. For instance, in Subsection 6.3.1, the equilibria E_2 and E_1 are the same for $N = 2$, and the center manifolds may exist near the equilibrium. Then a more careful analysis is necessary for $N = 2$, therefore, it will be addressed in future work.

The next subsection presents the mathematical settings to consider the dynamical systems associated with the radially symmetric stationary problem of (6.1.1). The main results of this chapter are shown in Section 6.2. The relations between our results and that of [21] are discussed in Section 6.7 as well as Remarks in Section 6.2.

6.1.2 Preliminaries

The stationary problem of (6.1.1) is

$$-\Delta U = \frac{\mu + \delta|\nabla U|^2}{1-U}, \quad x \in \mathbb{R}^N, \quad U = U(x). \tag{6.1.7}$$

This chapter is devoted to the study of the radially symmetric solutions of (6.1.7):

$$U'' + \frac{N-1}{r}U' + \frac{\mu + \delta(U')^2}{1-U} = 0, \quad \left({}' = \frac{d}{dr} \quad \text{and} \quad {}'' = \frac{d^2}{dr^2} \right) \tag{6.1.8}$$

with $U = U(r)$ and $r = |x| > 0$. In elliptic equations, it is important to consider radially symmetric solutions when we investigate the structure of these solutions. By considering radially symmetric stationary solutions, we are led to the problem of considering ODEs. However, problems such as the existence of solutions are not easy to solve. Following [21], we divide the cases by the value of δ as follows:

(I) Case 1: $0 < \delta < 1$. Let $u(r) = 1 - (1 - U(r))^{1-\delta}$ and $\tilde{\mu} = (1-\delta)\mu > 0$. Then, $u(r)$ satisfies

$$u'' + \frac{N-1}{r}u' + \tilde{\mu}(1-u)^{-p} = 0, \quad p = \frac{1+\delta}{1-\delta} > 1. \tag{6.1.9}$$

Note that since $U < 1$ from this transformation, $u < 1$.

(II) Case 2: $\delta = 1$. Let $u(r) = -2\log(1 - U(r))$ and $\tilde{\mu} = 2\mu > 0$. Then, (6.1.8) becomes the following:

$$u'' + \frac{N-1}{r}u' + \tilde{\mu}e^u = 0. \tag{6.1.10}$$

From the antilogarithm condition, $U < 1$ must be satisfied.

(III) Case 3: $\delta > 1$. Let $u(r) = (1 - U(r))^{-(\delta-1)} - 1$ and $\tilde{\mu} = (\delta-1)\mu > 0$. From (6.1.8),

$$u'' + \frac{N-1}{r}u' + \tilde{\mu}(u+1)^p = 0, \quad p = \frac{\delta+1}{\delta-1} > 1 \tag{6.1.11}$$

holds. Note that since $U < 1$ from this transformation, $u > -1$.

Here we note that (6.1.9) and (6.1.11) correspond to (6.1.4)-(6.1.5) in the case that $(\alpha, \beta) = (-1, -p)$ and $(1, p)$, respectively. Additionally, (6.1.10) corresponds to (6.1.4)-(6.1.6). Still, the difference between them and our problem is the range of radius r, that is, we consider the solutions on $0 \le r < \infty$.

(6.1.9), (6.1.10), and (6.1.11) are non-autonomous systems, especially, $r = 0$ is a singular point. In order to study their solutions with the dynamical systems approach, we consider the following transformations that transform (6.1.9), (6.1.10), and (6.1.11) into the autonomous systems on $\mathbb{R}^2$ and remove the singularity $r = 0$ for each case.

(I) Case 1: $0 < \delta < 1$. As in [33, 41], we introduce the following change of variables:

$$t = \kappa \log r, \quad a(t) = r^{-\alpha}(1-u), \quad \alpha = 1 - \delta > 0, \quad \kappa = \pm 1. \tag{6.1.12}$$

Then, (6.1.9) is transformed into the following:

$$\ddot{a} + A\dot{a} + Ba - \tilde{\mu}a^{-p} = 0, \quad \left(\dot{} = \frac{d}{dt} \quad \text{and} \quad \ddot{} = \frac{d^2}{dt^2} \right), \tag{6.1.13}$$

equivalently

$$\begin{cases} \dot{a} = b, \\ \dot{b} = -Ab - Ba + \tilde{\mu} a^{-p}, \end{cases} \qquad \left(\dot{} = \frac{d}{dt} \right), \tag{6.1.14}$$

where we set

$$\begin{aligned} A &= \kappa(2\alpha + N - 2) = \kappa(N - 2\delta), \quad \kappa = \pm 1, \\ B &= \alpha(\alpha + N - 2) = (1 - \delta)(N - \delta - 1) > 0. \end{aligned}$$

Note that $A > 0$ holds when $\kappa = 1$, and $A < 0$ holds when $\kappa = -1$. If $\kappa = 1$, then $r \to \infty$ as $t = \log r \to \infty$ holds. Therefore, to discuss the behavior of the solution to (6.1.9) as $r \to \infty$, it is necessary to study the asymptotic behavior of the solutions of (6.1.13) as $t \to \infty$. Similarly, $r \to 0$ as $t \to \infty$ in the case that $\kappa = -1$.

(II) Case 2: $\delta = 1$. Consider the following change of variables:

$$t = \kappa \log r, \quad a(t) = r^2 e^u, \quad \kappa = \pm 1. \tag{6.1.15}$$

Note that since $a(t) = r^2 e^u > 0$, we only need to consider $a(t) > 0$. If we consider $r \to 0$, then $a \to 0$. Then we have

$$\begin{cases} \dot{a} = b, \\ \dot{b} = \dfrac{1}{a} b^2 - Ab - \tilde{\mu} a^2 + 2(N - 2)a, \end{cases} \qquad \left(\dot{} = \frac{d}{dt} \right), \tag{6.1.16}$$

where

$$A = \kappa(N - 2), \quad \kappa = \pm 1.$$

Note that $A > 0$ in the case that $\kappa = 1$, and $A < 0$ in the case that $\kappa = -1$.

(III) Case 3: $\delta > 1$. We make the following change of variables:

$$t = \kappa \log r, \quad a(t) = r^{-\alpha}(1 + u), \quad \alpha = 1 - \delta < 0, \quad \kappa = \pm 1, \tag{6.1.17}$$

then (6.1.11) is transformed to the following ODE:

$$\begin{cases} \dot{a} = b, \\ \dot{b} = -Ab - Ba - \tilde{\mu} a^p, \end{cases} \qquad \left(\dot{} = \frac{d}{dt} \right), \tag{6.1.18}$$

where

$$\begin{aligned} A &= \kappa(2\alpha + N - 2) = \kappa(N - 2\delta), \quad \kappa = \pm 1, \\ B &= \alpha(\alpha + N - 2) = (1 - \delta)(N - \delta - 1). \end{aligned}$$

Here, the sign of the constants A and B depends on the parameters δ and κ as shown in Table 6.1.

Then, by introducing transformations (6.1.12), (6.1.15), and (6.1.17) that remove the singularity of $r = 0$, we are led to the problem of studying the behavior of the two-dimensional ODE systems (6.1.14), (6.1.16), and (6.1.18). Further, as shown in [31, 33, 32, **?**, 49, 50], it is expected that there are solutions $(a(t), b(t))$ of (6.1.14)), (6.1.16) and (6.1.18) that blow up, i.e., $\|(a(t), b(t))\| \to \infty$ as $t \to \infty$. To study the behavior of them, it is necessary to study the dynamics of (6.1.14), (6.1.16) and (6.1.18) on $\mathbb{R}^2 \cup \{\|(a(t), b(t))\| = \infty\}$. Then, we can apply the Poincaré type compactification

κ	A or B	$1<\delta<\frac{N}{2}$	$\delta=\frac{N}{2}$	$\frac{N}{2}<\delta<N-1$	$\delta=N-1$	$\delta>N-1$
1	A	$+$	0	$-$	$-$	$-$
1	B	$-$	$-$	$-$	0	$+$
-1	A	$-$	0	$+$	$+$	$+$
-1	B	$-$	$-$	$-$	0	$+$

Table 6.1: The sign of A and B.

(Poincaré compactification, Poincaré-Lyapunov compactification) and geometric methods for desingularization of vector fields (blow-up technique) for (6.1.14), (6.1.16), and (6.1.18). Here we refer to [14, 31, 33, 32, 49] for the Poincaré type compactification, and [1, 14] for the blow-up technique. In other words, we expect that all solutions of (6.1.8) are classified in a similar way as in these previous studies. Furthermore, it is expected that the existence of connecting orbits in the dynamical systems including infinity not only proves the existence of the solutions of (6.1.8) corresponding to the connecting orbits but also provides its profiles. Additionally, the asymptotic behavior of the solutions of (6.1.8) as $r\to\infty$ and $r\to 0$ can be studied. As in [31, 49, 50], the dynamics obtained by the Poincaré compactification, which includes the dynamics at infinity, is represented by the dynamics on the Poincaré disk. Similarly, the corresponding one obtained by Poincaré-Lyapunov compactification is represented by the dynamics on the Poincaré-Lyapunov disk.

However, the classical results on the blow-up technique in this framework require us to impose the restriction $p\in\mathbb{N}$ (see [1, 8, 14] and references therein). Then, as shown in Case1 and Case 3, we consider (6.1.1) with the restriction that δ takes discrete values. More precisely, we consider (6.1.1) with the following situations.

- Case 1; Since $p=(1+\delta)/(1-\delta)$ as defined in (6.1.9), δ takes a discrete value so that $p\in\mathbb{N}$ and $\delta=(p-1)/(p+1)$ are satisfied. For instance, if $p=2,3,4,\cdots$, then $\delta=1/3,1/2,3/5,\cdots$.

- Case 3; If $p\in\mathbb{N}$, $p=(\delta+1)/(\delta-1)$, then δ is a discrete value satisfying $\delta=(p+1)/(p-1)$. For instance, if $p=2,3,4,\cdots$, then $\delta=3,2,5/3,\cdots$. Moreover, for each δ range, a restriction on N (and p) is added as follows (see also Table 6.1).

  (i) If $1<\delta<N/2$ holds, then one needs to impose that for $p=2,3,4,\cdots$, $N\geq 7, N\geq 5, N\geq 4,\cdots$, respectively.

  (ii) If $\delta=N/2$ holds, then $(p,N)=(2,6),(3,4),(5,3)$, and there is no $N\geq 3$ that satisfies $\delta=N/2$.

  (iii) If $N/2<\delta<N-1$, we only need to consider the case that $p=2,4$, and for $N\geq 3$, $N/2<\delta<N-1$ holds if and only if $N=5$ or 3.

  (iv) $\delta=N-1$ holds if and only if $(p,N)=(2,4),(3,3)$.

  (v) If $\delta>N-1$, we can only consider the case that $(p,N)=(2,3)$.

Under these restrictions, the objective is to classify all solutions of (6.1.8). In particular, we use a different Poincaré type compactification than in [21] to reveal the shapes and asymptotic behavior of the solutions. And this problem is a multi-dimensional version of Chapter 5 ([35]). It is expected that this will lead to a deeper understanding of the behavior of typical solutions to the MEMS equations. In addition, the authors have clarified the behavior and properties of (typical) solutions of various equations in the framework

described above (see [31, 33, 32, 35]). In this chapter, we are also investigating the question of how far we can investigate the structure of solutions in a unified way using this framework.

This chapter is organized as follows. In the next section, we state the main results of this chapter. In Section 6.3, we obtain the dynamics of (6.1.14) on the Poincaré disk via Poincaré compactification and blow-up technique. The dynamics on the Poincaré-Lyapunov disk in (6.1.16) corresponding to Case 2 are discussed in Section 6.4. Similarly, those discussions for Case 3 are in Section 6.5. The proof of Theorems will be completed in Section 6.6. Section 6.7 is devoted to the concluding remarks.

6.2 Main results

In this section, the main results of this chapter are described. Hereinafter, note that the meaning of the symbol $F(\eta) \sim G(\eta)$ as $\eta \to +\infty$ is as follows:

$$\lim_{\eta\to+\infty} \left| \frac{F(\eta)}{G(\eta)} \right| = 1.$$

First, the following two results are obtained for Case 1 with $0 < \delta < 1$.

Theorem 6.2.1
Assume that $3 \le N \in \mathbb{N}$, $\mu > 0$, $p \in \mathbb{N}$, and $0 < \delta < 1$ with $\delta = (p-1)/(p+1)$. Then (6.1.8) has a radially symmetric stationary solution (which corresponds to an orbit of (6.1.14)) with the singularity at $r \to +\infty$. Moreover, this solution $U(r)$ satisfies the following:

- $\lim_{r\to 0} U(r) = 1 - C \quad (C > 0), \quad \lim_{r\to 0} U'(r) = 0 \quad \lim_{r\to+\infty} U(r) = -\infty.$
- *$U(r) < 1$ and $U'(r) < 0$ hold for $r \in (0, +\infty)$.*

In addition, the asymptotic behavior for $r \to +\infty$ is

$$U(r) \sim \begin{cases} 1 - \{K_1 r^{\alpha+\sigma_1} + K_2 r^{\alpha+\sigma_2} + M_1 r^{\alpha}\}^{\frac{1}{1-\delta}}, & (D > 0), \\ 1 - \left\{ r^{\frac{2-N}{2}} K(r) + M_1 r^{\alpha} \right\}^{\frac{1}{1-\delta}}, & (D < 0). \end{cases} \tag{6.2.1}$$

Here, $\alpha = 1 - \delta > 0$, $\tilde{\mu} = (1-\delta)\mu > 0$, and the following hold:

$$\begin{aligned} &\sigma_1 = \frac{-A + \sqrt{D}}{2}, \quad \sigma_2 = \frac{-A - \sqrt{D}}{2}, \\ &M_1 = (\tilde{\mu}/B)^{\frac{1}{p+1}} > 0, \quad D = (N-2)^2 - 4(\delta+1)(N-2) + 4(\delta+1)(\delta-1), \\ &K(r) = K_3 \sin[\frac{\sqrt{|D|}}{2} \log r] + K_4 \cos[\frac{\sqrt{|D|}}{2} \log r], \end{aligned}$$

where K_j $(1 \le j \le 4)$ are constants.

Remark 6.2.1
In this Theorem 6.2.1, no specific evaluation of the position of $1 - C$ has been obtained. We also do not have an evaluation of $r_0 \in (0, +\infty)$, where $U(r_0) = 0$. Note that the asymptotic behavior of $U(r)$ and $U'(r)$ in $r \to 0$ cannot be shown explicitly. This requires information up to the higher-order terms of the ODE, which is difficult to analyze, so this is an open problem. Also note that there is no N and δ such that $D = 0$, as described

later in Remark 6.3.1. This result should be related to the result on regular solutions in [21]. However, since the constants mentioned above have not been evaluated, we cannot conclude the relations precisely. We leave it open here.

Theorem 6.2.2
Assume that $3 \leq N \in \mathbb{N}$, $\mu > 0$, $p \in \mathbb{N}$, *and* $0 < \delta < 1$ *with* $\delta = (p-1)/(p+1)$. *Then* (6.1.8) *has a family of radially symmetric stationary solutions (which corresponds to a family of the orbits of* (6.1.14)*) with the singularities at* $r = 0$ *and* $r \to +\infty$. *Moreover, each solution* $U(r)$ *satisfies the following:*

- $\lim_{r\to 0} U(r) = -\infty, \quad \lim_{r\to 0} U'(r) = +\infty \quad \lim_{r\to+\infty} U(r) = -\infty.$
- $U(r) < 1$ *holds for* $r \in (0, +\infty)$.
- *There exists a constant* $r_* \in (0, +\infty)$ *such that the following holds:* $U'(r) > 0$ *for* $r \in (0, r_*)$, $U'(r_*) = 0$ *and* $U'(r) < 0$ *for* $r \in (r_*, +\infty)$.

In addition, the asymptotic behavior of $U(r)$ *and* $U'(r)$ *for* $r \to 0$ *are*

$$\begin{cases} U(r) \sim 1 - A_1 r^{-\frac{N-2}{1-\delta}} \\ U'(r) \sim A_2 r^{-\frac{N-1-\delta}{1-\delta}} \end{cases} \quad \text{as} \quad r \to 0 \tag{6.2.2}$$

with positive constants A_1 *and* A_2, *and the asymptotic behavior for* $r \to +\infty$ *is* (6.2.1).

Remark 6.2.2
In Theorem 6.2.2, there is no specific evaluation of the position of r_* *and* $U(r_*)$. *We also know that there exists* $r_\pm \in (0, +\infty)$ *such that* $U(r_\pm) = 0$, *however, we do not have a specific evaluation for this either. A note on the shape of* U *is in order. We only know that the value* $U(r_*)$ *at the extreme point* r_* *is less than* 1. *However, since we are considering a family of trajectories connecting the equilibria of the source point and sink point, we should be able to choose a trajectory that realizes* $0 < U(r_*) < 1$. *It should be noted that this is a new result not mentioned in [21].*

Second, the following result is obtained for Case 2 with $\delta = 1$.

Theorem 6.2.3
Assume that $3 \leq N \in \mathbb{N}$, $\mu > 0$, *and* $\delta = 1$. *Then* (6.1.8) *has a radially symmetric stationary solution (which corresponds to the orbit of* (6.1.16)*) with the singularity at* $r \to +\infty$. *Moreover, its solution* $U(r)$ *satisfies the following:*

- $\lim_{r\to 0} U(r) = 1 - C, \quad \lim_{r\to 0} U'(r) = 0, \quad \lim_{r\to+\infty} U(r) = -\infty, \quad$ *with* $C > 0$.
- $U(r) < 1$ *holds for* $r \in (0, +\infty)$.

In addition, the asymptotic behavior for $r \to +\infty$ *is*

$$U(r) \sim \begin{cases} 1 - \exp\left(\log r - \dfrac{1}{2}\log(K_1 r^{\sigma_1} + K_2 r^{\sigma_2} + M_4)\right), & (N \geq 11) \\ 1 - \exp\left(\log r - \dfrac{1}{2}\log\{K_3 r^{\sigma} \log r + K_4 r^{\sigma} + M_4\}\right), & (N = 10) \\ 1 - \exp\left[\log r - \dfrac{1}{2}\log\left\{r^{-\frac{A}{2}} K(r) + M_4\right\}\right]. & (N \leq 9) \end{cases} \tag{6.2.3}$$

Here, $\tilde{\mu} = 2\mu > 0$, and the following hold:

$$\sigma_1 = \frac{-A+\sqrt{P}}{2}, \quad \sigma_2 = \frac{-A-\sqrt{P}}{2}, \quad \sigma = -\frac{A}{2},$$
$$M_4 = 2\tilde{\mu}^{-1}(N-2) > 0, \quad P = (N-2)(N-10).$$
$$K(r) = K_5 \sin[\frac{\sqrt{|P|}}{2}\log r] + K_6 \cos[\frac{\sqrt{|P|}}{2}\log r],$$

where K_j $(1 \le j \le 6)$ are constants.

We can impose the same remarks on this theorem as on Remark 6.2.1. Next, we state the following result was obtained in Case 3, i.e., when $1 < \delta < N/2$.

Theorem 6.2.4
Assume that $3 \le N \in \mathbb{N}$, $\mu > 0$, $p \in \mathbb{N}$, and $1 < \delta < N/2$ with $\delta = (p+1)/(p-1)$. Then (6.1.8) *has a radially symmetric stationary solution (which corresponds to the orbit of* (6.1.18)*) with the singularity at $r \to +\infty$. Moreover, its solution $U(r)$ satisfies the following:*

- $\lim_{r\to 0} U(r) = 1 - C, \quad \lim_{r\to 0} U'(r) = 0, \quad \lim_{r\to+\infty} U(r) = -\infty, \quad$ *with $C > 0$.*
- *$U(r) < 1$ holds for $r \in (0, +\infty)$.*

In addition, the asymptotic behavior for $r \to +\infty$ is

$$U(r) \sim \begin{cases} 1 - \left\{K_1 r^{\alpha+\sigma_1} + K_2 r^{\alpha+\sigma_2} + L_1 r^{\alpha}\right\}^{-\frac{1}{\delta-1}}, & (D > 0) \\ 1 - \left\{r^{\frac{2-N}{2}} K(r) + L_1 r^{\alpha}\right\}^{-\frac{1}{\delta-1}}. & (D < 0) \end{cases} \tag{6.2.4}$$

Here, $\alpha = 1 - \delta < 0$, $\tilde{\mu} = (\delta-1)\mu > 0$, and the following hold:

$$\sigma_1 = \frac{-A+\sqrt{D}}{2}, \quad \sigma_2 = \frac{-A-\sqrt{D}}{2}, \quad L_1 = \left(-\frac{B}{\tilde{\mu}}\right)^{\frac{1}{p-1}} > 0$$
$$D = D(N,\delta) = (N-2)^2 - 4(\delta+1)(N-2) + 4(\delta+1)(\delta-1),$$
$$K(r) = K_3 \sin[\frac{\sqrt{|D|}}{2}\log r] + K_4 \cos[\frac{\sqrt{|D|}}{2}\log r],$$

where K_j $(1 \le j \le 4)$ are constants.

We can impose the same remarks on this theorem as on Remark 6.2.1. Next, we state the theorem obtained for the case $\delta = N/2$. For this case, the following result is shown in [21].

Theorem 6.2.5 ([21], Theorem 1.2 (iii))
Let $N \ge 2$. Assume $\delta = N/2$. Then all the radial regular solutions of (6.1.3) *can be described as*

$$(\mu, U(r)) = (2N\alpha(1-\alpha), \alpha(1-r^2)), \quad 0 < \alpha < 1.$$

Further, for $\delta = N/2$, we obtain the behavior of the radially symmetric solutions of (6.1.8) in the case that

$$\mu \neq 2N\alpha(1-\alpha)$$

as follows.

Theorem 6.2.6
Assume that $3 \leq N \in \mathbb{N}$, $\mu > 0$, $p \in \mathbb{N}$, and $\delta = N/2$ with $\delta = (p+1)/(p-1)$. As mentioned earlier, in this case, we only need to consider $p = 2, 3, 5$, and correspondingly $N = 6, 4, 3$. Then (6.1.8) has a radially symmetric stationary solution (which corresponds to the orbit of (6.1.18)) with the singularity at $r \to +\infty$. Moreover, its solution $U(r)$ satisfies the following:

- $\lim_{r\to 0} U(r) = 1-C, \quad \lim_{r\to 0} U'(r) = 0, \quad \lim_{r\to+\infty} U(r) = \lim_{r\to+\infty} U'(r) = -\infty \quad$ *with* $C > 0$.
- $U(r) < 1$ *holds for* $r \in (0, +\infty)$.

In addition, the asymptotic behavior of $U(r)$ and $U'(r)$ for $r \to \infty$ are

$$\begin{cases} U(r) \sim 1 - K_1 r^2, \\ U'(r) \sim -K_2 r, \end{cases} \qquad \text{as} \quad r \to \infty, \tag{6.2.5}$$

with positive constants K_j $(j = 1, 2)$.

Note that no specific evaluation of the position of $1 - C$ has been obtained. We also do not have an evaluation of $r_0 \in (0, +\infty)$, where $U(r_0) = 0$. It can be seen that the behavior of the solution as $r \to 0$ is qualitatively the same for Theorem 6.2.1, Theorem 6.2.3, Theorem 6.2.4, and Theorem 6.2.6. It should be noted that the asymptotic behavior of $U(r)$ as $r \to 0$ has the same form as the exact solution at $\mu = 2N\alpha(1-\alpha)$ in [21].

Finally, we state the theorem obtained for the case $N/2 < \delta < N-1$. The claim of this theorem gives not only (6.2.7), such that the asymptotic behavior as $r \to 0$ is completely consistent with that of [21], but also (6.2.8), which is more detailed.

Theorem 6.2.7
Assume that $3 \leq N \in \mathbb{N}$, $\mu > 0$, $p \in \mathbb{N}$, and $N/2 < \delta < N-1$ with $\delta = (p+1)/(p-1)$. As mentioned earlier, in this case, we only need to consider $p = 2, 4$ and correspondingly $N = 5, 3$. Then (6.1.8) has a radially symmetric stationary solution (which corresponds to the orbit of (6.1.18)) with the singularity at $r \to 0$ and $r \to +\infty$. Moreover, its solution $U(r)$ satisfies the following:

- $\lim_{r\to 0} U(r) = \lim_{r\to 0} \left(1 - \sqrt{\dfrac{\mu}{N-1-\delta}}\, r\right) = 1, \quad \lim_{r\to 0} U'(r) = -\sqrt{\dfrac{\mu}{N-1-\delta}}.$
- $\lim_{r\to+\infty} U(r) = \lim_{r\to+\infty} U'(r) = -\infty$
- $U(r) < 1$ *holds for* $r \in (0, +\infty)$.

In addition, the asymptotic behavior of $U(r)$ and $U'(r)$ for $r \to \infty$ are

$$\begin{cases} U(r) \sim 1 - A_1 r^{\frac{N-2}{\delta-1}}, \\ U'(r) \sim -A_2 r^{\frac{N-\delta-1}{\delta-1}}, \end{cases} \qquad \text{as} \quad r \to \infty \tag{6.2.6}$$

with positive constants A_j $(j = 1, 2)$. Furthermore, the asymptotic behavior $U(r)$ for $r \to 0$ are

$$U(r) \sim 1 - \sqrt{\frac{\mu}{N-1-\delta}}\, r \quad \text{as} \quad r \to 0 \tag{6.2.7}$$

$$\sim \begin{cases} 1 - \left\{K_1 r^{\alpha-\sigma_1} + K_2 r^{\alpha-\sigma_2} + L_1 r^{\alpha}\right\}^{-\frac{1}{\delta-1}}, & (D > 0) \\ 1 - \left\{r^{\frac{2-N}{2}} K(r) + L_1 r^{\alpha}\right\}^{-\frac{1}{\delta-1}}, & (D < 0) \end{cases} \tag{6.2.8}$$

Here, $\alpha = 1-\delta < 0$, $\tilde{\mu} = (\delta-1)\mu > 0$, and the following hold:

$$\sigma_1 = \frac{-A+\sqrt{D}}{2}, \quad \sigma_2 = \frac{-A-\sqrt{D}}{2}, \quad L_1 = \left(-\frac{B}{\tilde{\mu}}\right)^{\frac{1}{p-1}} > 0$$
$$D = D(N,\delta) = (N-2)^2 - 4(\delta+1)(N-2) + 4(\delta+1)(\delta-1),$$
$$K(r) = K_3 \sin[\frac{\sqrt{|D|}}{2}\log r] + K_4 \cos[\frac{\sqrt{|D|}}{2}\log r],$$

where K_j $(1 \le j \le 4)$ are constants.

Remark 6.2.3
In Theorem 6.2.7, note that there is no N and δ such that $D = 0$, as described later in Subsection 6.5.4. By deriving the asymptotic behavior in a similar way as [33, 32] in the derivation process, we obtain (6.2.8)*. As can be seen from the proof of this theorem, which is omitted in the statement of the theorem, the asymptotic behavior of $U'(r)$ in $r \to 0$ can be displayed explicitly. Furthermore, by selecting the principal terms in the derivation process, we can obtain* (6.2.7)*.*

Remark 6.2.4
In Theorem 6.2.7, the asymptotic behavior (6.2.7) *is in perfect agreement with the results obtained in (1.10) of [21], indicating that we have followed up the results of previous studies with an approach based on different ideas. Here, [21] investigates the global behavior by considering Lyapunov functions for ODE systems derived with different transformations than* (6.1.17) *(in Section 6.1 of this chapter), while this chapter uses Poincaré-Lyapunov compactification to investigate the dynamics of* (6.1.18) *to infinity.*

As described in Section 6.7, we did not obtain a clear result in $\delta \ge N-1$. The reason for this is that there is a restriction on the range of existence of the transformations U and u, and u and a.

6.3 Dynamics of (6.1.14) to infinity

In this section, all the dynamics of (6.1.14) on $\mathbb{R}^2 \cup \{\|(a,b)\| = +\infty\}$ will be obtained by using Poincaré compactification. n other words, we can enumerate all the solutions to (6.1.8) that satisfy $0 < \delta < 1$ by revealing all the trajectories, including those to infinity. In fact, for the case of $\tilde{\mu} = 1$ in (6.1.14), the objective has already been achieved by Ichida-Sakamoto [33] (see Chapter 4). However, for the sake of clarity in the description of the proof of the theorem that follows, and for the convenience of the reader, we give brief details as a general $\tilde{\mu} > 0$.

Before starting the detailed analysis, we study the dynamics near finite equilibrium of (6.1.14). If p is even (resp. p is odd), then (6.1.14) has an equilibrium $E_A : (a,b) = (M_1, 0)$ (resp. have the equilibria $\pm E_A : (a,b) = (\pm M_1, 0)$) with $M_1 = (\tilde{\mu}/B)^{\frac{1}{p+1}}$.

Let J_A be the Jacobian matrix of the vector field (6.1.14) at E_A. J_A is

$$J_A = \begin{pmatrix} 0 & 1 \\ -B(1+p) & -A \end{pmatrix}.$$

Then, the behavior of the solution around E_A is different by the sign of D (which is defined in Theorem 6.2.1). For instance, the matrix J_A has the real distinct eigenvalues if $D > 0$, and other cases can be concluded similarly. In addition, if $\kappa = 1$, then the real parts of all eigenvalues of J_A are negative. Therefore, we conclude that E_A is a sink in the case that $\kappa = 1$. Similarly, we can determine that E_A is a source in the case that $\kappa = -1$.

Remark 6.3.1
As defined in Theorem 6.2.1, D is

$$D = (N-2)^2 - 4(1+\delta)(N-\delta-1) = (N-2)^2 - 4(\delta+1)(N-2) + 4(\delta+1)(\delta-1).$$

By setting $Q = N-2 > 0$, we get

$$D(Q) = Q^2 - 4(\delta+1)Q + 4(\delta+1)(\delta-1).$$

By examining the solution of this quadratic equation, we know that $D(Q) < 0$ and $D(Q) > 0$ hold. However, since Q and δ are discrete values, we need to verify that $D(Q) = 0$. Since

$$Q = 2(\delta+1) + 2\sqrt{2(\delta+1)} = \frac{4p}{p+1} + 4\sqrt{\frac{p}{p+1}}, \quad \left(\delta = \frac{p-1}{p+1}\right)$$

holds, it is not possible to go from $1 < p \in \mathbb{N}$ to $Q \in \mathbb{N}$. In other words, $D(Q) = D(N,\delta) = 0$ is never true. Correspondingly, the case of $D = 0$ is eliminated in Theorem 6.2.1. Note that the equation of Q obtained here agrees with the one obtained in [42].

In order to study the dynamics of (6.1.14) on the Poincaré disk, we desingularize it by the time-scale desingularization

$$ds/dt = a^{-p} \quad \text{for} \quad p \in 2\mathbb{N}. \tag{6.3.1}$$

Since we assume that p is even, the direction of the time does not change via this desingularization. Then, we have

$$\begin{cases} a' = a^p b, \\ b' = -Aa^p b - Ba^{p+1} + \tilde{\mu}, \end{cases} \qquad \left(' = \frac{d}{ds}\right). \tag{6.3.2}$$

First, we only discuss the case that p is even. The odd case is discussed in the later subsection (see Subsection 6.3.6).

Remark 6.3.2
It should be noted that the time scale desingularization (6.3.1) *is simply multiplying the vector field by a^p. Then, except for the singularity $\{a = 0\}$, the solution curves of the system (vector field) remain the same but are parameterized differently. Still, we refer to Section 7.7 of [44] and references therein for the analytical treatments of desingularization with the time rescaling. In what follows, we use the similar time rescaling (re-parameterization of the solution curves) repeatedly to desingularize the vector fields.*

Now we can consider the dynamics of (6.3.2) on the charts $\overline{U}_j$ and $\overline{V}_j$.

6.3.1 Dynamics on the chart $\overline{U}_2$

To obtain the dynamics on the chart $\overline{U}_2$, we introduce coordinates (λ, x) by the formulas

$$a(s) = x(s)/\lambda(s), \quad b(s) = 1/\lambda(s).$$

In this chart, it corresponds to $a \to 0$ and $b \to +\infty$, and the direction in which x is positive corresponds to the direction in which a is positive. For a geometric image, see Section 1.1 in this thesis and the figure in Section 2 of [31, 33, 32]. Then,

$$\begin{cases} \lambda' = A\lambda^{-p+1}x^p + B\lambda^{-p+1}x^{p+1} - \tilde{\mu}\lambda^2, \\ x' = \lambda^{-p}x^p + A\lambda^{-p}x^{p+1} + B\lambda^{-p}x^{p+2} - \tilde{\mu}\lambda x, \end{cases} \qquad \left(' = \frac{d}{ds}\right) \tag{6.3.3}$$

holds. Time-scale desingularization $d\tau/ds = \lambda^{-p}$ yields

$$\begin{cases} \lambda_\tau = A\lambda x^p + B\lambda x^{p+1} - \tilde{\mu}\lambda^{p+2}, \\ x_\tau = x^p + Ax^{p+1} + Bx^{p+2} - \tilde{\mu}\lambda^{p+1}x, \end{cases} \tag{6.3.4}$$

where $\lambda_\tau = d\lambda/d\tau$ and $x_\tau = dx/d\tau$. The system (6.3.4) has the equilibria

$$E_0^+ : (\lambda, x) = (0, 0),$$
$$E_1 : (\lambda, x) = \left(0, \frac{-A-(N-2)}{2B}\right), \quad E_2 : (\lambda, x) = \left(0, \frac{-A+(N-2)}{2B}\right).$$

The Jacobian matrices of the vector field (6.3.4) at these equilibria are

$$E_0^+ : \begin{pmatrix} 0 & 0 \\ 0 & 0 \end{pmatrix}, \quad E_1 : \begin{pmatrix} \left(\frac{-A-(N-2)}{2B}\right)^p \frac{A-(N-2)}{2} & 0 \\ 0 & \left(\frac{-A-(N-2)}{2B}\right)^{p-1} \frac{(N-2)(N-2+A)}{2B} \end{pmatrix},$$
$$E_2 : \begin{pmatrix} \left(\frac{-A+(N-2)}{2B}\right)^p \frac{A+(N-2)}{2} & 0 \\ 0 & \left(\frac{-A+(N-2)}{2B}\right)^{p-1} \frac{(N-2)(N-2-A)}{2B} \end{pmatrix}.$$

Therefore, if $\kappa = 1$, then E_1 is a saddle and E_2 is a source. Similarly, if $\kappa = -1$, then E_1 is a sink and E_2 is a saddle. However, the equilibrium E_0^+ is not hyperbolic. The desingularization of vector fields by the blow-up technique is an effective method to study the behavior near its equilibrium (see Section 1.2 in this thesis and Section 3 of [14] and references therein). That is, we desingularize E_0^+ by introducing the following blow-up coordinates:

$$\lambda = \varepsilon^{p-1}\bar{\lambda}, \quad x = \varepsilon^{p+1}\bar{x}.$$

Since we are interested in the dynamics on the Poincaré disk, we consider the dynamics of blow-up vector fields on the chart $\{\bar{\lambda} = 1\}$ and $\{\bar{x} = \pm 1\}$.

Dynamics on the chart $\{\bar{\lambda} = 1\}$

By the change of coordinates $\lambda = \varepsilon^{p-1}$, $x = \varepsilon^{p+1}\bar{x}$,

$$\begin{cases} \varepsilon_\tau = (p-1)^{-1}(A\varepsilon^{p^2+p+1}\bar{x}^p + B\varepsilon^{p^2+2p+2}\bar{x}^{p+1} - \tilde{\mu}\varepsilon^{p^2}), \\ \bar{x}_\tau = \varepsilon^{p^2-1}\bar{x}^p + 2(p-1)^{-1}(-A\varepsilon^{p^2+p}\bar{x}^{p+1} - B\varepsilon^{p^2+2p+1}\bar{x}^{p+2} + \tilde{\mu}\varepsilon^{p^2-1}\bar{x}) \end{cases} \tag{6.3.5}$$

holds. The time-rescaling $d\eta/d\tau = \varepsilon^{p^2-1}$ yields

$$\begin{cases} \varepsilon_\eta = (p-1)^{-1}(A\varepsilon^{p+2}\bar{x}^p + B\varepsilon^{2p+3}\bar{x}^{p+1} - \tilde{\mu}\varepsilon), \\ \bar{x}_\eta = \bar{x}^p + 2(p-1)^{-1}(-A\varepsilon^{p+1}\bar{x}^{p+1} - B\varepsilon^{2p+2}\bar{x}^{p+2} + \tilde{\mu}\bar{x}), \end{cases} \tag{6.3.6}$$

where $\varepsilon_\eta = d\varepsilon/d\eta$ and $\bar{x}_\eta = d\bar{x}/d\eta$. The equilibria of (6.3.6) on $\{\varepsilon = 0\}$ are

$$\overline{E}_0^+ : (\varepsilon, \bar{x}) = (0, 0), \quad \overline{E}_p^+ : (\varepsilon, \bar{x}) = (0, M_2), \quad M_2 = -|-2\tilde{\mu}/(p-1)|^{\frac{1}{p-1}} < 0.$$

The Jacobian matrices of the vector fields (6.3.6) at these equilibria are

$$\overline{E}_0^+ : \begin{pmatrix} -\dfrac{\tilde{\mu}}{p-1} & 0 \\ 0 & \dfrac{2\tilde{\mu}}{p-1} \end{pmatrix}, \quad \overline{E}_p^+ : \begin{pmatrix} -\dfrac{\tilde{\mu}}{p-1} & 0 \\ 0 & -2\tilde{\mu} \end{pmatrix}.$$

Therefore, the equilibrium $\overline{E}_0^+$ is a saddle, and $\overline{E}_p^+$ is a sink.

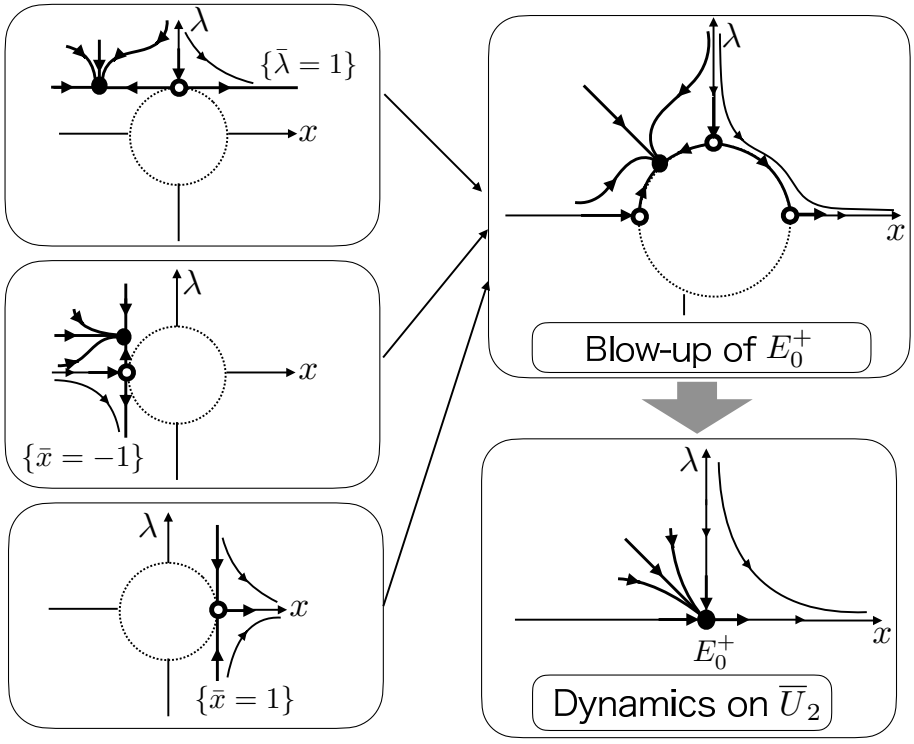

Figure 6.3.1: Schematic pictures of the dynamics of the blow-up vector fields and $\overline{U}_2$.

Dynamics on the chart $\{\bar{x}=1\}$

The change of coordinates $\lambda=\varepsilon^{p-1}\bar{\lambda}$, $x=\varepsilon^{p+1}$, and time-rescaling $d\eta/d\tau=\varepsilon^{p^2-1}$ yields

$$\begin{cases}\varepsilon_\eta=(p+1)^{-1}(\varepsilon+A\varepsilon^{p+2}+B\varepsilon^{2p+3}-\tilde{\mu}\varepsilon\bar{\lambda}^{p+1}),\\ \bar{\lambda}_\eta=(p+1)^{-1}(-(p-1)\bar{\lambda}+2A\varepsilon^{p+1}\bar{\lambda}+2B\varepsilon^{2p+2}\bar{\lambda}-2\tilde{\mu}\bar{\lambda}^{p+2}).\end{cases}\tag{6.3.7}$$

The equilibrium on $\{\varepsilon=0,\bar{\lambda}\geq 0\}$ is $(\varepsilon,\bar{\lambda})=(0,0)$. Eigenvalues of the Jacobian matrix are $(p+1)^{-1}$ and $-(p-1)/(p+1)$ with corresponding eigenvectors $(1,0)^T$ and $(0,1)^T$, respectively. Therefore, the equilibrium $(0,0)$ is a saddle.

Dynamics on the chart $\{\bar{x}=-1\}$

The change of coordinates $\lambda=\varepsilon^{p-1}\bar{\lambda}$, $x=-\varepsilon^{p+1}$, and time-rescaling $d\eta/d\tau=\varepsilon^{p^2-1}$ yields

$$\begin{cases}\varepsilon_\tau=-(p+1)^{-1}(\varepsilon-A\varepsilon^{p+2}+B\varepsilon^{2p+3}+\tilde{\mu}\varepsilon\bar{\lambda}^{p+1}),\\ \bar{\lambda}_\tau=(p+1)^{-1}((p-1)\bar{\lambda}+2A\varepsilon^{p+1}\bar{\lambda}-2B\varepsilon^{2p+2}\bar{\lambda}-2\tilde{\mu}\bar{\lambda}^{p+2}).\end{cases}\tag{6.3.8}$$

The equilibria on $\{\varepsilon=0,\bar{\lambda}\geq 0\}$ are

$$(\varepsilon,\bar{\lambda})=(0,0),\quad (\varepsilon,\bar{\lambda})=\left(0,[(p-1)/2\tilde{\mu}]^{\frac{1}{p+1}}\right).$$

By the further computations, the equilibrium $(0,0)$ is a saddle, and $\left(0,[(p-1)/2\tilde{\mu}]^{\frac{1}{p+1}}\right)$ is a sink.

Combining the dynamics on the charts $\{\bar{\lambda}=1\}$ and $\{\bar{x}=\pm 1\}$, the dynamics on the chart $\overline{U}_2$ can be obtained (see Figure 6.3.1).

6.3.2 Dynamics on the chart $\overline{V}_2$

In this chart, it corresponds to $a \to 0$ and $b \to -\infty$ and the direction in which x is negative corresponds to the direction in which a is positive. The change of coordinates

$$a(s) = -x(s)/\lambda(s), \quad b(s) = -1/\lambda(s)$$

give the projected dynamics of (6.3.2) on the chart $\overline{V}_2$:

$$\begin{cases} \lambda_\tau = A\lambda x^p + B\lambda x^{p+1} + \tilde{\mu}\lambda^{p+2}, \\ x_\tau = x^p + Ax^{p+1} + Bx^{p+2} + \tilde{\mu}\lambda^{p+1}x, \end{cases} \tag{6.3.9}$$

where τ is the new time introduced by $d\tau/ds = \lambda^{-p}$. The system (6.3.9) can be transformed into (6.3.4) by the change of coordinates Therefore, it is sufficient to consider the blow-up singularity $E_0^- : (\lambda, x) = (0, 0)$ by the formulas

$$\lambda = \varepsilon^{p-1}, \quad x = \varepsilon^{p+1}\bar{x} \quad \text{with} \quad \bar{\lambda} = 1.$$

Then,

$$\begin{cases} \varepsilon_\eta = (p-1)^{-1}(A\varepsilon^{p+2}\bar{x}^p + B\varepsilon^{2p+3}\bar{x}^{p+1} + \tilde{\mu}\varepsilon), \\ \bar{x}_\eta = \bar{x}^p + 2(p-1)^{-1}(-A\varepsilon^{p+1}\bar{x}^{p+1} - B\varepsilon^{2p+2}\bar{x}^{p+2} - \tilde{\mu}\bar{x}) \end{cases} \tag{6.3.10}$$

holds. Here, note that η satisfies $d\eta/d\tau = \varepsilon^{p^2-1}$. The equilibria of (6.3.10) on $\{\varepsilon = 0\}$ are

$$\overline{E}_0^- : (\varepsilon, \bar{x}) = (0, 0), \quad \overline{E}_p^- : (\varepsilon, \bar{x}) = (0, [2\tilde{\mu}/(p-1)]^{1/(p-1)}).$$

The equilibrium $\overline{E}_0^-$ is a saddle with the eigenvalues $\tilde{\mu}(p-1)^{-1}$ and $-2\tilde{\mu}(p-1)^{-1}$ whose corresponding eigenvectors are $(1, 0)^T$ and $(0, 1)^T$, respectively. Further, the equilibrium $\overline{E}_p^-$ is a source with the eigenvalues $\tilde{\mu}(p-1)^{-1}$ and $2\tilde{\mu}$ whose corresponding eigenvectors are $(1, 0)^T$ and $(0, 1)^T$, respectively.

6.3.3 Dynamics on the chart $\overline{U}_1$

Let us study the dynamics on the chart $\overline{U}_1$. In this chart, it corresponds to $a \to +\infty$ and $b \to 0$. The transformations

$$a(s) = 1/\lambda(s), \quad b(s) = x(s)/\lambda(s)$$

yield

$$\begin{cases} \lambda_\tau = -\lambda x, \\ x_\tau = -Ax - B + \tilde{\mu}\lambda^{p+1} - x^2, \end{cases} \tag{6.3.11}$$

via time-rescaling $d\tau/ds = \lambda^{-p}$. The system (6.3.11) has the equilibria

$$E_3 : (\lambda, x) = \left(0, 2^{-1}[-A - (N-2)]\right), \quad E_4 : (\lambda, x) = \left(0, 2^{-1}[-A + (N-2)]\right).$$

If κ is $\kappa = 1$, then the Jacobian matrices of the vector field (6.3.11) at these equilibria are

$$E_3 : \begin{pmatrix} \alpha + N - 2 & 0 \\ 0 & N - 2 \end{pmatrix}, \quad E_4 : \begin{pmatrix} \alpha & 0 \\ 0 & -(N-2) \end{pmatrix}.$$

Therefore, E_3 is a source, and E_4 is a saddle.

Similarly, if $\kappa = -1$, then

$$E_3 : \begin{pmatrix} -\alpha & 0 \\ 0 & N-2 \end{pmatrix}, \quad E_4 : \begin{pmatrix} -(\alpha+N-2) & 0 \\ 0 & -(N-2) \end{pmatrix}$$

holds. Therefore, E_3 is a saddle, and E_4 is a sink. Here, the solutions near E_3 are approximated as

$$\begin{cases} \lambda(\tau) = C_1 e^{-\alpha\tau}(1+o(1)), \\ x(\tau) - \alpha = C_2 e^{(N-2)\tau}(1+o(1)), \end{cases} \quad \text{as} \quad \tau \to +\infty. \tag{6.3.12}$$

If $\kappa = -1$, then $2^{-1}[-A-(N-2)] = \alpha$ holds. Further, the solutions near E_4 are approximated as

$$\begin{cases} \lambda(\tau) = C_1 e^{-(\alpha+N-2)\tau}(1+o(1)), \\ x(\tau) - M_3 = C_2 e^{-(N-2)\tau}(1+o(1)), \end{cases} \quad \text{as} \quad \tau \to +\infty \tag{6.3.13}$$

with $M_3 = (-A+(N-2))/2$.

6.3.4 Dynamics on the chart $\overline{V}_1$

In this chart, it corresponds to $a \to -\infty$ and $b \to 0$. The transformations

$$a(s) = -1/\lambda(s), \quad b(s) = -x(s)/\lambda(s)$$

yield

$$\begin{cases} \lambda_\tau = -\lambda x, \\ x_\tau = -Ax - B - \tilde{\mu}\lambda^{p+1} - x^2, \end{cases} \tag{6.3.14}$$

via time-rescaling $d\tau/ds = \lambda^{-p}$. We can see that the system (6.3.14) can be transformed into the system (6.3.11) by the change of coordinates:

$$(\lambda, x) \mapsto (-\lambda, x).$$

Therefore, the dynamics (6.3.14) is equivalent to the reflected one of (6.3.11) with respect to $\{\lambda = 0\}$.

6.3.5 Dynamics and connecting orbits on the Poincaré disk

Combining the dynamics on the charts $\overline{U}_j$ and $\overline{V}_j$ $(j = 1, 2)$, we obtain the dynamics on the Poincaré disk that is equivalent to the dynamics of (6.1.14) on $\mathbb{R}^2 \cup \{\|(a,b)\| = +\infty\}$ in the case that p is even as following Proposition (see Figure 6.3.2). Note that in Figure 6.3.2, the circumference corresponds to $\{\|(a,b)\| = +\infty\}$. We set Φ_1 as follows:

$$\Phi_1 = \{(a,b) \in \mathbb{R}^2 \cup \{\|(a,b)\| = +\infty\}\}.$$

Proposition 6.3.1
Assume that $3 \le N \in \mathbb{N}$, $\mu > 0$, $p \in \mathbb{N}$, and $0 < \delta < 1$ with $\delta = (p-1)/(p+1)$. Then, the dynamics on the Poincaré disk of the system (6.1.14) *is expressed as Figure 6.3.2.*

Proof. The proof of the connected orbit is exactly similar to that in [31, 33]. □

The proof is based on the Poincaré-Bendixson theorem. There are two notes on connecting orbits.

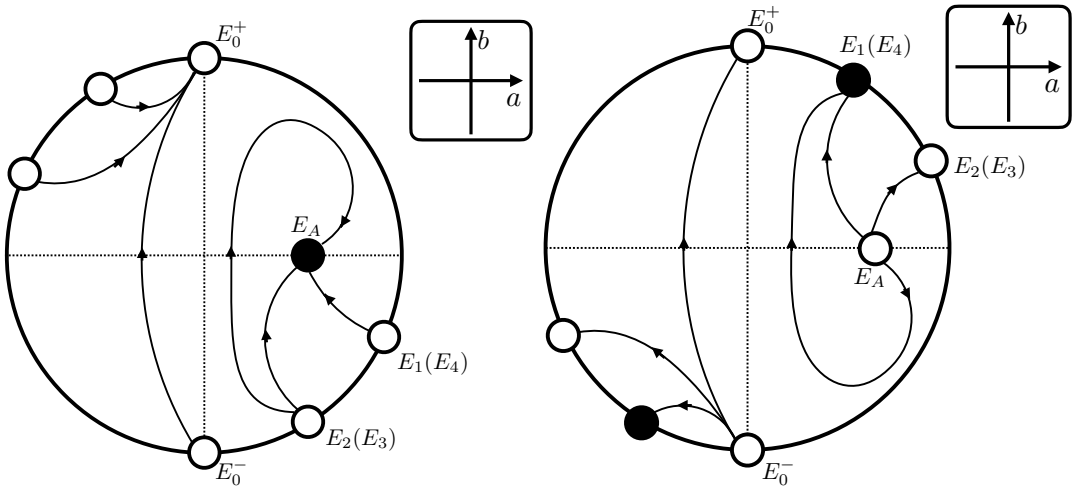

Figure 6.3.2: Schematic pictures of the dynamics on the Poincaré disk in the case that $0 < \delta < 1$, $p \in 2\mathbb{N}$, $D > 0$. In other words, these pictures are the dynamics of (6.1.14) on $\mathbb{R}^2 \cup \{\|(a,b)\| = +\infty\}$. [Left: Case $\kappa = 1$.] [Right: Case $\kappa = -1$.]

Remark 6.3.3
The key to the proof of this proposition is that da/db takes the same value except for $\{a = 0\}$, as mentioned in [31, 33]. That is, the flow on $\{(a,b) \in \Phi_1 \mid a > 0\}$ and $\{(a,b) \in \Phi_1 \mid a < 0\}$ are separated by the line $\{a = 0\}$.

Remark 6.3.4
Note that $t \to \infty$ of the picture in the case that $\kappa = 1$ is corresponding to $t \to -\infty$ of it in the case that $\kappa = -1$. The reverse is also true. As mentioned in [33], the existence of connecting orbits in Figure 6.3.2 corresponds to the existence of a function satisfying (6.1.8) *on a finite interval or $(0, +\infty)$ with parameter r. Furthermore, since all connecting orbits are known, all candidate solutions are enumerated such that* (6.1.8) *is satisfied. With this information, the asymptotic behavior corresponding to each connecting orbit can be studied.*

6.3.6 Dynamics on the Poincaré disk in the case that p is odd

In this subsection, we consider the dynamics (6.1.14) on the Poincaré disk in the case that p is odd. We desingularize it by the time-scale desingularization

$$ds/dt = a^{-p-1}.$$

Then,

$$\begin{cases} a' = a^{p+1}b, \\ b' = -Aa^{p+1}b - Ba^{p+2} + \tilde{\mu}a, \end{cases} \qquad \left(' = \frac{d}{ds}\right) \tag{6.3.15}$$

holds. In a similar argument as [33], since the direction of the time does not change via (6.3.1) on $\Phi_{a>0} = \{(a,b) \in \Phi_1 \mid a > 0\}$ for both even and odd cases, the flow of (6.3.15) on $\Phi_{a>0}$ for $p \in 2\mathbb{N} - 1$ is similar to that of (6.3.2) on $\Phi_{a>0}$ for $p \in 2\mathbb{N}$. Moreover, (6.3.15) is invariant under the mapping $(a,b) \mapsto -(a,b)$. Therefore, we can draw the phase portraits on the Poincaré disk of (6.1.14) (or (6.3.15)) when p is odd as shown in Figure 6.3.3 (cf. the flow on $\{a > 0\}$ of Figure 6.3.2).

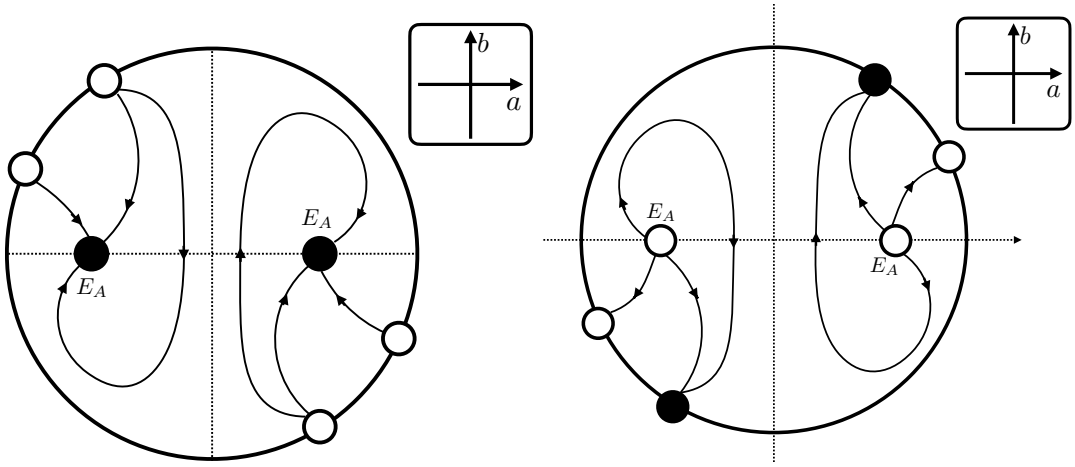

Figure 6.3.3: Schematic pictures of the dynamics on the Poincaré disk in the case that $0 < \delta < 1$, $D > 0$, and p is odd. [Left: Case $\kappa = 1$.] [Right: Case $\kappa = -1$.]

Remark 6.3.5
In this section, we have obtained all the dynamics on the Poincare disk of (6.1.14) *with* $p \in \mathbb{N}$. *As mentioned in Remark 6.3.4, now that we understand the dynamics including infinity, we can discuss the existence of functions that satisfy* (6.1.8) *corresponding to each orbit and the asymptotic behavior of their solutions. However, in the present problem,* U *and* u *are not defined in the entire domain, and a restriction is imposed on the range in which each exists. Therefore, even if we know the behavior of* $a(t)$ *or* $b(t)$*, when we restore it to* u *or* U*, it may not be suitable for the range of its existence. This is also true for the other cases, Case 2 and Case 3.*

Remark 6.3.6
In this Case 1, we consider the dynamics of the system obtained by introducing a transformation such as (6.1.12). *Based on the transformation given in [41], we can also introduce the following transformation:*

$$t = \kappa \log r, \quad a(t) = r^{-\alpha}(1-u), \quad b(t) = r^{-(\alpha-1)}u_r, \quad \alpha = 1-\delta > 0, \quad \kappa = \pm 1.$$

In other words, from the above transformation, we can also consider the following system:

$$\begin{cases} \dot{a} = -\kappa\alpha a - \kappa b, \\ \dot{b} = -\kappa M b - \kappa\tilde{\mu}a^{-p}, \end{cases} \qquad M = \alpha + N - 2.$$

Note that this system gives the same results as Theorem 6.2.1 and Theorem 6.2.2, although a different transformation is applied.

6.4 Dynamics of (6.1.16) to infinity

In this section, the dynamics of (6.1.16) on $\mathbb{R}^2 \cup \{\|(a,b)\| = +\infty\}\backslash\{a < 0\}$ are studied in a similar way as in Section 6.3. The reason for excluding $a < 0$ is that it is necessary to consider a region where the transformation (6.1.15), which will be introduced later, does not change the direction of time. However, we will use "the Poincaré-Lyapunov compactification" (the directional compactification) instead of "the Poincaré compactification" in order to consider the quasi-homogeneity of the vector field. Considering the

quasi-homogeneity, we need to retain the original vector field information. In order to correctly extract the structure at infinity, we use the Poincaré-Lyapunov compactification, which is an extension of the Poincaré compactification idea (see [35, 49, 50]). Note that the geometric image can be regarded as similar to Poincaré compactification (for instance, Figure 2 of [31]), namely, the Poncaré disk is called the Poincaré-Lyapunov one.

Before starting the detailed analysis, (6.1.16) has a finite equilibrium $E_B : (a, b) = (M_4, 0)$ with $M_4 = 2\tilde{\mu}^{-1}(N-2)$. Let J_B be the Jacobian matrix of the vector field (6.1.16) at E_B. J_B is the following:

$$J_B = \begin{pmatrix} 0 & 1 \\ -2(N-2) & -A \end{pmatrix}.$$

The eigenvalues are $2^{-1}(-A \pm \sqrt{(N-2)(N-10)})$. Then, the behavior of the solution around E_B is different by the sign of $N-10$. In other words, the behavior of the solution changes depending on the number of dimensions N. For instance, the matrix J_B has the real distinct eigenvalues if $N-10>0$, i.e., $3 \leq N \leq 9$, and other cases can be concluded similarly. This classification by the number of dimensions, such as $3 \leq N \leq 9$ and $N = 10$, and $N \geq 11$, is consistent with that of bifurcation carves in [21]. In addition, if $\kappa = 1$, then the real parts of all eigenvalues of J_B are negative. Therefore, we conclude that E_B is a sink in the case that $\kappa = 1$. Similarly, we can determine that E_B is a source in the case that $\kappa = -1$.

In order to study the dynamics of (6.1.16) on the Poincaré-Lyapunov disk, we desingularize it by the time-scale desingularization

$$ds/dt = a^{-1}. \tag{6.4.1}$$

Note that since we are considering $a \geq 0$, this transformation does not change the direction of time. By the same argument as in Remark 6.3.3, we note that this dynamics is closed in the region $\{a \geq 0\}$. Then,

$$\begin{cases} a' = ab, \\ b' = b^2 - Aab - \tilde{\mu}a^3 + 2(N-2)a^2, \end{cases} \qquad \left(' = \frac{d}{ds}\right) \tag{6.4.2}$$

holds. The system (6.4.2) has the equilibrium $E_O : (a, b) = (0, 0)$. The Jacobian matrix of the vector field (6.4.2) at E_O is

$$E_O : \begin{pmatrix} 0 & 0 \\ 0 & 0 \end{pmatrix}.$$

The equilibrium E_O is not hyperbolic.

6.4.1 Dynamics of (6.4.2) near $(0, 0)$

As before, in order to determine the dynamics near E_O, we desingularize it by introducing the following blow-up coordinates:

$$a = \varepsilon\bar{a}, \quad b = \varepsilon\bar{b}.$$

Since we are interested in the dynamics near E_O, we consider the dynamics of blow-up vector fields on the charts $\{\bar{a} = 1\}$ and $\{\bar{b} = \pm 1\}$. The reason we do not consider the case $\{\bar{a} = -1\}$ is that we are considering $a \geq 0$.

Dynamics on the chart $\{\bar{a} = 1\}$

By the change of coordinates $a = \varepsilon$, $b = \varepsilon\bar{b}$ and time-rescaling $d\sigma/ds = \varepsilon$, we have

$$\begin{cases} \varepsilon_\sigma = \varepsilon\bar{b}, \\ \bar{b}_\sigma = -A\bar{b} - \tilde{\mu}\varepsilon + 2(N-2), \end{cases} \tag{6.4.3}$$

where ε_σ and $\bar{b}_\sigma$ are $\varepsilon_\sigma = d\varepsilon/d\sigma$, $\bar{b}_\sigma = d\bar{b}/d\sigma$, respectively. The equilibria can be classified according to the value of $\kappa = \pm 1$ as follows:

- When $\kappa = 1$, this system has the equilibrium $\overline{E}_O^1 : (\varepsilon, \bar{b}) = (0, 2)$.
- When $\kappa = -1$, it is $\overline{E}_O^2 : (\varepsilon, \bar{b}) = (0, -2)$.

The Jacobian matrices of the vector field (6.4.3) at these equilibria are

$$\overline{E}_O^1 : \begin{pmatrix} 2 & 0 \\ -\tilde{\mu} & -(N-2) \end{pmatrix}, \quad \overline{E}_O^2 : \begin{pmatrix} -2 & 0 \\ -\tilde{\mu} & N-2 \end{pmatrix}.$$

Therefore, $\overline{E}_O^1$ and $\overline{E}_O^2$ are saddles.

We now derive the solution around $\overline{E}_O^2$ ($\kappa = -1$) for later use. Let $z(\sigma) := \varepsilon(\sigma) - 0$ and $w(\sigma) := \bar{b}(\sigma) + 2$. Then, they satisfy the following:

$$\frac{d}{d\sigma}\begin{pmatrix} z(\sigma) \\ w(\sigma) \end{pmatrix} = \begin{pmatrix} -2 & 0 \\ -\tilde{\mu} & N-2 \end{pmatrix}\begin{pmatrix} z(\sigma) \\ w(\sigma) \end{pmatrix}.$$

By solving these differential equations, we obtain

$$\begin{aligned} z(\sigma) &= C_1 e^{-2\sigma}, \\ w(\sigma) &= \frac{\tilde{\mu}}{N} C_3 e^{-2\sigma} + C_2 e^{(N-2)\sigma} \sim C_2 e^{(N-2)\sigma}, \quad \text{as} \quad \sigma \to +\infty, \end{aligned}$$

where C_j are constants. Therefore, the solution at $\overline{E}_O^2$ are approximated as

$$\begin{cases} \varepsilon(\sigma) = C_1 e^{-2\sigma}(1 + o(1)), \\ \bar{b}(\sigma) + 2 = C_2 e^{(N-2)\sigma}(1 + o(1)), \end{cases} \quad \text{as} \quad \sigma \to +\infty. \tag{6.4.4}$$

Dynamics on the chart $\{\bar{b} = 1\}$

By the change of coordinates $a = \varepsilon\bar{a}$, $b = \varepsilon$ and time-rescaling $d\sigma/ds = \varepsilon$, we have

$$\begin{cases} \varepsilon_\sigma = \varepsilon - A\varepsilon\bar{a} - \tilde{\mu}\varepsilon^2\bar{a}^3 + 2(N-2)\varepsilon\bar{a}^2, \\ \bar{a}_\sigma = \bar{a}^2(A + \tilde{\mu}\varepsilon\bar{a}^2 - 2(N-2)\bar{a}) \end{cases} \tag{6.4.5}$$

The equilibria can be classified according to the value of $\kappa = \pm 1$ as follows:

- When $\kappa = 1$, this system has the equilibria $\overline{E}_O^3 : (\varepsilon, \bar{a}) = (0, 0)$ and $\overline{E}_O^4 : (\varepsilon, \bar{a}) = \left(0, 2^{-1}\right)$.
- When $\kappa = -1$, the equilibrium on $\{\varepsilon = 0, \bar{a} \geq 0\}$ is $\overline{E}_O^3 : (\varepsilon, \bar{a}) = (0, 0)$.

The Jacobian matrices of the vector field (6.4.5) at these equilibria are

$$\overline{E}_O^3 : \begin{pmatrix} 1 & 0 \\ 0 & 0 \end{pmatrix}, \quad \overline{E}_O^4 : \begin{pmatrix} 1 & 0 \\ \dfrac{\tilde{\mu}}{16} & -\dfrac{1}{2}(N-2) \end{pmatrix}$$

Therefore, $\overline{E}_O^4$ is a saddle, and the center manifold theory is applicable to study the dynamics near $\overline{E}_O^3$ (for instance, see [9]). However, it is not possible to obtain the approximation of the (graph of) center manifold explicitly. This is due to the fact that $\bar{a} = 0$ is invariant, so the center manifold is not unique. From

$$\begin{aligned} \bar{a}_\sigma|_{\varepsilon=0,\kappa=1} &= 2(N-2)\bar{a}^2\left(\frac{1}{2} - \bar{a}\right) > 0, \\ \bar{a}_\sigma|_{\varepsilon=0,\kappa=-1} &= -2(N-2)\bar{a}^2\left(\frac{1}{2} + \bar{a}\right) < 0 \end{aligned}$$

hold with $0 < \bar{a} < 1/2$, the dynamics near $\overline{E}_O^3$ restricted on $\varepsilon = 0$ (i.e. the line of $\{\bar{b} = 1\}$) can be determined (see Figure 6.4.1 and Figure 6.4.2).

Dynamics on the chart $\{\bar{b} = -1\}$

By the change of coordinates $a = \varepsilon\bar{a}$, $b = -\varepsilon$ and time-rescaling $d\sigma/ds = \varepsilon$, we have

$$\begin{cases} \varepsilon_\sigma = -\varepsilon - A\varepsilon\bar{a} + \tilde{\mu}\varepsilon^2\bar{a}^3 - 2(N-2)\varepsilon\bar{a}^2, \\ \bar{a}_\sigma = A\bar{a}^2 - \tilde{\mu}\varepsilon\bar{a}^4 + 2(N-2)\bar{a}^3. \end{cases} \tag{6.4.6}$$

The equilibria can be classified according to the value of $\kappa = \pm 1$ as follows:

- When $\kappa = 1$, the equilibrium on $\{\varepsilon = 0, \bar{a} \geq 0\}$ is $\overline{E}_O^5 : (\varepsilon, \bar{a}) = (0, 0)$.
- When $\kappa = -1$, this system has the equilibria $\overline{E}_O^5 : (\varepsilon, \bar{a}) = (0, 0)$ and $\overline{E}_O^6 : (\varepsilon, \bar{a}) = \left(0, 2^{-1}\right)$.

The Jacobian matrices of the vector field (6.4.6) at these equilibria are

$$\overline{E}_O^5 : \begin{pmatrix} -1 & 0 \\ 0 & 0 \end{pmatrix}, \quad \overline{E}_O^6 : \begin{pmatrix} -1 & 0 \\ -\dfrac{\tilde{\mu}}{16} & \dfrac{1}{2}(N-2) \end{pmatrix}.$$

Therefore, $\overline{E}_O^6$ is a saddle. As with $\overline{E}_O^3$ above, the center manifold theory is applicable to study the dynamics near $\overline{E}_O^5$. Although the approximation of the (graph of) center manifold is not obtained, the dynamics near $\overline{E}_O^3$ restricted on $\varepsilon = 0$ (i.e. the line of $\{\bar{b} = 1\}$) can be determined from the following calculations:

$$\begin{aligned} \bar{a}_\sigma|_{\varepsilon=0,\kappa=1} &= 2(N-2)\bar{a}^2\left(\frac{1}{2} + \bar{a}\right) > 0 \\ \bar{a}_\sigma|_{\varepsilon=0,\kappa=-1} &= -2(N-2)\bar{a}^2\left(\frac{1}{2} - \bar{a}\right) < 0 \end{aligned}$$

with $0 < \bar{a} < 1/2$ (see Figure 6.4.1 and Figure 6.4.2).

Combining the dynamics on the charts $\{\bar{a} = 1\}$ and $\{\bar{b} = \pm 1\}$, we can obtain the dynamics near E_O (see Figure 6.4.1 and Figure 6.4.2).

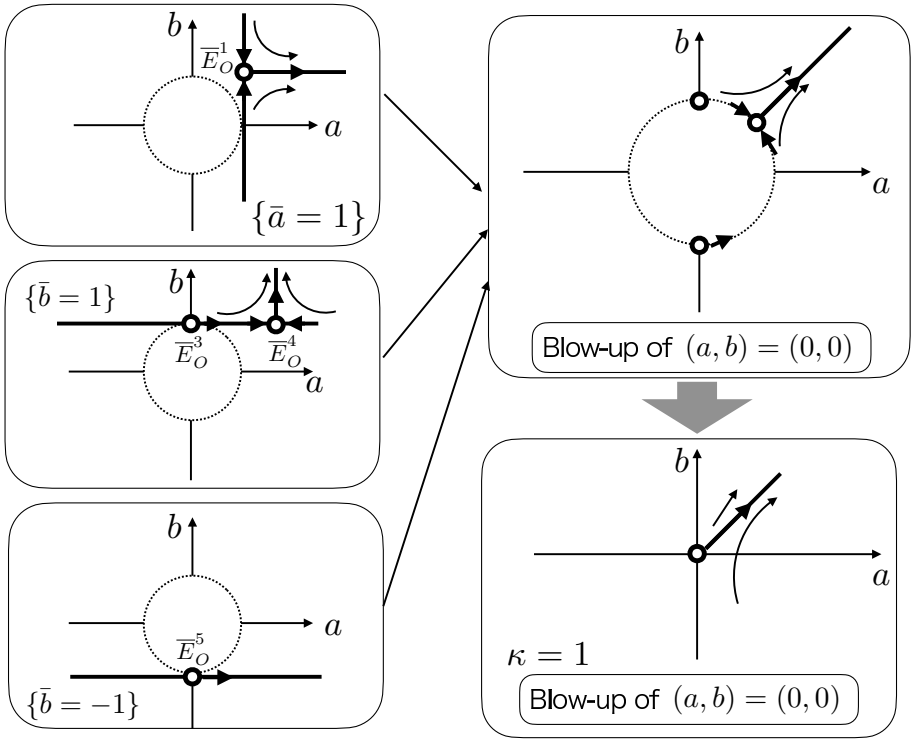

Figure 6.4.1: Schematic picture of the dynamics near E_O in the case that $\kappa = 1$.

6.4.2 Asymptotically quasi-homogeneous vector field

Before we consider the dynamics of (6.4.2) on the charts $\overline{U}_j$ and $\overline{V}_j$, we state the type and order of this vector field (6.4.2). Let $f = (f_1(a,b), f_2(a,b))$ be $f_1(a,b) = ab$ and $f_2(a,b) = b^2 - Aab - \tilde{\mu}a^3 + 2(N-2)a^2$. Then, we have the following observation (see [35, 49, 50] for more details).

Lemma 6.4.1
The vector field f is asymptotically quasi-homogeneous of type $(2,3)$ and order 4 at infinity.

Proof. Let a type be (α_1, α_2), $R \in \mathbb{R}$ and an order be $k+1$ with $k \geq 1$. For all $(a,b) \in \mathbb{R}^2$, the following holds:

$$\begin{aligned} f_1(R^{\alpha_1}a, R^{\alpha_2}b) &= R^{k+\alpha_1} f_1(a,b), \\ f_2(R^{\alpha_1}a, R^{\alpha_2}b) &= R^{k+\alpha_2} f_2(a,b). \end{aligned}$$

Using (6.4.2), the left-hand sides above are calculated as:

$$\begin{aligned} f_1(R^{\alpha_1}a, R^{\alpha_2}b) &= R^{\alpha_1+\alpha_2}ab, \\ f_2(R^{\alpha_1}a, R^{\alpha_2}b) &= R^{2\alpha_2}b^2 - AR^{\alpha_1+\alpha_2}ab - \tilde{\mu}R^{3\alpha_1}a^3 + 2(N-2)R^{2\alpha_1}a^2. \end{aligned}$$

By comparing the order parts, we get

$$\begin{cases} \alpha_1 + \alpha_2 = k + \alpha_1, \\ 2\alpha_2 = k + \alpha_2, \\ \alpha_1 + \alpha_2 = k + \alpha_2, \\ 3\alpha_1 = k + \alpha_2, \\ 2\alpha_1 = k + \alpha_2. \end{cases} \tag{6.4.7}$$

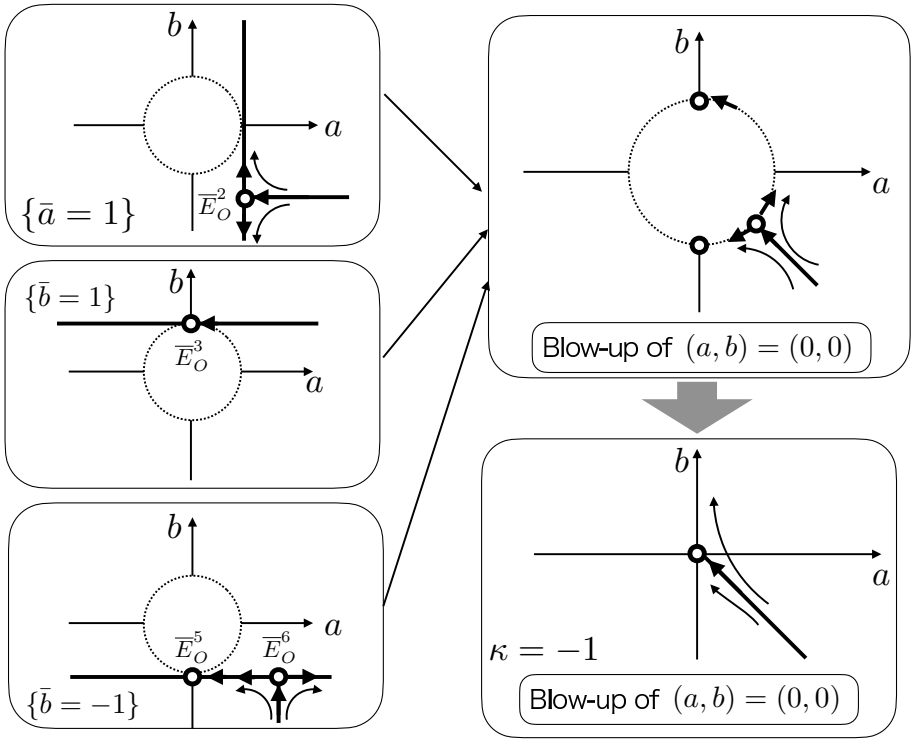

Figure 6.4.2: Schematic picture of the dynamics near E_O in the case that $\kappa = -1$.

Here, since the first and fourth equations in (6.4.7) correspond to the maximum order in (6.4.2), $(\alpha_1, \alpha_2) = (2, 3)$ and $k = 3$ are obtained from them. These then satisfy the second equation in (6.4.7). Furthermore, they satisfy as follows:

$$\lim_{R\to+\infty} R^{-(k+\alpha_1)}\big\{ f_1(R^{\alpha_1}a, R^{\alpha_2}b) - R^{k+\alpha_1}(f_{\alpha,k})_1(a,b) \big\} \equiv 0,$$
$$\lim_{R\to+\infty} R^{-(k+\alpha_2)}\big\{ f_2(R^{\alpha_1}a, R^{\alpha_2}b) - R^{k+\alpha_2}(f_{\alpha,k})_2(a,b) \big\} = 0,$$

where $(f_{\alpha,k})_1$ and $(f_{\alpha,k})_2$ are $(f_{\alpha,k})_1 = ab$ and $(f_{\alpha,k})_2 = b^2 - \tilde{\mu}a^3$, respectively. From the above results, we can see that the vector field f is asymptotically quasi-homogeneous of type $(2, 3)$ and order 4 at infinity. □

Note that if we follow a similar procedure in (6.3.2), the type becomes $(1, 1)$. Now we can consider the dynamics of (6.4.2) on the charts $\overline{U}_j$ $(j = 1, 2)$ and $\overline{V}_2$ since we are considering $a \geq 0$.

6.4.3 Dynamics on the chart $\overline{U}_2$

To obtain the dynamics on the chart $\overline{U}_2$, we introduce coordinates (λ, x) by the formulas

$$a(s) = x(s)/\{\lambda(s)\}^2, \quad b(s) = 1/\{\lambda(s)\}^3.$$

Here, note that the exponents of λ are derived from the type found in Lemma 6.4.1. The discussion on the directionality of the a and x-axis of the local coordinates is the same as in Subsection 6.3.1. Then, these transformations yield

$$\begin{cases} \lambda_\tau = 3^{-1}(-\lambda + A\lambda^2 x + \tilde{\mu}\lambda x^3 - 2(N-2)\lambda^3 x^2), \\ x_\tau = 3^{-1}(x + 2A\lambda x^2 + 2\tilde{\mu}x^4 - 4(N-2)\lambda^2 x^3), \end{cases} \tag{6.4.8}$$

via time-rescaling $d\tau/ds = \lambda^{-3}$. This system has the equilibrium

$$E_5 : (\lambda, x) = (0, 0)$$

on $\{x \geq 0\}$. The Jacobian matrix of the vector field (6.4.8) at E_5 is

$$E_5 : \begin{pmatrix} -3^{-1} & 0 \\ 0 & 3^{-1} \end{pmatrix}.$$

Therefore, E_5 is a saddle.

6.4.4 Dynamics on the chart $\overline{V}_2$

The change of coordinates

$$a(s) = -x(s)/\{\lambda(s)\}^2, \quad b(s) = -1/\{\lambda(s)\}^3$$

give the projected dynamics of (6.4.2) on the chart $\overline{V}_2$:

$$\begin{cases} \lambda_\tau = 3^{-1}(\lambda - A\lambda^2 x + \tilde{\mu}\lambda x^3 + 2(N-2)\lambda^3 x^2), \\ x_\tau = 3^{-1}(-x - 2A\lambda x^2 + 2\tilde{\mu}x^4 + 4(N-2)\lambda^2 x^3), \end{cases} \tag{6.4.9}$$

where τ is the new time introduced by $d\tau/ds = \lambda^{-3}$. This system has the equilibrium

$$E_6 : (\lambda, x) = (0, 0)$$

on $\{x \leq 0\}$. The Jacobian matrix of the vector field (6.4.9) at E_6 is

$$E_6 : \begin{pmatrix} 3^{-1} & 0 \\ 0 & -3^{-1} \end{pmatrix}.$$

Therefore, E_6 is a saddle.

6.4.5 Dynamics on the chart $\overline{U}_1$

Let us study the dynamics on the chart $\overline{U}_1$. The transformations

$$a(s) = 1/\{\lambda(s)\}^2, \quad b(s) = x(s)/\{\lambda(s)\}^3$$

yield

$$\begin{cases} \lambda_\tau = -2^{-1}\lambda x, \\ x_\tau = -2^{-1}x^2 - A\lambda x - \tilde{\mu} + 2(N-2)\lambda^2, \end{cases} \tag{6.4.10}$$

via time-rescaling $d\tau/ds = \lambda^{-3}$. This system has no equilibria. It is important to note that the following holds:

$$x_\tau\big|_{\lambda=0} = -\frac{1}{2}x^2 - \tilde{\mu} < 0.$$

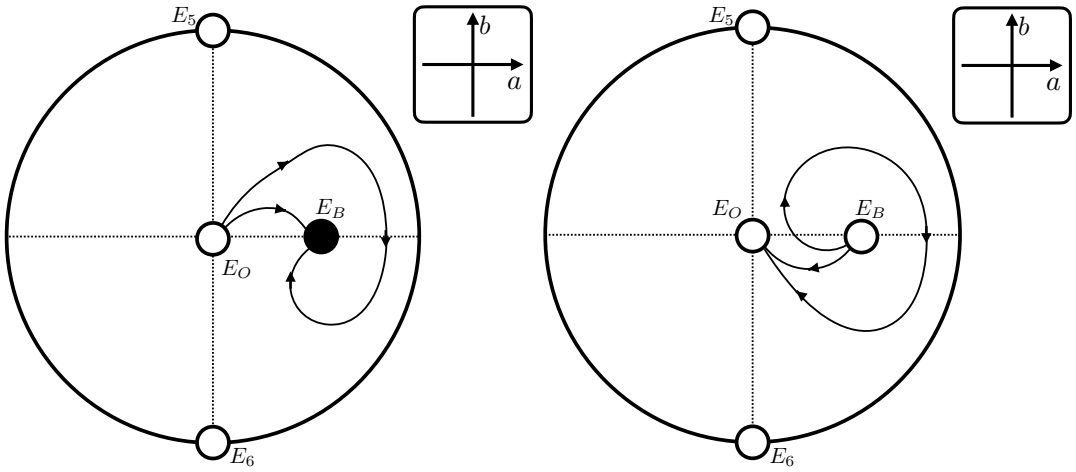

Figure 6.4.3: Roughly sketch of the dynamics on the Poincaré-Lyapunov disk in the Case 2 for the convenience. [Left: Case $\kappa = 1$.] [Right: Case $\kappa = -1$.]

6.4.6 Dynamics and connecting orbits on the Poincaré-Lyapunov disk

Combining the dynamics on the chart $\overline{U}_j$ $(j = 1, 2)$ and $\overline{V}_2$, we obtain the Poincaré-Lyapunov disk that is equivalent to the dynamics of (6.1.16) on $\mathbb{R}^2 \cup \{\|(a,b)\| = +\infty\} \setminus \{a < 0\}$ as following Proposition.

Let us prepare the symbols used in this subsection as follows:

- We set Φ_2 and Φ_3 as follows:

$$\Phi_2 = \{(a,b) \in \mathbb{R}^2 \cup \{\|(a,b)\| = +\infty\}\}$$

and

$$\Phi_3 = \{(a,b) \in \Phi_2 \mid a \geq 0\}.$$

- $\mathcal{W}^s(E_B)$ denotes the stable manifold of E_B in the dynamical system (6.1.16) in the case that $\kappa = 1$.
- $\mathcal{W}^u(E_B)$ denotes the unstable manifold of E_B in the dynamical system (6.1.16) in the case that $\kappa = -1$.
- $\overline{\mathcal{W}}^u(\overline{E}_O^1)$ denotes the unstable manifold of $\overline{E}_O^1$ in the dynamical system (6.4.3).
- $\overline{\mathcal{W}}^s(\overline{E}_O^2)$ denotes the stable manifold of $\overline{E}_O^2$ in the dynamical system (6.4.3).
- We denote by $\mathcal{W}^u(\overline{E}_O^1)$ the unstable set, which corresponds to $\overline{\mathcal{W}}^u(\overline{E}_O^1)$ on the blow-up vector field (6.4.3) of the equilibrium E_O of (6.4.2) (see Figure 6.4.1).
- We denote by $\mathcal{W}^s(\overline{E}_O^2)$ the stable set, which corresponds to $\overline{\mathcal{W}}^s(\overline{E}_O^2)$ on the blow-up vector field (6.4.3) of the equilibrium E_O of (6.4.2) (see Figure 6.4.2).

Proposition 6.4.1
Assume that $N \geq 3$, $\delta = 1$, and $\tilde{\mu} > 0$. Then, there exists a connecting orbit between the points of $\mathcal{W}^u(E_B)$ (resp. $\mathcal{W}^s(E_B)$) and the points of $\mathcal{W}^s(\overline{E}_O^2)$ (resp. $\mathcal{W}^u(\overline{E}_O^1)$) on the Poincaré-Lyapunov disk in the case that $\kappa = -1$ (resp. $\kappa = 1$) (see Figure 6.4.3).

Proof. **(I)** Since the line $\{a = 0\}$ is invariant under the flow of (6.4.2), any trajectories start from the points in $\{(a, b) \in \Phi_2 \mid a > 0\}$ cannot go to $\{(a, b) \in \Phi_2 \mid a < 0\}$. Similarly, any trajectories start from the points in $\{(a, b) \in \Phi_2 \mid a < 0\}$ cannot go to $\{(a, b) \in \Phi_2 \mid a > 0\}$. In other words, in (6.4.2) only $a \geq 0$ completes the behavior.
(II) When we consider the parameter s on the disk, the point E_O is the equilibrium of (6.4.2). However, E_O is a point on the line $\{a = 0\}$ with singularity about the parameter t. We can see that da/db takes the same values on the vector fields defined by (6.1.16) and (6.4.2) by excepting the singularity $\{a = 0\}$. If the trajectories start from (resp. come in) the equilibrium E_O about the parameter s, then they start from (resp. come in) it about t.
(III) What we show here is the existence of a connecting orbit between the points of $\mathcal{W}^u(E_B)$ and the points of $\mathcal{W}^s(\overline{E}_O^2)$ in the case that $\kappa = -1$. Assume that $\kappa = -1$. If $0 < a < M_4$, then we obtain

$$\dot{b}|_{b=0,0<a<M_4} = -\tilde{\mu}a^2 + 2(N-2)a > 0.$$

The only unstable point in the region $a \geq 0$ is E_B. Then the trajectory starting from the point on $\mathcal{W}^u(E_B)$ can only go to E_O on the $b < 0$ sides from the above **(II)** argument and the nullcline. Therefore, among the trajectories that depart from a point on $\mathcal{W}^u(E_B)$, there must be a trajectory that goes to a point on $\mathcal{W}^s(\overline{E}_O^2)$. All other trajectories eventually reach the region bounded by the stable manifold and the $b < 0$ sides of the b-axis and go to the origin along the b-axis. Thus, there exists a connecting orbit between the points of $\mathcal{W}^u(E_B)$ and the points of $\mathcal{W}^s(\overline{E}_O^2)$ in the case that $\kappa = -1$. This stable manifold plays the role of a boundary at $b < 0$ near the origin.
(IV) What remains to be shown is the existence of a trajectory connecting the points on $\mathcal{W}^u(\overline{E}_O^1)$ and the points on $\mathcal{W}^s(E_B)$ for $\kappa = 1$. In (6.1.16), switching $\kappa = \pm 1$ is equivalent to introducing the following transformation:

$$b \mapsto -b, \quad t \mapsto -t.$$

In fact, the change from $\kappa = -1$ to $\kappa = 1$ in (6.1.16) causes only the sign of A to switch. On the other hand, even if we introduce the above transformation, it only changes the sign of A in (6.1.16). Thus, we conclude that the connecting orbits at $\kappa = -1$ obtained in **(III)** also exist at $\kappa = 1$ due to the symmetry of the transformation $b \mapsto -b$, $t \mapsto -t$. Therefore, there exists a connecting orbit between E_O and E_B on the Poincaré-Lyapunov disk for both $\kappa = 1$ and $\kappa = -1$. This completes the proof of Proposition 6.4.1. □

6.5 Dynamics of (6.1.18) to infinity

In this section, we study the dynamics of (6.1.18) on $\mathbb{R}^2 \cup \{\|(a, b)\| = +\infty\}$ (i.e., Poincaré-Lyapunov disk) using the Poincaré-Lyapunov compactification as in Section 6.4. In the following, let set Φ_4 be as follows:

$$\Phi_4 = \{(a, b) \in \mathbb{R}^2 \cup \{\|(a, b)\| = +\infty\}\}.$$

Note that (6.1.18) is invariant under the following transformation if and only if p is odd.

$$(a, b) \mapsto -(a, b).$$

Furthermore, there is a clear difference between the detailed analysis in (6.1.18) and that in Section 6.4. This difference is that this equation does not have a singularity, so there

is no need to apply time-scale desingularization. That is, unlike Proposition 6.3.1 in Section 6.3 and Proposition 6.4.1 in Section 6.4, a trajectory starting from a point on $\{(a,b) \in \Phi_4 \mid a < 0\}$ may pass through the line $\{a = 0\}$ and reach $\{(a,b) \in \Phi_4 \mid a > 0\}$. This implies that there may be a sign-changing solution for a as the corresponding solution.

However, due to the relationship between U and u transformations in Case 3, the constraint $u > -1$ is imposed in this problem. Accordingly, from the relationship between u and a, we obtain

$$u > -1 \iff 1 + u > 0 \iff a = r^{-\alpha}(1+u) > 0.$$

From this argument, we can study all dynamics on Φ_4 by Poincaré-Lyapunov compactification, however, we can only focus on the trajectories that are attracted to the equilibrium on $\Phi_4 \backslash \{a < 0\}$ in deriving the asymptotic behavior of $U(r)$ for the solution corresponding to each connecting orbit. In order to find possible trajectories to study, we first consider the dynamics of (6.1.18) on the local coordinates $\overline{U}_j$ $(j = 1, 2)$ and $\overline{V}_2$ using that. Reversing the order of discussion in Section 6.4, the discussion on finite equilibria in this equation will be presented later.

Before performing the Poincaré-Lyapunov compactification, we study the type and order of the vector field (6.1.18) similarly to Lemma 6.4.1 in Subsection 6.4.2. Let $f = (f_1(a,b), f_2(a,b))$ be $f_1(a,b) = b$ and $f_2(a,b) = -Ab - Ba - \tilde{\mu}a^p$.

Lemma 6.5.1
The vector field f is asymptotically quasi-homogeneous of type $(2, p+1)$ and order p at infinity.

Proof. It is shown similarly to Lemma 6.4.1. □

6.5.1 Dynamics on the chart $\overline{U}_2$

The transformations

$$a(t) = x(t)/\{\lambda(t)\}^2, \quad b(t) = 1/\{\lambda(t)\}^{p+1}$$

yield

$$\begin{cases} \lambda_\tau = (p+1)^{-1}(A\lambda^p + B\lambda^{2p-1}x + \tilde{\mu}\lambda x^p), \\ x_\tau = 1 + 2(p+1)^{-1}(A\lambda^{p-1}x + B\lambda^{2p-2}x^2 + \tilde{\mu}x^{p+1}), \end{cases} \tag{6.5.1}$$

via time-scaling $d\tau/dt = \lambda^{-p+1}$. The equilibria of this system can be classified according to whether p is even or odd as follows:

- When p is even, the equilibrium is $E_7 : (\lambda, x) = (0, L_2)$ with $L_2 = -|-(p+1)/(2\tilde{\mu})|^{1/(p+1)} < 0$.
- If p is an odd greater than or equal to 3, then this system has no equilibria.

Through further computations, we determine that the equilibrium E_7 is a source. However, this equilibrium is infinitely far in the region $\Phi_4 \backslash \{a > 0\}$, which is not consistent with the objective stated at the beginning of Section 6.5.

6.5.2 Dynamics on the chart $\overline{V}_2$

By the transformations

$$a(t) = -x(t)/\{\lambda(t)\}^2, \quad b(t) = -1/\{\lambda(t)\}^{p+1},$$

and time-scaling $d\tau/dt = \lambda^{-p+1}$, we have

$$\begin{cases} \lambda_\tau = (p+1)^{-1}(A\lambda^p + B\lambda^{2p-1}x - (-1)^p\tilde{\mu}\lambda x^p), \\ x_\tau = 1 + 2(p+1)^{-1}(A\lambda^{p-1}x + B\lambda^{2p-2}x^2 - (-1)^p\tilde{\mu}x^{p+1}). \end{cases} \tag{6.5.2}$$

The equilibria of this system can be classified according to whether p is even or odd as follows:

- When p is even, the equilibrium is $E_8 : (\lambda, x) = (0, L_3)$ with $L_3 = \{(p+1)/(2\tilde{\mu})\}^{1/(p+1)} > 0$.
- If p is an odd greater than or equal to 3, this system has no equilibria.

By a similar calculation as before, we find that the equilibrium E_8 is a sink. Note, however, that E_8 is not our objective equilibrium, since it also exists in the region where $\Phi_4\backslash\{a > 0\}$, as in Subsection 6.5.1.

6.5.3 Dynamics on the chart $\overline{U}_1$

The transformations

$$a(t) = 1/\{\lambda(t)\}^2, \quad b(t) = x(t)/\{\lambda(t)\}^{p+1}$$

yield

$$\begin{cases} \lambda_\tau = -2^{-1}\lambda x, \\ x_\tau = -A\lambda^{p-1}x - B\lambda^{2p-2} - \tilde{\mu} - 2^{-1}(p+1)x^2, \end{cases} \tag{6.5.3}$$

via time-scaling $d\tau/dt = \lambda^{-p+1}$. This system has no equilibria. It is important to note that the following holds:

$$x_\tau\big|_{\lambda=0} = -\tilde{\mu} - 2^{-1}(p+1)x^2 < 0.$$

Combining the dynamics on the chart $\overline{U}_j$ $(j = 1, 2)$ and $\overline{V}_2$, it is clear that there are no infinitely far equilibrium on $\Phi_4\backslash\{a < 0\}$ when p is both even and odd.

6.5.4 Dynamics near finite equilibria

Based on the conclusions given at the end of Subsections 6.5.1, 6.5.2, and 6.5.3, we now investigate the finite equilibria in (6.1.18). In the Poincaré-Lyapunov compactification, we did not need to consider the case of the range of δ, as shown in Table 6.1. However, when discussing finite equilibria, it is necessary to consider this.

The case $1 < \delta < N/2$

For $1 < \delta < N/2$, (6.1.18) has the following finite equilibria, depending on whether p is even or odd:

- When p is even, the equilibria are $E_{O'} : (a, b) = (0, 0)$, $E_C : (a, b) = (L_1, 0)$ with $L_1 = (-B/\tilde{\mu})^{1/(p-1)} > 0$.

- If p is an odd greater than or equal to 3, the equilibria are $E_{O'} : (a, b) = (0, 0)$, $E_C : (a, b) = (\pm L_1, 0)$.

The Jacobian matrices of the vector field (6.1.18) at these equilibria are

$$E_{O'} : \begin{pmatrix} 0 & 1 \\ -B & -A \end{pmatrix} = J_1, \quad \pm E_C : \begin{pmatrix} 0 & 1 \\ (p-1)B & -A \end{pmatrix} = J_2.$$

First, the eigenvalues of the matrix J_1 are $-\alpha > 0$ and $-\alpha - N + 2 < 0$ when $\kappa = 1$, and the corresponding eigenvectors are $(1, -\alpha)$ and $(1, -\alpha - N + 2)$, respectively. Therefore, when $\kappa = 1$, the equilibrium $E_{O'}$ is a saddle. On the other hand, when $\kappa = -1$, we determine that this equilibrium is a saddle similarly.

Then, the behavior of the solution around E_C depends on the sign of D from the calculation of the eigenvalues of the matrix J_2 (D is defined in Theorem 6.2.4). In addition, if $\kappa = 1$, then the real parts of all eigenvalues of J_2 are negative. Therefore, we can conclude that E_C is asymptotically stable when $\kappa = 1$. Similarly, we can determine that E_C can be unstable when $\kappa = -1$.

Since equilibria at infinity do not exist on $\Phi_4 \backslash \{a < 0\}$, the existence of a connecting orbit connecting $E_{O'}$ and E_C in this region is expected in order to satisfy the restriction on the range of existence of the solution $U(r)$ described at the beginning of this section, whether p is even or odd. The existence of connecting orbits will be proved in Subsection 6.5.5 (see Proposition 6.5.1).

Remark 6.5.1
As defined in Theorem 6.2.4, D is

$$D = D(N, \delta) = (N-2)^2 - 4(\delta+1)(N-2) + 4(\delta+1)(\delta-1).$$

By setting $Q = N - 2 > 0$ in a similar way as in Remark 6.3.1, we obtain

$$D(Q) = Q^2 - 4(\delta+1)Q + 4(\delta+1)(\delta-1).$$

From a similar argument as in Remark 6.3.1, it is not possible to have $D(Q) = D(N, \delta) = 0$. Correspondingly, the case of $D = 0$ is eliminated in Theorem 6.2.4.

The case $\delta = N/2$

For $\delta = N/2$, (6.1.18) has the following finite equilibrium, depending on whether p is even or odd:

- When p is even, the equilibria are $E_{O'} : (a, b) = (0, 0)$, $E_C : (a, b) = (L_1, 0)$ with $L_1 = (-B/\tilde{\mu})^{1/(p-1)} > 0$.
- If p is an odd greater than or equal to 3, the equilibria are $E_{O'} : (a, b) = (0, 0)$, $E_C : (a, b) = (\pm L_1, 0)$.

By a similar argument as in Subsection 6.5.4, the existence of a connecting orbit connecting $E_{O'}$ and E_C in this region is expected in order to satisfy the restriction on the range of existence of the solution $U(r)$ described at the beginning of this section, whether p is even or odd. The existence of connecting orbits will be proved in Subsection 6.5.5 (see Proposition 6.5.2). The Jacobian matrices of the vector field (6.1.18) at these equilibria are

$$E_{O'} : \begin{pmatrix} 0 & 1 \\ -B & 0 \end{pmatrix} = J_3, \quad \pm E_C : \begin{pmatrix} 0 & 1 \\ (p-1)B & 0 \end{pmatrix} = J_4.$$

The eigenvalues of the matrix J_3 are $2^{-1}(N-2) > 0$ and $-2^{-1}(N-2) < 0$ from $B = -4^{-1}(N-2)^2 < 0$, and the corresponding eigenvectors are $(1, 2^{-1}(N-2))$ and $(1, -2^{-1}(N-2))$, respectively. Therefore, the equilibrium $E_{O'}$ is a saddle. On the other hand, the eigenvalues of the matrix J_4 are $\pm\sqrt{-(p-1)B}i$. Hence, it is generally difficult to determine the dynamics around the equilibrium E_C at $\delta = N/2$ since the eigenvalues are purely imaginary numbers.

However, in this $\delta = N/2$ case, (6.1.18) turns out to be a Hamiltonian system, and we can understand the dynamics around this equilibrium. In fact, let $H = H(a,b)$ be the constant C as follows:

$$H(a,b) = \frac{1}{2}Ba^2 + \frac{\tilde{\mu}}{p+1}a^{p+1} + \frac{1}{2}b^2 + C.$$

Then,

$$\begin{cases} \dfrac{\partial H}{\partial b} = b, \\ \dfrac{\partial H}{\partial a} = Ba + \tilde{\mu}a^p \end{cases}$$

holds. Therefore, H is a conserved quantity of this equation. From these, we can conclude that the dynamics around E_C.

Remark 6.5.2
In Section 5 of [21], the existence of periodic orbits is claimed by presenting conserved quantity for equations derived by a different transformation from ours in the case that $\delta = N/2$. Note that the existence of the periodic orbits agrees with the result of [21].

The case $N/2 < \delta < N-1$

As mentioned in Section 6.1, for $N/2 < \delta < N-1$, we can only consider the cases $p = 2$ and $p = 4$. The system (6.1.18) has the equilibria

$$E_{O'} : (a,b) = (0,0), \quad E_C : (a,b) = (L_1, 0).$$

The Jacobian matrices of this vector field at these equilibria are

$$E_{O'} : \begin{pmatrix} 0 & 1 \\ -B & -A \end{pmatrix}, \quad \pm E_C : \begin{pmatrix} 0 & 1 \\ (p-1)B & -A \end{pmatrix}.$$

Compared to the case of $1 < \delta < N/2$, the sign reversal of A and the switch of $\kappa = \pm 1$ correspond (see Table 6.1). A similar calculation as in Subsection 6.5.4 shows that the equilibrium $E_{O'}$ is a saddle. In addition, E_C is unstable when $\kappa = 1$, and E_C is asymptotically stable when $\kappa = -1$. Thus, as in the above subsection, $p \in \mathbb{N}$, and in the region where $\Phi_4 \cup \{a > 0\}$, we are interested in the existence of a connecting orbit between $E_{O'}$ and E_C and the asymptotic behavior of the corresponding solution derived from it. The existence of connecting orbits will be proved in Subsection 6.5.5 (see Proposition 6.5.3).

From a similar argument as in Remark 6.5.1, note that it is not possible to have $D(Q) = D(N,\delta) = 0$. Correspondingly, note that the case of $D = 0$ is eliminated in Theorem 6.2.7.

The case $\delta = N - 1$

For $\delta = N - 1$, (6.1.18) has only finite equilibrium $(a, b) = (0, 0)$. Therefore, there are no trajectories connecting equilibria in $\Phi_4 \backslash \{a < 0\}$ including equilibria at infinity. Although each orbit in this region may imply the existence of solutions to (6.1.8), this analysis method does not investigate detailed information on the shape and asymptotic behavior of the solutions. We leave it open here.

The case $\delta > N - 1$

As mentioned in Section 6.1, for this case, we can only consider the case $p = 2$. The system (6.1.18) has the equilibria

$$(a, b) = (0, 0), \quad (a, b) = (L_4, 0), \quad L_4 = -|-B\tilde{\mu}^{-1}|^{1/(p-1)} < 0.$$

Therefore, there are no trajectories connecting equilibria in $\Phi_4 \backslash \{a < 0\}$ including equilibria at infinity. Therefore, there are no trajectories connecting equilibria in $\Phi_4 \backslash \{a < 0\}$ including equilibria at infinity.

6.5.5 Dynamics and connecting orbits on the Poincaré-Lyapunov disk

By combining the previous arguments in local coordinates and finite equilibria, we obtain the following propositions.

Proposition 6.5.1
Assume that $3 \leq N \in \mathbb{N}$, $\tilde{\mu} > 0$, $p \in \mathbb{N}$ and $1 < \delta < N/2$ with $\delta = (p + 1)/(p - 1)$. Then, there exists a connecting orbit between the points of $\mathcal{W}^u(E_{O'})$ (resp. $\mathcal{W}^s(E_{O'})$) on the region of $\Phi_4 \backslash \{a < 0\}$, and the points of $\mathcal{W}^s(E_C)$ (resp. $\mathcal{W}^u(E_C)$) on the Poincaré-Lyapunov disk in the case that $\kappa = 1$ (resp. $\kappa = -1$).

Proof. **(I)** First, assume that $p \in 2\mathbb{N}$ and $\kappa = 1$. This is shown by the proof by contradiction. We assume that the trajectory starting from a point on $\mathcal{W}^u(E_{O'})$ in the region $\Phi_4 \backslash \{a < 0\}$ never reaches a point on $\mathcal{W}^s(E_C)$. Then, since it is a two-dimensional system, the trajectory starting from a point on it can only go to a point on $\mathcal{W}^s(E_8)$. However, the trajectory to reach a point on $\mathcal{W}^s(E_C)$ will intersect this trajectory, which is a contradiction. Therefore, a trajectory starting from a point on $\mathcal{W}^u(E_{O'})$ in the region $\Phi_4 \backslash \{a < 0\}$ must reach a point on $\mathcal{W}^s(E_C)$.
(II) Next, assume that $p \in 2\mathbb{N}$ and $\kappa = -1$. As in Proposition 6.4.1, switching $\kappa = \pm 1$ is equivalent to performing the following transformation:

$$b \mapsto -b, \quad t \mapsto -t.$$

Thus, the existence of a connecting orbit between the equilibrium E_C and $E_{O'}$ is proved even in the case of $\kappa = -1$.
(III) Finally, this is proved for the case where p is odd in a similar way as the argument for the even case. □

Furthermore, in the cases that $\delta = N/2$ and $N/2 < \delta < N - 1$, we can prove the existence of connecting orbits between equilibrium at $\Phi_4 \backslash \{a < 0\}$ in a similar way as for Proposition 6.4.1 and Proposition 6.5.1.

Proposition 6.5.2
Assume that $3 \leq N \in \mathbb{N}$, $\tilde{\mu} > 0$, $p \in \mathbb{N}$ and $\delta = N/2$ with $\delta = (p+1)/(p-1)$. As mentioned earlier, in this case, we only need to consider $p = 2, 3, 5$, and correspondingly $N = 6, 4, 3$. Then, there exists a connecting orbit between the points of $\mathcal{W}^u(E_{O'})$ in the region of $\Phi_4 \backslash \{a < 0\}$, and the points of $\mathcal{W}^s(E_{O'})$ in this region.

Proposition 6.5.3
Assume that $3 \leq N \in \mathbb{N}$, $\tilde{\mu} > 0$, $p \in \mathbb{N}$ and $N/2 < \delta < N - 1$ with $\delta = (p+1)/(p-1)$. As mentioned earlier, in this case, we only need to consider $p = 2, 4$ and correspondingly $N = 5, 3$. Then, there exists a connecting orbit between the points of $\mathcal{W}^u(E_{O'})$ (resp. $\mathcal{W}^s(E_{O'})$) on the region of $\Phi_4 \backslash \{a < 0\}$, and the points of $\mathcal{W}^s(E_C)$ (resp. $\mathcal{W}^u(E_C)$) on the Poincaré-Lyapunov disk in the case that $\kappa = -1$ (resp. $\kappa = 1$).

6.6 Proof of Theorem

In this section, the proofs of our main results are given. If the initial data are located on $\mathbb{R}^2 \backslash \{a = 0\}$, the existence of the solutions follows from the standard theory of ordinary differential equations. Therefore, we only consider the existence of the trajectories that connect equilibria and the detailed dynamics near the equilibria on Φ_1 (see Subsection 6.3.5).

6.6.1 Proof of Theorem 6.2.1

Proof. The proof of the existence of the connecting orbits between E_A and E_4 (resp. E_3) on the chart $\overline{U}_1$ for $p \in 2\mathbb{N}$, $p \in 2\mathbb{N} + 1$, and $\kappa = 1$ (resp. $\kappa = -1$) is obtained in Proposition 6.3.1 and Subsection 6.3.6. That is, equation (6.1.8) has a family of radially symmetric stationary solutions which corresponds to a family of the orbits of (6.1.14). Furthermore, since these trajectories exist for $\{(a, b) \in \Phi_1 \mid a > 0\}$, the expression for the transformation in Case 1 shows that $U(r) < 1$ ($r \in (0, +\infty)$).

Therefore, it is sufficient to show that (6.2.1) and

$$\lim_{r \to 0} U(r) = 1 - C \quad (C > 0), \quad \lim_{r \to 0} U'(r) = 0.$$

Note that if we can derive (6.2.1), then the following is also proved.

$$\lim_{r \to +\infty} U(r) = -\infty.$$

Next, the asymptotic behavior for $r \to 0$ is derived as follows. We recall from (6.3.12) that the solutions near a saddle point E_3 are approximated

$$\begin{cases} \lambda(\tau) = C_1 e^{-\alpha\tau}(1 + o(1)), \\ x(\tau) - \alpha = C_2 e^{(N-2)\tau}(1 + o(1)), \end{cases} \quad \text{as} \quad \tau \to +\infty,$$

where $\alpha = (-A-(N-2))/2$, C_1 and C_2 are constants. Note that we focus on the direction of stable manifold $\mathcal{W}^s(E_3)$. We choose $C_1 e^{-\alpha\tau}$ as "the principal term". Using (6.3.12), we then have

$$\frac{d\tau}{dt} = \frac{d\tau}{ds}\frac{ds}{dt} = \lambda^{-p} \cdot a^{-p} = 1.$$

This yields $t(\tau) = \tau + C_3$ ($C_3 \in \mathbb{R}$). We can see $t(\tau) \to +\infty$ as $\tau \to +\infty$ since we focus on the points on $\mathcal{W}^s(E_3)$, and we get

$$\tau(t) = t + C_4, \quad (C_4 \in \mathbb{R}).$$

Therefore, we obtain

$$\begin{aligned} a(t) = \frac{1}{\lambda} = \lambda^{-1} &\sim \left\{C_1 e^{-\alpha\tau}(1+o(1))\right\}^{-1} \\ &\sim C_5 e^{\alpha\tau} = C_5 e^{\alpha(t+C_4)} = C_6 e^{\alpha t} \quad \text{as} \quad t \to +\infty, \end{aligned}$$

where C_j are constants. Since, the trajectories are lying on $\{a > 0\}$, it follows that $C_6 > 0$.

On the other hand, we obtain

$$\begin{aligned} b(t) &= \lambda^{-1} x \\ &\sim \{C_1 e^{-\alpha\tau}(1+o(1))\}^{-1} \cdot \{C_2 e^{(N-2)\tau}(1+o(1)) + \alpha\} \\ &\sim C_7 e^{\alpha\tau}. \end{aligned}$$

Note that the last "$\sim$" ignore the x term in order to extract the components in the stable manifold direction, as described above. This idea has already been adopted in [35] and is effective for obtaining more accurate asymptotic behavior. Thus,

$$b(t) \sim C_8 e^{\alpha t} \quad \text{as} \quad t \to +\infty.$$

Since, the trajectories are lying on $\{b > 0\}$, it follows that $C_8 > 0$. From these arguments, the following follows

$$\dot{a} \sim b \quad \text{as} \quad t \to +\infty$$

and $C_8 = \alpha C_6$.

From these results, we can obtain

$$\lim_{r\to 0} u(r) = \lim_{r\to 0}(1 - r^\alpha a) = \lim_{r\to 0}(1 - r^\alpha C_6 e^{\alpha t}) = 1 - C_6$$

and

$$\lim_{r\to 0} u'(r) = \lim_{r\to 0}\{r^{\alpha-1}(-\alpha a + b)\} = \lim_{r\to 0}\{r^{\alpha-1}(-\alpha C_6 + C_8) r^{-\alpha}\} = 0$$

with $C_9 > 0$. Therefore, we derive the following from the relationship between u and U transformations in Case 1.

$$\lim_{r\to 0} U(r) = 1 - C \quad (C > 0), \quad \lim_{r\to 0} U'(r) = 0.$$

Finally, we derive the asymptotic behavior for $r \to +\infty$. The idea of this proof has already been used in [33, 32], see also. We focus our attention on the dynamics around E_A. It is divided into two cases by the value of $D = D(N, \delta)$. Then, we derive the asymptotic behavior for the two cases $D > 0$ and $D < 0$, respectively. Note that Remark 6.3.1 states that the case $D = 0$ cannot occur. We define

$$\tilde{a} = a - M_1, \quad \tilde{b} = b - 0.$$

(i) Let us consider the case that $D > 0$, namely, the matrix J_A has the real distinct eigenvalues

$$\sigma_1 = \frac{-A + \sqrt{D}}{2}, \quad \sigma_2 = \frac{-A - \sqrt{D}}{2}.$$

The eigenvectors corresponding to each eigenvalues are

$$\mathbf{v}_1 = \begin{pmatrix} 1 \\ \sigma_1 \end{pmatrix}, \quad \mathbf{v}_2 = \begin{pmatrix} 1 \\ \sigma_2 \end{pmatrix}.$$

We then obtain the following asymptotic behavior:

$$\begin{pmatrix} \tilde{a}(t) \\ \tilde{b}(t) \end{pmatrix} = K_1 \begin{pmatrix} 1 \\ \sigma_1 \end{pmatrix} e^{\sigma_1 t} + K_2 \begin{pmatrix} 1 \\ \sigma_2 \end{pmatrix} e^{\sigma_2 t}$$

with any constants K_1 and K_2. Therefore, the solution around the equilibrium E_A is

$$\begin{cases} a(t) \sim K_1 e^{\sigma_1 t} + K_2 e^{\sigma_2 t} + M_1, \\ b(t) \sim K_1 \sigma_1 e^{\sigma_1 t} + K_2 \sigma_2 e^{\sigma_2 t}, \end{cases} \qquad M_1 = \left(\frac{\tilde{\mu}}{B}\right)^{\frac{1}{p+1}}.$$

Moreover, by using $\kappa = 1$ in (6.1.12), we have

$$\begin{aligned} u(r) &= 1 - r^\alpha a \\ &\sim 1 - r^\alpha (K_1 e^{\sigma_1 t} + K_2 e^{\sigma_2 t} + M_1) \\ &= 1 - K_1 r^\alpha e^{\sigma_1 \log r} - K_2 r^\alpha e^{\sigma_2 \log r} - M_1 r^\alpha \\ &= 1 - K_1 r^{\alpha+\sigma_1} - K_2 r^{\alpha+\sigma_2} - M_1 r^\alpha \quad \text{as} \quad r \to +\infty. \end{aligned}$$

Since $0 < \delta < 1$, it holds that

$$\alpha + \sigma_1 < 0, \quad \alpha + \sigma_2 < 0.$$

Hence, from the relationship between u and U transformations in Case1, we obtain as follows:

$$\begin{aligned} U(r) &= 1 - (1-u)^{\frac{1}{1-\delta}} \\ &\sim 1 - \left\{K_1 r^{\alpha+\sigma_1} + K_2 r^{\alpha+\sigma_2} + M_1 r^\alpha\right\}^{\frac{1}{1-\delta}} \quad \text{as} \quad r \to +\infty \end{aligned}$$

where K_1 and K_2 are constants.

(ii) Consider the case that $D < 0$, namely, the matrix J_A has the complex eigenvalues

$$\sigma = \mu \pm i\nu = \frac{-A}{2} \pm i\frac{1}{2}\sqrt{|D|}.$$

The eigenvectors corresponding to each eigenvalue are

$$\mathbf{v} = \mathbf{p} \pm i\mathbf{q} = \begin{pmatrix} 1 \\ -\dfrac{A}{2} \end{pmatrix} \pm i \begin{pmatrix} 0 \\ \dfrac{1}{2}\sqrt{|D|} \end{pmatrix}.$$

The function $\tilde{a}(t)$ and $\tilde{b}(t)$ are expressed as follows:

$$\begin{pmatrix} \tilde{a}(t) \\ \tilde{b}(t) \end{pmatrix} = z(t)\mathbf{q} + w(t)\mathbf{p} = z(t) \begin{pmatrix} 0 \\ \dfrac{1}{2}\sqrt{|D|} \end{pmatrix} + w(t) \begin{pmatrix} 1 \\ -\dfrac{A}{2} \end{pmatrix},$$

where

$$\begin{pmatrix} z(t) \\ w(t) \end{pmatrix} := e^{\mu t} \begin{pmatrix} \cos \nu t & -\sin \nu t \\ \sin \nu t & \cos \nu t \end{pmatrix} \begin{pmatrix} z(0) \\ w(0) \end{pmatrix}.$$

Therefore, the solution $a(t)$ around the equilibrium E_A is

$$a(t) = e^{-\frac{A}{2}t} \left(z(0) \sin \frac{\sqrt{|D|}}{2} t + w(0) \cos \frac{\sqrt{|D|}}{2} t \right) + M_1.$$

Using $\kappa = 1$ in (6.1.12), we can derive the following:

$$\begin{aligned} u(r) &= 1 - r^{\alpha} a \\ &= 1 - r^{\frac{2-N}{2}} \left(K_3 \sin[\frac{\sqrt{|D|}}{2} \log r] + K_4 \cos[\frac{\sqrt{|D|}}{2} \log r] \right) - M_1 r^{\alpha} \quad \text{as} \quad r \to \infty \end{aligned}$$

with $K_3 = z(0)$ and $K_4 = w(0)$. Hence, from the relationship between u and U transformations in Case 1, the asymptotic behavior for $r \to +\infty$ is

$$U(r) \sim 1 - \left\{ r^{\frac{2-N}{2}} \left(K_3 \sin[\frac{\sqrt{|D|}}{2} \log r] + K_4 \cos[\frac{\sqrt{|D|}}{2} \log r] \right) + M_1 r^{\alpha} \right\}^{\frac{1}{1-\delta}}.$$

Therefore, we obtain (6.2.1). This completes the proof of Theorem 6.2.1. □

Remark 6.6.1
The existence of a trajectory such that it passes through the line $b = -\alpha a$ on the disk corresponds to the existence of $r = r_*$ such that $U'(r_*) = 0$. In fact, the equation of this line can be derived as follows:

$$U' = 0 \iff u' = 0 \iff r^{\alpha - 1}(-\alpha a - b) = 0 \iff b = -\alpha a.$$

From the conclusion of Theorem 6.2.1, this line is the line passing through the origin and E_3 on this disk. And we know that E_3 for $\kappa = -1$ is the point at infinity on this line (see Figure 6.3.2 and Figure 6.3.3).

6.6.2 Proof of Theorem 6.2.2

As in the proof of Theorem 6.2.1, the proof of the existence of the connecting orbits between E_A and E_3 (resp. E_4) on the chart $\overline{U}_1$ for $p \in 2\mathbb{N}$, $p \in 2\mathbb{N} + 1$, and $\kappa = 1$ (resp. $\kappa = -1$) is obtained. Therefore, these trajectories correspond to the radially symmetric stationary solution in (6.1.8). Moreover, these trajectories exist in $\{a > 0\}$, so $U(r) < 1$ ($r \in (0, +\infty)$) from the transformation in Case 1. The existence of a constant $r_* \in (0, +\infty)$ such that $U'(r_*)$ is shown from Remark 6.6.1. This is because the connecting orbits between E_A and E_4 pass through a straight line that passes through the origin and E_3 for $\kappa = -1$ (see Figure 6.3.2).

Therefore, it is sufficient to show that (6.2.2). If these are proved, then the following is also shown

$$\lim_{r \to 0} U(r) = -\infty, \quad \lim_{r \to 0} U'(r) = \infty.$$

Using (6.3.13), we then have

$$\frac{d\tau}{dt} = \frac{d\tau}{ds}\frac{ds}{dt} = \lambda^{-p} a^{-p} = \lambda^{-p} \left(\frac{1}{\lambda} \right)^{-p} = 1.$$

This yields $t(\tau) = \tau + C_3$ with a constant $C_3 \in \mathbb{R}$. We can see $t(\tau) \to +\infty$ as $\tau \to +\infty$ since we focus on the points on $\mathcal{W}^s(E_4)$. This relationship shows that

$$\tau(t) = t + C_4, \quad (C_4 \in \mathbb{R})$$

holds. Therefore, we obtain

$$\begin{aligned} a(t) = \frac{1}{\lambda} &\sim \left\{ C_1 e^{-(\alpha+N-2)\tau}(1+o(1)) \right\}^{-1} \\ &\sim C_5 e^{(\alpha+N-2)\tau} \\ &= C_6 e^{(\alpha+N-2)t} \quad \text{as} \quad t \to +\infty \end{aligned}$$

and

$$\begin{aligned} b(t) = \frac{x}{\lambda} &\sim \left\{ C_1 e^{-(\alpha+N-2)\tau}(1+o(1)) \right\}^{-1} \cdot \left\{ C_2 e^{-(N-2)\tau}(1+o(1)) + M_3 \right\} \\ &\sim C_7 e^{(\alpha+N-2)\tau} \cdot \left\{ C_2 e^{-(N-2)\tau}(1+o(1)) + M_3 \right\} \\ &\sim C_7 M_3 e^{(\alpha+N-2)\tau} \\ &= C_8 e^{(\alpha+N-2)t} \quad \text{as} \quad t \to \infty \end{aligned}$$

where C_j are constants. Since, the trajectories are lying on $\{a > 0\}$, it follows that $C_6 > 0$. From these arguments, the following follows

$$\dot{a} \sim b \quad \text{as} \quad t \to +\infty$$

and $C_8 = C_5(\alpha + N - 2) > 0$.

By using $\kappa = -1$ in (6.1.12), we have

$$\begin{aligned} u(r) &= 1 - r^\alpha a \sim 1 - C_5 r^{-(N-2)} \quad \text{as} \quad r \to 0, \\ u'(r) &= r^{\alpha-1}(-\alpha a + b) \sim C_9 r^{-(N-1)} \quad \text{as} \quad r \to 0 \end{aligned}$$

with a positive constant C_9. Hence, from the relationship between u and U transformations in Case 1, we obtain (6.2.2). This completes the proof of Theorem 6.2.2. □

6.6.3 Proof of Theorem 6.2.3

Next, the proof of our main result related to Case 2 is given. It should be noted that if the initial data are located on $\mathbb{R}^2 \backslash \{a \le 0\}$, the existence of the solutions follows from the standard theory of ordinary differential equations.

Proof. The proof of the existence of the connecting orbit between the points of $\mathcal{W}^u(E_B)$ (resp. $\mathcal{W}^s(E_B)$) and the points of $\mathcal{W}^s(\overline{E}_O^2)$ (resp. $\mathcal{W}^u(\overline{E}_O^1)$) is obtained in Proposition 6.4.1. That is, (6.1.8) has a radially symmetric stationary solution that corresponds to the orbit of (6.1.16). Moreover, these trajectories exist in $\{a > 0\}$, so $U(r) < 1$ ($r \in (0, +\infty)$) from the transformation in Case 2. Therefore, it is sufficient to show that (6.2.3) and

$$\lim_{r \to 0} U(r) = 1 - C, \quad \lim_{r \to 0} U'(r) = 0$$

Let us derive the asymptotic behavior for $r \to 0$. The idea of the proof is almost similar to the proof of Theorem 6.2.1. Using (6.4.4), we then have $d\sigma/dt = 1$. It shows that $\sigma(t) = t + A_1$ holds. Therefore, we can obtain

$$\begin{cases} a(t) \sim A_2 e^{-2t}, \\ b(t) \sim A_3 e^{-2t}, \end{cases} \quad \text{as} \quad t \to +\infty$$

with $A_3 = -2A_2 < 0$. By using $\kappa = -1$ in (6.1.15), we have

$$\begin{cases} \lim_{r\to 0} u(r) = \lim_{r\to 0}(-2\log r + \log a) = A_4, \\ \lim_{r\to 0} u'(r) = \lim_{r\to 0}\left(-2\frac{1}{r} - \frac{1}{r}\frac{1}{a}\dot{a}\right) = 0 \end{cases}$$

with a constant A_4. Hence, from the relationship between u and U transformations in Case 2, we can obtain as follows:

$$\lim_{r\to 0} U(r) = 1 - C, \quad \lim_{r\to 0} U'(r) = 0$$

The derivation process of (6.2.3) is similar to the proof of Theorem 6.2.1 and can be divided into three cases according to the sign of $N - 10$. In particular, see [33, 32] for the derivation process of the asymptotic behavior in the case of $N = 10$. Therefore, this completes the proof of Theorem 6.2.3. □

6.6.4 Proof of Theorem 6.2.4

Proof. The proof of the existence of the connecting orbit between $E_{O'}$ and E_C is obtained in Proposition 6.5.1. Therefore, the existence of a radially symmetric stationary solution can be shown by similar arguments as before. (6.2.4) is derived in much the same way as in Theorem 6.2.1 and Theorem 6.2.3. The same applies to the proof of

$$\lim_{r\to 0} U(r) = 1 - C, \quad \lim_{r\to 0} U'(r) = 0.$$

Therefore, this completes the proof of Theorem 6.2.4. □

6.6.5 Proof of Theorem 6.2.6

The existence of a connecting orbit starting from the points on the unstable manifold of $E_{O'}$ and reaching the points on the stable manifold of $E_{O'}$ was obtained in Proposition 6.5.2. Therefore, the existence of a radially symmetric stationary solution can be shown by similar arguments as before. (6.2.5) and

$$\lim_{r\to 0} U(r) = 1 - K_1, \quad \lim_{r\to 0} U'(r) = 0$$

are derived by a similar procedure as before arguments. Therefore, this completes the proof of Theorem 6.2.6. □

6.6.6 Proof of Theorem 6.2.7

The proof of the existence of the connecting orbit between $E_{O'}$ and E_C is obtained in Proposition 6.5.3. The existence of a radially symmetric stationary solution can be shown by similar arguments as before. Therefore, it is sufficient to show that (6.2.6), (6.2.7), (6.2.8), and

$$\lim_{r\to 0} U'(r) = -\sqrt{\frac{\mu}{N-1-\delta}}.$$

Note that (6.2.8) is derived in much the same way as in Theorem 6.2.1, Theorem 6.2.3, and Theorem 6.2.4. In addition, (6.2.6) is derived by a similar procedure as before

arguments. Then, all we need to do is derive (6.2.7). This can be derived by performing the work of selecting the principal term in the calculation process to derive (6.2.8). The same is true for the behavior of $U'(r)$ as $r \to 0$.

In order to derive (6.2.7), we focus our attention on the dynamics around E_C in the case that $N/2 < \delta < N-1$ and $\kappa = -1$. Similarly, as in Subsection 6.6.1, the solution around this equilibrium is

$$\begin{cases} a(t) \sim K_1 e^{\sigma_1 t} + K_2 e^{\sigma_2 t} + L_1 \sim L_1, \\ b(t) \sim K_1 \sigma_1 e^{\sigma_1 t} + K_2 \sigma_2 e^{\sigma_2 t}, \end{cases} \qquad L_1 = \left(-\frac{B}{\tilde{\mu}}\right)^{\frac{1}{p-1}} > 0, \quad \text{as} \quad t \to \infty$$

when $D > 0$. The same is true for the solution around it when $D < 0$. Note that we have chosen the principal term in the expression for $a(t)$. By using $\kappa = -1$ in (6.1.17), we have

$$\begin{cases} u(r) = r^\alpha - 1 \sim L_1 r^\alpha - 1 \\ u'(r) = (1-\delta) r^{-\delta} a - r^{-\delta} b \sim (1-\delta) r^{-\delta} L_1 \end{cases} \qquad \text{as} \quad r \to 0$$

for both $D > 0$ and $D < 0$. From this result, we can conclude that

$$U(r) \sim 1 - (L_1 r^\alpha)^{-\frac{1}{\delta-1}} = 1 - \sqrt{\frac{\mu}{N-1-\delta}}\, r \quad \text{as} \quad r \to 0$$

with $L_1^{-\frac{1}{\delta-1}} = \left(\dfrac{\mu}{N-1-\delta}\right)^{\frac{1}{2}}$. Thus, (6.2.7) can be derived. Similarly,

$$\lim_{r\to 0} U'(r) = \lim_{r \to 0} \frac{1}{\delta - 1} (1-U)^\delta u' = -\sqrt{\frac{\mu}{N-1-\delta}} < 0$$

holds. Therefore, this completes the proof of Theorem 6.2.7. □

6.7 Concluding remarks

In this chapter, we studied the existence, information about their shape, and the asymptotic behavior of radially symmetric stationary solutions of (6.1.1). These are studied by applying the framework that combines Poincaré type compactification, classical dynamical systems theory, and geometric methods for desingularization of vector fields (blow-up technique).

Motivated by the previous study [21], this chapter considers the question of how far we can investigate the structure of solutions in a unified way by applying this framework. Then, our framework allowed us to obtain results that were not obtained in [21] (mainly, Theorem 6.2.2, (6.2.8) in Theorem 6.2.7) and results that were partially included in the results there (Theorem 6.2.1, 6.2.3, 6.2.4, 6.2.6).

As mentioned in Section 6.1, one of the advantages of using these methods is that it is possible to reveal all the dynamics of the ODEs of interest, including infinity. That is, we expect to enumerate all solutions of (6.1.8).

However, in this problem, restrictions are imposed on the range of existence of each of the conversions from U to u and from u to a. This also restricts the possible regions in these ODEs, and we were not able to study the case of $\delta \geq N-1$. The structure of the solution in this range has been obtained by [21]. It remains to be seen how close we can get to this conclusion in the framework of this chapter, or whether we can extend this conclusion.

Since the theory of blow-up (desingularization of the vector fields) is not applicable for the non-polynomial vector fields, we cannot deal with the general case that $p \in \mathbb{R}$. Therefore, the need to impose $p \in \mathbb{N}$ led us to consider discrete values for δ. Hence, we leave it open here.

Chapter 7

Traveling wave solutions for degenerate nonlinear parabolic equations

Abstract

We consider the traveling wave solutions of the degenerate nonlinear parabolic equation $u_t = u^p(u_{xx} + u)$ which arises in the model of heat combustion, solar flares in astrophysics, plane curve evolution problems and the resistive diffusion of a force-free magnetic field in a plasma confined between two walls. We also deal with the equation $v_\tau = v^p(v_{xx} + v - v^{-p+1})$ related with it. We first give a result on the whole dynamics on the phase space $\mathbb{R}^2$ with including infinity about two-dimensional ordinary differential equation that introduced the traveling wave coordinates: $\xi = x - ct$ by applying the Poincaré compactification and dynamical system approach. Second, we focus on the connecting orbits on it and give a result on the existence of the weak traveling wave solutions with quenching for $c > 0$ and $p \in 2\mathbb{N}$. Moreover, we give the detailed information about the asymptotic behavior of $u(\xi)$, $u'(\xi)$, $v(\xi)$ and $v'(\xi)$ for $p \in 2\mathbb{N}$. In the case that $p \in 2\mathbb{N} + 1$, it is too complicated to determine the dynamics near the singularities on the Poincaré disk, however, we classify the connecting orbits and corresponding traveling wave solutions and obtain their asymptotic behavior. This chapter is based on the following published paper ([32]):

> Ichida, Y., Sakamoto, T.O.: Traveling wave solutions for degenerate nonlinear parabolic equations, J. Elliptic Parabol. Equ. **6**, 795–832 (2020).

7.1 Introduction

In this chapter, we consider the following degenerate nonlinear parabolic equation

$$u_t = u^p(u_{xx} + u), \quad (t, x) \in (0, T) \times \mathbb{R}, \tag{7.1.1}$$

where $p \in \mathbb{N}$ and $0 < T < \infty$. This equation arises in the modeling of heat combustion, solar flares in astrophysics, plane curve evolution problems and the resistive diffusion of a force-free magnetic field in a plasma confined between two walls (see [4], [46], [47], [62] and references therein).

In particular, we briefly introduce the derivation from plane curve evolution problems. Let $\mathcal{C}(t)$ be a smooth Jordan curve at time t in the plane $\mathbb{R}^2$. The curve $\mathcal{C}(t)$ is

parameterized by $\boldsymbol{X}(u,t)$ for $u \in [0,1]$ and moves by

$$\dot{\boldsymbol{X}} = V(u,t)\boldsymbol{N}(u,t) + W(u,t)\boldsymbol{T}(u,t), \quad \left(\dot{\boldsymbol{X}} = \partial \boldsymbol{X}/\partial t\right).$$

Here $\boldsymbol{T}$ is the unit tangent vector, $\boldsymbol{N} = -\boldsymbol{T}^{\perp}$ is the unit outward normal vector, V is the normal velocity in $\boldsymbol{N}$-direction and W is the tangent velocity in $\boldsymbol{T}$-direction. Also, we denote by κ and θ the curvature and tangential angle of the curve $\mathcal{C}(t)$, respectively. Then, we can see that the classical curvature flow equation $V = -\kappa$ corresponds to (7.1.1) in the case that $p = 2$ (see [71] for the details).

Poon [62] (and references therein) considered the following equation:

$$u_t = u^p(u_{xx} + u), \quad (t,x) \in (0,T) \times (-L,L), \tag{7.1.2}$$

where $p \in \mathbb{R}$ and $T < \infty$. He studied that the non-negative solutions with either the Dirichlet boundary condition or periodic boundary condition. As a result, the upper bound and lower bound of the blow-up rate were obtained if a non-negative solution of (7.1.2) blows up of type II in finite time. In these studies, the rescaled function

$$v(\tau,x) = (pT)^{\frac{1}{p}} e^{-\tau} u(t,x), \quad t = T(1 - e^{-p\tau}), \quad \tau \in [0,+\infty)$$

plays important role. One can see that if $u(t,x)$ is a solution of (7.1.2), then $v(\tau,x)$ is a non-negative solution of the rescaled equation

$$v_\tau = v^p(v_{xx} + v - v^{-p+1}), \qquad (\tau,x) \in (0,+\infty) \times (-L,L). \tag{7.1.3}$$

In [62], the lower bound of the blow-up rate is obtained with considering the traveling wave solutions of (7.1.3). Similarly, the equation (7.1.1) can be transformed into the following equation

$$v_\tau = v^p(v_{xx} + v - v^{-p+1}), \quad (\tau,x) \in (0,\infty) \times \mathbb{R}. \tag{7.1.4}$$

Since the traveling wave solutions are not only upper (or lower) solutions as discussed in [62] but also the entire solutions of the equations, we study that of (7.1.1) and (7.1.4).

In order to consider the traveling waves of (7.1.1), we introduce the following change of variables:

$$u(t,x) = \phi(\xi), \quad \xi = x - ct, \quad c > 0.$$

We seek the solution $\phi(\xi)$ of the following equation:

$$-c\phi' = \phi^p\phi'' + \phi^{p+1}, \quad \xi \in \mathbb{R}, \quad ' = \frac{d}{d\xi}, \tag{7.1.5}$$

or equivalently,

$$\begin{cases} \phi' = \psi, \\ \psi' = -c\phi^{-p}\psi - \phi. \end{cases} \tag{7.1.6}$$

Similarly, in terms of (7.1.4), we introduce the following change of variables:

$$v(\tau,x) = \phi(\xi), \quad \xi = x - c\tau, \quad c > 0.$$

We also seek the solution $\phi(\xi)$ of the following equation:

$$-c\phi' = \phi^p\phi'' + \phi^{p+1} - \phi, \quad \xi \in \mathbb{R}, \quad ' = \frac{d}{d\xi}, \tag{7.1.7}$$

or equivalently,

$$\begin{cases} \phi' = \psi, \\ \psi' = -c\phi^{-p}\psi - \phi + \phi^{-p+1}. \end{cases} \tag{7.1.8}$$

Combining the equation (7.1.5) and (7.1.7), we obtain the following equation:

$$-c\phi' = \phi^p\phi'' + \phi^{p+1} - \delta\phi, \quad \xi \in \mathbb{R}, \quad ' = \frac{d}{d\xi},$$

or equivalently,

$$\begin{cases} \phi' = \psi, \\ \psi' = -c\phi^{-p}\psi - \phi + \delta\phi^{-p+1}, \end{cases} \tag{7.1.9}$$

where $\delta = 0$ or 1. Here we note that the case when $\delta = 0$ corresponds to (7.1.6) and the case that $\delta = 1$ corresponds to (7.1.8).

We expect that the negative powers nonlinear term ϕ^{-p} and $\delta\phi^{-p+1}$ could induce the singularity in finite time (see [31, 33, 49, 50]). Therefore, we apply the Poincaré compactification (see Section 1.1) to the dynamical system of (7.1.9) to obtain the detailed information of the traveling wave solutions (in weak sense) for (7.1.1) and (7.1.4).

Before we state the main results of this chapter, we state the Definition of weak traveling wave solutions with quenching for (7.1.1) and (7.1.4) as follows.

Definition 7.1.1
Let $u(\xi)$ be a quasi traveling waves with quenching of (7.1.1) *on a semi-infinite interval (ξ_*, ∞) satisfying*

$$\lim_{\xi\to\xi_*+0} |u'(\xi)| = \infty \quad \textit{and} \quad \lim_{\xi\to\xi_*+0} u(\xi) = 0$$

(see Definition 2.1.3 or Definition 3 of [31]). Then, we say that a function

$$u^*(\xi) = \begin{cases} 0, & \xi \in (-\infty, \xi_*], \\ u(\xi), & \xi \in (\xi_*, \infty) \end{cases}$$

is a weak traveling wave solution with quenching of (7.1.1).

The above Definition implies that $u^*(\xi)$ satisfies

$$\int_{\mathbb{R}} \left[c\, u\varphi' + p(u^{p-1}u'\varphi - u^p\varphi')u' - u^{p+1}(\varphi'' + \varphi) \right] d\xi = 0$$

for all $\varphi \in C_0^\infty(\mathbb{R})$. We define a weak traveling wave solution with quenching of (7.1.4) similarly.

We then state the main results of this chapter:

Theorem 7.1.1
Assume that $p \in 2\mathbb{N}$. Then, for a given positive constant c, the equation (7.1.1) *has a family of weak traveling wave solutions with quenching (which corresponds to a family of the orbits of* (7.1.6)*). Moreover, each weak traveling wave solution with quenching $u(\xi)$ satisfies the following:*

- $$\begin{cases} \lim\limits_{\xi\to\xi_*+0} u(\xi) = 0, & \lim\limits_{\xi\to+\infty} u(\xi) = 0, \\ \lim\limits_{\xi\to\xi_*+0} u'(\xi) = +\infty, & \lim\limits_{\xi\to+\infty} u'(\xi) = 0. \end{cases}$$
- *$u(\xi) > 0$ holds for $\xi \in (\xi_*, +\infty)$ and $u(\xi) = 0$ holds for $\xi \in (-\infty, \xi_*]$.*

- *There exists a constant $\xi_0 \in (\xi_*, +\infty)$ such that the following holds: $u'(\xi) > 0$ for $\xi \in (\xi_*, \xi_0)$, $u'(\xi_0) = 0$ and $u'(\xi) < 0$ for $\xi \in (\xi_0, +\infty)$.*

In addition, asymptotic behavior of $u(\xi)$ are

$$\begin{cases} u(\xi) \sim A(\xi - \xi_*)^{\frac{1}{p}} \\ u'(\xi) \sim A(\xi - \xi_*)^{-\frac{p-1}{p}} \end{cases} \quad \text{as} \quad \xi \to \xi_* + 0 \tag{7.1.10}$$

and

$$\begin{cases} u(\xi) \sim (p\xi/c)^{-\frac{1}{p}} \\ u'(\xi) \sim c(p\xi/c)^{-\frac{p+1}{p}} \end{cases} \quad \text{as} \quad \xi \to +\infty, \tag{7.1.11}$$

where $A > 0$ is a constant.

Asymptotic behavior of $u'(\xi)$ for $\xi \to \xi_* + 0$ that is more accurate than in [32] was obtained after publication of the paper. Note that this was obtained by refining the asymptotic form, as will be discussed later in the proof.

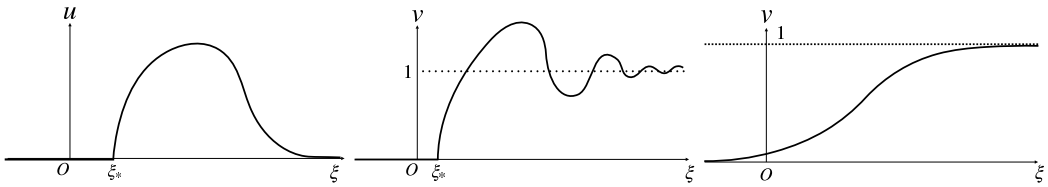

Figure 7.1.1: Schematic picture of the traveling wave solutions obtained in Theorems. Here it should be noted that the position of the quenching point ξ_* is not determined in our studies, however, they are shown in the figures for the convenience. [Left: The weak traveling wave solution with quenching in Theorem 7.1.1.] [Middle: The weak traveling wave solution with quenching in Theorem 7.1.2 in the case that $D < 0$.] [Right: The traveling wave solution on $\xi \in \mathbb{R}$ obtained in Theorem 7.1.3 in the case that $D > 0$.]

Theorem 7.1.2
Assume that $p \in 2\mathbb{N}$. Then, for a given positive constant c, the equation (7.1.4) has a family of weak traveling wave solutions with quenching (which corresponds to a family of the orbits of (7.1.8)). Moreover, each weak traveling wave solution with quenching $v(\xi)$ satisfies the following:

- $$\begin{cases} \lim\limits_{\xi \to \xi_* + 0} v(\xi) = 0, & \lim\limits_{\xi \to +\infty} v(\xi) = 1, \\ \lim\limits_{\xi \to \xi_* + 0} v'(\xi) = +\infty, & \lim\limits_{\xi \to +\infty} v'(\xi) = 0. \end{cases}$$

- *$v(\xi) > 0$ holds for $\xi \in (\xi_*, +\infty)$ and $v(\xi) = 0$ holds for $\xi \in (-\infty, \xi_*]$.*

Furthermore, the asymptotic behavior of $v(\xi)$ and $v'(\xi)$ for $\xi \to +\infty$ are

$$v(\xi) \sim \begin{cases} B_1 e^{\omega_1 \xi} + B_2 e^{\omega_2 \xi} + 1 \quad (D > 0), \\ (B_3 \xi + B_4) e^{\omega \xi} + 1 \quad (D = 0), \\ e^{-\frac{c}{2}\xi} \left(B_5 \cdot [\sin \frac{\sqrt{|D|}}{2} \xi] + B_6 [\cos \frac{\sqrt{|D|}}{2} \xi] \right) + 1 \quad (D < 0), \end{cases} \tag{7.1.12}$$

and

$$v'(\xi) \sim \begin{cases} c^2(B_1\lambda_1 e^{\omega_1\xi} + B_2\omega_2 e^{\lambda_2\xi}) \quad (D>0), \\ c^2\left\{-\dfrac{c}{2}(B_3\xi + B_4)e^{\omega\xi} + B_3\left(1-\dfrac{c}{2}\alpha\right)e^{\omega\xi}\right\} \quad (D=0), \\ \dfrac{c^2}{2}\sqrt{|D|}\cdot e^{-\frac{c}{2}\xi}\left(B_5\cdot[\sin\dfrac{\sqrt{|D|}}{2}\xi] - B_6\cdot[\cos\dfrac{\sqrt{|D|}}{2}\xi]\right) \\ \quad -\dfrac{c^3}{2}\cdot e^{-\frac{c}{2}\xi}\left(B_5\cdot[\sin\dfrac{\sqrt{|D|}}{2}\xi] + B_6\cdot[\cos\dfrac{\sqrt{|D|}}{2}\xi]\right) \quad (D<0), \end{cases} \tag{7.1.13}$$

where B_j are constants and

$$\omega_1 = \frac{-c+\sqrt{D}}{2}, \quad \omega_2 = \frac{-c-\sqrt{D}}{2}, \quad \omega = -\frac{c}{2}, \quad D = c^2 - 4p.$$

In addition, the asymptotic behavior of $v(\xi)$ and $v'(\xi)$ for $\xi \to \xi_* + 0$ are

$$\begin{cases} v(\xi) \sim A(\xi-\xi_*)^{\frac{1}{p}} \\ v'(\xi) \sim A(\xi-\xi_*)^{-\frac{p-1}{p}} \end{cases} \quad \text{as} \quad \xi \to \xi_* + 0. \tag{7.1.14}$$

Asymptotic behavior of $v'(\xi)$ for $\xi \to \xi_* + 0$ that is more accurate than in [32] was obtained after publication of the paper. Note that this was obtained by refining the asymptotic form, as will be discussed later in the proof.

Theorem 7.1.3
Assume that $p \in 2\mathbb{N}$. Then, for a given positive constant c, the equation (7.1.4) *has a family of traveling wave solutions (which corresponds to a family of the orbits of* (7.1.8)*). Each traveling wave solution $v(\xi)$ satisfies the following:*

- $\begin{cases} \lim\limits_{\xi\to-\infty} v(\xi) = 0, & \lim\limits_{\xi\to+\infty} v(\xi) = 1, \\ \lim\limits_{\xi\to-\infty} v'(\xi) = 0, & \lim\limits_{\xi\to+\infty} v'(\xi) = 0. \end{cases}$
- *$v(\xi) > 0$ holds for $\xi \in \mathbb{R}$.*

In addition, the asymptotic behavior of $v(\xi)$ and $v'(\xi)$ for $\xi \to +\infty$ are expressed as (7.1.12) *and* (7.1.13)*.*

This chapter is organized as follows. In the next section, we obtain the dynamics of (7.1.9) with $p \in 2\mathbb{N}$ on the Poincaré disk via Poincaré compactification and basic theory of the dynamical systems. The proof of Theorems will be completed in Section 7.3. In Section 7.4, we consider the case that $p \in 2\mathbb{N}+1$. Section 7.5 is devoted to the conclusions and remarks.

7.2 Dynamics on the Poincaré disk of (7.1.9) with $p \in 2\mathbb{N}$

In order to study the dynamics of (7.1.9) on the Poincaré disk, we desingularize it by the time-scale desingularization

$$ds/d\xi = \{\phi(\xi)\}^{-p} \quad \text{for} \quad p \in 2\mathbb{N}. \tag{7.2.1}$$

Since we assume that p is even, the direction of the time does not change via this desingularization. Then we have

$$\begin{cases} \phi' = \phi^p\psi, \\ \psi' = -c\psi - \phi^{p+1} + \delta\phi, \end{cases} \quad \left(' = \frac{d}{ds}\right), \tag{7.2.2}$$

where $\delta = 0$ or $\delta = 1$.

It should be noted that the time scale desingularization (7.2.1) is simply multiplying the vector field by ϕ^p. Then, except the singularity $\{\phi = 0\}$, the solution curves of the system (vector field) remain the same but are parameterized differently. Still, we refer to Section 7.7 of [44] and references therein for the analytical treatments of desingularization with the time rescaling. In what follows, we use the similar time rescaling (re-parameterization of the solution curves) repeatedly to desingularize the vector fields.

The system (7.2.2) has the equilibrium $E_O : (\phi, \psi) = (0, 0)$ for $\delta = 0$. Also, it has the equilibria E_O and E_δ for $\delta = 1$. We will determine the stability of E_δ in Section 3.7. We study the stability of E_O. The behavior of solutions for $\delta = 0$ and $\delta = 1$ are different.

7.2.1 Dynamics of (7.2.2) near $(0, 0)$: the case $\delta = 0$

When the parameter δ is $\delta = 0$, the Jacobian matrix of the vector field (7.2.2) at E_O is

$$E_O : \begin{pmatrix} 0 & 0 \\ 0 & -c \end{pmatrix}.$$

Then, the center manifold theory is applicable to study the dynamics near E_O (for instance, see [9]). It implies that there exists a function $h(\phi)$ satisfying

$$h(0) = \frac{dh}{d\phi}(0) = 0$$

such that the center manifold of (7.2.2) is represented as $\{(\phi, \psi) \,|\, \psi = h(\phi)\}$ near $(0, 0)$. Differentiating it with respect to s, we have

$$-ch(\phi) - \phi^{p+1} = \frac{dh}{d\phi} \cdot \phi^p h(\phi).$$

Then, we can obtain the approximation of the (graph of) center manifold as follows:

$$\left\{(\phi, \psi) \,|\, \psi = -\phi^{p+1}/c + O(\phi^{3p+1})\right\}. \tag{7.2.3}$$

Therefore, the dynamics of (7.2.2) near $(0, 0)$ is topologically equivalent to the dynamics of the following equation:

$$\phi' = -\phi^{2p+1}/c + O(\phi^{4p+1}). \tag{7.2.4}$$

These results give us the dynamics of (7.2.2) near $(0, 0)$ for $\delta = 0$.

7.2.2 Dynamics of (7.2.2) near $(0, 0)$: the case $\delta = 1$

When the parameter δ is $\delta = 1$, the Jacobian matrix of the vector field (7.2.2) at E_O is

$$E_O : \begin{pmatrix} 0 & 0 \\ 1 & -c \end{pmatrix}.$$

It has the real distinct eigenvalues 0 and $-c$. The eigenvectors corresponding to each eigenvalue are

$$\mathbf{v}_1 = \begin{pmatrix} c \\ 1 \end{pmatrix}, \quad \mathbf{v}_2 = \begin{pmatrix} 0 \\ 1 \end{pmatrix}.$$

We set matrix T as $T = (\mathbf{v}_1, \mathbf{v}_2)$. Then, we can obtain the following:

$$\begin{aligned}\begin{pmatrix} \phi'(s) \\ \psi'(s) \end{pmatrix} &= \begin{pmatrix} 0 & 0 \\ 1 & -c \end{pmatrix} \begin{pmatrix} \phi(s) \\ \psi(s) \end{pmatrix} + \begin{pmatrix} \phi^p\psi \\ -\phi^{p+1} \end{pmatrix} \\ &= T \begin{pmatrix} 0 & 0 \\ 0 & -c \end{pmatrix} T^{-1} \begin{pmatrix} \phi(s) \\ \psi(s) \end{pmatrix} + \begin{pmatrix} \phi^p\psi \\ -\phi^{p+1} \end{pmatrix}.\end{aligned}$$

By multiplying T^{-1} to both sides from left,

$$T^{-1} \begin{pmatrix} \phi'(s) \\ \psi'(s) \end{pmatrix} = \begin{pmatrix} 0 & 0 \\ 0 & -c \end{pmatrix} T^{-1} \begin{pmatrix} \phi(s) \\ \psi(s) \end{pmatrix} + T^{-1} \begin{pmatrix} \phi^p\psi \\ -\phi^{p+1} \end{pmatrix}. \tag{7.2.5}$$

We set $\begin{pmatrix} \tilde{\phi}(s) \\ \tilde{\psi}(s) \end{pmatrix} = T^{-1} \begin{pmatrix} \phi(s) \\ \psi(s) \end{pmatrix}$. Then, we can see the following equations:

$$\phi^p\psi = c^p\tilde{\phi}^{p+1} + c^p\tilde{\phi}^p\tilde{\psi}, \quad -\phi^{p+1} = -c^{p+1}\tilde{\phi}^{p+1}.$$

Therefore, the equation (7.2.5) is

$$\frac{d}{ds} \begin{pmatrix} \tilde{\phi}(s) \\ \tilde{\psi}(s) \end{pmatrix} = \begin{pmatrix} 0 & 0 \\ 0 & -c \end{pmatrix} \begin{pmatrix} \tilde{\phi}(s) \\ \tilde{\psi}(s) \end{pmatrix} + \begin{pmatrix} c^{p-1}\tilde{\phi}^{p+1} + c^{p-1}\tilde{\phi}^p\tilde{\psi} \\ -c^{p-1}\tilde{\phi}^{p+1} - c^{p-1}\tilde{\phi}^p\tilde{\psi} - c^{p+1}\tilde{\phi}^{p+1} \end{pmatrix},$$

namely,

$$\begin{cases} \tilde{\phi}'(s) = c^{p-1}\tilde{\phi}^{p+1} + c^{p-1}\tilde{\phi}^p\tilde{\psi}, \\ \tilde{\psi}'(s) = -c\tilde{\psi} - c^{p-1}\tilde{\phi}^{p+1} - c^{p-1}\tilde{\phi}^p\tilde{\psi} - c^{p+1}\tilde{\phi}^{p+1}, \end{cases} \qquad \left(\ ' \ = \frac{d}{ds} \right). \tag{7.2.6}$$

As in the case that $\delta = 0$, the center manifold theory is applicable to study the dynamics of (7.2.6). It implies that there exists a function $h(\tilde{\phi})$ satisfying

$$h(0) = \frac{dh}{d\tilde{\phi}}(0) = 0$$

such that the center manifold of (7.2.6) is represented as $\{(\tilde{\phi}, \tilde{\psi}) \,|\, \tilde{\psi}(s) = h(\tilde{\phi}(s))\}$ near $(0, 0)$. Differentiating it with respect to s, we have

$$-ch(\tilde{\phi}) - c^{p-1}\tilde{\phi}^{p+1} - c^{p-1}\tilde{\phi}^p h(\tilde{\phi}) - c^{p+1}\tilde{\phi}^{p+1} = \frac{dh}{d\tilde{\phi}} \left(c^{p-1}\tilde{\phi}^{p+1} + c^{p-1}\tilde{\phi}^p h(\tilde{\phi}) \right).$$

Then, we can obtain the approximation of the (graph of) center manifold as follows:

$$\left\{ (\tilde{\phi}, \tilde{\psi}) \,|\, \tilde{\psi}(s) = -c^{p-2}(c^2+1)\tilde{\phi}(s)^{p+1} + O(\tilde{\phi}^{p+2}) \right\}. \tag{7.2.7}$$

Therefore, the dynamics of (7.2.6) near $(0, 0)$ is topologically equivalent to the dynamics of the following equation:

$$\tilde{\phi}'(s) = c^{p-1}\tilde{\phi}^{p+1} - c^{2p-3}(c^2+1)\tilde{\phi}^{2p+1}.$$

Note that $\tilde{\phi}$ and $\tilde{\psi}$ are $\tilde{\phi} = \phi/c$, $\tilde{\psi} = \psi - \phi/c$. We conclude that the approximation of the (graph of) center manifold are

$$\psi(s) = \phi/c - [(c^2+1)\phi^{p+1}]/c^3 \tag{7.2.8}$$

and the dynamics of (7.2.2) near $(0, 0)$ is topologically equivalent to the dynamics of the following equation:

$$\phi'(s) = \phi^{p+1}/c - [(c^2+1)\phi^{2p+1}]/c^3. \tag{7.2.9}$$

These results give us the dynamics of (7.2.2) near $(0, 0)$ for $\delta = 1$. Now we can consider the dynamics of (7.2.2) on the charts $\overline{U}_j$ and $\overline{V}_j$.

7.2.3 Dynamics on the chart $\overline{U}_2$

To obtain the dynamics on the chart $\overline{U}_2$, we introduce coordinates (λ, x) by the formulas

$$\phi(s) = x(s)/\lambda(s), \quad \psi(s) = 1/\lambda(s).$$

Then we have

$$\begin{cases} \lambda' = c\lambda + \lambda^{1-p}x^{p+1} - \delta\lambda x, \\ x' = \lambda^{-p}x^p + cx + \lambda^{-p}x^{p+2} - \delta x^2. \end{cases}$$

Time-scale desingularization $d\sigma/ds = \lambda(s)^{-p}$ yields

$$\begin{cases} \lambda_\sigma = c\lambda^{p+1} + \lambda x^{p+1} - \delta\lambda^{p+1}x, \\ x_\sigma = x^p + c\lambda^p x + x^{p+2} - \delta\lambda^p x^2, \end{cases} \tag{7.2.10}$$

where $\lambda_\sigma = d\lambda/d\sigma$ and $x_\sigma = dx/d\sigma$. The system (7.2.10) has the equilibrium

$$E_0^+ : (\lambda, x) = (0, 0).$$

The Jacobian matrix of the vector field (7.2.10) at its equilibrium is

$$E_0^+ : \begin{pmatrix} 0 & 0 \\ 0 & 0 \end{pmatrix}.$$

The equilibrium E_0^+ is not hyperbolic. Therefore, to determine the dynamics near E_0^+, we desingularize it by introducing the following blow-up coordinates:

$$\lambda = r^{p-1}\bar{\lambda}, \quad x = r^p\bar{x}$$

(see Section 1.2 in this thesis and Section 3 of [14] for the desingularizations of vector fields by the blow-up). Since we are interested in the dynamics on the Poincaré disk, we consider the dynamics of blow-up vector fields on the charts $\{\bar{\lambda} = 1\}$ and $\{\bar{x} = \pm 1\}$.

Dynamics on the chart $\{\bar{\lambda} = 1\}$

By the change of coordinates $\lambda = r^{p-1}$, $x = r^p\bar{x}$, we have

$$\begin{cases} r_\sigma = (p-1)^{-1}(cr^{p^2-p+1} + r^{p^2+p+1}\bar{x}^{p+1} - \delta r^{p^2+1}\bar{x}), \\ \bar{x}_\sigma = (p-1)^{-1}(-cr^{p^2-p}\bar{x} - r^{p^2+p}\bar{x}^{p+2} + \delta r^{p^2}\bar{x}^2) + r^{p^2-p}\bar{x}^p. \end{cases}$$

The time-rescaling $d\eta/d\sigma = r^{p^2-p}$ yields

$$\begin{cases} r_\eta = (p-1)^{-1}(cr + r^{2p+1}\bar{x}^{p+1} - \delta r^{p+1}\bar{x}), \\ \bar{x}_\eta = (p-1)^{-1}(-c\bar{x} - r^{2p}\bar{x}^{p+2} + \delta r^p\bar{x}^2) + \bar{x}^p. \end{cases} \tag{7.2.11}$$

The equilibria of (7.2.11) on $\{r = 0\}$ are

$$\overline{E}_0^+ : (r, \bar{x}) = (0, 0), \quad \overline{E}_p^+ : (0, [c/(p-1)]^{\frac{1}{p-1}}).$$

The Jacobian matrices of the vector field (7.2.11) at these equilibria are

$$\overline{E}_0^+ : \begin{pmatrix} \dfrac{c}{p-1} & 0 \\ 0 & -\dfrac{c}{p-1} \end{pmatrix}, \quad \overline{E}_p^+ : \begin{pmatrix} \dfrac{c}{p-1} & 0 \\ 0 & c \end{pmatrix}.$$

Therefore, $\overline{E}_0^+$ is a saddle, and $\overline{E}_p^+$ is a source for $c > 0$.

The solutions are approximated as

$$\begin{cases} r(\eta) \sim A_1 e^{\frac{c}{p-1}\eta}(1 + o(1)), \\ \bar{x}(\eta) - P \sim A_2 e^{c\eta}(1 + o(1)), \end{cases} \qquad P := \left(\frac{c}{p-1}\right)^{\frac{1}{p-1}}$$

with constants A_j.

Dynamics on the chart $\{\bar{x} = 1\}$

By the change of coordinates $\lambda = r^{p-1}\bar{\lambda}$, $x = r^p$, and time-rescaling $d\eta/d\sigma = r^{p^2-p}$, we have

$$\begin{cases} r_\eta = p^{-1}(r + cr\bar{\lambda}^p + r^{2p+1} - \delta r^{p+1}\bar{\lambda}^p), \\ \bar{\lambda}_\eta = p^{-1}\{-(p-1)\bar{\lambda} + c\bar{\lambda}^{p+1} + r^{2p}\bar{\lambda} - \delta r^p\bar{\lambda}^{p+1}\}. \end{cases}$$

The equilibria on $\{r = 0\}$ are

$$(r, \bar{\lambda}) = (0, 0), \quad (r, \bar{\lambda}) = (0, [p - 1/c]^{\frac{1}{p}}).$$

By the further computations, we can see that $(0, 0)$ is a saddle, and $(0, [p - 1/c]^{\frac{1}{p}})$ is a source.

Dynamics on the chart $\{\bar{x} = -1\}$

By the change of coordinates $\lambda = r^{p-1}\bar{\lambda}$, $x = -r^p$, and time-rescaling $d\eta/d\sigma = r^{p^2-p}$, we have

$$\begin{cases} r_\eta = p^{-1}(-r + cr\bar{\lambda}^p - r^{2p+1} + \delta r^{p+1}\bar{\lambda}^p), \\ \bar{\lambda}_\eta = p^{-1}\{(p-1)\bar{\lambda} + c\bar{\lambda}^{p+1} - r^{2p}\bar{\lambda} + \delta r^p\bar{\lambda}^{p+1}\}. \end{cases}$$

The equilibrium on $\{r = 0, \bar{\lambda} \geq 0\}$ is $(0, 0)$. The linearized eigenvalues are $-p^{-1}$ and $(p-1)/p$ with corresponding eigenvectors $(1, 0)$ and $(0, 1)$, respectively. Therefore, $(r, \bar{\lambda}) = (0, 0)$ on the chart $\{\bar{x} = -1\}$ is a saddle.

Combining the dynamics on the charts $\{\bar{\lambda} = 1\}$ and $\{\bar{x} = \pm 1\}$, we obtain the dynamics on $\overline{U}_2$ (see Figure 7.2.1).

7.2.4 Dynamics on the chart $\overline{V}_2$

The change of coordinates

$$\phi(s) = -x(s)/\lambda(s), \quad \psi(s) = -1/\lambda(s)$$

gives the projected dynamics of (7.2.2) on the chart $\overline{V}_2$:

$$\begin{cases} \lambda_\sigma = c\lambda^{p+1} + \lambda x^{p+1} - \delta\lambda^{p+1}x, \\ x_\sigma = x^p + c\lambda^p x + x^{p+2} - \delta\lambda^p x^2, \end{cases} \tag{7.2.12}$$

where σ is the new time introduced by $d\sigma/ds = \lambda(s)^{-p}$. We can see that the system (7.2.12) and (7.2.10) are same.

7.2.5 Dynamics on the chart $\overline{U}_1$

Let us study the dynamics on the chart $\overline{U}_1$. The transformations

$$\phi(s) = 1/\lambda(s), \quad \psi(s) = x(s)/\lambda(s)$$

yield

$$\begin{cases} \lambda_\sigma = -\lambda x, \\ x_\sigma = -c\lambda^p x + \delta\lambda^p - 1 - x^2 \end{cases} \tag{7.2.13}$$

via time-rescaling $d\sigma/ds = \lambda(s)^{-p}$. When the parameter δ is $\delta = 0$, the system (7.2.13) has no equilibria. If $\delta = 1$, then the equilibrium of (7.2.13) is $(\lambda, x) = (1, 0)$ that coincides with the equilibrium $(\phi, \psi) = (1, 0)$ of (7.1.9).

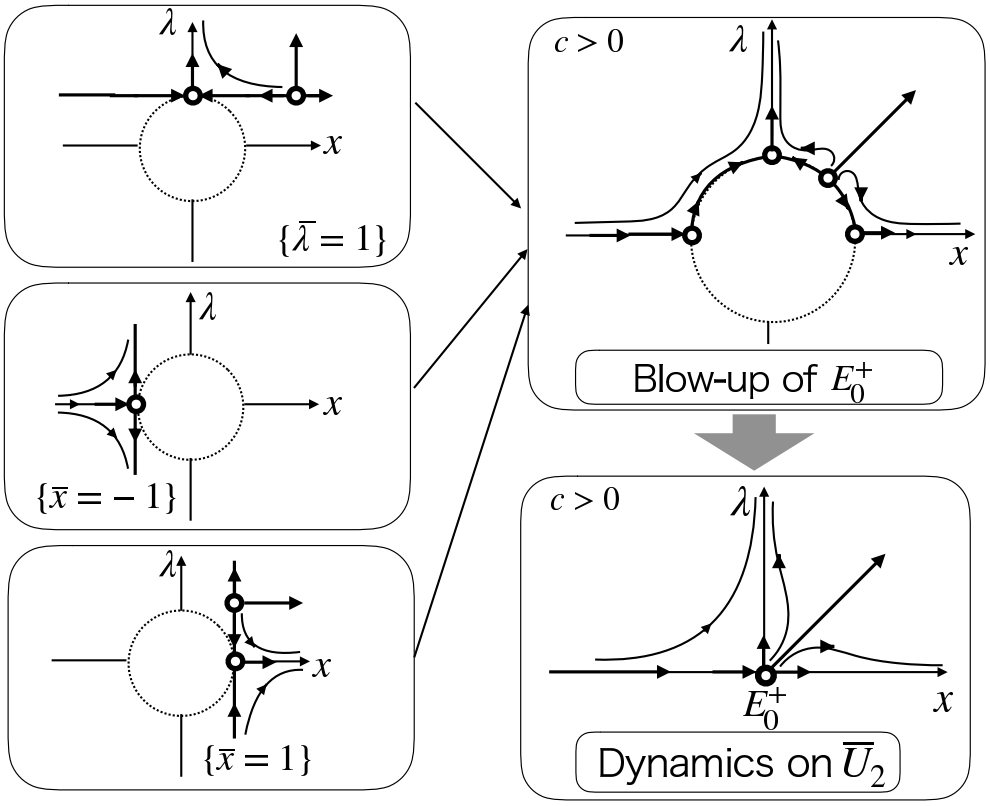

Figure 7.2.1: Schematic pictures of the dynamics of the blow-up vector fields and $\overline{U}_2$ in the case that $c > 0$ and $p \in 2\mathbb{N}$.

7.2.6 Dynamics on the chart $\overline{V}_1$

The transformations

$$\phi(s) = -1/\lambda(s), \quad \psi(s) = -x(s)/\lambda(s)$$

yield

$$\begin{cases} \lambda_\sigma = -\lambda x, \\ x_\sigma = -c\lambda^p x + \delta\lambda^p - 1 - x^2 \end{cases} \tag{7.2.14}$$

via time-rescaling $d\sigma/ds = \lambda(s)^{-p}$. We can see that the system (7.2.14) can be coincided with (7.2.13).

7.2.7 Dynamics on the Poincaré disk

In order to see the dynamics on the Poincaré disk, we study the dynamics near finite-equilibria of (7.1.9). If $\delta = 1$ and p is even , then (7.1.9) has the equilibria $\pm E_\delta : (\phi, \psi) = (\pm 1, 0)$. Let J_1 be the Jacobian matrix of the vector field (7.1.9) at E_δ. Then, the behavior of the solution around E_δ is different by the sign of D (which is defined in Theorem 7.1.2). For instance, the matrix J_1 has the real distinct eigenvalues if $D > 0$ and other cases can be concluded similarly. In addition, if $c > 0$, then the real part of all eigenvalues of J_1 are negative. Therefore, we determine that the the equilibria $\pm E_\delta : (\phi, \psi) = (\pm 1, 0)$ are sink.

Combining dynamics on the chart $\overline{U}_j$ and $\overline{V}_j$, we obtain the dynamics on the Poincaré disk in the case that p is even (see Figure 7.2.2). If the E_δ is asymptotically stable, then E_δ is a stable node for $D \geq 0$ and is a stable focus (spiral sink) for $D < 0$.

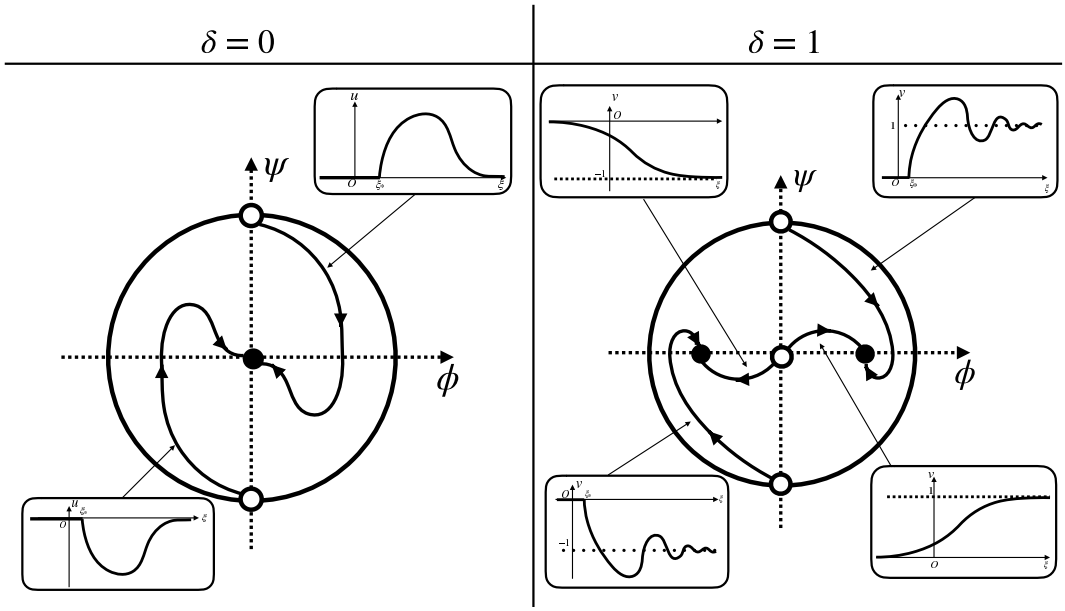

Figure 7.2.2: Schematic picture of the dynamics on the Poincaré disk and corresponding (weak) traveling wave solutions in the case that p is even with $D < 0$ and $c > 0$.

Remark 7.2.1
In Figure7.2.2, we need to be careful about the handling of the point $E_O : (\phi, \psi) = (0, 0)$ for $\delta = 0$ and $\delta = 1$. When we consider the parameter s on the disk, the point E_O is the equilibrium of (7.2.2)*. However, E_O is a point on the line $\{\phi = 0\}$ with singularity about the parameter ξ. We can see that $d\phi/d\psi$ takes the same values on the vector fields defined by* (7.2.2) *and* (7.1.9) *by excepting the singularity $\{\phi = 0\}$. If the trajectories start (resp. come in) the equilibrium E_O about the parameter s, then they start from (resp. come in) the point E_O about ξ.*

7.3 Proof of the Theorems

In this section, we prove our main results. If the initial data are located on $H_+ \backslash \{\phi = 0\}$, the existence of the solutions follows from the standard theory for the ordinary differential equations. Therefore, we consider the existence of the trajectories that connect equilibria and the detailed dynamics near the equilibria on the Poincaré disk and their asymptotic behavior.

Proof of Theorem 7.1.1

Since the point $(y_1, y_2, y_3) = (0, 1, 0)$ on the Poincaré disk corresponds to $E_0^+ : (\phi, \psi) = (0, +\infty)$, we denote it by E_0^+ as well. Similarly, we denote $(y_1, y_2, y_3) = (0, 0, 1)$ by E_O, which corresponds to the equilibrium $(\phi, \psi) = (0, 0)$.

First, we prove the existence of connecting orbit between E_0^+ and E_O on the Poincaré disk (see Figure 7.2.2).

For a given compact subset $W \subset H_+$, there are no equilibrium or closed orbit in W. Therefore, by the Poincaré-Bendixson theorem, any trajectories starting from the points in W cannot stay in W with increasing s. This implies that the trajectories in H_+ go to $E_O : (\phi, \psi) = (0, 0)$ from $\mathbb{S}^1$, which corresponds to $\{\|(\phi, \psi)\| = \infty\}$. Since the line $\{\phi = 0\}$

is invariant under the flow of (7.2.2), therefore, any trajectories start from the points in $\{y \in H_+ \,|\, y_1 > 0\}$ cannot go to $\{y \in H_+ \,|\, y_1 < 0\}$.

Then, let $\overline{\mathcal{W}}^u(\overline{E}_p^+)$ be a unstable manifold of $\overline{E}_p^+$ (which is the equilibrium of the system (7.2.11)). We denote by $\mathcal{W}^u(\overline{E}_p^+)$ the unstable set, which corresponds to $\overline{\mathcal{W}}^u(\overline{E}_p^+)$ on the blow-up vector filed (7.2.11) of the equilibrium E_0^+ of (7.2.10). Similarly, we denote by $\mathcal{W}^c(E_O)$ the stable set of E_O, corresponding to the stable center manifold of E_O on the blow-up vector field (7.2.2).

Consider the trajectories start from the points on $\mathcal{W}^u(\overline{E}_p^+) \subset \{y \in H_+ \,|\, y_1 > 0\}$. The trajectories cannot stay in any compact subset on H_+, and cannot go to $\{y \in H_+ \,|\, y_1 < 0\}$, therefore, they go to E_O with lying on $\mathcal{W}^c(E_O)$. This implies that the system (7.1.9) and (7.2.2) possess the orbits that connect E_0^+ and E_O on the Poincaré disk. Also we recall Remark 7.2.1. Thus, there are orbits connecting $(\phi, \psi) = (0, +\infty)$ and $(0, 0)$ on the original vector field (7.1.9).

Second, we prove the existence of a constant $\xi_0 \in (\xi_*, +\infty)$. It is sufficient to show the connecting orbits pass through the line $\{\psi = 0\}$. Considering (7.1.9) for $\delta = 0$, $\phi'|_{\psi=0} = 0$ and $\psi'|_{\psi=0} = -\phi$. Note that we focus on $\{y \in H_+ \,|\, y_1 > 0\}$, $\psi'|_{\psi=0}$ satisfies $\psi'|_{\psi=0} < 0$ for $\phi > 0$. Therefore, any trajectories start from the points on $\mathcal{W}^u(\overline{E}_p^+) \subset \{y \in H_+ \,|\, y_1 > 0\}$ must pass $\psi = 0$, and go to E_O with lying on $\mathcal{W}^c(E_O)$.

Finally, we compute the asymptotic behavior of the trajectories near the equilibria E_0^+ and E_O as follows:

(i) As shown in [31] and [33], we can obtain the asymptotic behavior of $u(\xi)$ and $u'(\xi)$ at E_0^+. Indeed,

$$\begin{aligned}
\frac{d\eta}{d\xi} &= \frac{ds}{d\xi} \cdot \frac{d\sigma}{ds} \cdot \frac{d\eta}{d\sigma} = \phi^{-p} \cdot \lambda^{-p} \cdot r^{p^2-p} \\
&= r^{-p} \bar{x}^{-p} \\
&\sim \left(A_1 e^{\frac{c}{p-1}\eta} (1 + o(1)) \right)^{-p} \cdot (A_2 e^{c\eta}(1 + o(1)) + P)^{-p} \\
&\sim A_3 e^{\frac{-pc}{p-1}\eta} \cdot (A_2 e^{c\eta}(1 + o(1)) + P)^{-p} \\
&= A_3 e^{\frac{-pc}{p-1}\eta} \cdot \frac{1}{(A_2 e^{c\eta}(1 + o(1)) + P)^p} \\
&= A_3 e^{\frac{-pc}{p-1}\eta} \cdot \frac{1}{\{A_2 e^{c\eta}(1 + o(1))\}^p + p\{A_2 e^{c\eta}(1 + o(1))\}^{p-1} P + \cdots + P^p} \\
&\sim A e^{\frac{-pc}{p-1}\eta} \quad \text{as} \quad \eta \to -\infty
\end{aligned}$$

holds with constants A and A_j. Note that this argument is a refinement of [33]. Here, " $f(x) \sim g(x)$ as $x \to a$" means that $f(x) - g(x) = o(g(x))$ as $x \to a$, equivalently,

$$\lim_{x \to a} \left| \frac{f(x)}{g(x)} \right| = 1.$$

This yields

$$\xi(\eta) \sim A e^{\frac{pc}{p-1}\eta} + \tilde{A}, \quad (\tilde{A} \in \mathbb{R}).$$

Set $\xi_* = \lim_{\eta \to -\infty} \xi(\eta)$, then we have

$$\xi_* = A \int_{-\infty}^{0} e^{\frac{pc}{p-1}\eta} d\eta < +\infty.$$

Therefore,

$$\xi - \xi_* \sim Ae^{\frac{pc}{p-1}\eta} \quad (\eta \to -\infty)$$

holds. Finally, we obtain

$$\begin{aligned} u(\xi) = \phi(\xi) &= r\bar{x} \\ &\sim \left\{ A_1 e^{\frac{c}{p-1}\eta}(1+o(1)) \right\} \cdot \{A_2 e^{c\eta}(1+o(1)) + P\} \\ &\sim A_4 e^{\frac{c}{p-1}\eta} \cdot \{A_2 e^{c\eta}(1+o(1)) + P\} \\ &= A_5 e^{\frac{c}{p-1}\eta} e^{c\eta} + A_4 \cdot P \cdot e^{\frac{c}{p-1}\eta} \\ &= A_5 e^{\frac{pc}{p-1}\eta} + A_4 \cdot P \cdot e^{\frac{c}{p-1}\eta} \\ &\sim Ae^{\frac{c}{p-1}\eta}. \end{aligned}$$

Here, in last relation, since $e^{\frac{pc}{p-1}\eta} < e^{\frac{c}{p-1}\eta}$ $(\eta < 0)$ is satisfied by $pc/(p-1) > c/(p-1)$, we choose the term with the greater influence when $\eta \to -\infty$. Therefore, we have

$$u(\xi) = \phi(\xi) \sim Ae^{\frac{c}{p-1}\eta} \sim A(\xi - \xi_*)^{\frac{1}{p}} \quad (\xi \to \xi_* + 0).$$

Since the trajectories are lying on $\{\phi > 0\}$, it holds that $A > 0$.

Similarly, we can obtain the rate for $u'(\xi) = c^2\psi(\xi)$ as $\xi \to \xi_*$.

(ii) If the initial value is on the center manifold, the solution at the around E_O on Poincaré disk has the form

$$\begin{cases} \phi(s) = \sqrt[2p]{\dfrac{1}{\frac{2}{c}ps - 2p\tilde{A}}}, \\ \psi(s) = -\dfrac{1}{c}\left(\dfrac{1}{\frac{2}{c}ps - 2p\tilde{A}}\right)^{\frac{p+1}{2p}}. \end{cases} \tag{7.3.1}$$

Since the initial value $\phi(0)$ is located on $\{\phi > 0\}$, it holds that $\tilde{A} < 0$. These results follow from (7.2.3) and (7.2.4). We then have

$$\frac{ds}{d\xi} = \phi^{-p} = \left(\frac{2p}{c}s(\xi) - 2p\tilde{A}\right)^{\frac{1}{2}}.$$

Therefore, there exists a solution $s(\xi)$ such that the following holds

$$s(\xi) = \frac{p\xi^2 + 2Bp\xi + 2\tilde{A}c^2 + B^2p}{2c} \tag{7.3.2}$$

with a constant B. Substituting (7.3.2) into (7.3.1), we have

$$\begin{cases} \phi(\xi) \sim (p\xi/c)^{-\frac{1}{p}} \\ \psi(\xi) \sim \left[-(p\xi/c)^{-\frac{p+1}{p}} \right] /c \end{cases} \quad \text{as} \quad \xi \to +\infty.$$

Therefore, we can obtain the asymptotic behavior (7.1.10) and (7.1.11). We then obtain the weak traveling wave solutions with quenching that consist of the functions $u(x-ct) = \phi(\xi)$ on (ξ_*, ∞) and $u(x-ct) = 0$ on $(-\infty, \xi_*]$ (see Figure 7.1.1).

This completes the proof. □

Proof of Theorem 7.1.2

As in the previous proof of Theorem 7.1.1, it is necessary to find the orbits that connect E_0^+ and E_δ on the Poincaré disk (see Figure 7.2.2). We note that the flow on $\{(\phi,\psi) \in H_+ \cup \mathbb{S}^2 \,|\, \phi > 0\}$ and $\{(\phi,\psi) \in H_+ \cup \mathbb{S}^2 \,|\, \phi < 0\}$ are separated by the line $\{\phi = 0\}$. In other words, any trajectories start from the point on the unstable manifold $\mathcal{W}^u(\overline{E}_p^+)$ of $\overline{E}_p^+$ which corresponds the equilibrium E_0^+ of (7.2.10) cannot go to $\{(\phi,\psi) \in H_+ \cup \mathbb{S}^2 \,|\, \phi < 0\}$ in the case that $\delta = 1$. Since E_O is unstable, any trajectories start from the point on $\mathcal{W}^u(\overline{E}_p^+)$ must go to the equilibrium E_δ. Then it holds that there exist the connecting orbits from E_0^+ to E_δ.

As in the proof of Theorem 7.1.1, we can obtain the rates (7.1.14) for $v(\xi)$ and $v'(\xi)$ as $\xi \to \xi_*$ in the case that $p \in 2\mathbb{N}$, therefore, we only consider the dynamics near E_δ. We define

$$\Phi(\xi) := \phi(\xi) - 1 \quad \text{and} \quad \Psi(\xi) := \psi(\xi).$$

Then, there are three cases to consider:

(i) Let us consider the case that $D > 0$, namely, the matrix J_1 has the real distinct eigenvalues

$$\omega_1 = \frac{-c + \sqrt{D}}{2}, \quad \omega_2 = \frac{-c - \sqrt{D}}{2}.$$

The eigenvectors corresponding to each eigenvalue are

$$\mathbf{v}_1 = \begin{pmatrix} 1 \\ \omega_1 \end{pmatrix}, \quad \mathbf{v}_2 = \begin{pmatrix} 1 \\ \omega_2 \end{pmatrix}.$$

We then obtain the following behavior:

$$\begin{pmatrix} \Phi(\xi) \\ \Psi(\xi) \end{pmatrix} = B_1 \begin{pmatrix} 1 \\ \omega_1 \end{pmatrix} e^{\omega_1 \xi} + B_2 \begin{pmatrix} 1 \\ \omega_2 \end{pmatrix} e^{\omega_2 \xi}$$

with any constants B_1 and B_2. Therefore, the solution around the equilibrium E_δ is

$$\begin{cases} \phi(\xi) \sim B_1 e^{\omega_1 \xi} + B_2 e^{\omega_2 \xi} + 1, \\ \psi(\xi) \sim B_1 \omega_1 e^{\omega_1 \xi} + B_2 \omega_2 e^{\omega_2 \xi}. \end{cases}$$

Using $v(\xi) = \phi(\xi)$ and $v'(\xi) = c^2 \psi$, we can derive the following:

$$\begin{cases} v(\xi) \sim B_1 e^{\omega_1 \xi} + B_2 e^{\omega_2 \xi} + 1, \\ v'(\xi) \sim c^2 (B_1 \omega_1 e^{\omega_1 \xi} + B_2 \omega_2 e^{\omega_2 \xi}). \end{cases}$$

Since $c > 0$, it hold that $\omega_1 < 0$ and $\omega_2 < 0$.

(ii) Consider the case that $D = 0$, namely, the matrix J_1 has a multiple real eigenvalue $\omega = -\dfrac{c}{2}$. The eigenvector $\mathbf{v}_1$ and the generalized eigenvector corresponding to the eigenvalue $\mathbf{v}_2$ are

$$\mathbf{v}_1 = \begin{pmatrix} 1 \\ -\dfrac{c}{2} \end{pmatrix}, \quad \mathbf{v}_2 = \begin{pmatrix} \alpha \\ 1 - \dfrac{c}{2}\alpha \end{pmatrix}$$

with α is arbitrary constant. Therefore, the solution around the equilibrium E_δ is

$$\begin{cases} \phi(\xi) \sim (B_3 \xi + B_4) e^{\omega \xi} + 1, \\ \psi(\xi) \sim -\dfrac{c}{2}(B_3 \xi + B_4) e^{\omega \xi} + B_3 \left(1 - \dfrac{c}{2}\alpha\right) e^{\omega \xi}. \end{cases}$$

Then, we can derive the following:

$$\begin{cases} v(\xi) \sim (B_3\xi + B_4)e^{\omega\xi} + 1, \\ v'(\xi) \sim c^2 \left\{ -\frac{c}{2}(B_3\xi + B_4)e^{\omega\xi} + B_3 \left(1 - \frac{c}{2}\alpha\right) e^{\omega\xi} \right\}. \end{cases}$$

Since $c > 0$, it holds that $\omega < 0$. Note that we can determine

$$\lim_{\xi \to +\infty} (B_3\xi + B_4)e^{\omega\xi} = 0$$

by the L'Hôpital's rule.

(iii) Consider the case that $D < 0$, namely, the matrix J_1 has the complex eigenvalues $\omega = \mu \pm i\nu = -\frac{c}{2} \pm i\frac{1}{2}\sqrt{|D|}$. The eigenvectors corresponding to each eigenvalue are

$$\mathbf{v} = \begin{pmatrix} 1 \\ -\frac{c}{2} \end{pmatrix} \pm i \begin{pmatrix} 0 \\ \frac{1}{2}\sqrt{|D|} \end{pmatrix}.$$

The function $\Phi(\xi)$ and $\Psi(\xi)$ are expressed as following:

$$\begin{pmatrix} \Phi(\xi) \\ \Psi(\xi) \end{pmatrix} = z(\xi) \begin{pmatrix} 0 \\ \frac{1}{2}\sqrt{|D|} \end{pmatrix} + w(\xi) \begin{pmatrix} 1 \\ -\frac{c}{2} \end{pmatrix},$$

where

$$\begin{pmatrix} z(\xi) \\ w(\xi) \end{pmatrix} = e^{\mu\xi} \begin{pmatrix} \cos\nu\xi & -\sin\nu\xi \\ \sin\nu\xi & \cos\nu\xi \end{pmatrix} \begin{pmatrix} z(0) \\ w(0) \end{pmatrix}.$$

Therefore, the solution $\phi(\xi)$ around the equilibrium E_δ is

$$\phi(\xi) = e^{-\frac{c}{2}\xi} \left([\sin \frac{\sqrt{|D|}}{2}\xi] \cdot z(0) + [\cos \frac{\sqrt{|D|}}{2}\xi] \cdot w(0) \right) + 1.$$

Similarly, $\psi(\xi)$ is

$$\begin{aligned} \psi(\xi) = \frac{1}{2}\sqrt{|D|} \cdot e^{-\frac{c}{2}\xi} \left([\sin \frac{\sqrt{|D|}}{2}\xi] \cdot z(0) - [\cos \frac{\sqrt{|D|}}{2}\xi] \cdot w(0) \right) \\ - \frac{c}{2} \cdot e^{-\frac{c}{2}\xi} \left([\sin \frac{\sqrt{|D|}}{2}\xi] \cdot z(0) + [\cos \frac{\sqrt{|D|}}{2}\xi] \cdot w(0) \right). \end{aligned}$$

Then, we can derive the following:

$$\begin{cases} v(\xi) \sim e^{-\frac{c}{2}\xi} \left([\sin \frac{\sqrt{|D|}}{2}\xi] \cdot z(0) + [\cos \frac{\sqrt{|D|}}{2}\xi] \cdot w(0) \right) + 1, \\ v_\xi(\xi) \sim \frac{c^2}{2}\sqrt{|D|} \cdot e^{-\frac{c}{2}\xi} \left([\sin \frac{\sqrt{|D|}}{2}\xi] \cdot z(0) - [\cos \frac{\sqrt{|D|}}{2}\xi] \cdot w(0) \right) \\ \qquad -\frac{c^3}{2} \cdot e^{-\frac{c}{2}\xi} \left([\sin \frac{\sqrt{|D|}}{2}\xi] \cdot z(0) + [\cos \frac{\sqrt{|D|}}{2}\xi] \cdot w(0) \right). \end{cases}$$

Therefore, we can obtain the asymptotic behavior (7.1.12), (7.1.13), (7.1.14). We then obtain the weak traveling wave solutions with quenching that consist of the functions $v(x - c\tau) = \phi(\xi)$ on (ξ_*, ∞) and $v(x - c\tau) = 0$ on $(-\infty, \xi_*]$ (see Figure 7.1.1).

This completes the proof. □

Proof of Theorem 7.1.3

As in the previous proofs of Theorem 7.1.1 and 7.1.2, it is necessary to find the orbits that connect E_O and E_δ on the Poincaré disk (see Figure 7.2.2). Note that the point E_O exists on the singularity line $\{\phi = 0\}$ about the parameter ξ. By Remark 7.2.1, the trajectories start from the point on $\mathcal{W}^c(E_O)$ must go to the equilibrium E_δ. Then it holds that there exist the connecting orbits from E_O to E_δ.

To complete the proof, we have to show that

$$\lim_{\xi\to-\infty} v(\xi) = \lim_{\xi\to-\infty} v'(\xi) = 0. \tag{7.3.3}$$

Consider the dynamics near $E_O : (\phi, \psi) = (0, 0)$ with $\delta = 1$ that given by (7.2.9) and (7.2.8). That is, dynamics on the center manifold (7.2.7) is locally topologically equivalent to the dynamics of the following equation:

$$\phi' = \phi^{p+1}/c - [(c^2+1)\phi^{2p+1}]/c^3 + h.o.t.$$

Let us consider the equation up to lower order terms that determine the dynamics near the equilibrium:

$$\phi' = \phi^{p+1}/c.$$

This yields

$$\phi(s) = [-p(A + s/c)]^{-\frac{1}{p}}$$

with a constant A. Then, we have

$$\frac{ds}{d\xi} = \phi^{-p} = -p(A + s/c).$$

This yields

$$s/c + A = Be^{-p\xi/c}.$$

Finally, we have

$$\phi(s) = Ce^{\xi/c}.$$

with a constant C . This yields (7.3.3). □

7.4 Dynamics on the Poincaré disk of (7.1.9) : p is odd

We complete the proof of main Theorems, still, we continue to consider the case that $p \in 2\mathbb{N} + 1$. Similarly as in the even case, we consider the dynamics (7.1.9) near $(0, 0)$ and the dynamics (7.1.9) on the Poincaré disk. We desingularize it by the time-scale desingularization

$$ds/d\xi = \{\phi(\xi)\}^{-p-1}.$$

Then, we have

$$\begin{cases} \phi'(s) = \phi^{p+1}\psi, \\ \psi'(s) = -c\phi\psi - \phi^{p+2} + \delta\phi^2, \end{cases} \qquad \left(\ ' \ = \frac{d}{ds} \right), \tag{7.4.1}$$

where $\delta = 0$ or $\delta = 1$.

As in the previous section, we can consider the dynamics of (7.4.1) on the charts $\overline{U}_j$ and $\overline{V}_j$. Here we note that the flow of (7.4.1) on $\{\phi > 0\}$ is the same to that of (7.1.9) on $\{\phi > 0\}$.

The system (7.4.1) has the equilibrium $E_O : (\phi, \psi) = (0, 0)$ for $\delta = 0$ and $\delta = 1$. The Jacobian matrix of the vector field (7.4.1) at E_O is

$$E_O : \begin{pmatrix} 0 & 0 \\ 0 & 0 \end{pmatrix}.$$

The equilibrium E_O is not hyperbolic. In order to determine the dynamics near E_O, we desingularize it by introducing the following blow-up coordinates. Since the terms of $\delta\phi^2$ is the principal part of (7.4.1), the blow-up coordinates for $\delta = 0$ and $\delta = 1$ are different.

Also, we note that if $\delta = 1$ and p is odd, then (7.1.9) has the equilibrium

$$E_\delta : (\phi, \psi) = (1, 0)$$

and the Jacobian matrix and stability around it are the same as in the even case.

7.4.1 Dynamics of (7.4.1) near $(0, 0)$: the case $\delta = 0$

In order to determine the dynamics near E_O, we desingularize it by introducing the following blow-up coordinates for $\delta = 0$:

$$\phi = \varepsilon\bar{\phi}, \quad \psi = \varepsilon^{p+1}\bar{\psi}.$$

Since we are interested in the dynamics near $(0, 0)$, we consider the dynamics of blow-up vector fields on the charts $\{\bar{\phi} = \pm 1\}$ and $\{\bar{\psi} = \pm 1\}$.

Dynamics on the chart $\{\bar{\phi} = 1\}$

By the change of coordinates $\phi = \varepsilon$, $\psi = \varepsilon^{p+1}\bar{\psi}$ and time-rescaling $d\sigma/ds = \varepsilon$, we have

$$\begin{cases} \varepsilon_\sigma = \varepsilon^{2p+1}\bar{\psi}, \\ \bar{\psi}_\sigma = -(p+1)\varepsilon^{2p}\bar{\psi}^2 - c\bar{\psi} - 1, \end{cases} \tag{7.4.2}$$

where $\varepsilon_\sigma = d\varepsilon/d\sigma$ and $\bar{\psi}_\sigma = d\bar{\psi}/d\sigma$. This system has the equilibrium on $\{\varepsilon = 0\}$

$$\overline{E}_O^+ : (\varepsilon, \bar{\psi}) = \left(0, -\frac{1}{c}\right).$$

The Jacobian matrix of the vector field (7.4.2) at $\overline{E}_O^+$ is

$$\overline{E}_O^+ : \begin{pmatrix} 0 & 0 \\ 0 & -c \end{pmatrix}.$$

In order to apply the center manifold theory, we set

$$\varepsilon(\sigma) = 0 + U(\sigma), \quad \bar{\psi}(\sigma) = -\frac{1}{c} + V(\sigma).$$

Then, we can obtain the following equation:

$$\begin{cases} U_\sigma = -U^{2p+1}/c + U^{2p+1}V, \\ V_\sigma = -[(p+1)U^{2p}/c^2] + [2(p+1)U^{2p}V]/c - (p+1)U^{2p}V^2 - cV. \end{cases} \tag{7.4.3}$$

There exists a function $h(U)$ satisfying

$$h(0) = \frac{dh}{dU}(0) = 0$$

such that the center manifold of (7.4.3) is represented as $\{(U,V)\,|\,V=h(U)\}$ near $(0,0)$. Differentiating it with respect to σ, we have

$$-\frac{p+1}{c^2}U^{2p}+\frac{2(p+1)}{c}U^{2p}h-(p+1)U^{2p}h^2-ch=\frac{dh}{dU}\left(-\frac{1}{c}U^{2p+1}+U^{2p+1}h\right).$$

Then, we can obtain the approximation of the (graph of) center manifold as follows:

$$\left\{(U,V)\,|\,V=-(p+1)U^{2p}/c^3+O(U^{4p})\right\}. \tag{7.4.4}$$

Therefore, the dynamics of (7.4.3) near $(0,0)$ is topologically equivalent to the dynamics of the following equation:

$$U_\sigma=\left(-\frac{1}{c}-\frac{p+1}{c^3}U^{2p}\right)U^{2p+1}+O(U^{6p+1}).$$

Dynamics on the chart $\{\bar{\phi}=-1\}$

By the change of coordinates $\phi=-\varepsilon$, $\psi=\varepsilon^{p+1}\bar{\psi}$ and time-rescaling $d\sigma/ds=\varepsilon$, we have

$$\begin{cases}\varepsilon_\sigma=-\varepsilon^{2p+1}\bar{\psi},\\ \bar{\psi}_\sigma=(p+1)\varepsilon^{2p}\bar{\psi}^2+c\bar{\psi}+1.\end{cases} \tag{7.4.5}$$

This system has the equilibrium on $\{\varepsilon=0\}$

$$\overline{E}_O^-:(\varepsilon,\bar{\psi})=\left(0,-\frac{1}{c}\right).$$

The Jacobian matrix of the vector field (7.4.5) at $\overline{E}_O^-$ is

$$\overline{E}_O^-:\begin{pmatrix}0&0\\0&c\end{pmatrix}.$$

In order to apply the center manifold theory, we set

$$\varepsilon(\sigma)=0+U(\sigma),\quad \bar{\psi}(\sigma)=-\frac{1}{c}+V(\sigma).$$

Then, we can obtain the following equation:

$$\begin{cases}U_\sigma=U^{2p+1}/c-U^{2p+1}V,\\ V_\sigma=[(p+1)U^{2p}/c^2]-[2(p+1)U^{2p}V]/c+(p+1)U^{2p}V^2+cV.\end{cases} \tag{7.4.6}$$

As the previous discussion, we can obtain the approximation of the (graph of) center manifold as follows:

$$\left\{(U,V)\,|\,V=-(p+1)U^{2p}/c^3+O(U^{4p})\right\}.$$

Therefore, the dynamics near $(0,0)$ is topologically equivalent to the dynamics of the following equation:

$$U_\sigma=\left(\frac{1}{c}+\frac{p+1}{c^3}U^{2p}\right)U^{2p+1}+O(U^{6p+1}).$$

Dynamics on the chart $\{\bar{\psi} = 1\}$

By the change of coordinates $\phi = \varepsilon\bar{\phi}$, $\psi = \varepsilon^{p+1}$ and time-rescaling $d\sigma/ds = \varepsilon$, we have

$$\begin{cases} \varepsilon_\sigma = (p+1)^{-1}(-c\varepsilon\bar{\phi} - \varepsilon\bar{\phi}^{p+2}), \\ \bar{\phi}_\sigma = (p+1)^{-1}(c\bar{\phi}^2 + \bar{\phi}^{p+3}) + \varepsilon^{2p}\bar{\phi}^{p+1}. \end{cases}$$

The equilibrium on $\{\varepsilon = 0\}$ is $(0,0)$. The Jacobian matrix of this vector field at its equilibrium is

$$\begin{pmatrix} 0 & 0 \\ 0 & 0 \end{pmatrix}.$$

Therefore, this equilibrium $(\varepsilon, \bar{\phi}) = (0,0)$ is not hyperbolic again. Here we shall not consider more complicated analysis for dynamics near $(\varepsilon, \bar{\phi}) = (0,0)$, however, it will be studied that the asymptotic behavior of the connecting orbits from (or to) E_O in a latter subsection.

Dynamics on the chart $\{\bar{\psi} = -1\}$

By the change of coordinates $\phi = \varepsilon\bar{\phi}$, $\psi = -\varepsilon^{p+1}$ and time-rescaling $d\sigma/ds = \varepsilon$, we have

$$\begin{cases} \varepsilon_\sigma = (p+1)^{-1}(-c\varepsilon\bar{\phi} + \varepsilon\bar{\phi}^{p+2}), \\ \bar{\phi}_\sigma = (p+1)^{-1}(c\bar{\phi}^2 - \bar{\phi}^{p+3}) - \varepsilon^{2p}\bar{\phi}^{p+1}. \end{cases}$$

This system has the equilibria on $\{\varepsilon = 0\}$

$$(\varepsilon, \bar{\phi}) = (0,0), \quad (\varepsilon, \bar{\phi}) = (0, \pm c^{\frac{1}{p+1}}).$$

The Jacobian matrices of this vector field at these equilibria are

$$(0,0) : \begin{pmatrix} 0 & 0 \\ 0 & 0 \end{pmatrix}, \quad (0, \pm c^{\frac{1}{p+1}}) : \begin{pmatrix} 0 & 0 \\ 0 & \mp c^{\frac{p+2}{p+1}} \end{pmatrix}.$$

The dynamics around the equilibria $(0, \pm c^{\frac{1}{p+1}})$ are same as $\overline{E}_O^{\pm}$. As in the previous discussion, we conclude that the dynamics near $(0,0)$ cannot be completely determined.

Combining the dynamics on the charts $\{\bar{\phi} = \pm 1\}$ and $\{\bar{\psi} = \pm 1\}$, we obtain the dynamics near E_O (see Figure 7.4.1).

7.4.2 Dynamics of (7.4.1) near $(0,0)$: the case $\delta = 1$

In order to determine the dynamics near E_O, we desingularize it by introducing the following blow-up coordinates for $\delta = 1$:

$$\phi = \varepsilon\bar{\phi}, \quad \psi = \varepsilon\bar{\psi}.$$

Since we are interested in the dynamics near $(0,0)$, we consider the dynamics of blow-up vector fields on the charts $\{\bar{\phi} = \pm 1\}$ and $\{\bar{\psi} = \pm 1\}$.

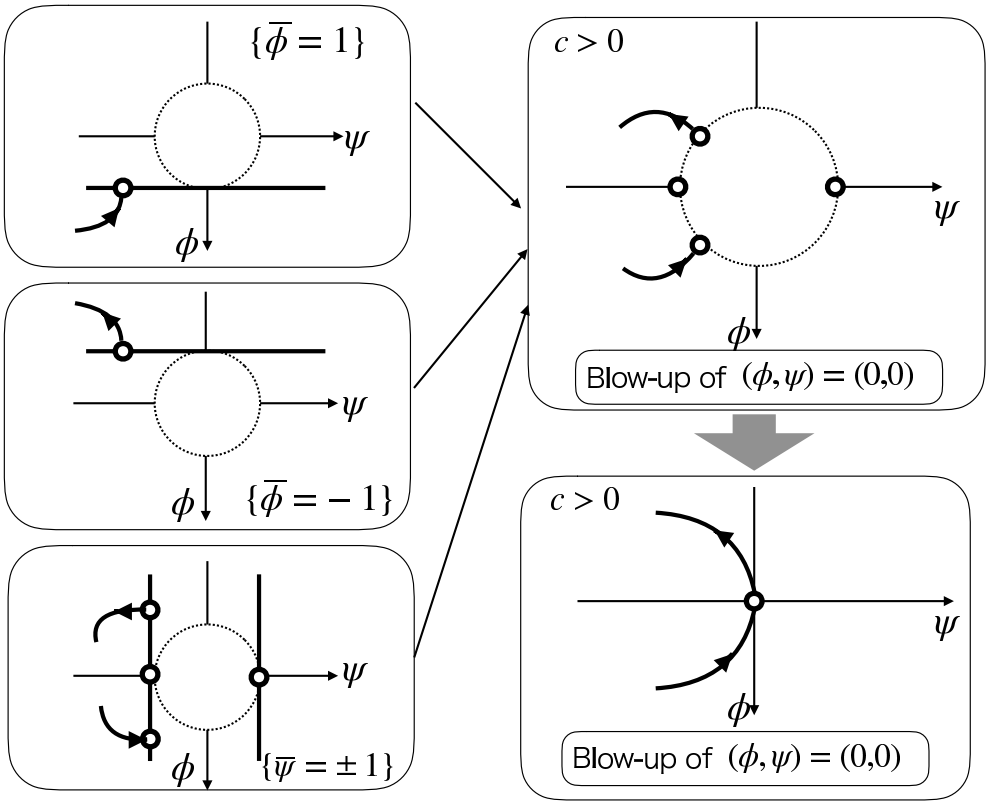

Figure 7.4.1: Schematic pictures of the dynamics near E_O in the case that $c>0$, $\delta=0$ and p is odd.

Dynamics on the chart $\{\bar{\phi}=1\}$

By the change of coordinates $\phi=\varepsilon$, $\psi=\varepsilon\bar{\psi}$ and time-rescaling $d\sigma/ds=\varepsilon$, we have

$$\begin{cases} \varepsilon_\sigma = \varepsilon^{p+1}\bar{\psi}, \\ \bar{\psi}_\sigma = -\varepsilon^p\bar{\psi}^2 - c\bar{\psi} - \varepsilon^p + 1. \end{cases} \tag{7.4.7}$$

This system has the equilibrium on $\{\varepsilon=0\}$

$$\overline{E}^+_{O'} : (\varepsilon,\bar{\psi}) = \left(0, \frac{1}{c}\right).$$

The Jacobian matrix of the vector field (7.4.7) at its equilibrium is

$$\overline{E}^+_{O'} : \begin{pmatrix} 0 & 0 \\ 0 & -c \end{pmatrix}.$$

In order to apply the center manifold theory, we set

$$\varepsilon(\sigma) = 0 + U(\sigma), \quad \bar{\psi}(\sigma) = \frac{1}{c} + V(\sigma).$$

Then, we can obtain the following equation:

$$\begin{cases} U_\sigma = U^{p+1}/c + U^{p+1}V, \\ V_\sigma = -[(c^2+1)U^p/c^2] - [2U^pV]/c - U^pV^2 - cV. \end{cases} \tag{7.4.8}$$

There exists a function $h(U)$ satisfying

$$h(0) = \frac{dh}{dU}(0) = 0$$

such that the center manifold of (7.4.8) is represented as $\{(U,V) \,|\, V = h(U)\}$ near $(0,0)$. Differentiating it with respect to σ, we have

$$-\frac{c^2+1}{c^2}U^p - \frac{2}{c}U^p h - U^p h^2 - ch = \frac{dh}{dU}\left(\frac{1}{c}U^{p+1} + U^{p+1}h\right).$$

Then, we can obtain the approximation of the (graph of) center manifold as follows:

$$\left\{(U,V) \,|\, V = -(c^2+1)U^p/c^3 + O(U^{2p})\right\}. \tag{7.4.9}$$

Therefore, the dynamics of (7.4.8) near $(0,0)$ is topologically equivalent to the dynamics of the following equation:

$$U_\sigma = \left(\frac{1}{c} - \frac{c^2+1}{c^3}U^p\right)U^{p+1} + O(U^{3p+1}).$$

Dynamics on the chart $\{\bar{\phi} = -1\}$

By the change of coordinates $\phi = -\varepsilon$, $\psi = \varepsilon\bar{\psi}$ and time-rescaling $d\sigma/ds = \varepsilon$, we have

$$\begin{cases} \varepsilon_\sigma = -\varepsilon^{p+1}\bar{\psi}, \\ \bar{\psi}_\sigma = \varepsilon^p\bar{\psi}^2 + c\bar{\psi} + \varepsilon^p + 1. \end{cases} \tag{7.4.10}$$

This system has the equilibrium on $\{\varepsilon = 0\}$

$$\overline{E}^-_{O'} : (\varepsilon, \bar{\psi}) = \left(0, -\frac{1}{c}\right).$$

The Jacobian matrix of the vector field (7.4.10) at $\overline{E}^-_{O'}$ is

$$\overline{E}^-_{O'} : \begin{pmatrix} 0 & 0 \\ 0 & c \end{pmatrix}.$$

In order to apply the center manifold theory, we set

$$\varepsilon(\sigma) = 0 + U(\sigma), \quad \bar{\psi}(\sigma) = -\frac{1}{c} + V(\sigma).$$

Then, we can obtain the following equation:

$$\begin{cases} U_\sigma = U^{p+1}/c - U^{p+1}V, \\ V_\sigma = [(c^2+1)U^{2p}/c^2] - [2U^pV]/c + U^pV^2 + cV. \end{cases}$$

As the previous discussion, we can obtain the approximation of the (graph of) center manifold as follows:

$$\left\{(U,V) \,|\, V = -(c^2+1)U^p/c^3 + O(U^{2p})\right\}.$$

Therefore, the dynamics near $(0,0)$ is topologically equivalent to the dynamics of the following equation:

$$U_\sigma = \left(\frac{1}{c} + \frac{c^2+1}{c^3}U^p\right)U^{p+1} + O(U^{3p+1}).$$

Dynamics on the chart $\{\bar{\psi} = 1\}$

By the change of coordinates $\phi = \varepsilon\bar{\phi}$, $\psi = \varepsilon$ and time-rescaling $d\sigma/ds = \varepsilon$, we have

$$\begin{cases} \varepsilon_\sigma = -c\varepsilon\bar{\phi} - \varepsilon^{p+1}\bar{\phi}^{p+2} + \varepsilon\bar{\phi}^2, \\ \bar{\phi}_\sigma = c\bar{\phi}^2 + \varepsilon^p\bar{\phi}^{p+3} - \bar{\phi}^3 + \varepsilon^p\bar{\phi}^{p+1}. \end{cases}$$

The equilibria on $\{\varepsilon = 0\}$ are $(0,0)$ and $(0,c)$. The Jacobian matrices of this vector field at these equilibria are

$$(0,0) : \begin{pmatrix} 0 & 0 \\ 0 & 0 \end{pmatrix}, \quad (0,c) : \begin{pmatrix} 0 & 0 \\ 0 & -c^2 \end{pmatrix}.$$

The dynamics around the equilibrium $(0,c)$ is same as $\overline{E}^+_{O'}$. Therefore, this equilibrium $(r,\bar{\phi}) = (0,0)$ is not hyperbolic again. Here we shall not consider more complicated analysis, however, it will be studied that the asymptotic behavior of the connecting orbits from (or to) $\overline{E}^+_{O'}$ in a latter subsection.

Dynamics on the chart $\{\bar{\psi} = -1\}$

By the change of coordinates $\phi = \varepsilon\bar{\phi}$, $\psi = -\varepsilon$ and time-rescaling $d\sigma/ds = \varepsilon$, we have

$$\begin{cases} \varepsilon_\sigma = -c\varepsilon\bar{\phi} + \varepsilon^{p+1}\bar{\phi}^{p+2} - \varepsilon\bar{\phi}^2, \\ \bar{\phi}_\sigma = c\bar{\phi}^2 - \varepsilon^p\bar{\phi}^{p+3} + \bar{\phi}^3 - \varepsilon^p\bar{\phi}^{p+1}. \end{cases}$$

The equilibria on $\{\varepsilon = 0\}$ are $(0,0)$ and $(0,-c)$. The Jacobian matrices of this vector field at these equilibria are

$$(0,0) : \begin{pmatrix} 0 & 0 \\ 0 & 0 \end{pmatrix}, \quad (0,-c) : \begin{pmatrix} 0 & 0 \\ 0 & c^2 \end{pmatrix}.$$

The dynamics around the equilibrium $(0,-c)$ is same as $\overline{E}^-_{O'}$. Therefore, this equilibrium $(r,\bar{\phi}) = (0,0)$ is not hyperbolic again, however, we shall not consider more complicated analysis here.

Combining the dynamics on the charts $\{\bar{\phi} = \pm 1\}$ and $\{\bar{\psi} = \pm 1\}$, we obtain the dynamics near E_O (see Figure 7.4.2).

7.4.3 Dynamics on the chart $\overline{U}_2$

To obtain the dynamics on the chart $\overline{U}_2$, we introduce coordinates (λ, x) by the formulas

$$\phi(s) = x(s)/\lambda(s), \quad \psi(s) = 1/\lambda(s).$$

Then we have

$$\begin{cases} \lambda' = cx + \lambda^{-p}x^{p+2} - \delta x^2, \\ x' = \lambda^{-p-1}x^{p+1} + c\lambda^{-1}x^2 + \lambda^{-p-1}x^{p+3} - \delta\lambda^{-1}x^3. \end{cases} \tag{7.4.11}$$

Time-scale desingularization $d\sigma/ds = \lambda(s)^{-p-1}$ yields

$$\begin{cases} \lambda_\sigma = c\lambda^{p+1}x + \lambda x^{p+2} - \delta\lambda^{p+1}x^2, \\ x_\sigma = x^{p+1} + c\lambda^p x^2 + x^{p+3} - \delta\lambda^p x^3, \end{cases} \tag{7.4.12}$$

where $\lambda_\sigma = d\lambda/d\sigma$ and $x_\sigma = dx/d\sigma$. The system (7.4.12) has the equilibrium

$$E^+_{0'} : (\lambda, x) = (0,0). \tag{7.4.13}$$

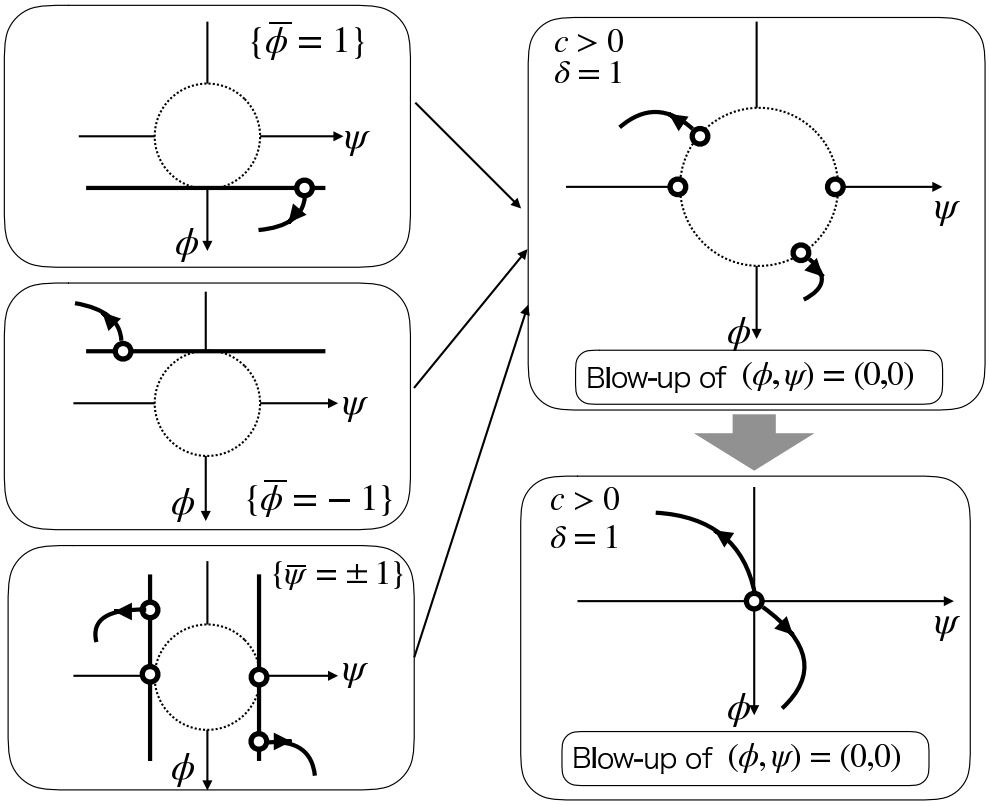

Figure 7.4.2: Schematic pictures of the dynamics near E_O in the case that $c>0$, $\delta=1$ and p is odd.

The Jacobian matrix of the vector field (7.4.12) at its equilibrium is

$$E_{0'}^{+}:\begin{pmatrix}0&0\\0&0\end{pmatrix}.$$

The equilibrium $E_{0'}^{+}$ is not hyperbolic. As in the previous section, to determine the dynamics near $E_{0'}^{+}$, we desingularize it by introducing the following blow-up coordinates with excepting $p=1$:

$$\lambda=r^{p-1}\bar{\lambda},\quad x=r^{p}\bar{x}.$$

Since we are interested in the dynamics on the Poincaré disk, we consider the dynamics of blow-up vector fields on the charts $\{\bar{\lambda}=1\}$ and $\{\bar{x}=\pm 1\}$.

Dynamics on the chart $\{\bar{\lambda}=1\}$

By the change of coordinates $\lambda=r^{p-1}$, $x=r^{p}\bar{x}$ and time-rescaling $d\eta/d\sigma=r^{p^2}$, we have

$$\begin{cases} r_\eta=(p-1)^{-1}(cr\bar{x}+r^{2p+1}\bar{x}^{p+2}-\delta r^{p+1}\bar{x}^2),\\ \overline{x}_\eta=(p-1)^{-1}(-c\bar{x}^2-r^{2p}\bar{x}^{p+3}+\delta r^{p}\bar{x}^3)+\bar{x}^{p+1}. \end{cases} \tag{7.4.14}$$

The equilibria of (7.4.14) on $\{r=0\}$ are $\overline{E}_{0'}^{+}:(r,\bar{x})=(0,0)$ and

$$\pm\overline{E}_{p'}^{+}:(r,\bar{x})=(0,\pm q),\quad q:=[c/(p-1)]^{\frac{1}{p-1}}.$$

The Jacobian matrices of the vector field (7.4.14) at these equilibria are

$$\overline{E}_{0'}^{+}:\begin{pmatrix}0&0\\0&0\end{pmatrix},\quad \pm\overline{E}_{p'}^{+}:\begin{pmatrix}\pm q^p&0\\0&\pm(p-1)q^p\end{pmatrix}.$$

Therefore, $+\overline{E}^+_{p'}$ (resp. $-\overline{E}^+_{p'}$) is a source (resp. sink) for $c > 0$. Also, $\overline{E}^+_{0'}$ is not hyperbolic again. The dynamics of (7.4.14) near $\overline{E}^+_{0'}$ cannot be completely determined, however, we can study the detailed behavior of the trajectories along the unstable (resp. stable) manifolds of $\overline{E}^+_{p'}$ (resp. $-\overline{E}^+_{p'}$) of (7.4.14). For instance, the solutions near $\overline{E}^+_{p'}$ are approximated as follows.

$$r(\eta) \sim C_1 e^{q^p \eta}(1 + o(1)), \tag{7.4.15}$$

$$\bar{x}(\eta) \sim C_2 e^{(p-1)q^p \eta}(1 + o(1)) + q. \tag{7.4.16}$$

Dynamics on the chart $\{\bar{x} = 1\}$

By the change of coordinates $\lambda = r^{p-1}\bar{\lambda}$, $x = r^p$, and time-rescaling $d\eta/d\sigma = r^{p^2}$, we have

$$\begin{cases} r_\eta = p^{-1}(r + cr\bar{\lambda}^p + r^{2p+1} - \delta r^{p+1}\bar{\lambda}^p), \\ \bar{\lambda}_\eta = p^{-1}\{-(p-1)\bar{\lambda} + c\bar{\lambda}^{p+1} + r^{2p}\bar{\lambda} - \delta r^p \bar{\lambda}^{p+1}\}. \end{cases}$$

The equilibria on $\{r = 0\}$ are

$$(r, \bar{\lambda}) = (0, 0), \quad (r, \bar{\lambda}) = (0, [p - 1/c]^{\frac{1}{p}})$$

for $c > 0$. By the further computations, we can see that $(0, 0)$ is a saddle, and $(0, [p-1/c]^{\frac{1}{p}})$ is a source.

Dynamics on the chart $\{\bar{x} = -1\}$

By the change of coordinates $\lambda = r^{p-1}\bar{\lambda}$, $x = -r^p$, and time-rescaling $d\eta/d\sigma = r^{p^2}$, we have

$$\begin{cases} r_\eta = p^{-1}(-r - cr\bar{\lambda}^p - r^{2p+1} - \delta r^{p+1}\bar{\lambda}^p), \\ \bar{\lambda}_\eta = p^{-1}\{(p-1)\bar{\lambda} - c\bar{\lambda}^{p+1} - r^{2p}\bar{\lambda} - \delta r^p \bar{\lambda}^{p+1}\}. \end{cases}$$

The equilibria on $\{r = 0\}$ are

$$(r, \bar{\lambda}) = (0, 0), \quad (r, \bar{\lambda}) = (0, [p - 1/c]^{\frac{1}{p}})$$

for $c > 0$. By the further computations, we can see that $(0, 0)$ is a saddle, and $(0, [p-1/c]^{\frac{1}{p}})$ is a sink.

Combining the dynamics on the charts $\{\bar{\lambda} = 1\}$ and $\{\bar{x} = \pm 1\}$, we obtain the dynamics on $\overline{U}_2$ (see Figure 7.4.3).

7.4.4 Dynamics on the chart $\overline{V}_2$

The change of coordinates

$$\phi(s) = -x(s)/\lambda(s), \quad \psi(s) = -1/\lambda(s)$$

give the projected dynamics of (7.2.2) on the chart $\overline{V}_2$:

$$\begin{cases} \lambda_\sigma = -c\lambda^{p+1}x + \lambda x^{p+2} + \delta\lambda^{p+1}x^2, \\ x_\sigma = x^{p+1} - c\lambda^p x^2 + x^{p+3} + \delta\lambda^p x^3, \end{cases} \tag{7.4.17}$$

where τ is the new time introduced by $d\sigma/ds = \lambda(s)^{-p-1}$. The system (7.4.17) can be transformed into (7.4.12) by the change of coordinates $(\lambda, x) \to (-\lambda, x)$. Therefore, it is sufficient to consider the blow-up of singularity $E^-_{0'} : (\lambda, x) = (0, 0)$ by the formulas

$$\lambda = r^{p-1}\bar{\lambda}, \quad x = r^p \bar{x} \quad \text{with} \quad \bar{\lambda} = 1.$$

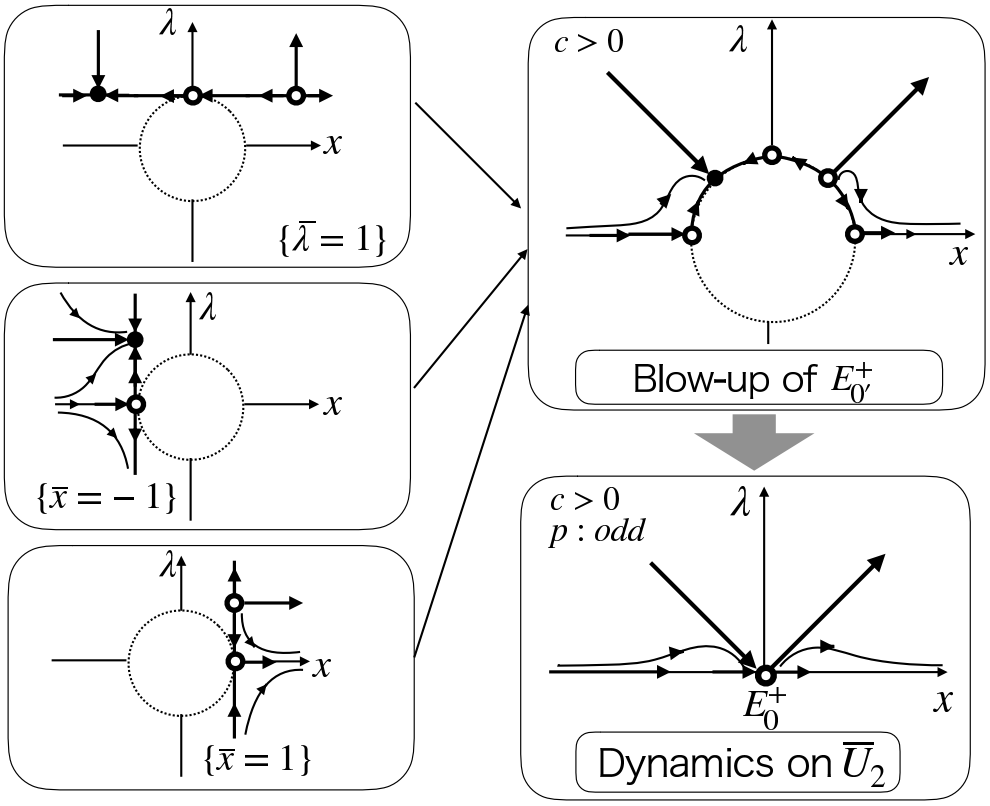

Figure 7.4.3: Schematic pictures of the dynamics of the blow-up vector fields and $\overline{U}_2$ in the case that $c > 0$ and p is odd.

Then, we have

$$\begin{cases} r_\eta = (p-1)^{-1}(-cr\bar{x} + r^{2p+1}\bar{x}^{p+2} + \delta r^{p+1}\bar{x}^2), \\ \overline{x}_\eta = (p-1)^{-1}(c\bar{x}^2 - r^{2p}\bar{x}^{p+3} - \delta r^p\bar{x}^3) + \bar{x}^{p+1}, \end{cases}$$

where η satisfies $d\eta/d\sigma = \{r(\tau)\}^{p^2}$. The equilibrium on $\{r = 0\}$ is $(0, 0)$ with 0 eigenvalues for $c > 0$. Therefore, this equilibrium is not hyperbolic again. We shall not consider the more complicated analysis here.

7.4.5 Dynamics on the chart $\overline{U}_1$

Let us study the dynamics on the chart $\overline{U}_1$. The transformations

$$\phi(s) = 1/\lambda(s), \quad \psi(s) = x(s)/\lambda(s)$$

yield

$$\begin{cases} \lambda_\sigma = -\lambda x, \\ x_\sigma = -c\lambda^p x + \delta\lambda^p - 1 - x^2 \end{cases} \tag{7.4.18}$$

via time-rescaling $d\sigma/ds = \{\lambda(s)\}^{-p-1}$. When the parameter δ is $\delta = 0$, the system (7.4.18) has no equilibria. If $\delta = 1$, then the equilibrium of (7.4.18) is $(\lambda, x) = (1, 0)$ that coincides with the equilibrium $(\phi, \psi) = (1, 0)$ of (7.1.9).

7.4.6 Dynamics on the chart $\overline{V}_1$

Let us study the dynamics on the chart $\overline{V}_1$. The transformations

$$\phi(s) = -1/\lambda(s), \quad \psi(s) = -x(s)/\lambda(s).$$

yield

$$\begin{cases} \lambda_\sigma = -\lambda x, \\ x_\sigma = c\lambda^p x - \delta\lambda^p - 1 - x^2 \end{cases} \tag{7.4.19}$$

via time-rescaling $d\sigma/ds = \{\lambda(s)\}^{-p-1}$. The system (7.4.19) has no equilibria.

7.4.7 Classification of the connecting orbits in odd case

As studied previous subsections, there are equilibria that are not hyperbolic in the blow-up vector fields (7.4.2),(7.4.5),(7.4.7),(7.4.10) and (7.4.14). Therefore, we cannot determine the dynamics near the singularities explicitly. However, if the center, stable and unstable manifolds of the equilibria on each blow-up vector field are inherited to the vector filed on the Poincaré disk and the connecting orbits between each other are exist, then they correspond to the functions satisfying (7.1.9). In this subsection, we classify the connecting orbits and the functions corresponding them. It should be noted that if there is a quasi traveling wave with quenching, we can find the weak traveling wave solutions with quenching of (7.1.1) (for $\delta = 0$) and (7.1.4) (for $\delta = 1$). The proofs of Theorems (computations of asymptotic behavior) for the odd case are similar as the even case.

Let us prepare the symbols used in this subsection as follows:

- $\mathcal{W}^{cs}(\overline{E}_O^+)$ denotes the center-stable manifold of $\overline{E}_O^+$ in the dynamical system (7.4.2).
- $\mathcal{W}^{cu}(\overline{E}_O^-)$ denotes the center-unstable manifold of $\overline{E}_O^-$ in the dynamical system (7.4.5).
- $\mathcal{W}^{cu}(\overline{E}_{O'}^+)$ denotes the center-unstable manifold of $\overline{E}_{O'}^+$ in the dynamical system (7.4.7).
- $\mathcal{W}^{cu}(\overline{E}_{O'}^-)$ denotes the center-stable manifold of $\overline{E}_{O'}^-$ in the dynamical system (7.4.10).
- $\mathcal{W}^{s}(-\overline{E}_{p'}^+)$ denotes the stable manifold of $-\overline{E}_{p'}^+$ in the dynamical system (7.4.14).
- $\mathcal{W}^{u}(\overline{E}_{p'}^+)$ denotes the unstable manifold of $\overline{E}_{p'}^+$ in the dynamical system (7.4.14).

First, we state the result for $\delta = 0$.

Theorem 7.4.1
Assume that $c > 0$, $\delta = 0$, $p \in 2\mathbb{N} + 1$ and the following:

- *The equilibrium $E_O : (y_1, y_2, y_3) = (0, 0, 1)$ on the Poincaré disk of (7.2.2) has the center-stable manifold $\mathcal{W}^{cs}(E_O)$ and center-unstable manifold $\mathcal{W}^{cu}(E_O)$ that corresponds to $\mathcal{W}^{cs}(\overline{E}_O^+)$ and $\mathcal{W}^{cu}(\overline{E}_O^-)$, respectively.*
- *The equilibrium $E_{O'}^+$ (which is defined in (7.4.13)) on the Poincaré disk of (7.2.2) has the stable manifold $\mathcal{W}^{s}(E_{O'}^+)$ and unstable manifold $\mathcal{W}^{u}(E_{O'}^+)$ that corresponds to $\mathcal{W}^{s}(-\overline{E}_{p'}^+)$ and $\mathcal{W}^{u}(\overline{E}_{p'}^+)$, respectively.*

Then, the following holds:

(I) If there exits a connecting orbit Γ^+ that connects $\mathcal{W}^{cs}(E_O)$ and $\mathcal{W}^{u}(E_{O'}^+)$, then (7.1.1) has a weak traveling wave solutions with quenching. In addition, it hold that

$$\begin{cases} u(\xi) \sim (p\xi/c)^{-\frac{1}{p}} \quad as \quad \xi \to \infty \\ \lim\limits_{\xi \to +\infty} u'(\xi) = 0 \end{cases}$$

and

$$\begin{cases} u(\xi) \sim A(\xi - \xi_*)^{\frac{1}{p}} \\ u'(\xi) \sim A(\xi - \xi_*)^{-\frac{p-1}{p}} \end{cases} \quad as \quad \xi \to \xi_* + 0$$

where $|\xi_*| < \infty$, $A > 0$ *are constants* (ξ_* *is the quenching point). In addition,* $u(\xi) > 0$ *holds for* $\xi \in (\xi_*, \infty)$ *and* $u(\xi) = 0$ *for* $\xi \in (-\infty, \xi_*)$.

(II) If there exits a connecting orbit Γ^- *that connects* $\mathcal{W}^{cu}(E_O)$ *and* $\mathcal{W}^s(E^+_{O'})$, *then* (7.1.1) *has a weak traveling wave solutions with quenching and its profile is obtained by the mapping* $u(\xi) \mapsto -u(-\xi)$, *where* $u(\xi)$ *is a weak traveling wave solutions with quenching corresponding to* Γ^+.

Proof of (I) As discussed Section 7.4, the dynamics on the center manifold (7.4.4) that gives dynamics near $\overline{E}^+_O$ is topologically equivalent to the dynamics of the following system:

$$\frac{dU}{d\sigma} = -U^{2p+1}/c + h.o.t \tag{7.4.20}$$

with

$$U(\sigma) = \phi(\sigma) \quad \text{and} \quad \frac{d\sigma}{d\xi} = \frac{d\sigma}{ds} \cdot \frac{ds}{d\xi} = \phi^{-p}.$$

Then, (7.4.20) yields

$$\phi(\sigma) \sim (A + 2p\sigma/c)^{-\frac{1}{2p}} \quad \text{as} \quad \sigma \to \infty$$

with a constant $A > 0$. Therefore, we have

$$\frac{d\sigma}{d\xi} \sim \sqrt{A + 2p\sigma/c}.$$

holds near $\sigma = \infty$. This implies that

$$\sigma \sim (p^2\xi^2 + 2Bp^2\xi - Ac^2 + B^2p^2)/(2cp) \quad \text{as} \quad \sigma \to \infty$$

with a constant B. Therefore,

$$u(\xi) = \phi(\xi) \sim (p\xi/c)^{-\frac{1}{p}}.$$

Let us consider the dynamics near $\overline{E}^+_{p'}$ of (7.4.14). We recall (7.4.15), (7.4.16) and

$$\begin{aligned}
\frac{d\eta}{d\xi} &= \frac{d\eta}{d\sigma}\frac{d\sigma}{ds}\frac{ds}{d\xi} = r^{p^2} \cdot \lambda^{-p-1} \cdot \phi^{-p-1} = r^{-p}\bar{x}^{-p-1} \\
&\sim \left\{C_1 e^{q^p\eta}(1 + o(1))\right\}^{-p} \cdot \left\{C_2 e^{(p-1)q^p\eta}(1 + o(1)) + q\right\}^{-p-1} \\
&\sim C_3 e^{-pq^p\eta} \cdot \left\{C_2 e^{(p-1)q^p\eta}(1 + o(1)) + q\right\}^{-p-1} \quad \eta \to -\infty \\
&= C_3 e^{-pq^p\eta} \cdot \frac{1}{\left\{C_2 e^{(p-1)q^p\eta}(1 + o(1)) + q\right\}^{p+1}} \\
&= C_3 e^{-pq^p\eta} \cdot \frac{1}{\left\{C_2 e^{(p-1)q^p\eta}(1 + o(1))\right\}^{p+1} + (p+1)\left\{C_2 e^{(p-1)q^p\eta}(1 + o(1))\right\}^{p} \cdot q + \cdots + q^p} \\
&\sim Ce^{-pq^p\eta} \quad \text{as} \quad \eta \to -\infty.
\end{aligned}$$

We then have

$$\frac{d\xi}{d\eta} = Ce^{pq^p\eta}.$$

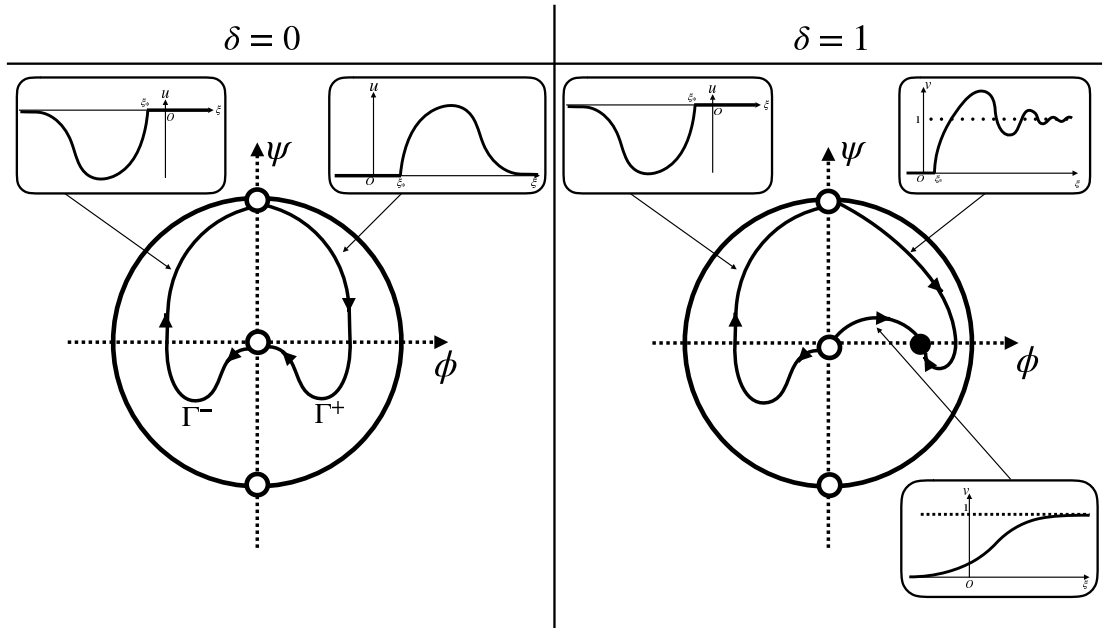

Figure 7.4.4: Roughly sketch of the dynamics on the Poincaré disk and corresponding (weak) traveling wave solutions in the case that the assumptions of Theorems are satisfied with $D < 0$ and $c > 0$.

This yields

$$\xi - \xi_* \sim Ce^{pq^p\eta} \quad \text{as} \quad \eta \to -\infty.$$

We then have

$$\begin{aligned} u(\xi) = \phi(\xi) &= \frac{x}{\lambda} = \frac{r^p}{r^{p-1}}\overline{x} = r\overline{x} \\ &\sim \left\{C_1 e^{q^p\eta}(1+o(1))\right\}\left\{C_2 e^{(p-1)q^p\eta}(1+o(1)) + q\right\} \\ &\sim C_4 e^{q^p\eta}\cdot\left\{C_2 e^{(p-1)q^p\eta}(1+o(1)) + q\right\} \\ &= C_5 e^{q^p\eta}e^{(p-1)q^p\eta} + C_4\cdot q\cdot e^{q^p\eta} \\ &= C_5 e^{pq^p\eta} + C_4\cdot q\cdot e^{q^p\eta} \\ &\sim Ae^{q^p\eta}. \end{aligned}$$

Here, in last relation, since $e^{pq^p\eta} < e^{q^p\eta}$ $(\eta < 0)$ is satisfied by $pq^p > q^p$, we choose the term with the greater influence when $\eta \to -\infty$. Therefore, we have

$$u(\xi) = \phi(\xi) \sim Ae^{q^p\eta} \sim A(\xi - \xi_*)^{\frac{1}{p}} \quad \text{as} \quad \xi \to \xi_* + 0.$$

Similarly, since $\psi(\xi) = 1/\lambda = r^{1-p}$, it holds that

$$\psi(\xi) \sim Ae^{pq^p\eta} \sim A\left(\xi - \xi_*\right)^{-\frac{p-1}{p}} \quad \text{as} \quad \xi \to \xi_* + 0.$$

Proof of (II) Since (7.4.1) with $\delta = 0$ is invariant under the mapping: $\phi(\xi) \mapsto -\phi(-\xi)$, the statement holds. □

Second, we state the result for $\delta = 1$. There are three types of connecting orbits that correspond to the (weak) traveling wave solutions of (7.1.4).

Theorem 7.4.2
Assume that $c > 0$, $\delta = 1$, $p \in 2\mathbb{N}+1$ and the following:

- *The equilibrium $E^+_{O'}$ (which is defined in (7.4.13)) on the Poincaré disk of (7.2.2) has the unstable manifold $\mathcal{W}^u(E^+_{O'})$ that corresponds to $\mathcal{W}^u(\overline{E}^+_{p'})$.*

If there exists a connecting orbit that connects $\mathcal{W}^u(E^+_{O'})$ and $\mathcal{W}^s(E_\delta)$, then (7.1.4) has a weak traveling wave solutions with quenching. The asymptotic behavior for $\xi \to \infty$ are given by (7.1.12) and (7.1.13) in Theorem 7.1.2. In addition, the asymptotic behavior near the quenching point ξ_* are given by the following:

$$\begin{cases} v(\xi) \sim A(\xi - \xi_*)^{\frac{1}{p}} \\ v'(\xi) \sim A(\xi - \xi_*)^{-\frac{p-1}{p}} \end{cases} \quad \text{as} \quad \xi \to \xi_* + 0.$$

Proof Since dynamics of (7.4.1) on $\{\phi > 0\}$ is equivalent to the dynamics of (7.2.2) on $\{\phi > 0\}$, asymptotic behavior for $\xi \to \infty$ is exactly same to (7.1.12) and (7.1.13) in Theorem 7.1.2. In order to prove the Theorem, it is sufficient to compute the asymptotic behavior along $\mathcal{W}^u(E^+_{p'})$.

We recall the dynamics on the chart $\overline{U}_2$ given by (7.4.15) and (7.4.16). Then, we have

$$\frac{d\eta}{d\xi} = \frac{d\eta}{d\sigma}\frac{d\sigma}{ds}\frac{ds}{d\xi} = Ae^{-pq^p\eta},$$

where $A > 0$ is a constant. This yields

$$\xi - \xi_* \sim Ce^{pq^p\eta} \quad \text{as} \quad \eta \to -\infty.$$

Further computations yield

$$v(\xi) = \phi(\xi) = r\bar{x} \sim A(\xi - \xi_*)^{\frac{1}{p}} \quad \text{as} \quad \xi \to \xi_* + 0$$

and

$$v'(\xi) = c^2\psi(\xi) = c^2 r^{1-p} \sim A\,(\xi - \xi_*)^{-\frac{p-1}{p}} \quad \text{as} \quad \xi \to \xi_* + 0.$$

□

Theorem 7.4.3
Assume that $c > 0$, $\delta = 1$, $p \in 2\mathbb{N}+1$ and the following:

- *The equilibrium $E_O : (y_1, y_2, y_3) = (0, 0, 1)$ on the Poincaré disk of (7.2.2) has the center-unstable manifold $W^{cu}(E_O)$ that corresponds to $\mathcal{W}^{cu}(\overline{E}^+_{O'})$.*

Then, if there exist a connecting orbit that connects $\mathcal{W}^{cu}(E_O)$ and $\mathcal{W}^s(E_\delta)$, then (7.1.4) has a traveling wave solution that satisfies $v(\xi) > 0$ for $\xi \in \mathbb{R}$,

$$\lim_{\xi\to-\infty} v(\xi) = \lim_{\xi\to-\infty} v'(\xi) = 0,$$

$$\lim_{\xi\to\infty} v(\xi) = 1 \quad \textit{and} \quad \lim_{\xi\to\infty} v'(\xi) = 0.$$

Proof The dynamics near E_δ of (7.4.1)is equivalent to that of (7.2.2). Let us consider the dynamics along $\mathcal{W}^{cu}(E_O)$. We recall that the dynamics on the center manifold (7.4.9) is locally topologically equivalent to the dynamics of the following system

$$\frac{dU}{d\sigma} = U^{p+1}/c + h.o.t.$$

This yields

$$U(\sigma) \sim [-p(\sigma/c + A)]^{-\frac{1}{p}}.$$

Then we have

$$\frac{d\sigma}{d\xi} = \frac{d\sigma}{ds}\frac{ds}{d\xi} = \phi^{-p} = -p(\sigma/c + A).$$

Therefore, we have $\sigma = Be^{-p\xi/c} - A$ and

$$v(\xi) = \phi(\xi) = U(\sigma(\xi)) = Ce^{\xi/c} \to 0 \quad \text{as} \quad \xi \to -\infty,$$

where $C > 0$ is a constant that depend on p. □

Theorem 7.4.4
Assume that $c > 0$, $\delta = 1$, $p \in 2\mathbb{N} + 1$ and the following:

- *The equilibrium $E_O : (y_1, y_2, y_3) = (0, 0, 1)$ on the Poincaré disk of (7.2.2) has the center-unstable manifold $\mathcal{W}^{cu}(E_O)$ that corresponds to $\mathcal{W}^{cu}(\overline{E}^-_{O'})$.*
- *The equilibrium $E^+_{O'}$ (which is defined in (7.4.13)) on the Poincaré disk of (7.2.2) has the stable manifold $\mathcal{W}^s(E^+_{O'})$ that corresponds to $\mathcal{W}^s(-\overline{E}^+_{p'})$.*

If there exists a connecting orbit that connects $\mathcal{W}^{cu}(E_O)$ and $\mathcal{W}^s(E^+_{O'})$, then (7.1.4) has a weak traveling wave solutions with quenching. In addition,

$$\lim_{\xi \to -\infty} v(\xi) = \lim_{\xi \to -\infty} v'(\xi) = 0$$

and

$$\begin{cases} v(\xi) \sim A(\xi_* - \xi)^{\frac{1}{p}} \\ v'(\xi) \sim A(\xi_* - \xi)^{-\frac{p-1}{p}} \end{cases} \quad \text{as} \quad \xi \to \xi_* - 0$$

hold. Here, $A < 0$ is a constant and ξ_* ($|\xi_*| < \infty$) is a quenching point, that is, $v(\xi) < 0$ for $\xi \in (-\infty, \xi_*)$ and $v(\xi) = 0$ for $\xi \in [\xi_*, +\infty)$ hold.

Proof Dynamics along $\mathcal{W}^{cu}(\overline{E}^-_{O'})$ is determined by the equation (7.4.6). Therefore, asymptotic behavior for $\xi \to -\infty$ can be obtained as similar to the proof previous Theorem.

Let us consider the dynamics along $\mathcal{W}^s(-\overline{E}^+_{p'})$. We recall (7.4.14) and Jacobian matrix at

$$-\overline{E}^+_{p'} : (r, \bar{x}) = (0, -[c/(p-1)]^{\frac{1}{p-1}}).$$

Dynamics near $-\overline{E}^+_{p'}$ are

$$r(\eta) \sim C_1 e^{-q^p \eta}(1 + o(1)) \quad \text{and} \quad \bar{x}(\eta) \sim C_2 e^{-(p-1)q^p \eta}(1 + o(1)) - q, \quad q = [c/(p-1)]^{\frac{1}{p-1}}$$

(cf. (7.4.15) and (7.4.16)). Further computations yield

$$\xi(\eta) = Ae^{-pq^p \eta} + \tilde{A} \quad \text{as} \quad \eta \to +\infty.$$

Let $\tilde{A} = \xi_*$ (i.e., $\xi_* = \lim_{\eta \to +\infty} \xi(\eta)$) , then the asymptotic behavior can be obtained by the similar computations in the proof of Theorem 7.4.2. □

The roughly sketch of the Poincaré disk in the case that the assumptions of Theorems are satisfied is shown in Figure 7.4.4. We note that if the E_δ is asymptotically stable, then E_δ is a stable node for $D \geq 0$ and is a stable focus (spiral sink) for $D < 0$.

7.5 Conclusions and Remarks

In this chapter, we studied whole dynamics of (7.1.9) on the phase space $\mathbb{R}^2 \cup \{(\phi, \psi) \mid \|(\phi, \psi)\| = +\infty\}$ and asymptotic behavior of the solutions on $\mathbb{R}$ of (7.1.1) and (7.1.4) by applying the Poincaré compactification and dynamical system approach.

We remark that since the theory of blow-up (desingularization of the vector fields) is not applicable for the non-polynomial vector fields, we cannot deal with the general case that $p \in \mathbb{R}$. Hence, we leave it open here.

Further, the stabilities of the (weak) traveling waves were not discussed here. To do that, it will be necessary another approach to (7.1.1) and (7.1.4). Therefore, also we leave it open here.

In addition, the case that $p = 1$ is not discussed. The reason is that the type and degree of the vector fields on the each local chart (for instance, see (7.4.11)) cannot be determined through the Newton polyhedra (for instance, see [8]). Therefore, it is necessary to more detailed analysis for the case that $p = 1$. It will be addressed in future works.

Let us return our attention to the relationship between (7.1.1) and (7.1.4). If $v(\xi) = v(x - c\tau)$ is a (weak) traveling wave solution of (7.1.4), then the function

$$u(x,t) = p^{-\frac{1}{p}} \left(\frac{1}{T-t}\right)^{\frac{1}{p}} v\left(x - \frac{c}{p}\log\left(\frac{T}{T-t}\right)\right)$$

satisfies (7.1.1) on $\mathbb{R} \times (0, T)$. This results give us the profiles of blow-up solutions for (7.1.1) and (7.1.4) associated with the traveling wave solutions.

Chapter 8

A refined asymptotic behavior of traveling wave solutions for degenerate nonlinear parabolic equations

Abstract

In this chapter, we consider the asymptotic behavior of traveling wave solutions of a certain degenerate nonlinear parabolic equation for $\xi \equiv x - ct \to -\infty$ with $c > 0$. We give a refined one of them, which was not obtained in the preceding work [32], by an appropriate asymptotic study and properties of the Lambert W function. This chapter is based on the following published paper ([30]):

> Ichida, Y., Matsue, K., Sakamoto, T.O.: A refined asymptotic behavior of traveling wave solutions for degenerate nonlinear parabolic equations, JSIAM Lett., **12**, 65–68 (2020).

8.1 Introduction

In this chapter, we consider the degenerate nonlinear parabolic equation

$$u_t = u^p(u_{xx} + u) - \delta u, \quad t > 0, \quad x \in \mathbb{R}, \tag{8.1.1}$$

where $\delta = 0$ or 1, $p \in 2\mathbb{N}$.

When $\delta = 0$, this equation arises in the modeling of heat combustion, solar flares in astrophysics, plane curve evolution problems and the resistive diffusion of a force-free magnetic field in a plasma confined between two walls (see [4, 46, 47, 62] and references therein). Also, there are many studies on blow-up solution to (8.1.1) (for instance, see [4, 62] and references therein).

On the other hand, the equation (8.1.1) with $\delta = 1$ can be obtained by transforming solution of (8.1.1) with $\delta = 0$ (see [62]). In [62], the traveling wave solutions of (8.1.1) play important roles. More precisely, the lower bound of the blow-up rate is obtained by means of the traveling wave solutions of (8.1.1) under either the Dirichlet boundary condition or the periodic boundary condition in the case that $\delta = 1$ and x is restricted to $x \in (-L, L)$.

In addition, the traveling wave solutions are not only upper (or lower) solutions as discussed in [62] but also the entire solutions of the equation. These facts motivate us to study detailed information of the traveling wave solutions to (8.1.1).

In order to consider the traveling waves of (8.1.1), we introduce the following change of variables:

$$u(t,x)=\phi(\xi),\quad \xi=x-ct,\quad c>0.$$

The equation of $\phi(\xi)$ solving (8.1.1) is then reduced to

$$-c\phi'=\phi^p\phi''+\phi^{p+1}-\delta\phi,\quad \xi\in\mathbb{R},\quad {}'=\frac{d}{d\xi},$$

equivalently

$$\begin{cases}\phi'=\psi,\\ \psi'=-c\phi^{-p}\psi-\phi+\delta\phi^{-p+1},\end{cases}\tag{8.1.2}$$

where $\delta=0$ or 1.

In [32], a result on the whole dynamics on the phase space $\mathbb{R}^2$ including infinity generated by the two-dimensional ordinary differential equation (ODE for short) (8.1.2) is obtained by applying the dynamical system approach and the Poincaré compactification (for instance, see Section 1.1 and [14] for the details of the Poincaré compactification). Further, connecting orbits on it are focused and several results on the existence of (weak) traveling wave solutions are given. The following theorem is one of main results obtained in [32].

Theorem 8.1.1 (Theorem 7.1.3 ([32], Theorem 3))
Assume that $p\in 2\mathbb{N}$ and $\delta=1$. Then, for a given positive constant c, the equation (8.1.1) *has a family of traveling wave solutions (which correspond to a family of the orbits of* (8.1.2)*). Each traveling wave solution $u(t,x)=\phi(\xi)$ satisfies the following.*

- $\begin{cases}\lim\limits_{\xi\to-\infty}\phi(\xi)=0, & \lim\limits_{\xi\to+\infty}\phi(\xi)=1,\\ \lim\limits_{\xi\to-\infty}\phi'(\xi)=0, & \lim\limits_{\xi\to+\infty}\phi'(\xi)=0.\end{cases}$
- $\phi(\xi)>0$ *holds for* $\xi\in\mathbb{R}$.

Figure 8.2.1 shows dynamics on the Poincaré disk of (8.1.2) (see [14] for the definition of the Poincaré disk). In addition, the asymptotic behavior of the traveling wave solutions (obtained in Theorem 8.1.1) for $\xi\to+\infty$ is also given in [32], while the asymptotic behavior as $\xi\to-\infty$ is not obtained there.

In this chapter, we give a refined asymptotic behavior of the traveling wave solutions, which contributes to extraction of their characteristic nature. The main theorem of this chapter is the following.

Theorem 8.1.2
The asymptotic behavior of $\phi(\xi)$ obtained in Theorem 8.1.1 as $\xi\to-\infty$ is

$$\phi(\xi)\sim\left(\frac{\mu c^2}{\mu(c^2+1)-e^{-\frac{p}{c}\xi}}\right)^{\frac{1}{p}},\quad \text{as}\quad \xi\to-\infty,$$

where $\mu<0$ is a constant that depends on the initial state $\phi_0=\phi(0)$.

During our proof of the theorem, we see that the Lambert W function plays a key role in describing the asymptotic behavior. Evaluation of integrals including the Lambert W function is necessary to obtain the asymptotic behavior in the present form. Our argument here is based on an asymptotic study of solutions in the different form from that provided in e.g. [32, 50], which can be applied to asymptotic analysis towards further applications in various phenomena including their numerical calculations.

8.2 Preliminaries

In this section, we partially reproduce calculations in Chapter 7 and [32] for the readers' convenience.

First, we study the dynamics near bounded equilibria of (8.1.2). If $\delta = 1$ and p is even, then (8.1.2) has the equilibria $\pm E_1 : (\phi, \psi) = (\pm 1, 0)$. Let J_1 be the Jacobian matrix of the vector field (8.1.2) at E_1. Then, the behavior of the solution around E_1 is different by the sign of $D = c^2 - 4p$. For instance, the matrix J_1 has the real distinct eigenvalues if $D > 0$ and other cases can be concluded similarly. In addition, if $c > 0$, then the real part of all eigenvalues of J_1 are negative. Therefore, we determine that the equilibria $\pm E_1 : (\phi, \psi) = (\pm 1, 0)$ are sink.

Second, in order to study the dynamics of (8.1.2) on the Poincaré disk, we desingularize it by the time-scale desingularization

$$ds/d\xi = \{\phi(\xi)\}^{-p} \quad \text{for} \quad p \in 2\mathbb{N}. \tag{8.2.1}$$

Since p is assumed to be even, the direction of the time does not change via this desingularization. Then we have

$$\left\{ \begin{array}{l} \phi' = \phi^p \psi, \\ \psi' = -c\psi - \phi^{p+1} + \delta\phi, \end{array} \right. \qquad \left(\ ' \ = \frac{d}{ds} \right), \tag{8.2.2}$$

where $\delta = 0$ or $\delta = 1$.

It should be noted that the time-scale desingularization (8.2.1) is simply the multiplication of ϕ^p to the vector field. Then, except the singularity $\{\phi = 0\}$, the solution curves of the system (vector field) remain the same but are parameterized differently (see also Section 7.7 of [44]).

The system (8.2.2) has the equilibrium $E_O : (\phi, \psi) = (0, 0)$. When $\delta = 1$, the Jacobian matrix of the vector field (8.2.2) at E_O is

$$E_O : \left(\begin{array}{cc} 0 & 0 \\ 1 & -c \end{array} \right).$$

It has the real distinct eigenvalues 0 and $-c$. The eigenvectors corresponding to each eigenvalue are

$$\mathbf{v}_1 = \left(\begin{array}{c} c \\ 1 \end{array} \right), \quad \mathbf{v}_2 = \left(\begin{array}{c} 0 \\ 1 \end{array} \right).$$

We set a matrix T as $T = (\mathbf{v}_1, \mathbf{v}_2)$. Then we obtain

$$\begin{aligned} \left(\begin{array}{c} \phi' \\ \psi' \end{array} \right) &= \left(\begin{array}{cc} 0 & 0 \\ 1 & -c \end{array} \right) \left(\begin{array}{c} \phi \\ \psi \end{array} \right) + \left(\begin{array}{c} \phi^p \psi \\ -\phi^{p+1} \end{array} \right) \\ &= T \left(\begin{array}{cc} 0 & 0 \\ 0 & -c \end{array} \right) T^{-1} \left(\begin{array}{c} \phi \\ \psi \end{array} \right) + \left(\begin{array}{c} \phi^p \psi \\ -\phi^{p+1} \end{array} \right). \end{aligned}$$

Let $\begin{pmatrix} \tilde{\phi} \\ \tilde{\psi} \end{pmatrix} = T^{-1} \begin{pmatrix} \phi \\ \psi \end{pmatrix}$. We then obtain the following system:

$$\begin{cases} \tilde{\phi}' = c^{p-1}\tilde{\phi}^{p+1} + c^{p-1}\tilde{\phi}^p\tilde{\psi}, \\ \tilde{\psi}' = -c\tilde{\psi} - c^{p-1}\tilde{\phi}^{p+1} - c^{p-1}\tilde{\phi}^p\tilde{\psi} - c^{p+1}\tilde{\phi}^{p+1}. \end{cases} \tag{8.2.3}$$

The center manifold theory (e.g. [9]) is applicable to study the dynamics of (8.2.3). It implies that there exists a function $h(\tilde{\phi})$ satisfying

$$h(0) = \frac{dh}{d\tilde{\phi}}(0) = 0$$

such that the center manifold of E_O for (8.2.3) is locally represented as $\{(\tilde{\phi}, \tilde{\psi}) \,|\, \tilde{\psi}(s) = h(\tilde{\phi}(s))\}$. Differentiating it with respect to s, we have

$$\begin{aligned} -ch(\tilde{\phi}) - c^{p-1}\tilde{\phi}^{p+1} - c^{p-1}\tilde{\phi}^p h(\tilde{\phi}) - c^{p+1}\tilde{\phi}^{p+1} \\ = \frac{dh}{d\tilde{\phi}}\left(c^{p-1}\tilde{\phi}^{p+1} + c^{p-1}\tilde{\phi}^p h(\tilde{\phi})\right). \end{aligned}$$

Then we obtain the approximation of the (graph of) center manifold as follows:

$$\left\{(\tilde{\phi}, \tilde{\psi}) \,|\, \tilde{\psi} = -c^{p-2}(c^2+1)\tilde{\phi}(s)^{p+1} + O(\tilde{\phi}^{p+2})\right\}. \tag{8.2.4}$$

Therefore, the dynamics of (8.2.3) near E_O is topologically equivalent to the dynamics of the following equation:

$$\tilde{\phi}'(s) = c^{p-1}\tilde{\phi}^{p+1} - c^{2p-3}(c^2+1)\tilde{\phi}^{2p+1}.$$

We conclude that the approximation of the (graph of) center manifold is

$$\psi(s) = \phi/c - [(c^2+1)\phi^{p+1}]/c^3$$

and the dynamics of (8.2.2) near E_O is topologically equivalent to the dynamics of the following equation:

$$\phi'(s) = \phi^{p+1}/c - [(c^2+1)\phi^{2p+1}]/c^3. \tag{8.2.5}$$

Finally, we obtain the dynamics on the Poincaré disk in the case that p is even (see Figure 8.2.1). This argument indicates that the asymptotic behavior of ϕ through the present system is calculated as a function of s and that an additional asymptotic study is required to obtain the behavior of ϕ in terms of the original frame coordinate ξ.

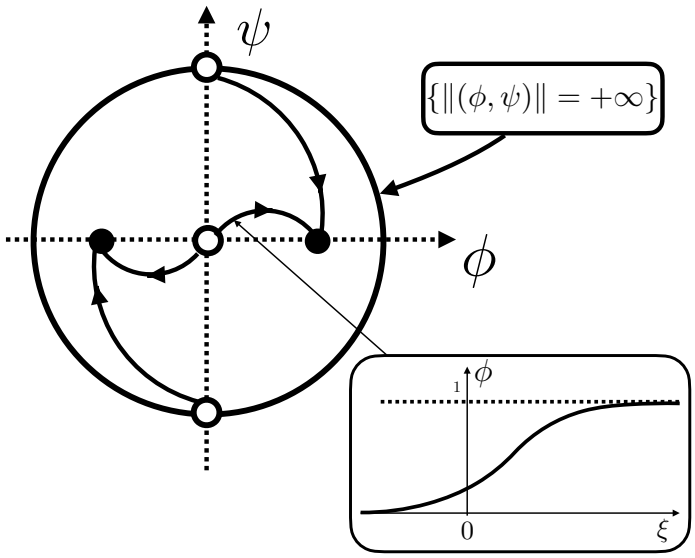

Figure 8.2.1: Schematic picture of the dynamics on the Poincaré disk and corresponding traveling wave solutions in the case that $\delta = 1$ and p is even with $D = c^2 - 4p > 0$ and $c > 0$.

Remark 8.2.1 ([32], Remark 1)
In Figure 8.2.1, we need to be careful about the handling of the point E_O. When we consider the parameter s on the disk, E_O is the equilibrium of (8.2.2)*. However, E_O is a point on the line $\{\phi = 0\}$ with singularity about the parameter ξ. We see that $d\phi/d\psi$ takes the same values on the vector fields defined by* (8.2.2) *and* (8.1.2) *except the singularity $\{\phi = 0\}$. If the trajectories start the equilibrium E_O about the parameter s, then they start from the point E_O about ξ.*

8.3 Proof of Theorem 8.1.2

The proof is divided into four steps. In Step I, we derive an ODE describing the behavior of s with respect to ξ. It turns out to contain the Lambert W function. In Step II, we confirm that $\xi(s) \to -\infty$ as $s \to -\infty$, which is used for the direct derivation of $\phi(\xi)$ in the asymptotic sense. Step III is devoted to obtain the relationship between ϕ and ξ. According to preceding studies such as [32, 50], the asymptotic behavior of $\phi(\xi)$ can be obtained in the composite form $\phi(s(\xi))$, which can require multiple integrations of differential equations. Except special cases, lengthy calculations are necessary towards an explicit and meaningful expression of the targeting asymptotics. Instead, we directly derive the relationship of ϕ to ξ without solving the ODE obtained in Step I and calculate the asymptotic behavior of the function $\xi(\phi)$ as $\phi \to 0$ associated with the center manifold (8.2.4), which works well even if integrands include the Lambert W function. We finally obtain the asymptotic behavior of $\phi(\xi)$ in Step IV via inverse function arguments.

Remark 8.3.1
The Lambert W function $y = W(x)$ is defined as the inverse function of $x = ye^y$. We easily see the following properties which we shall use below:

- *$W(x) > 0$ for $x > 0$;*
- *$W(x) < \log x$ for $x > e$.*

See e.g. [12] and references therein for further properties.

Proof. (I): First we set

$$w(s) := \phi(s)^{-p} > 0.$$

With the aid of (8.2.5), we have

$$w'(s) = -p/c + [p(c^2+1)/c^3 w] = A + Bw^{-1}, \tag{8.3.1}$$

where

$$A = -p/c < 0 \quad \text{and} \quad B = [p(c^2+1)/c^3] > 0.$$

The solution of (8.3.1) satisfies the following.

$$|1 + Aw/B|\, e^{-\left(\frac{A}{B}w+1\right)} = |A/B|\, e^{-\frac{A^2}{B}s - \frac{A^2C_1+B}{B}}$$

with a constant C_1. Since the dynamics of $\phi(s)$ near 0 (i.e., $\phi(s) \approx 0$) is our interest, we may assume that $w(s)$ is sufficiently large, which implies that $[A/B]w + 1 < 0$. Then we have

$$-(1 + Aw/B)\, e^{-\left(\frac{A}{B}w+1\right)} = -Ae^{-\frac{A^2}{B}s - \frac{A^2C_1+B}{B}}/B.$$

By using $w = \phi(s)^{-p}$ and the Lambert W function, we obtain

$$\phi(s) = \left[-B\left\{W\left(E(s)\right) + 1\right\}/A\right]^{-\frac{1}{p}},$$

where $E(s) = -[A/B]e^{-\frac{A^2}{B}s - \frac{A^2C_1+B}{B}}$. We consequently have

$$\frac{ds}{d\xi} = \phi^{-p} = -B\left\{W\left(E(s)\right) + 1\right\}/A. \tag{8.3.2}$$

(II): We shall prove

$$\xi(s) \to -\infty \quad \text{as} \quad s \to -\infty.$$

We note that $E(\cdot)$ is positive on $\mathbb{R}$ and hence $W(E(s)) > 0$ holds for $s \in \mathbb{R}$. Integrating (8.3.2) on $(-\infty, 0]$, we have

$$\xi(0) - \xi_- = \int_{-\infty}^{0} \left[-B\left\{W\left(E(s)\right) + 1\right\}/A\right]^{-1} ds,$$

where

$$\xi_- = \lim_{s\to-\infty} \xi(s).$$

Without loss of generality, we may set $\xi(0) = 0$.

By using properties of the Lambert W function, for a negative constant s_* satisfying $|s_*| \gg 1$, we have

$$\begin{aligned}
-\xi_- &= \int_{-\infty}^{0} \left[-B\left\{W\left(E(s)\right)+1\right\}/A\right]^{-1} ds \\
&> -\frac{A}{B}\left[\int_{s_*}^{0} \left\{W\left(E(s)\right)+1\right\}^{-1} ds \right. \\
&\qquad \left. + \int_{-\infty}^{s_*} \left\{\log(E(s))+1\right\}^{-1} ds\right] \\
&> -\frac{A}{B}\int_{-\infty}^{s_*} \left[\log\left(-[A/B]e^{-\frac{A^2}{B}s-\frac{A^2C_1+B}{B}}\right)+1\right]^{-1} ds \\
&= -\frac{A}{B}\int_{-\infty}^{s_*} \left[\log(-[A/B])\right. \\
&\qquad \left. -(A^2s+A^2C_1+B)/B+1\right]^{-1} ds \\
&= -\lim_{s\to-\infty}\frac{A}{B}\left[(-B/A^2)\log\left|(-A^2/B)s+C_2\right|\right]_s^{s_*},
\end{aligned}$$

where

$$C_2 = \log(-A/B) - (A^2C_1+B)/B + 1.$$

Since $A < 0 < B$ holds, we have

$$\begin{aligned}
-\xi_- &> (1/A)\log\{(-A^2/B)s_* + C_2\} \\
&\quad + (-1/A)\lim_{s\to-\infty}\log\{(-A^2/B)s + C_2\} = +\infty.
\end{aligned}$$

Therefore the asymptotic behavior of $\phi(s)$ as $s \to -\infty$ is equivalent to that of $\phi(\xi)$ as $\xi \to -\infty$.

(III): Next, we represent ξ as a function of ϕ. We rewrite (8.3.2) as

$$\frac{d\xi}{ds} = \phi^p.$$

Using (8.2.5), we obtain

$$\begin{aligned}
\xi + C_3 &= \int \{\phi(s)\}^p ds = \int \phi^p \frac{ds}{d\phi} d\phi \\
&= \int \phi^p \left(\frac{1}{c}\phi^{p+1} - \frac{c^2+1}{c^3}\phi^{2p+1}\right)^{-1} d\phi \\
&= \int \frac{c^3}{\phi\{c^2-(c^2+1)\phi^p\}} d\phi
\end{aligned}$$

with a constant C_3. Introducing $\varphi = \phi^p$, we further have

$$\begin{aligned}
\xi + C_3 &= \int \frac{c^3}{\phi\{c^2 - (c^2+1)\phi^p\}} d\phi \\
&= \frac{c^3}{p} \int \frac{1}{\varphi\{c^2 - (c^2+1)\varphi\}} d\varphi \\
&= \frac{c^3}{p} \int \left\{ \frac{1}{c^2}\frac{1}{\varphi} + \left(1 + \frac{1}{c^2}\right) \frac{1}{c^2 - (c^2+1)\varphi} \right\} d\varphi \\
&= \frac{c}{p} \log \left| \frac{\varphi}{(c^2+1)\varphi - c^2} \right| \\
&= \frac{c}{p} \log \left| \frac{\phi^p}{(c^2+1)\phi^p - c^2} \right|.
\end{aligned}$$

Then the constant C_3 is given by

$$C_3 = \frac{c}{p} \log \left| \frac{\phi_0^p}{(c^2+1)\phi_0^p - c^2} \right|,$$

where $\phi(0) = \phi_0$. Moreover, it holds that $C_3 < 0$ regardless of the value of c, provided $\phi_0 \ll 1$. Indeed, it holds that

$$0 < \phi_0 < \left(c^2/[c^2+2]\right)^{\frac{1}{p}} \qquad (0 < \phi_0 \ll 1).$$

(IV): Finally, we aim to represent ϕ as a function of ξ. As mentioned above, we obtain

$$\xi + \frac{c}{p} \log \left| \frac{\phi_0^p}{(c^2+1)\phi_0^p - c^2} \right| = \frac{c}{p} \log \left| \frac{\phi^p}{(c^2+1)\phi^p - c^2} \right|.$$

This yields

$$\frac{\phi^p}{(c^2+1)\phi^p - c^2} = \pm \left| \frac{\phi_0^p}{(c^2+1)\phi_0^p - c^2} \right| e^{\frac{p}{c}\xi}.$$

Therefore, we have

$$\phi^p = \frac{\mu e^{\frac{p}{c}\xi} c^2}{\mu e^{\frac{p}{c}\xi}(c^2+1) - 1}, \quad \mu = \pm \left| \frac{\phi_0^p}{(c^2+1)\phi_0^p - c^2} \right|.$$

If $\mu > 0$, there exists a finite ξ such that $\mu e^{\frac{p}{c}\xi}(c^2+1) - 1 = 0$ holds. However, as in Theorem 8.1.1, the traveling wave solutions $\phi(\xi)$ that correspond to the connecting orbits between E_O and E_1 have no singularities for $\xi \in \mathbb{R}$. Therefore, μ must be negative. This yields

$$\frac{\mu e^{\frac{p}{c}\xi} c^2}{\mu e^{\frac{p}{c}\xi}(c^2+1) - 1} > 0 \quad \text{with} \quad \mu = -\left| \frac{\phi_0^p}{(c^2+1)\phi_0^p - c^2} \right|.$$

Since p is even, we obtain the following.

$$\phi(\xi) = \left(\frac{\mu c^2}{\mu(c^2+1) - e^{-\frac{p}{c}\xi}} \right)^{\frac{1}{p}} \to 0, \quad \text{as} \quad \xi \to -\infty,$$

where $\mu < 0$ is the constant that depends on the initial state ϕ_0. □

8.4 Conclusion

In this chapter, we give a refined asymptotic behavior of the traveling wave solutions of (8.1.1) as $\xi \to -\infty$. As shown in Step III of the proof, the present result is obtained by considering the asymptotic behavior of $\xi(\phi)$ without taking the relationship between ξ and s into account. This is a key idea to get over the difficulties of treatment of the Lambert W function to obtain the asymptotic behavior for $u(t,x) = \phi(\xi)$. We expect that our approach can be applied to the asymptotic behavior of typical solutions as well as that of singular solutions.

Chapter 9

Classification of nonnegative traveling wave solutions for the 1D degenerate parabolic equations

Abstract

Traveling wave solutions for the one-dimensional degenerate parabolic equations are considered. The purpose of this chapter is to classify the nonnegative traveling wave solutions including sense of weak solutions of these equations and to present their existence, information about their shape and asymptotic behavior. These are studied by applying the framework that combines Poincaré compactification and classical dynamical systems theory. We also aim to use these results to generalize the results of our previous studies. The key to this is the introduction of a transformation, which overcomes the generalization difficulties faced by these studies. This chapter is based on the following published paper ([38]):

> Ichida, Y: Classification of nonnegative traveling wave solutions for the 1D degenerate parabolic equations, Discrete Contin. Dyn. Syst., Ser. B, **28** (2023), no. 2, 1116–1132.

9.1 Introduction

In this chapter, we consider the following spatial one-dimensional degenerate nonlinear parabolic equation

$$u_t = uu_{xx} - \gamma(u_x)^2 + ku^2 - \delta pu, \quad t > 0, \quad x \in \mathbb{R}, \tag{9.1.1}$$

where $0 < \gamma < 1$, $k > 0$, $1 < p \in \mathbb{R}$, and $\delta = 0$ or 1. This equation (9.1.1) can be obtained by setting $u(t, x) = (U(t, x))^p$ in equation

$$U_t = U^p(U_{xx} + \mu U) - \delta U, \quad t > 0, \quad x \in \mathbb{R} \tag{9.1.2}$$

with $\mu > 0$. Note that $\gamma = (p - 1)/p$ and $k = \mu p$ hold.

The equation (9.1.2) is also a kind of spatial 1D degenerate nonlinear parabolic equation. In addition, this equation with $\delta = 0$ is such an equation that has many phenomena in its background. See, for instance, [4, 32, 30, 62] and references therein for background

phenomena. For instance, in the curve shortening problem, we can see that the classical curvature flow equation $V = -\kappa$ corresponds to (9.1.2) in the case that $p = 2$ (see [5, 20, 22]). Here, we denote by κ and V the curvature and outward normal velocity of a curve, respectively. In addition, this equation arises in the modeling of the resistive diffusion of a force-free magnetic field in a plasma confined between two walls. See [46, 47] and references therein for derivation of equation (9.1.2) from plasma phenomena. Other examples include heat combustion, solar flares in astrophysics.

In the equation (9.1.2), there have been many studies on blow-up solutions, and the derivation of blow-up rates has been of particular mathematical interest. It is known that blow-up occurs in general higher dimensional problems, but the blow-up rate is not well understood (see [3, 61]). One of the intrinsic difficulties of this problem is U^p, which comes from degeneracy, and many problems still remain for the blow-up analysis of this type of equation, even in the spatial one-dimensional case (see [4, 62]). In the following, we will focus on problems in 1D.

We briefly review [5, 62], which also motivated our study. According to [5], the traveling wave solutions correspond to special self-similar solutions of curve shortening which evolves by rotating and contracting simultaneously. They gave the blow-up rate of (9.1.2) with $\delta = 0$ for $p \geq 2$ under periodic boundary condition and x is restricted to $x \in (-L, L)$. Self-similarity is known to play an important role in blow-up analysis, and it can be said that the problem of investigating the structure of traveling wave solutions was derived from this fact. In [62], Poon gave the upper and lower bounds of the blow-up rate of (9.1.2) with $\delta = 0$ for $p \geq 2$ under either the Dirichlet boundary condition or the periodic boundary condition and x is restricted to $x \in (-L, L)$. In particular, the equation (9.1.2) with $\delta = 1$ can be obtained by transformed solution of (9.1.2) with $\delta = 0$, and the traveling wave solution of this equation plays important roles in deriving the lower bound. More precisely, let $\tilde{U} = \tilde{U}(\tau, x)$ be the solution of (9.1.2) for $\delta = 1$ and $U = U(t, x)$ $(t \in (0, T))$ be the solution of (9.1.2) for $\delta = 0$, then the following relation of transformation is satisfied:

$$\tilde{U}(\tau, x) = (pT)^{\frac{1}{p}} e^{-\tau} U(t, x), \quad t = T(1 - e^{-p\tau}), \quad \tau \in (0, +\infty)$$

(see also [32, 62]).

Next, we briefly explain why considering traveling wave solutions leads to blow-up analysis, based on [5, 62] and references therein. The proof of the main theorem in [62] (e.g., Section 3 in [62]) suggests that investigating the evaluation of $\tilde{U}(\tau, 0)$ and behavior of $\tilde{U}(\tau, 0)$ for $\tau \to +\infty$ are the first steps in blow-up analysis. Under these symbols, let

$$U(\xi) = \tilde{U}(x - c\tau), \quad \xi = x - c\tau, \quad c > 0$$

be the traveling wave solution in (9.1.2), and we can consider the problem of investigating the behavior for $\xi \to -\infty$ corresponding to $\tau \to +\infty$. Therefore, based on the above explanation and discussion in [5, 62], it is important to classify the traveling wave solutions in (9.1.2). In particular, by focusing on the asymptotic behavior for $\xi \to -\infty$, it will provide a new perspective for future blow-up analysis (see also Remark 9.2.7).

With the motivation of contributing to the derivation of a more refined blow-up rate by examining in more detail the traveling wave solution studied by [62], in [32, 30], they restrict to $1 < p \in \mathbb{N}$, set $\mu = 1$, and give the classification of traveling wave solutions of (9.1.2) for both $\delta = 0$ and $\delta = 1$. Ichida-Sakamoto [32] shows that results on the classification (existence only for $p \in 2\mathbb{N}$, shapes, and asymptotic behavior) of (weak) traveling wave solutions are given by applying the dynamical system approach, the Poincaré compactification, and geometric methods for desingularization of vector fields called blow-up

technique (for instance, see Chapter 1 in this thesis and [14] for the details of the Poincaré compactification and blow-up technique). Here, the meaning of the classification of this solutions comes from the fact that we have revealed all dynamics to infinity of the ordinary differential equations (hereinafter, ODEs) obtained by introducing traveling wave coordinates by using these methods. In addition, Ichida-Matsue-Sakamoto [30] gave a refined asymptotic behavior, which was not obtained in the preceding work [32], by an appropriate asymptotic study and properties of the Lambert W function.

In Chapter 7 and Chapter 8 ([32, 30]), the following issues are specified as future main works.

- There is no discussion in general $p \in \mathbb{R}$. This is because, in using the blow-up technique, it is necessary to assume $p \in \mathbb{N}$ from its existing results [1, 8, 14]. It is difficult to extend these results and make them usable in the general case.
- In Chapter 7 ([32]), when p is odd, we face the problem of not being able to determine the dynamics in the neighborhood of the singularity points. To be more precise, it is a problem in which a new singularity point appears even if the singularity is desingularized by performing a blow-up transformation on a not hyperbolic equilibrium in the two-dimensional ODE system under its consideration. Therefore, it could not completely prove the existence of connecting orbits in this case, and gave a conclusion assuming the existence of orbits. This problem in the case where p is odd should be solved if the existence of the corresponding connecting orbits can be proved without facing a similar problem with $p \in \mathbb{N}$.

With overcoming these problems, we do not deal with equation (9.1.2) as it is, but rather with equation (9.1.1), which is obtained by transformation, as mentioned at the beginning of this section. That is, (9.1.1) is obtained by setting $u = U^p$ in (9.1.2), which is assumed $1 < p \in \mathbb{R}$. It is important to emphasize that by introducing this transformation, p is transferred to the coefficients from the degree. This is the key to not having to request $p \in \mathbb{N}$, as we will see in the analysis that follows. This transformation is also used in [2]. In [2], they investigate decay and blow-up of solutions in the initial-boundary value problem for general nonnegative initial functions.

In this chapter, in order to investigate the properties and structure of the nonnegative traveling wave solution of (9.1.2) in general $1 < p \in \mathbb{R}$, we will study its structure in (9.1.1). We then introduce the following change of variables:

$$\phi(\xi) = u(t, x), \quad \xi = x - ct, \quad 0 < c \in \mathbb{R}.$$

The equation of $\phi(\xi)$ solving (9.1.1) is then reduced to

$$\phi\phi'' = -c\phi' + \gamma(\phi')^2 - k\phi^2 + \delta p\phi, \quad \left({}' = \frac{d}{d\xi}, \quad {}'' = \frac{d^2}{d\xi^2} \right). \tag{9.1.3}$$

Then, (9.1.3) is equivalent to

$$\begin{cases} \phi' = \psi, \\ \psi' = -c\phi^{-1}\psi + \gamma\phi^{-1}\psi^2 - k\phi + \delta p, \end{cases} \qquad \left({}' = \frac{d}{d\xi} \right). \tag{9.1.4}$$

Since this system of ODEs has ϕ^{-1}, it turns out to have a singularity at $\phi = 0$, which is not easy to analyze about its dynamics. However, as shown in [31, 33, 32, 49, 50], it is possible to study the dynamics of these ODEs to infinity in the framework that combines Poincaré compactification (for instance, see Section 2 of [31] and [14, 33, 32, 49, 50] for

the details of it) and classical dynamical systems theory. Note that, unlike the literature cited above, we do not use blow-up technique in our analysis, and therefore do not include it in this framework. By using these methods, the whole dynamics on the phase space $\mathbb{R}^2$ including infinity (denoted by Poincaré disk) generated by the two-dimensional ODE (9.1.4) is obtained without assuming $p \in \mathbb{N}$. The results can be shown that the nonnegative traveling wave solutions corresponding to each connecting orbit in the Poincaré disk are classified. Thus, the existence of each traveling wave solution is revealed, and information about its shape and asymptotic behavior can be obtained.

The conclusions about the traveling wave solution in (9.1.1), obtained without requiring $p \in \mathbb{N}$, can be reflected in (9.1.2) by $u = U^p$. This means that we can obtain a generalized results without the restriction $p \in \mathbb{N}$ in the conclusion obtained for (9.1.2) ([32, 30]). This automatically proves the existence of unproven connecting orbits in the case that p is odd, which was an issue in these studies under considering nonnegative solutions.

These arguments may be unique to this type of equation. However, to the best of the author's knowledge, there is no study that classifies the typical and characteristic solutions of these equations by the dynamical systems approach. In this sense, we believe that the classification obtained in this chapter can make a significant contribution to future research on the derivation of the blow-up rate in (9.1.2), and lead to a deeper study of the solution structure of this equation.

This chapter is organized as follows. In the next section, we state the main results of this chapter. In Section 9.3, we obtain the dynamics of (9.1.4) on the Poincaré disk via Poincaré compactification and classical dynamical systems theory. The proof of Theorems will be completed in Section 9.4. In Section 9.5 is devoted to the concluding remarks.

9.2 Main results

Before, we state the main results of this chapter, we first state the definition of a quasi traveling wave with singularity for (9.1.1) as follows.

Definition 9.2.1
We say that a function $u(t,x) \equiv \phi(\xi)$ is a quasi traveling wave with singularity of (9.1.1) *if the function $u(t,x)$ is a quasi traveling wave of* (9.1.1) *on a semi-infinite interval such that ϕ reaches* 0 *and only right differentiation is possible and it becomes a constant at finite end point of the semi-infinite interval. More precisely, the function $\phi(\xi)$ is a solution of* (9.1.3) *on a semi-infinite interval $(\xi_*, +\infty)$ ($\phi(\xi) \in C^2(\xi_*, +\infty)$, $|\xi_*| < \infty$), and satisfies*

$$\lim_{\xi \searrow \xi_* + 0} \phi(\xi) = 0 \quad \text{and} \quad \lim_{\xi \searrow \xi_* + 0} \phi'(\xi) = C$$

with $C > 0$.

Remark 9.2.1
In the above definition, see Definition 2.1.2 (Definition 2 in [31]) and Definition 2.1 in [37] for the definition of a quasi traveling wave of (9.1.1) *on a semi-infinite interval. Furthermore, note that although this definition is similar to a quasi traveling wave with quenching as defined in these papers, the meaning of singularity is different. It is important to emphasize that a quasi traveling wave is not a general term.*

Next, we state the definition of a weak traveling wave solution with singularity for (9.1.1) as follows. Note that $u = 0$ is the trivial solution to this equation. This definition is an analogue of Definition 7.1.1 (Definition 1 in [32]).

Definition 9.2.2
Let $u(\xi)$ be a quasi traveling wave with singularity of (9.1.3) *on a semi-infinite interval (ξ_*, ∞) satisfying*

$$\lim_{\xi \searrow \xi_* + 0} u'(\xi) = C \quad \textit{and} \quad \lim_{\xi \searrow \xi_* + 0} u(\xi) = 0$$

with a positive constant C. Then, we say that a function

$$u^*(\xi) = \begin{cases} 0, & \xi \in (-\infty, \xi_*], \\ u(\xi), & \xi \in (\xi_*, +\infty) \end{cases}$$

is a weak traveling wave solution with singularity of (9.1.3). *Singularity here means having a point ξ_* that is not differentiable.*

The above Definition implies that $u^*(\xi)$ satisfies

$$\int_{\mathbb{R}} \left[u\varphi_\xi (c - u_\xi) + (\gamma + 1)(u_\xi)^2 \varphi - u^2(\varphi_{\xi\xi} + k\varphi) + \delta p u \varphi \right] d\xi = 0$$

for all $\varphi \in C_0^\infty(\mathbb{R})$.

Under these definitions, the main results of this chapter are described. Note that $\phi(\xi) = u(\xi)$ and $\phi'(\xi) = \psi(\xi) = u_\xi(\xi)$ hold. Hereinafter, note that the meaning of the symbol $f(\xi) \sim g(\xi)$ as $\xi \to a$ is as follows:

$$\lim_{\xi \to a} \left| \frac{f(\xi)}{g(\xi)} \right| = 1.$$

Theorem 9.2.1
Assume that $1 < p \in \mathbb{R}$, $k > 0$, $\mu > 0$, and $\delta = 0$. Then, for a given positive constant c, the equation (9.1.1) *has a family of weak traveling wave solutions with singularity (which corresponds to a family of the orbits of* (9.1.4)*). Moreover, each weak traveling wave solution with singularity $u(\xi)$ satisfies the following:*

- $\lim_{\xi \searrow \xi_* + 0} u(\xi) = \lim_{\xi \to +\infty} u(\xi) = \lim_{\xi \to +\infty} u'(\xi) = 0$, $\lim_{\xi \searrow \xi_* + 0} u'(\xi) = C$ *with a positive constant C.*
- $u(\xi) > 0$ *holds for $\xi \in (\xi_*, +\infty)$ and $u(\xi) = 0$ holds for $\xi \in (-\infty, \xi_*]$.*
- *There exists a constant $\xi_0 \in (\xi_*, +\infty)$ such that the following holds: $u'(\xi) > 0$ for $\xi \in (\xi_*, \xi_0)$, $u'(\xi_0) = 0$ and $u'(\xi) < 0$ for $\xi \in (\xi_0, +\infty)$.*

In addition, the asymptotic behavior of $u(\xi)$ for $\xi \searrow \xi_* + 0$ is

$$u(\xi) \sim A(\xi - \xi_*) \quad \text{as} \quad \xi \searrow \xi_* + 0, \tag{9.2.1}$$

where A is a positive constant, and the asymptotic behavior of $u(\xi)$ and $u'(\xi)$ for $\xi \to +\infty$ are

$$\begin{cases} u(\xi) \sim \dfrac{c}{k} \xi^{-1}, \\ u'(\xi) \sim -\dfrac{c}{k} \xi^{-2}, \end{cases} \qquad \text{as} \quad \xi \to +\infty. \tag{9.2.2}$$

Figure 9.2.1 shows the schematic pictures of the traveling wave solutions obtained in Theorem 9.2.1 and the following theorems.

From the result of the above theorem and the relations $U = u^{1/p}$ and $U' = p^{-1}U^{-p+1}u'$, the following holds for U. That is, the following follows immediately from the result of this theorem. The following result corresponds to a generalization of the results in Theorem 7.1.1 and Theorem 7.4.1 in this thesis (Theorem 1 and Theorem 4 of [32]).

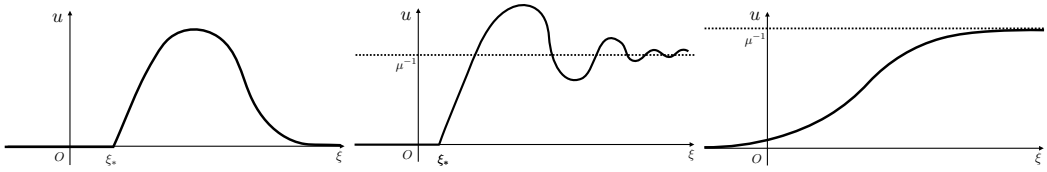

Figure 9.2.1: Schematic picture of the traveling wave solutions obtained in Theorems. Here it should be noted that the position of the singularity point ξ_* is not determined in our studies, however, they are shown in the figures for the convenience. [Left: The weak traveling wave solution with singularity in Theorem 9.2.1.] [Middle: The weak traveling wave solution with singularity in Theorem 9.2.2 in the case that $D < 0$.] [Right: The traveling wave solution on $\xi \in \mathbb{R}$ obtained in Theorem 9.2.3 in the case that $D > 0$.]

Corollary 9.2.1
Assume that $1 < p \in \mathbb{R}$, $k > 0$, $\mu > 0$, and $\delta = 0$. Then, for a given positive constant c, the equation (9.1.2) has a family of weak traveling wave solutions with quenching. Moreover, each weak traveling wave solution with quenching $U(\xi)$ satisfies the following:

- $\begin{cases} \lim\limits_{\xi \searrow \xi_* + 0} U(\xi) = 0, & \lim\limits_{\xi \to +\infty} U(\xi) = 0, \\ \lim\limits_{\xi \searrow \xi_* + 0} U'(\xi) = +\infty, & \lim\limits_{\xi \to +\infty} U'(\xi) = 0. \end{cases}$
- *$U(\xi) > 0$ holds for $\xi \in (\xi_*, +\infty)$ and $U(\xi) = 0$ holds for $\xi \in (-\infty, \xi_*]$.*
- *There exists a constant $\xi_0 \in (\xi_*, +\infty)$ such that the following holds: $U'(\xi) > 0$ for $\xi \in (\xi_*, \xi_0)$, $U'(\xi_0) = 0$ and $U'(\xi) < 0$ for $\xi \in (\xi_0, +\infty)$.*

In addition, the asymptotic behavior of $U(\xi)$ and $U'(\xi)$ for $\xi \searrow \xi_* + 0$ are

$$\begin{cases} U(\xi) \sim A_1 (\xi - \xi_*)^{\frac{1}{p}}, \\ U'(\xi) \sim A_2 (\xi - \xi_*)^{-\frac{p-1}{p}}, \end{cases} \quad \text{as} \quad \xi \searrow \xi_* + 0, \tag{9.2.3}$$

where A_1 and A_2 are positive constants, and the asymptotic behavior of $U(\xi)$ and $U'(\xi)$ for $\xi \to +\infty$ are

$$\begin{cases} U(\xi) \sim \left(\dfrac{k}{c}\xi\right)^{-\frac{1}{p}}, \\ U'(\xi) \sim -\dfrac{1}{p}\left(\dfrac{k}{c}\right)^{-\frac{1}{p}} \xi^{-\frac{p+1}{p}}, \end{cases} \quad \text{as} \quad \xi \to +\infty. \tag{9.2.4}$$

Remark 9.2.2
A several remarks about the results obtained in Corollary 9.2.1. As mentioned above, this result is a generalization of the result of previous studies. See Fig. 7.1.1, Fig. 7.2.2 and Fig. 7.4.4 in Chapter 7 (Fig. 1, Fig. 4 and Fig. 8 in [32]) for schematic pictures of this solution. Note that (9.2.4) is consistent with the result obtained by restricting to $\mu = 1$ (i.e., $k = p$) and $p \in \mathbb{N}$ in Theorem 7.1.1 and Theorem 7.4.1 in this thesis (Theorem 1 and Section 4.1 of [32]). On the other hand, (9.2.3) differs in the exponential part from $U'(\xi)$ obtained in Theorem 7.1.1 (Theorem 1 of [32]). The reason for this is that, after the publication of it, we chose more appropriate principal terms in the computational process of deriving the asymptotic behavior, which resulted in a higher accuracy. This improvement has already been introduced into [35, 37]. However, the underlying idea is similar to the previous ones.

Remark 9.2.3
It should be emphasized that, as will be discussed in Section 9.5, the only nonnegative traveling wave solution to (9.1.2) *with* $\delta = 0$ *is the one concluded in Corollary 9.2.1.*

Theorem 9.2.2
Assume that $1 < p \in \mathbb{R}$, $k > 0$, $\mu > 0$, *and* $\delta = 1$. *Then, for a given positive constant* c, *the equation* (9.1.1) *has a family of weak traveling wave solutions with singularity (which corresponds to a family of the orbits of* (9.1.4)*). Moreover, each weak traveling wave solution with singularity* $u(\xi)$ *satisfies the following:*

- $\lim_{\xi \searrow \xi_* + 0} u(\xi) = 0$, $\lim_{\xi \to +\infty} u(\xi) = \mu^{-1}$, $\lim_{\xi \searrow \xi_* + 0} u'(\xi) = C$ *with a positive constant* C.
- $u(\xi) > 0$ *holds for* $\xi \in (\xi_*, +\infty)$ *and* $u(\xi) = 0$ *holds for* $\xi \in (-\infty, \xi_*]$.

In addition, the asymptotic behavior of $u(\xi)$ *for* $\xi \searrow \xi_* + 0$ *is expressed as* (9.2.1), *and the asymptotic behavior of* $u(\xi)$ *for* $\xi \to +\infty$ *is*

$$u(\xi) \sim \frac{1}{\mu} \sim \begin{cases} B_1 e^{\omega_1 \xi} + B_2 e^{\omega_2 \xi} + \dfrac{1}{\mu}, & (D > 0), \\ (B_3 \xi + B_4) e^{\omega \xi} + \dfrac{1}{\mu}, & (D = 0), \\ e^{-\frac{\mu c}{2} \xi} \left(B_5 \cdot \sin[\frac{\sqrt{|D|}}{2} \xi] + B_6 \cdot \cos[\frac{\sqrt{|D|}}{2} \xi] \right) + \dfrac{1}{\mu}, & (D < 0), \end{cases} \quad \text{as} \quad \xi \to +\infty \tag{9.2.5}$$

where B_j $(1 \le j \le 6)$ *are constants and*

$$\omega_1 = \frac{-\mu c + \sqrt{D}}{2} < 0, \quad \omega_2 = \frac{-\mu c - \sqrt{D}}{2} < 0, \quad \omega = -\frac{\mu c}{2} < 0, \quad D = \mu^2 c^2 - 4k.$$

As can be seen from the proof oh this theorem, which is omitted in the statement of the theorem, the asymptotic behavior of $u'(\xi)$ for $\xi \to +\infty$ can be displayed explicitly (see [32]). From the result of the above theorem and the relation $u = U^p$ between u and U, we can see that, in the same way as in Corollary 9.2.1, the following follows immediately.

Corollary 9.2.2
Assume that $1 < p \in \mathbb{R}$, $k > 0$, $\mu > 0$, *and* $\delta = 1$. *Then, for a given positive constant* c, *the equation* (9.1.2) *has a family of weak traveling wave solutions with quenching. Moreover, each weak traveling wave solution with quenching* $U(\xi)$ *satisfies the following:*

- $\lim_{\xi \searrow \xi_* + 0} U(\xi) = 0$, $\lim_{\xi \to +\infty} U(\xi) = \mu^{-\frac{1}{p}}$, $\lim_{\xi \searrow \xi_* + 0} U'(\xi) = +\infty$.
- $U(\xi) > 0$ *holds for* $\xi \in (\xi_*, +\infty)$ *and* $U(\xi) = 0$ *holds for* $\xi \in (-\infty, \xi_*]$.

In addition, the asymptotic behavior of $U(\xi)$ *for* $\xi \searrow \xi_* + 0$ *is expressed as* (9.2.3), *and the asymptotic behavior of* $U(\xi)$ *for* $\xi \to +\infty$ *is*

$$U(\xi) \sim \mu^{-\frac{1}{p}} \sim \begin{cases} \left(B_1 e^{\omega_1 \xi} + B_2 e^{\omega_2 \xi} + \dfrac{1}{\mu} \right)^{\frac{1}{p}}, & (D > 0), \\ \left((B_3 \xi + B_4) e^{\omega \xi} + \dfrac{1}{\mu} \right)^{\frac{1}{p}}, & (D = 0), \\ \left(e^{-\frac{\mu c}{2} \xi} \left(B_5 \cdot \sin[\frac{\sqrt{|D|}}{2} \xi] + B_6 \cdot \cos[\frac{\sqrt{|D|}}{2} \xi] \right) + \dfrac{1}{\mu} \right)^{\frac{1}{p}}, & (D < 0), \end{cases} \tag{9.2.6}$$

where B_j $(1 \le j \le 6)$ *are constants.*

Remark 9.2.4
This result is also a generalization of the results in Theorem 7.1.2 and Theorem 7.4.2 in this thesis (Theorem 2 and Theorem 5 of [32]). See Fig. 7.1.1, Fig. 7.2.2 and Fig. 7.4.4 in Chapter 7 (Fig. 1, Fig. 4 and Fig. 8 in [32]) for schematic pictures of this solution. Note that for the principal term $\mu^{-1/p}$ in (9.2.6)*, if we set $\mu = 1$, the result is the same as that of Theorem 7.1.2 obtained in this thesis (Theorem 2 obtained in [32]). Although the asymptotic behavior of* (9.2.6) *does not seem to fully match the results of [32], the principal term does. It should be possible to confirm this consistency by examining the higher oder. However, this is a subject for future work.*

Theorem 9.2.3
Assume that $1 < p \in \mathbb{R}$, $k > 0$, $\mu > 0$, and $\delta = 1$. Then, for a given positive constant c, the equation (9.1.1) *has a traveling wave solution (which corresponds to an orbit of* (9.1.4)*). Moreover, its traveling wave solution $u(\xi)$ satisfies the following:*

- $\lim_{\xi \to -\infty} u(\xi) = 0, \quad \lim_{\xi \to +\infty} u(\xi) = \mu^{-1}$.
- $u(\xi) > 0$ *holds for* $\xi \in \mathbb{R}$.

In addition, the asymptotic behavior of $u(\xi)$ for $\xi \to \infty$ is expressed as (9.2.5)*, and the asymptotic behavior of $u(\xi)$ for $\xi \to -\infty$ is*

$$u(\xi) \sim \frac{Mc^2 e^{\frac{p}{c}\xi}}{M(\mu c^2 + 1)e^{\frac{p}{c}\xi} - 1} \quad \text{as} \quad \xi \to -\infty, \tag{9.2.7}$$

where $M < 0$ is a constant that depends on the initial state $\phi(0) = \phi_0$.

From the result of the above theorem and the relation $u = U^p$ between u and U, we can see that, in the same way as in Corollary 9.2.1 and Corollary 9.2.2, the following holds.

Corollary 9.2.3
Assume that $1 < p \in \mathbb{R}$, $k > 0$, $\mu > 0$, and $\delta = 1$. Then, for a given positive constant c, the equation (9.1.2) *has a traveling wave solution. Moreover, this traveling wave solution $U(\xi)$ satisfies the following:*

- $\lim_{\xi \to -\infty} U(\xi) = 0, \quad \lim_{\xi \to +\infty} U(\xi) = \mu^{-\frac{1}{p}}$.
- $U(\xi) > 0$ *holds for* $\xi \in \mathbb{R}$.

In addition, the asymptotic behavior of $U(\xi)$ for $\xi \to \infty$ is expressed as (9.2.6)*, and the asymptotic behavior of $U(\xi)$ for $\xi \to -\infty$ is*

$$U(\xi) \sim \left(\frac{Mc^2 e^{\frac{p}{c}\xi}}{M(\mu c^2 + 1)e^{\frac{p}{c}\xi} - 1} \right)^{\frac{1}{p}} \quad \text{as} \quad \xi \to -\infty, \tag{9.2.8}$$

where $M < 0$ is a constant that depends on the initial state $\phi(0) = \phi_0$.

Remark 9.2.5
This result is also a generalization of the result in Theorem 8.1.2 in this thesis (Theorem 2 of [30]). See Fig. 8.2.1 (Fig. 1 in [30]) for schematic picture of this solution. Note that (9.2.8) *is consistent with the result obtained in Theorem 8.1.2 (Theorem 2 of [30]).*

Remark 9.2.6
It should be emphasized that there are only two type of nonnegative traveling wave solutions in (9.1.2) *with* $\delta = 1$*, which are concluded in Corollary 9.2.2 and Corollary 9.2.3. The reason for this will be discussed in Section 9.5.*

Remark 9.2.7
As mentioned in Section 9.1, the derivation of the asymptotic behavior of the obtained traveling wave solutions for $\xi \searrow -\infty$ *or* $\xi \searrow \xi_* + 0$ *are expected to contribute to a more accurate derivation of the blow-up rate. As can be also seen from the results in [62], the results in Theorem 9.2.2 and Corollary 9.2.2 can be used for blow-up analysis (see also top right of Figure 9.2.1). To the best of the authors' knowledge, no conclusion has given the existence of* $\xi_* > -\infty$ *or their asymptotic behavior there, except for our previous works Chapter 7 and Chapter 8 ([32, 30]).*

Remark 9.2.8
The stability of the (weak) traveling wave solutions obtained by main results is not known in the framework of the analysis in this chapter. It is necessary that more detailed (and hard) analysis in order to study the stability. However, since the main purpose of this chapter is to investigate the existence, shape and asymptotic behavior of (weak) traveling wave solutions of (9.1.2) *from the dynamical system view point (especially, the Poincaré compactification), we leave it open here.*

9.3 Dynamics on the Poincaré disk of (9.1.4)

In this section, we study $\mathbb{R}^2 \cup \{(\phi, \psi) \mid \|(\phi, \psi)\| = +\infty\}$ called the dynamics on the Poincaré disk, by the Poincaré compactification. The analysis used in this section is basically the same in idea as the analysis in Chapter 7 and Chapter 8 ([32, 30]), except that the blow-up technique is not used. For the reader's convenience, the calculation process is described here.

9.3.1 Dynamics near finite equilibria

First, we study the dynamics near finite equilibria of (9.1.4). If $\delta = 1$, then this equation has the equilibrium $E_1 : (\phi, \psi) = (\mu^{-1}, 0)$ for $\{\phi > 0\}$. Note that $\phi = 0$ has singularity. The Jacobian matrix of the vector field (9.1.4) at E_1 is

$$E_1 : \begin{pmatrix} 0 & 1 \\ -k & -c\mu \end{pmatrix}.$$

Let J_1 be this matrix. Then, the behavior of the solution around E_1 is different by the sign of $D = \mu^2 c^2 - 4k$. For instance, the matrix J_1 has the real distinct eigenvalues if $D > 0$ and other cases can be concluded similarly. In addition, if $c > 0$, then the real part of all eigenvalues of J_1 are negative. Therefore, we determine that the equilibrium E_1 is asymptotically stable. E_1 is a stable node for $D \geq 0$ and is a stable focus (spiral sink) for $D < 0$.

Second, in order to study the dynamics of (9.1.4) on the Poincaré disk, we desingularize it by the time-scale desingularization

$$ds/d\xi = \phi^{-1}. \tag{9.3.1}$$

Note that this allows us to include $\phi = 0$. Since we are considering a nonnegative solution, i.e., $\phi \geq 0$, the direction of the time does not change via this desingularization in this

region. Then we have

$$\begin{cases} \phi' = \phi\psi, \\ \psi' = -c\psi + \gamma\psi^2 - k\phi^2 + \delta p\phi, \end{cases} \qquad \left(' = \frac{d}{ds}\right). \tag{9.3.2}$$

Remark 9.3.1
It should be noted that the time scale desingularization (9.3.1) *is simply multiplying the vector field by* ϕ*. Then, except the singularity* $\{\phi = 0\}$*, the solution curves of the system (vector field) remain the same but are parameterized differently. Still, we refer to Section 7.7 of [44] and references therein for the analytical treatments of desingularization with the time rescaling. In what follows, we use the similar time rescaling (re-parameterization of the solution curves) repeatedly to desingularize the vector fields.*

If $\delta = 0$, the system (9.3.2) has the equilibria

$$E_0 : (\phi, \psi) = (0, 0), \quad E_2 : (\phi, \psi) = \left(0, c\gamma^{-1}\right), \quad 0 < \gamma < 1.$$

The Jacobian matrices of the vector field (9.3.2) at these equilibria are

$$E_0 : \begin{pmatrix} 0 & 0 \\ 0 & -c \end{pmatrix}, \quad E_2 : \begin{pmatrix} c\gamma^{-1} & 0 \\ 0 & c \end{pmatrix}.$$

Therefore, E_2 is a source since the linearized eigenvalues are $c\gamma^{-1} > 0$ and $c > 0$ with corresponding eigenvectors $(1, 0)^T$ and $(0, 1)^T$, respectively. Then, the center manifold theory is applicable to study the dynamics near E_0 (for instance, see [9]). We can obtain the approximation of the (graph of) center manifold as follows:

$$\{(\phi, \psi) \mid \psi(s) = -kc^{-1}\phi^2 + O(\phi^4)\}. \tag{9.3.3}$$

Hence, the dynamics of (9.3.2) near $E_0 : (0, 0)$ is topologically equivalent to the dynamics of the following equation:

$$\phi'(s) = -kc^{-1}\phi^3 + O(\phi^5) \tag{9.3.4}$$

(see Subsection 3.2 of [32] for more details of this process).

On the other hand, the system (9.3.2) has the equilibria

$$E_0 : (\phi, \psi) = (0, 0), \quad E_1 : (\phi, \psi) = (\mu^{-1}, 0), \quad E_2 : (\phi, \psi) = (0, c\gamma^{-1}), \quad 0 < \gamma < 1$$

in the case that $\delta = 1$. E_1 is described above. The Jacobian matrices of the vector field (9.3.2) at these equilibria are

$$E_0 : \begin{pmatrix} 0 & 0 \\ p & -c \end{pmatrix}, \quad E_2 : \begin{pmatrix} c\gamma^{-1} & 0 \\ p & c \end{pmatrix}.$$

Note that the behavior of solutions around E_0 and E_2 for $\delta = 0$ and $\delta = 1$ are different. E_2 is a source since the linearized eigenvalues are $c\gamma^{-1} > 0$ and $c > 0$ with corresponding eigenvectors $(1, c^{-1}p(\gamma^{-1} - 1)^{-1})^T$ and $(0, 1)^T$, respectively. By the same argument as in Subsection 3.2 of [32] and Section 2 of [30], we can study the dynamics around the equilibrium E_0 for $\delta = 1$. We conclude that the approximation of the (graph of) center manifold is

$$\left\{(\phi, \psi) \mid \psi(s) = \frac{p}{c}\phi - \frac{p}{c^3}(\mu c^2 + 1)\phi^2 + O(\phi^3)\right\} \tag{9.3.5}$$

and the dynamics of (9.3.2) near E_0 is topologically equivalent to the dynamics of the following equation:

$$\phi'(s) = \frac{p}{c}\phi^2 - \frac{p}{c^3}(\mu c^2 + 1)\phi^3 + O(\phi^4). \tag{9.3.6}$$

These results give us the dynamics near finite equilibria of (9.3.2).

From the next subsection, we can consider the dynamics of this equation on the charts $\overline{U}_j$ $(j = 1, 2)$ and $\overline{V}_2$ since we are considering $\phi \geq 0$.

9.3.2 Dynamics on the chart $\overline{U}_2$

To obtain the dynamics on the chart $\overline{U}_2$, we introduce the coordinates (λ, x) by the formulas

$$\phi(s) = x(s)/\lambda(s), \quad \psi(s) = 1/\lambda(s).$$

In this chart, it corresponds to $\phi \to 0$ and $\psi \to +\infty$ and the direction in which x is positive corresponds to the direction in which ϕ is positive. For a geometric image, see Fig. 2 of [31] and Fig. 2 of [32]. Then, we have

$$\begin{cases} \lambda' = c\lambda - \gamma + kx^2 - \delta p\lambda x, \\ x' = p^{-1}\lambda^{-1}x + cx + k\lambda^{-1}x^3 - \delta p x^2. \end{cases} \tag{9.3.7}$$

By using the time-scale desingularization $d\tau/ds = \lambda^{-1}$, we can obtain

$$\begin{cases} \lambda_\tau = c\lambda^2 - \gamma\lambda + k\lambda x^2 - \delta p\lambda^2 x, \\ x_\tau = p^{-1}x + c\lambda x + kx^3 - \delta p\lambda x^2, \end{cases} \tag{9.3.8}$$

where $\lambda_\tau = d\lambda/d\tau$ and $x_\tau = dx/d\tau$. The equilibrium of the system (9.3.8) on $\{\lambda = 0\}$ is $E_3 : (\lambda, x) = (0, 0)$. E_3 is a saddle since the linearized eigenvalues are $-\gamma$ and p^{-1} with corresponding eigenvectors $(1, 0)^T$ and $(0, 1)^T$, respectively.

Remark 9.3.2
A similar argument shows that the origin is also the equilibrium in the argument of [32]. However, it is essentially different from the present result in that all components of the Jacobi matrix at this equilibrium are zero. In [32], the blow-up technique was used to solve this problem. On the other hand, since E_3 is a hyperbolic, it should be emphasized that we were able to study the behavior of the solution around this point without using this technique. This is undoubtedly one of the major factors that allow us to investigate without imposing $p \in \mathbb{N}$.

9.3.3 Dynamics on the chart $\overline{V}_2$

In this chart, it corresponds to $\phi \to 0$ and $\psi \to -\infty$ and the direction in which x is negative corresponds to the direction in which ϕ is positive. The change of coordinates

$$\phi(s) = -x(s)/\lambda(s), \quad \psi(s) = -1/\lambda(s)$$

give the projected dynamics of (9.3.2) on the chart $\overline{V}_2$:

$$\begin{cases} \lambda_\tau = c\lambda^2 + \gamma\lambda - k\lambda x^2 - \delta p\lambda^2 x, \\ x_\tau = -p^{-1}x + c\lambda x - kx^3 - \delta p\lambda x^2, \end{cases} \tag{9.3.9}$$

where τ is the new time introduced by $d\tau/ds = \lambda^{-1}$. The equilibrium of the system (9.3.9) on $\{\lambda = 0\}$ is $E_4 : (\lambda, x) = (0, 0)$. Eigenvalues of the the linearized matrix are γ and $-p^{-1}$ with corresponding eigenvectors $(1, 0)^T$ and $(0, 1)^T$, respectively. Therefore, the equilibrium E_4 is a saddle.

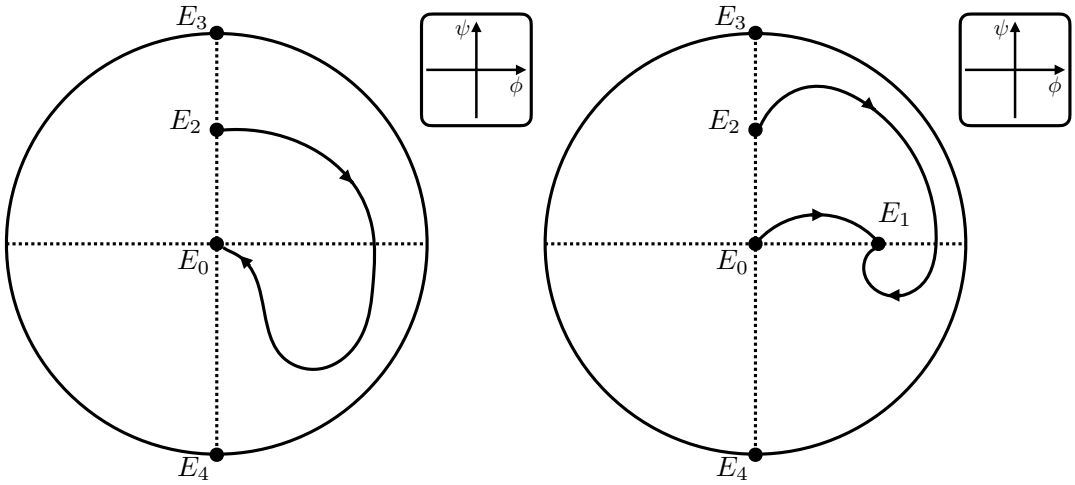

Figure 9.3.1: Schematic pictures of the dynamics on the Poincaré disk in the case that $\delta = 0$ or 1, $1 < p \in \mathbb{R}$. [Left: Case $\delta = 0$.] [Right: Case $\delta = 1$.]

9.3.4 Dynamics on the chart $\overline{U}_1$

In this chart, it corresponds to $\phi \to +\infty$ and $\psi \to 0$. The transformations $\phi(s) = 1/\lambda(s)$, $\psi(s) = x(s)/\lambda(s)$, and time-rescaling $d\tau/ds = \lambda^{-1}$ yield

$$\begin{cases} \lambda_\tau = -\lambda x, \\ x_\tau = -c\lambda x - p^{-1}x^2 - k + \delta p\lambda. \end{cases} \tag{9.3.10}$$

This system has no equilibria. It is important to emphasize that the following holds:

$$x_\tau\big|_{\lambda=0} = -p^{-1}x^2 - k < 0.$$

9.3.5 Dynamics and connecting orbits on the Poincaré disk

Combining the dynamics on the charts $\overline{U}_j$ $(j = 1, 2)$ and $\overline{V}_2$, we can obtain the dynamics on the Poincaré disk that is equivalent to the dynamics of (9.1.4) (or (9.3.2)) (see also Figure 9.3.1).

The purpose of this subsection is to prove the existence of connecting orbits. Before we do so, we will give some remarks about disks.

Remark 9.3.3
In Figure 9.3.1, we need to be careful about the handling of the point E_0. A note on this treatment is given for the reader's convenience, although it is a reproduction of [32, 30]. When we consider the parameter s on the disk, E_0 is the equilibrium of (9.3.2)*. However, E_0 is a point on the line $\{\phi = 0\}$ with singularity about the parameter ξ. We see that $d\phi/d\psi$ takes the same values on the vector fields defined by* (9.1.4) *and* (9.3.2) *except the singularity $\{\phi = 0\}$. If the trajectories start (resp. come in) the equilibrium E_0 about the parameter s, then they start from (resp. come in) the point E_0 about ξ. This is also the case for E_2.*

Let us prepare the symbols used in this subsection as follows:

- The set Φ denotes $\Phi = \{(\phi, \psi) \in \mathbb{R}^2 \cup \{\|(\phi, \psi)\| = +\infty\}\}$.

- $\mathcal{W}^{cs}(E_0)$ denotes the center-stable manifold of E_0 in the dynamical system (9.3.2) for $\delta = 0$. From Remark 9.3.3, $\mathcal{W}^{cs}(E_0)$ inherits the center-stable manifold of the singularity E_0 in the dynamical system (9.1.4) for $\delta = 0$.
- $\mathcal{W}^{cu}(E_0)$ denotes the center-unstable manifold of E_0 in the dynamical system (9.3.2) for $\delta = 1$. From Remark 9.3.3, $\mathcal{W}^{cu}(E_0)$ inherits the center-unstable manifold of E_0 in the dynamical system (9.1.4) for $\delta = 1$.
- $\mathcal{W}^{s}(E_1)$ denotes the stable manifold of E_1 in the dynamical system (9.1.4) for $\delta = 1$.
- $\mathcal{W}^{u}(E_2)$ denotes the unstable manifold of E_2 in the dynamical system (9.3.2) for both $\delta = 0$ and $\delta = 1$. From Remark 9.3.3, $\mathcal{W}^{u}(E_2)$ inherits the unstable manifold of the singularity E_2 in the dynamical system (9.1.4) for both $\delta = 0$ and $\delta = 1$.

Proposition 9.3.1
Assume that $\delta = 0$ or 1, $1 < p \in \mathbb{R}$, $\gamma = (p-1)/p$, $\mu > 0$, and $k = p\mu$. Then, the dynamics on the Poincaré disk of the system (9.1.4) *is expressed as Figure 9.3.1.*

Proof. (I). First, we shall prove the existence of trajectories between E_2 and E_0 that starts from the points on $\mathcal{W}^{u}(E_2)$ and reaches the points on $\mathcal{W}^{cs}(E_0)$ for $\delta = 0$. Since $\{\phi = 0\}$ is invariant in (9.3.2), any trajectory starting from the points in $\{(\phi, \psi) \in \Phi \mid \phi > 0\}$ cannot go to $\{(\phi, \psi) \in \Phi \mid \phi < 0\}$. Let us consider the trajectories starting from the points on $\mathcal{W}^{u}(E_2)$. Then, as in [32], from the Poincaré-Bendixson theorem and Remark 9.3.3, we know that these trajectories can only go to the points on $\mathcal{W}^{cs}(E_0)$ in (9.3.2). Here, as mentioned in Remark 9.3.3, since $d\phi/d\psi$ takes the same values on the vector fields defined by (9.1.4) and (9.3.2), we can see that these trajectories possessed by (9.3.2) is also inherited by (9.1.4). Thus, it is proved that there exists the connecting orbits between E_2 and E_0 for $\delta = 0$.
(II). Second, we shall prove the existence of trajectories between E_2 and E_1 that starts from the points on $\mathcal{W}^{u}(E_2)$ and reaches the points on $\mathcal{W}^{s}(E_1)$ for $\delta = 1$. From the discussion in (I), any trajectory starting from the points on $\mathcal{W}^{u}(E_2)$ cannot go to $\{(\phi, \psi) \mid \phi < 0\}$, and can only go to the points on $\mathcal{W}^{s}(E_1)$. Thus, we conclude that there exists the connecting orbits between E_2 and E_1 for $\delta = 1$.
(III). Finally, from the discussion in Remark 9.3.3 and (II), we can see that the trajectory starting from the points on $\mathcal{W}^{cu}(E_0)$ must go to the points on $\mathcal{W}^{s}(E_1)$.

Therefore, we prove that there exists the connecting orbits between E_0 and E_1 for $\delta = 1$. □

9.4 Proof of theorems

In this section, we prove our main results. If the initial data are located on $\Phi \backslash \{\phi < 0\}$, the existence of the solutions follows from the standard theory for the ODEs. Therefore, we consider the existence of the trajectories that connect equilibria and detailed dynamics near the equilibria on the Poincaré disk and their asymptotic behavior. Note from the proof of Proposition 9.3.1 that there are no orbits that pass through the ψ-axis, so there are no sign-changing solutions.

9.4.1 Proof of Theorem 9.2.1

The proof of existence of the connecting orbits between E_2 and E_0 for $\delta = 0$ is obtained in Proposition 9.3.1. Therefore, there exists a family of the quasi traveling waves with

singularity which corresponds to a family of the orbits of (9.1.4). By considering this result together with Definition 9.2.2, (9.1.1) has a family of weak traveling wave solutions with singularity. Moreover, these trajectories exist in $\{\phi \geq 0\}$, $u > 0$ holds for $\xi \in (\xi_*, \infty)$.

Next, we prove the existence of a constant $\xi_0 \in (\xi_*, \infty)$. The proof is presented in the same way as the proof of Theorem 1 in [32].

Then, we shall compute the asymptotic behavior of the trajectories near the equilibria E_2 and E_0. Note that the basic idea is the same as the proof of Theorem 1 in [32], however, that the ODEs we are dealing with are different.

Let us derive (9.2.1). The solutions around E_2 are approximated as

$$\begin{cases} \phi(s) = C_1 e^{\frac{c}{\gamma}s}(1 + o(1)), \\ \psi(s) = C_2 e^{cs}(1 + o(1)) + \dfrac{c}{\gamma} \end{cases}$$

with constants C_j $(j = 1, 2)$. Using this equation, we obtain

$$\frac{ds}{d\xi} = \phi^{-1} = \left\{ C_1 e^{\frac{c}{\gamma}s}(1 + o(1)) \right\}^{-1} \sim C_3 e^{-\frac{c}{\gamma}s} \quad \text{as} \quad s \to -\infty.$$

Here, note that the meaning of the symbol $F(s) \sim G(s)$ as $s \to -\infty$ is as follows:

$$\lim_{s \to -\infty} \left| \frac{F(s)}{G(s)} \right| = 1.$$

From this result, we can obtain $d\xi/ds \sim C_4 e^{\frac{c}{\gamma}s}$. This yields $\xi(s) \sim C_5 e^{\frac{c}{\gamma}s} + C_6$ $(C_6 \in \mathbb{R})$. Set

$$\xi_* = \lim_{s \to -\infty} \xi(s),$$

then we have

$$\xi - \xi_* \sim C_7 e^{\frac{c}{\gamma}s} \quad \text{as} \quad s \to -\infty$$

with constants C_j in the same discussion as [31, 33, 32, 50]. Therefore, we obtain

$$\begin{aligned} &\phi(\xi) = C_1 e^{\frac{c}{\gamma}s}(1 + o(1)) \sim C_1 e^{\frac{c}{\gamma}} \sim C_8(\xi - \xi_*) \quad \text{as} \quad \xi \searrow \xi_* + 0, \\ &\psi(\xi) = C_2 e^{cs}(1 + o(1)) + \frac{c}{\gamma} \sim \frac{\gamma}{c} \quad \text{as} \quad \xi \searrow \xi_* + 0. \end{aligned}$$

Since the trajectories are lying on $\{\phi > 0\}$, it holds that $C_8 > 0$. By using $u(\xi) = \phi(\xi)$ and $u_\xi = \psi(\xi)$, we can derive (9.2.1).

Finally, we shall derive (9.2.2). If the initial value is on the center manifold, the solution around E_0 on Poincaré disk has the form

$$\begin{cases} \phi(s) = \sqrt{\dfrac{1}{\dfrac{2k}{c}s - A_1}} = \left(\dfrac{2k}{c}s - A_1 \right)^{-\frac{1}{2}}, \\ \psi(s) = -\dfrac{k}{c}\left(\dfrac{2k}{c}s - A_1 \right)^{-1} = -\dfrac{k}{2ks - cA_1}. \end{cases} \tag{9.4.1}$$

Since the initial value $\phi(0)$ is located on $\{\phi > 0\}$, it holds that $A_1 < 0$. These results follow from (9.3.3) and (9.3.4). We then have

$$\frac{ds}{d\xi} = \phi^{-1} = \left(\frac{2k}{c}s - A_1 \right)^{\frac{1}{2}}.$$

Therefore, there exists a solution $s(\xi)$ such that the following holds:

$$s(\xi) = \frac{k}{2c}\xi^2 + A_2\xi + \frac{c}{2k}A_2^2 + \frac{c}{2k}A_1 \sim \frac{k}{2c}\xi^2 \quad \text{as} \quad \xi \to +\infty \tag{9.4.2}$$

with constants A_j. Substituting (9.4.2) into (9.4.1), we have

$$\begin{cases} \phi(\xi) = \left(\dfrac{2k}{c}s - A_1\right)^{-\frac{1}{2}} \sim \dfrac{c}{k}\xi^{-1}, \\ \psi(\xi) \sim -\dfrac{k}{c}\cdot\left(\dfrac{k^2}{c^2}\xi^2\right)^{-1} = -\dfrac{c}{k}\xi^{-2}, \end{cases} \qquad \text{as} \quad \xi \to +\infty.$$

In addition, we can see that $\phi' \sim \psi$ as $\xi \to +\infty$ holds. By using $u(\xi) = \phi(\xi)$ and $u_\xi = \psi(\xi)$, we can derive (9.2.2). This completes the proof. □

9.4.2 Proof of Theorem 9.2.2

The same arguments as in Theorem 9.2.1 can be used to obtain the existence of a family of weak traveling wave solutions with singularity and information about their shape. Then, all that remains to be shown is to derive (9.2.1) and (9.2.5). By focusing on E_1, (9.2.5) can be proved in the same way as proof of Theorem 2 in [32].

Finally, let us derive (9.2.1) in this case. Note that this is the same conclusion as Theorem 9.2.1, however, there is a difference in the solutions around E_2 since the linearized matrix in E_2 is different for $\delta = 0$ and $\delta = 1$. They are approximated as

$$\begin{cases} \phi(s) = A_1 e^{\frac{c}{\gamma}s}, \\ \psi(s) = A_1\dfrac{p(p-1)}{c}e^{\frac{c}{\gamma}s} + A_2 e^{cs} + \dfrac{c}{\gamma} \sim \dfrac{c}{\gamma}, \end{cases} \qquad \text{as} \quad s \to -\infty.$$

From this result, (9.2.1) can be shown in the same way as in the previous subsection (see Subsection 9.4.1). This completes the proof. □

9.4.3 Proof of Theorem 9.2.3

The same arguments as in Theorem 9.2.1 and Theorem 9.2.2 can be used to obtain the existence of a traveling wave solution and information about its shape. Therefore, we shall derive (9.2.7). The proof is almost the same as in [30]. However, there are some parts that are different. We briefly reproduce the proof and describe it below for the reader's convenience.

First we set $w(s) = \phi(s)^{-1} > 0$. With the aid of (9.3.6), we have

$$w'(s) = -\frac{p}{c} + \frac{p}{c^3}(\mu c^2 + 1)w^{-1} = A + Bw^{-1}, \tag{9.4.3}$$

where $A = -pc^{-1} < 0$ and $B = c^{-3}p(\mu c^2 + 1) > 0$. These are consistent with the results obtained in [30] when $\mu = 1$. The solution of (9.4.3) satisfies the following:

$$-(1 + Aw/B)e^{-\left(\frac{A}{B}w+1\right)} = -AB^{-1}e^{-\frac{A^2}{B}s - \frac{A^2C_1+B}{B}}$$

since the dynamics of $\phi(s)$ near 0 is our interest. That is, $w(s)$ is sufficiently large, which implies that $AB^{-1}w + 1 < 0$. Here C_1 is a constant. By using $w = \phi^{-1}$ and the Lambert W function (see [30] and references therein), we obtain

$$\phi(s) = [-A^{-1}B\{W(E(s)) + 1\}]^{-1}, \quad E(s) = -AB^{-1}e^{-\frac{A^2}{B}s - \frac{A^2C_1+B}{B}}.$$

We consequently have

$$\frac{ds}{d\xi} = \phi^{-1} = -\frac{B}{A}\{W(E(s)) + 1\}. \tag{9.4.4}$$

Second, we shall prove

$$\xi(s) \to -\infty \quad \text{as} \quad s \to -\infty.$$

This proof is given in [30] and is used properties of the Lambert W function.

Next, we represent ξ as a function of ϕ. We rewrite (9.4.4) as

$$\frac{d\xi}{ds} = \phi.$$

Using (9.3.6), we can obtain

$$\begin{aligned}
\xi + C_3 &= \int \phi(s)\, ds = \int \phi \frac{ds}{d\phi}\, d\phi \\
&= \int \phi \left(\frac{p}{c}\phi^2 - \frac{p}{c^3}(\mu c^2 + 1)\phi^3\right)^{-1} d\phi \\
&= \int \frac{c^3}{p\phi\{c^2 - (\mu c^2 + 1)\phi\}}\, d\phi \\
&= \frac{c^3}{p}\int \left[\frac{1}{c^2}\frac{1}{\phi} + \frac{1}{c^2}(\mu c^2 + 1)\frac{1}{c^2 - (\mu c^2 + 1)\phi}\right] d\phi \\
&= \frac{c}{p}\log|\phi| - \frac{c}{p}\log|(\mu c^2 + 1)\phi - c^2| \\
&= \frac{c}{p}\log\left|\frac{\phi}{(\mu c^2 + 1)\phi - c^2}\right|
\end{aligned}$$

with a constant C_3. Then the constant C_3 is given by

$$C_3 = \frac{c}{p}\log\left|\frac{\phi_0}{(\mu c^2 + 1)\phi_0 - c^2}\right|,$$

where $\phi(0) = \phi_0$. Note that we can conclude that $C_3 < 0$ in the same way as in [30].

Finally, we aim to represent ϕ as a function of ξ. As mentioned above, we obtain

$$\xi + \frac{c}{p}\log\left|\frac{\phi_0}{(\mu c^2 + 1)\phi_0 - c^2}\right| = \frac{c}{p}\log\left|\frac{\phi}{(\mu c^2 + 1)\phi - c^2}\right|.$$

Therefore, we have

$$\phi(\xi) = \frac{Mc^2 e^{\frac{p}{c}\xi}}{M(\mu c^2 + 1)e^{\frac{p}{c}\xi} - 1}, \quad M = -\left|\frac{\phi_0}{(\mu c^2 + 1)\phi_0 - c^2}\right|,$$

where $M < 0$ is the constant that depends on the initial state ϕ_0. This completes the proof. □

9.5 Concluding remarks

In this chapter, we studied whole dynamics of (9.1.4) on the phase space

$$\mathbb{R}^2 \cup \{\|(\phi, \psi)\| = +\infty\} \setminus \{\phi < 0\}$$

and all trajectories with $\{\phi \geq 0\}$ were classified. This allowed us to classify the nonnegative traveling wave solutions including weak traveling wave solutions with singularity of (9.1.1) and to present their existence, information about their shape and asymptotic behavior. These are studied by applying the framework that combines Poincaré compactification and classical dynamical systems theory.

By using the relation between u and U, we obtained the classification of the corresponding traveling wave solutions in (9.1.2). The present process does not require $p \in \mathbb{N}$ since it does not use the blow-up technique as in previous studies, concluding in a general $1 < p \in \mathbb{R}$ results. This solves the problem in (9.1.2) where the argument in $1 < p \in \mathbb{R}$ is not given and the existence of connecting orbits cannot be proved when p is odd. It can be argued that the results obtained in this chapter extend the results of Chapter 7 and Chapter 8 ([32, 30]) to the general case.

By studying the dynamics to infinity, we can see that there is only a family of orbits connecting E_0 and E_2 at $\delta = 0$ (see Figure 9.3.1). In other words, the only nonnegative traveling wave solution to (9.1.1) at $\delta = 0$ is the one given by Theorem 9.2.1. Furthermore, by following this transformation, we can conclude that the only nonnegative traveling wave solution for (9.1.2) with $\delta = 0$ is the one given by Corollary 9.2.1 as mentioned in Remark 9.2.3. A similar argument leads to the conclusion as in Remark 9.2.6 for $\delta = 1$.

This is essentially due to the introduction of the transformation $u = U^p$. This transformation has overcome the difficulty in extending the previous studies. There are problems that impose a similar $p \in \mathbb{N}$ constraint (see [31, 33, 35, 37]). However, this idea can only be used for this type of equation. It remains to be seen what methods will be effective in dealing with these problems.

Furthermore, as mentioned in Remark 9.2.8, the stability of the traveling wave solution obtained in this study has not been discussed. This problem has been an issue in Chapter 7 and Chapter 8 ([32, 30]), and will remain an issue in this chapter as well. The question of the stability of the traveling wave solutions (including in a weak sense) is important from the point of view of the phenomenon and blow-up analysis. Then, numerical simulation will play an important role in providing suggestions and conjectures. However, it is not easy due to influence of the degenerate parts of equations. We believe that the results in this chapter will provide a new perspective for the construction of stable numerical schemes. As noted in Remark 9.2.7, it will also contribute greatly to future blow-up analysis.

Chapter 10

Radially symmetric stationary solutions for certain chemotaxis systems in higher dimensions: a geometric approach

Abstract

This chapter reports results on the existence, shapes, and asymptotic behavior of positive radially symmetric stationary solutions for several models of chemotaxis in higher dimensions. The systems treated in this chapter are the simplest parabolic-elliptic Keller-Segel model and the simplest attraction-repulsion chemotaxis system, in which a positive-valued (resp. negative-valued) solution of one is a negative-valued (resp. positive-valued) solution of the other from symmetry. In particular, the construction of functions satisfying equations that diverge at the endpoints of finite intervals is an interesting result. The key to the discussion is to derive a scalar equation by using a transformation on the averaged mass for the equation satisfied by the radially symmetric stationary solution and to investigate the infinity dynamics as geometric information for the two-dimensional ordinary differential equations derived from it. To achieve this, we use a method that combines classical results from the continuous dynamical systems theory and Poincaré-Lyapunov compactification. In addition, the results for singular solutions are discussed in light of the results of previous studies. This chapter is based on the following published paper ([39]):

> Ichida, Y.: Radially symmetric stationary solutions for certain chemotaxis systems in higher dimensions: a geometric approach, Discrete Contin. Dyn. Syst., **43** (2023), no. 5, 1975–2001.

10.1 Introduction

Let $u = u(t, x)$ be the density of the cell population, $v = v(t, x)$ be the concentration of the chemotactic substance, $p = p(t, x)$ be the concentration of the attractant, $q = q(t, x)$ be the concentration of the repellent and $N \geq 3$. In this chapter, we consider the radially

symmetric stationary solutions of the following systems:

$$\begin{cases} u_t = \Delta u - \nabla \cdot (u \nabla v), & x \in \mathbb{R}^N, \quad t > 0, \\ 0 = \Delta v + u, & x \in \mathbb{R}^N, \quad t > 0 \end{cases} \tag{10.1.1}$$

and

$$\begin{cases} u_t = \Delta u - \alpha \nabla \cdot (u \nabla p) + \beta \nabla \cdot (u \nabla q), & x \in \mathbb{R}^N, \quad t > 0, \\ 0 = \Delta p + u, & x \in \mathbb{R}^N, \quad t > 0, \\ 0 = \Delta q + u, & x \in \mathbb{R}^N, \quad t > 0, \end{cases} \tag{10.1.2}$$

where α and β are positive constants. Assume that $\alpha < \beta$ below.

(10.1.1) and (10.1.2) are a kind of chemotaxis systems. (10.1.1) is a system of equations based on [43], which is considered to be the pioneering work on the model of chemotaxis, and simplified by [58]. This equation is called the simplest classical Keller-Segel or Keller-Segel-Patlak system, see for instance [11, 56, 57, 64], and references therein for related works. According to [56], the convective term $-\nabla \cdot (u \nabla v)$ in the first equation describes aggregation directed towards the origin with a velocity proportional to ∇v. Mathematically, the main studies are on well-posedness, boundedness, and blow-up solution; see the survey paper [29] and references therein. However, as also noted in [65], in many biological processes, not only attracting effects such as (10.1.1) but also repulsive effects are quite possible. One representative system is the attraction-repulsion chemotaxis system, and (10.1.2) is the simplest version of them. In terms of phenomena, (10.1.2) comes from the systems proposed in [48] and was introduced to explain the aggregation of microglia observed in Alzheimer's disease.

In (10.1.2), by setting $v = \beta q - \alpha p$, we obtain

$$\begin{cases} u_t = \Delta u + \nabla \cdot (u \nabla v), & x \in \mathbb{R}^N, \quad t > 0, \\ 0 = \Delta v + (\beta - \alpha) u, & x \in \mathbb{R}^N, \quad t > 0. \end{cases} \tag{10.1.3}$$

Note that the sign of the convective term in (10.1.1) is different in (10.1.3). It turns out that it is sufficient to examine the behavior of u in (10.1.3) in order to study the behavior of the solution u of equation (10.1.2).

In [57], by focusing on radially symmetric and radially symmetric stationary solutions of (10.1.1), [57] shows the optimal conditions on the initial data for the finite-time blow-up and the global existence of solutions. Discussions examining the properties of solutions to scalar equations involving the averaged mass of u (see (10.1.7)) play an important role. In addition, for $\alpha > 0$, let $\phi(r; \alpha)$ be a solution to the following equation:

$$(r^{N-1} \phi_r)_r + r^{N-1} e^{\phi} = 0, \quad \phi(0) = \alpha, \quad \phi_r(0) = 0. \tag{10.1.4}$$

We set

$$U(r; \alpha) = e^{\phi(r; \log \alpha)}, \quad V(r; \alpha) = \phi(r; \log \alpha) - \log \alpha \quad \text{for} \quad r \geq 0.$$

Then, it is stated in [57] that $(U, V) = (U(r; \alpha), V(r, \alpha))$ is a solution of the following equations:

$$0 = \nabla \cdot (\nabla U - U \nabla V), \quad 0 = \Delta V + U.$$

In [57], conclusions are drawn mainly based on these facts. In addition, in (10.1.4), the singular solution $\phi^*(r) = -2 \log r + \log(2N - 4)$ is shown to be unique by Mignot-Puel [52]. This is also shown in Miyamoto-Naito [53] with a generalized equation. In [7], they investigate the bifurcation problem for radially symmetric stationary solutions by focusing on (10.1.4) and this singular solution.

Generally speaking, a radially symmetric stationary solution is one of the special and typical solutions that play a fundamental and important role in studying the solution structure of partial differential equations in multidimensional space. Therefore, motivated by [57], this chapter attempts to clear the structure of radially symmetric stationary solutions of (10.1.1), (10.1.2) and (10.1.3) from a dynamical systems theory and geometric approach different from [57] (in particular, the infinite dynamics of differential equations based on the Poincaré type compactification). The goal is to discover new aspects of the abundant solution structure of the chemotaxis systems.

The Poincaré type compactification is one of the compactifications of the original phase space (the embedding of $\mathbb{R}^n$ into the unit upper hemisphere of $\mathbb{R}^{n+1}$). See [14, 31, 32, 33, 34, 49, 50] and their references for details. A brief overview is given in Section 1.1. In the following, the Poincaré type compactification includes both the Poincaré compactification and the Poincaré-Lyapunov compactification. The difference between the two is that the vector field is either homogeneous or quasi-homogeneous, respectively. For the quasi-homogeneity of a vector field, see Section 1.1 and [49, 50]. The most important feature of applying this method is that it allows us to investigate the global behavior of the system of ODEs of interest by revealing all its dynamics including infinity (see also [34]). This method has been used, for instance, in the analysis of the Liénard equation ([14] and references therein), and in the reconsideration of blow-up solutions of systems of ODEs in the view of dynamical systems ([49, 50]).

The author has used a kind of compactification of phase space called the Poincaré type compactification to investigate the structure of special solutions (e.g., the stationary solution, the traveling wave solution) of partial differential equations with negative powers nonlinearity and degenerate parabolic equation ([31, 32, 33, 38]). In particular, the classification of nonnegative traveling wave solutions for the 1D degenerate parabolic equations is given in [38]. It also reveals the global behavior of certain ODE systems, as described in [34]. To the best of the author's knowledge, there is no study of this method being applied to chemotaxis systems. Therefore, by applying this method, we clarify the existence, profiles, and asymptotic behavior of radially symmetric stationary solutions from a different angle from previous studies.

We derive a system of ordinary differential equations satisfying the radially symmetric stationary solutions of (10.1.1), (10.1.2), and (10.1.3). The equation satisfied by the radially symmetric solution $(u, v) = (u(t, r), v(t, r))$, $r = |x| > 0$, of equation (10.1.1) is

$$\begin{cases} r^{N-1}u_t = (r^{N-1}u_r)_r - (ur^{N-1}v_r)_r, \\ (r^{N-1}v_r)_r + r^{N-1}u = 0. \end{cases} \tag{10.1.5}$$

On the other hand, the equation for the radially symmetric solution of (10.1.3) derived from (10.1.2) is as follows:

$$\begin{cases} r^{N-1}u_t = (r^{N-1}u_r)_r + (ur^{N-1}v_r)_r, \\ (r^{N-1}v_r)_r + (\beta - \alpha)r^{N-1}u = 0. \end{cases} \tag{10.1.6}$$

Next, we introduce the following transformation:

$$w(t, r) := \frac{1}{r^N} \int_0^r s^{N-1}u(t, s)\, ds, \quad r > 0. \tag{10.1.7}$$

This transformation (10.1.7) involves the averaged mass of u being used, for instance, see [57, 64] and references therein. Here we consider solutions that satisfy the following

$$\lim_{r\to 0} r^N w(r, t) = 0. \tag{10.1.8}$$

(10.1.8) will be helpful in understanding the claims for singular solutions (see Subsection 10.5.1, Subsection 10.5.2).

Then, from (10.1.5), we can see that $w(t,r)$ satisfies the following scalar equation:

$$w_t = w_{rr} + \frac{N+1}{r}w_r + rww_r + Nw^2, \quad w = w(t,r), \quad r > 0. \tag{10.1.9}$$

Furthermore, from (10.1.6) we obtain

$$w_t = w_{rr} + \frac{N+1}{r}w_r + (\alpha-\beta)rww_r + (\alpha-\beta)Nw^2, \quad w = w(t,r), \quad r > 0. \tag{10.1.10}$$

Here, if $\alpha = 1$ and $\beta = 0$, (10.1.10) becomes (10.1.9), so it is sufficient to examine the behavior of the solution of (10.1.10). Note that we assume

$$r^{N-1}v_r(r) \to 0 \quad (r \to 0)$$

in this calculation process. In addition,

$$u(t,r) = rw_r(t,r) + Nw(t,r) \tag{10.1.11}$$

holds, and by differentiating both sides of (10.1.11) by r,

$$u_r(t,r) = rw_{rr}(t,r) + (N+1)w_r(t,r) \tag{10.1.12}$$

holds.

Since we consider the radially symmetric stationary solutions of the original systems of partial differential equations (10.1.1) and (10.1.2), this chapter is reduced to the problem of studying the behavior of the solutions of the following equation (second-order ordinary differential equation) satisfied by these stationary solutions $w(r)$ from (10.1.10):

$$w_{rr} + \frac{N+1}{r}w_r + (\alpha-\beta)rww_r + (\alpha-\beta)Nw^2 = 0, \quad w = w(r), \quad r > 0. \tag{10.1.13}$$

Note that $r^{N-1}u_r = ur^{N-1}v_r$ is naturally assumed in (10.1.5) since $w_t = 0$ from the above discussion. Similarly, $r^{N-1}u_r = -ur^{N-1}v_r$ is assumed in (10.1.6).

(10.1.13) is a non-autonomous system, especially, $r = 0$ is a singular point. Then, we consider the following transformations that transform (10.1.13) into the autonomous systems on $\mathbb{R}^2$ and remove the singularity $r = 0$:

$$t = \kappa \log r, \quad a(t) = r^2 w(r), \quad \kappa = \pm 1. \tag{10.1.14}$$

Then,

$$\begin{aligned} w &= r^{-2}a, \\ w_r &= -2r^{-3}a + \kappa r^{-3}\dot{a}, \\ w_{rr} &= 6r^{-4}a - 5\kappa r^{-4}\dot{a} + r^{-4}\ddot{a} \end{aligned}$$

hold. (10.1.13) is transformed into the following:

$$\ddot{a} + \kappa(N-4)\dot{a} + \kappa(\alpha-\beta)a\dot{a} - 2(N-2)a + (N-2)(\alpha-\beta)a^2 = 0, \tag{10.1.15}$$

equivalently

$$\begin{cases} \dot{a} = b, \\ \dot{b} = -\kappa(N-4)b - \kappa(\alpha-\beta)ab + 2(N-2)a - (N-2)(\alpha-\beta)a^2, \end{cases} \tag{10.1.16}$$

where we set $\dot{} = d/dt$ and $\ddot{} = d^2/dt^2$. This transformation (10.1.14) was also introduced in [33, 41]. When the parameter κ is $\kappa = 1$, we see that $r \to \infty$ as $t = \log r \to \infty$ holds. Therefore, to discuss the behavior of the solution to (10.1.13) as $r \to \infty$, we need to study the information of the solutions of (10.1.16) as $t \to \infty$. Similarly, $r \to 0$ as $t \to \infty$ in the case that $\kappa = -1$. Here, switching the positive and negative values of $\alpha - \beta$ is equivalent to applying the following transformation in (10.1.16):

$$(a, b) \mapsto (-a, -b). \tag{10.1.17}$$

That is, the solutions of (10.1.16) at $\alpha = 1$ and $\beta = 0$ correspond to the radially symmetric stationary solutions of the simplest parabolic-elliptic Keller-Segel model (10.1.1), and the solutions of (10.1.16) at $\alpha \neq \beta$ (in this chapter, especially $\alpha < \beta$) corresponds to the radially symmetric stationary solutions of the simplest attraction-repulsion chemotaxis model (10.1.2) or derived from it (10.1.3).

The purpose of this chapter is to focus on the radially symmetric stationary solutions of (10.1.1), (10.1.2), and (10.1.3) and to investigate what kind of solutions exist, information about their shapes, and their asymptotic behavior. For this purpose, in (10.1.16), we examine the dynamics in

(i) $\alpha = 1$ and $\beta = 0$ (special case of $\alpha > \beta$, see Section 10.3), and

(ii) $\alpha < \beta$ (from the results of (i) and the symmetry (10.1.17)),

respectively, the dynamics on $\mathbb{R}^2 \cup \{\|(a, b)\| = +\infty\}$. Therefore, the Poincaré-Lyapunov compactification is used as described above. The dynamics including infinity, obtained by Poincaré-Lyapunov's one is hereafter referred to as Poincaré-Lyapunov disk. The reason for choosing this compactification is to properly extract information at infinity in the original phase space, taking into account the quasi-homogeneity of (10.1.16), as described in Subsection 10.3.2 (see, for instance, Section 1.1 and [49, 50]). As noted in Section 1.1 and [49, 50], via these compactifications, the infinity for the original phase space corresponds to the boundary of compact manifolds. Here, we split the boundary and project each of them to some local charts, and study the dynamics. By combining this information from some local charts, we can obtain the dynamics including infinity. From these results, if all connecting orbits, including those up to infinity in the original phase space (i.e., all connecting orbits on the Poincaré-Lyapunov disk) are known, then it is expected to give the existence of solutions not revealed in previous studies, information about the shape, and asymptotic behavior.

Since this method can actually examine both positive-valued and negative-valued solutions at once, the focus of the discussion is on examining (10.1.16). The information of the positive-valued (resp. negative-valued) solutions of (10.1.1) corresponds to the information of the negative-valued (resp. positive-valued) solutions of (10.1.2) and (10.1.3). In other words, although the information on the negative-valued solution is unnecessary from the viewpoint of the phenomenon, this information plays an important role in the investigation of positive solutions of other chemotaxis models.

If we know the asymptotic behavior of $a(t)$ and $b(t)$ as $t \to t_+$ (the maximal existence time, $t_+ < +\infty$ or $t_+ = +\infty$), we can find the asymptotic behavior of $w(r)$ and $w_r(r)$ as $r \to r_-$ (the minimal existence interval, $0 < r_- < +\infty$ or $r_- = 0$) and $r \to r_+$ (the maximal existence interval, $0 < r_- < r_+ < +\infty$ or $r_+ = +\infty$) from (10.1.14), and we can derive it for $u(r)$ and $u_r(r)$ from (10.1.11) and (10.1.12).

In this chapter, we clarify the existence, shape, and asymptotic behavior of radially symmetric stationary solutions, which have not been clarified before (in particular, Theorem 10.2.2). However, the stability of this solution is not obtained. The author, who has

clarified the structure of special solutions of various partial differential equations using this method based on dynamical systems theory and geometric approaches, believes that their new attempts in this study will bring rich insights into solution behavior and solution structure of chemotaxis systems and giving rise to new research.

This chapter is organized as follows. In the next section, we state the main results of this chapter. In Section 10.3, we obtain the dynamics of (10.1.16) with $\alpha = 1$ and $\beta = 0$ on the Poincaré-Lyapunov disk via Poincaré-Lyapunov compactification and basic theory of the dynamical systems. We also use the symmetry in (10.1.17) to give the Poincaré-Lyapunov disk of (10.1.16) in $\alpha < \beta$ (see Subsection 10.3.8 for a detailed discussion). The proof of theorems will be completed in Section 10.4. Finally, in Section 10.5, we discuss the uniqueness of the singular solutions in previous studies, together with the conclusions drawn from this chapter.

10.2 Main results

The main key to obtain the main results is the availability of a phase portrait corresponding to the Poincaré-Lyapunov disk in (10.1.16), which will be explained in detail in a later section. Here and after, note that the meaning of the symbol $f(\xi) \sim g(\xi)$ as $\xi \to a$ is as follows:

$$\lim_{\xi \to a} \left| \frac{f(\xi)}{g(\xi)} \right| = 1.$$

First, we present one new result for a positive-valued radially symmetric stationary solution of (10.1.5).

Theorem 10.2.1
Assume that $N \geq 3$. Then, (10.1.5) has a radially symmetric stationary solution (which corresponds to an orbit of (10.1.16) in the case that $\alpha = 1$ and $\beta = 0$). Moreover, its solution $u(r)$ satisfies the following:

- *$u(r) > 0$ holds for $r \in (0, +\infty)$.*
- *$\lim_{r \to 0} u(r) = C$, $\lim_{r \to 0} u_r(r) = 0$, $\lim_{r \to +\infty} u(r) = 0$,*

where $C > 0$ is a constant. In addition, the asymptotic behavior of $u(r)$ for $r \to +\infty$ is

$$u(r) \sim 2(N-2)r^{-2} \tag{10.2.1}$$

$$\sim \begin{cases} 2(N-2)r^{-2} + A_1 r^{-2+\sigma_-} + A_2 r^{-2+\sigma_+}, & (N \geq 11) \\ 16r^{-2} + (A_3 \log r + A_4) r^{-6}, & (N = 10) \\ 2(N-2)r^{-2} + 2^{-1}(N-2) r^{-\frac{N+2}{2}} \overline{W} + 2^{-1}\sqrt{|D|} r^{-\frac{N+2}{2}} \overline{Z}, & (3 \leq N \leq 9) \end{cases} \tag{10.2.2}$$

where A_j are constants. Here, the following hold:

$$\begin{aligned} &\sigma_\pm = 2^{-1}\{-\kappa(N-2) \pm \sqrt{(N-2)(N-10)}\}, \\ &D = (N-2)(N-10), \\ &\overline{Z}(r) = B_1 \cos[2^{-1}\sqrt{|D|}\log r] - B_2 \sin[2^{-1}\sqrt{|D|}\log r], \\ &\overline{W}(r) = B_1 \sin[2^{-1}\sqrt{|D|}\log r] + B_2 \cos[2^{-1}\sqrt{|D|}\log r] \end{aligned}$$

where B_j are constants.

Remark 10.2.1
We give two remarks regarding Theorem 10.2.1.

(i) The behavior of the solution at $r \to +\infty$ depends on the number of dimensions N. In particular, for $3 \le N \le 9$, we can observe that $u(r)$ goes to $u = 0$ with damping oscillatory terms. The results of (10.2.1) *and* (10.2.2) *in $N \ge 10$ are consistent with the results of [57] and Lemma 2.1 of [66], which considered* (10.1.4)*. However, $3 \le N \le 9$ is new in that it is not derived from [57, 66].*

(ii) The explicit asymptotic form of u as $r \to 0$ is not obtained in this chapter. As we will be described in Subsection 10.4.1, this derivation requires attention to $(a, b) = (0, 0)$ in (10.1.16)*. This is because only the lowest order term is known about the solution behavior near the origin in* (10.1.16)*. We leave it open here.*

Next, we discuss a result for a sign-changing solution. This follows from the trajectory of the infinity dynamics obtained in Section 10.3, which gives another proof of Lemma 4.5 (i) for [57].

Proposition 10.2.1
Assume that $N \ge 3$. In (10.1.5)*, there is no sign-changing radially symmetric stationary solution. The same is true for* (10.1.6)*.*

Finally, we present new results that are constructing positive-valued functions on finite or semi-infinite intervals that satisfy (10.1.6). If $u \mapsto -u$ from the symmetry of (10.1.17), then the following results correspond to negative-valued solutions of (10.1.5).

Theorem 10.2.2
Assume that $N \ge 3$. Then, the following holds:

(i) There exists a family of the functions (which corresponds to a family of the orbits of (10.1.16) *in the case that $\alpha < \beta$) defined on the finite interval such that each function $u(r)$ satisfies* (10.1.6) *on a finite interval (r_-, r_+) $(0 < r_- < r_+ < +\infty)$. Moreover, for each function $u(r)$, the following holds:*

- *$u(r) > 0$ holds for $r \in (r_-, r_+)$.*
- *$\lim_{r \to r_- + 0} u(r) = +\infty$, $\lim_{r \to r_+ - 0} u(r) = +\infty$.*
- *There exists a constant $r_* \in (r_-, r_+)$ such that the following holds: $u_r(r) < 0$ for $r \in (r_-, r_*)$, $u_r(r_*) = 0$ and $u_r(r) > 0$ for $r \in (r_*, r_+)$.*
- *The asymptotic behavior for $r \to r_- + 0$ is*

$$u(r) \sim K r^{-2} (\log r - \log r_-)^{-2} [-(N-2)(\log r - \log r_-) + 1], \tag{10.2.3}$$

where $K > 0$ and $r \to r_+ - 0$ is

$$u(r) \sim K r^{-2} (\log r_+ - \log r)^{-2} [(N-2)(\log r_+ - \log r) + 1] \tag{10.2.4}$$

where $K > 0$.

(ii) There exists a function (which corresponds to an orbit of (10.1.16) *in the case that $\alpha < \beta$) defined on the semi-infinite interval such that its function $u(r)$ satisfies* (10.1.6) *on a semi-infinite interval $(r_-, +\infty)$ $(0 < r_- < +\infty)$. Moreover, for its function $u(r)$, the following holds:*

- $u(r) > 0$ *holds for* $r \in (r_-, +\infty)$.
- $\lim_{r\to r_-+0} u(r) = +\infty$, $\lim_{r\to+\infty} u(r) = 0$, $\lim_{r\to+\infty} u_r(r) = 0$.
- *The asymptotic behavior of* $u(r)$ *for* $r \to r_- + 0$ *is expressed as* (10.2.3).

(iii) There exists a function (which corresponds to an orbit of (10.1.16) *in the case that* $\alpha < \beta$*) defined on the finite interval such that its function* $u(r)$ *satisfies* (10.1.6) *on a finite interval* $[0, r_+)$ $(0 < r_+ < +\infty)$*. Moreover, for its function* $u(r)$*, the following holds:*

- $u(r) > 0$ *holds for* $r \in [0, r_+)$.
- $\lim_{r\to 0} u(r) = C$, $\lim_{r\to 0} u_r(r) = 0$, $\lim_{r\to r_+-0} u(r) = +\infty$, *where* $C > 0$.
- *The asymptotic behavior of* $u(r)$ *for* $r \to r_+ - 0$ *is expressed as* (10.2.4).

Remark 10.2.2
Here, the corresponding discussion in the proof indicates that the solution is constructed only on a finite or semi-infinite interval with respect to r*, so we express it as a function (or family of functions) that satisfies the equation. Some solutions obtained in above results satisfy the equation only on finite interval* (r_-, r_+) $(0 < r_- < r_+ < +\infty)$ *or semi-infinite interval. That is, even though we are considering equations in the whole domain, we are constructing solutions that cause singularity at the endpoints of a finite (or semi-infinite) interval. In this chapter, we do not discuss the behavior of the solutions* $u(r)$ *after* $u'(r)$ *becomes infinity (outside of the interval on that* $u(r)$ *satisfies* (10.1.6)*). A more detailed (and hard) analysis is needed. In addition, the main purpose of this chapter is to investigate the existence, shapes, and asymptotic behavior of solutions of* (10.1.6) *from the dynamical system viewpoint and geometric approaches, we leave it open here.*

10.3 Dynamics on the Poincaré-Lyapunov disk of (10.1.16)

In this section, all the dynamics of (10.1.16) on $\mathbb{R}^2 \cup \{\|(a,b)\| = +\infty\}$ in the case that $\alpha = 1$ and $\beta = 0$ will be obtained by using Poincaré-Lyapunov compactification. It is also given for the case $\alpha < \beta$. Considering symmetry (10.1.17), in this section we study (10.1.16) in the case that $\alpha = 1$ and $\beta = 0$. See Subsection 10.3.8 for the calculation process when $\alpha < \beta$.

10.3.1 Dynamics near finite equilibria of (10.1.16)

Before starting the detailed analysis, we study the dynamics near finite equilibrium of (10.1.16). The finite equilibria in (10.1.16) are as follows:

$$E_0 : (a,b) = (0,0), \quad E_1 : (a,b) = (2,0).$$

Let J_0 (resp. J_1) be the Jacobian matrix of the vector field (10.1.16) at E_0 (resp. E_1). J_0 and J_1 are

$$J_0 = \begin{pmatrix} 0 & 1 \\ 2(N-2) & -\kappa(N-4) \end{pmatrix}, \quad J_1 = \begin{pmatrix} 0 & 1 \\ -2(N-2) & -\kappa(N-2) \end{pmatrix}.$$

We can claim the following for the dynamics in the neighborhood of E_0 for each of $\kappa = \pm 1$.

(i) When $\kappa = 1$, the eigenvalues of matrix J_0 are 2 and $-(N-2)$, so E_0 is a saddle. The eigenvectors corresponding to the eigenvalues are $(1,2)^T$ and $(1,-(N-2))^T$, respectively, with T representing the transpose.

(ii) When $\kappa = -1$, the eigenvalues of matrix J_0 are $N-2$ and -2, so E_0 is a saddle. The eigenvectors corresponding to the eigenvalues are $(1,N-2)^T$ and $(1,-2)^T$, respectively.

Furthermore, the eigenvalues $\sigma_\pm$ of matrix J_1 are

$$\sigma_\pm = \frac{-\kappa(N-2) \pm \sqrt{(N-2)(N-10)}}{2}.$$

The corresponding eigenvectors are $(1,\sigma_+)^T$ and $(1,\sigma_-)^T$, respectively. When $\kappa = 1$, the real parts of all eigenvalues of J_1 are negative. Therefore, we conclude that E_1 is asymptotically stable. On the other hand, E_1 is unstable when $\kappa = -1$. From the eigenvalues, note that the behavior of the solution near E_1 in $N \geq 3$ depends on the value of $N-10$. For instance, if $3 \leq N \leq 9$, then matrix J_1 has two different complex eigenvalues. Other cases can be concluded similarly.

10.3.2 Asymptotically quasi-homogeneous vector field

Before we consider the dynamics of (10.1.16) on the charts $\overline{U}_j$ and $\overline{V}_j$, we derive the type and order of this vector field. See Section 1.1 for the definition (Definition 1.1.3) of local charts. Let $f = (f_1(a,b), f_2(a,b))$ be

$$f_1(a,b) = b, \quad f_2(a,b) = -\kappa(N-4)b - \kappa ab + 2(N-2)a - (N-2)a^2.$$

Then we have the following observation (see Section 1.1 and [49, 50] for more details).

Lemma 10.3.1
The vector field f is asymptotically quasi-homogeneous of type $(1,2)$ and order 2 at infinity.

Proof. Let a type be (α_1, α_2) and $R \in \mathbb{R}$. For all $(a,b) \in \mathbb{R}^2$, the following holds:

$$f_1(R^{\alpha_1}a, R^{\alpha_2}b) = R^{k+\alpha_1} f_1(a,b),$$
$$f_2(R^{\alpha_1}a, R^{\alpha_2}b) = R^{k+\alpha_2} f_2(a,b).$$

By comparing the order parts, we get

$$\begin{cases} \alpha_2 = k + \alpha_1, \\ \alpha_2 = k + \alpha_2, \\ \alpha_1 + \alpha_2 = k + \alpha_2, \\ \alpha_1 = k + \alpha_2, \\ 2\alpha_1 = k + \alpha_2. \end{cases} \tag{10.3.1}$$

Here since the first and third equations in (10.3.1) correspond to the maximum order in (10.1.16), $(\alpha_1, \alpha_2) = (1,2)$ and $k = 1$ are obtained from them. Furthermore, they satisfy as follows:

$$\lim_{R\to+\infty} R^{-(k+\alpha_1)} \left\{ f_1(R^{\alpha_1}a, R^{\alpha_2}b) - R^{k+\alpha_1}(f_{\alpha,k})_1(a,b) \right\} = 0,$$
$$\lim_{R\to+\infty} R^{-(k+\alpha_2)} \left\{ f_2(R^{\alpha_1}a, R^{\alpha_2}b) - R^{k+\alpha_2}(f_{\alpha,k})_2(a,b) \right\} = 0,$$

where $(f_{\alpha,k})_1$ and $(f_{\alpha,k})_2$ are $(f_{\alpha,k})_1 = b$ and $(f_{\alpha,k})_2 = -\kappa ab$, respectively. From the above results, we can see that the vector field f is asymptotically quasi-homogeneous of type $(1,2)$ and order $k+1=2$ at infinity. □

10.3.3 Dynamics on the chart $\overline{U}_2$

To obtain the dynamics on the chart $\overline{U}_2$, we introduce coordinates (λ, x) by the formulas

$$a = x/\lambda, \quad b = 1/\lambda^2.$$

Here, note that the exponents of λ are derived from the type found in Lemma 10.3.1. The image of the geometric position of these local coordinates is almost the same as in Figure 1.1.2. Then we have

$$\begin{cases} \dot{\lambda} = 2^{-1}\kappa(N-4)\lambda + 2^{-1}\kappa x - (N-2)\lambda^2 x + 2^{-1}(N-2)\lambda x^2, \\ \dot{x} = \lambda^{-1} + 2^{-1}\kappa(N-4)x + 2^{-1}\kappa\lambda^{-1}x^2 - (N-2)\lambda x^2 + 2^{-1}(N-2)x^3. \end{cases} \tag{10.3.2}$$

Time-scale desingularization $d\tau/dt = \lambda^{-1}$ yields

$$\begin{cases} \lambda_\tau = 2^{-1}\kappa(N-4)\lambda^2 + 2^{-1}\kappa\lambda x - (N-2)\lambda^3 x + 2^{-1}(N-2)\lambda^2 x^2, \\ x_\tau = 1 + 2^{-1}\kappa(N-4)\lambda x + 2^{-1}\kappa x^2 - (N-2)\lambda^2 x^2 + 2^{-1}(N-2)\lambda x^3, \end{cases} \tag{10.3.3}$$

where λ_τ and x_τ are $\lambda_\tau = d\lambda/d\tau$ and $x_\tau = dx/d\tau$, respectively. The equilibria in (10.3.3) and their stability by $\kappa = \pm 1$, respectively, are described as follows:

- If $\kappa = 1$, then there is no equilibrium and $x_\tau > 0$ at $\lambda = 0$.
- If $\kappa = -1$, then there exists equilibria

  $$E_2 : (\lambda, x) = (0, -\sqrt{2}), \quad E_3 : (\lambda, x) = (0, \sqrt{2}).$$

  The Jacobian matrices of vector field (10.3.3) at these equilibria are

  $$E_2 : \begin{pmatrix} 2^{-1}\sqrt{2} & 0 \\ -2^{-1}\sqrt{2}N & \sqrt{2} \end{pmatrix}, \quad E_3 : \begin{pmatrix} -2^{-1}\sqrt{2} & 0 \\ 2^{-1}\sqrt{2}N & -\sqrt{2} \end{pmatrix}.$$

  Therefore, E_2 is unstable and E_3 is asymptotically stable. Let J_3 be the Jacobian matrix of this vector field at E_3. The eigenvalues of matrix J_3 are $-2^{-1}\sqrt{2}$ and $-\sqrt{2}$. The eigenvectors corresponding to the eigenvalues are $(1, N)^T$ and $(0, 1)^T$, respectively.

10.3.4 Dynamics on the chart $\overline{V}_2$

The change of coordinates

$$a = -x/\lambda, \quad b = -1/\lambda^2$$

give the projected dynamics of (10.1.16) on the chart $\overline{V}_2$:

$$\begin{cases} \lambda_\tau = 2^{-1}\kappa(N-4)\lambda^2 - 2^{-1}\kappa\lambda x - (N-2)\lambda^3 x - 2^{-1}(N-2)\lambda^2 x^2, \\ x_\tau = 1 + 2^{-1}\kappa(N-4)\lambda x - 2^{-1}\kappa x^2 - (N-2)\lambda^2 x^2 - 2^{-1}(N-2)\lambda x^3, \end{cases} \tag{10.3.4}$$

where τ is the new time introduced by $d\tau/dt = \lambda^{-1}$. When $\kappa - 1$, there is no equilibrium, and when $\kappa = -1$, there are two equilibria,

$$E_4 : (\lambda, x) = (0, -\sqrt{2}), \quad E_5 : (\lambda, x) = (0, \sqrt{2}).$$

By examining the eigenvalues of the linearized matrix in Subsection 10.3.3, we conclude that E_4 is unstable and E_5 is asymptotically stable.

10.3.5 Dynamics on the chart $\overline{U}_1$

The change of coordinates $a = 1/\lambda$ and $b = x/\lambda^2$, and time-rescaling $d\tau/dt = \lambda^{-1}$ yield

$$\begin{cases} \lambda_\tau = -\lambda x, \\ x_\tau = -\kappa(N-4)\lambda x - \kappa x + 2(N-2)\lambda^2 - (N-2)\lambda - 2x^2. \end{cases} \tag{10.3.5}$$

If $\kappa = 1$, then the equilibria on $\{\lambda = 0\}$ are

$$E_6 : (\lambda, x) = (0, 0), \quad E_7 : (\lambda, x) = (0, -2^{-1}).$$

The Jacobian matrices of vector field (10.3.5) at these equilibria are

$$E_6 : \begin{pmatrix} 0 & 0 \\ -(N-2) & -1 \end{pmatrix} = J_6, \quad E_7 : \begin{pmatrix} 2^{-1} & 0 \\ -2^{-1}N & 1 \end{pmatrix}.$$

Therefore, E_7 is unstable and E_6 is not hyperbolic.

On the other hand, when $\kappa = -1$, the equilibria are

$$E_6 : (\lambda, x) = (0, 0), \quad E_8 : (\lambda, x) = (0, 2^{-1}).$$

In the same way as above, E_8 is found to be asymptotically stable.

Therefore, in the remainder of this subsection, we investigate the dynamical system around E_6. This can be done by applying the center manifold theory (for instance, see [9, 70]). A similar argument is made in [30, 32, 34, 38], but for the reader's convenience, we briefly describe the argument. The eigenvalues of matrix J_6 are 0 and $-\kappa$. The eigenvectors corresponding to the eigenvalues are

$$\mathbf{v}_1 = (\kappa, -(N-2))^T, \quad \mathbf{v}_2 = (0, 1)^T.$$

We set a matrix T as $T = (\mathbf{v}_1, \mathbf{v}_2)$. Then we obtain

$$\begin{aligned} \frac{d}{d\tau}\begin{pmatrix} \lambda \\ x \end{pmatrix} &= \begin{pmatrix} 0 & 0 \\ -(N-2) & -\kappa \end{pmatrix}\begin{pmatrix} \lambda \\ x \end{pmatrix} + \begin{pmatrix} -\lambda x \\ -\kappa(N-4)\lambda x + 2(N-2)\lambda^2 - 2x^2 \end{pmatrix} \\ &= T\begin{pmatrix} 0 & 0 \\ 0 & -\kappa \end{pmatrix} T^{-1}\begin{pmatrix} \lambda \\ x \end{pmatrix} + \begin{pmatrix} -\lambda x \\ -\kappa(N-4)\lambda x + 2(N-2)\lambda^2 - 2x^2 \end{pmatrix}. \end{aligned}$$

Let

$$\begin{pmatrix} \tilde{\lambda}(\tau) \\ \tilde{x}(\tau) \end{pmatrix} = T^{-1}\begin{pmatrix} \lambda(\tau) \\ x(\tau) \end{pmatrix}.$$

We then obtain the following system:

$$\begin{cases} \tilde{\lambda}_\tau = (N-2)\tilde{\lambda}^2 - \tilde{\lambda}\tilde{x}, \\ \tilde{x}_\tau = \tilde{x}[-\kappa + 2(N-1)\tilde{\lambda} - 2\tilde{x}]. \end{cases} \tag{10.3.6}$$

The center manifold theory is applicable to studying the dynamics of (10.3.6). It implies that there exists a function $h(\tilde{\lambda})$ satisfying

$$h(0) = \frac{dh}{d\tilde{\lambda}}(0) = 0$$

such that the center manifold of the origin for above system is locally represented as $\{(\tilde{\lambda}, \tilde{x}) \mid \tilde{x}(\tau) = h(\tilde{\lambda}(\tau))\}$. However, it is not immediately possible to express an approximate function h that defines the center manifold except for $\tilde{x} = 0$. This is because $\tilde{x} = 0$

is invariant from the second equation in (10.3.6). Note that in such cases, the center manifold is not necessarily unique, as described in [70]. By center manifold theory, assuming $\tilde{x} = 0$ as the (graph of) center manifold in (10.3.6), the dynamics near the origin are topologically equivalent to the following equation:

$$\tilde{\lambda}_\tau = (N-2)\tilde{\lambda}^2.$$

From $\lambda = \kappa\tilde{\lambda}$ and $x = -(N-2)\tilde{\lambda} + \tilde{x}$, the approximation of the (graph of) center manifold in (10.3.5) is

$$\{(\lambda, x) \mid x(\tau) = -\kappa(N-2)\lambda(\tau)\} \tag{10.3.7}$$

and the dynamics near E_6 is topologically equivalent to the dynamics of the following equation:

$$\lambda_\tau = \kappa(N-2)\lambda^2. \tag{10.3.8}$$

Note that in these equations derived from $\tilde{x} = 0$ only low-order information is available.

10.3.6 Dynamics on the chart $\overline{V}_1$

The transformations $a = -\lambda^{-1}$ and $b = -x/\lambda^2$ yield

$$\begin{cases} \lambda_\tau = -\lambda x, \\ x_\tau = -\kappa(N-4)\lambda x + \kappa x + 2(N-2)\lambda^2 + (N-2)\lambda - 2x^2 \end{cases} \tag{10.3.9}$$

via time-rescaling $d\tau/dt = \lambda^{-1}$. If $\kappa = 1$, then the equilibria on $\{\lambda = 0\}$ are

$$E_9 : (\lambda, x) = (0, 0), \quad E_{10} : (\lambda, x) = (0, 2^{-1}).$$

If $\kappa = -1$, then the equilibria on $\{\lambda = 0\}$ are E_9 and $E_{11} : (\lambda, x) = (0, -2^{-1})$. As before, by finding the linearized matrices at these equilibria, E_{10} is asymptotically stable, E_{11} is unstable, and E_9 is not hyperbolic. The dynamical system around E_9 can be understood by the center manifold theorem as in Subsection 10.3.5.

10.3.7 Dynamics and connecting orbits on the Poincaré-Lyapunov disk

Let us prepare the symbols used in this subsection as follows:

- $\mathcal{W}^s(E_0)$ denotes the stable manifold of E_0 in the dynamical system (10.1.16) in the case that $\kappa = -1$.
- $\mathcal{W}^u(E_0)$ denotes the unstable manifold of E_0 in the dynamical system (10.1.16) in the case that $\kappa = -1$.
- $\mathcal{W}^s(E_3)$ denotes the stable manifold of E_3 in the dynamical system (10.1.16) in the case that $\kappa = -1$.
- $\mathcal{W}^{cs}(E_6)$ denotes the center-stable manifold of E_6 in the dynamical system (10.1.16) in the case that $\kappa = -1$.

Combining the dynamics on the charts $\overline{U}_j$ and $\overline{V}_j$ $(j = 1, 2)$, we obtain the Poincaré-Lyapunov disk that is equivalent to the dynamics of (10.1.16) on $\mathbb{R}^2 \cup \{\|(a, b)\| = +\infty\}$ (see Figure 10.3.1). The purpose of this subsection is to classify the connecting orbits between these equilibria.

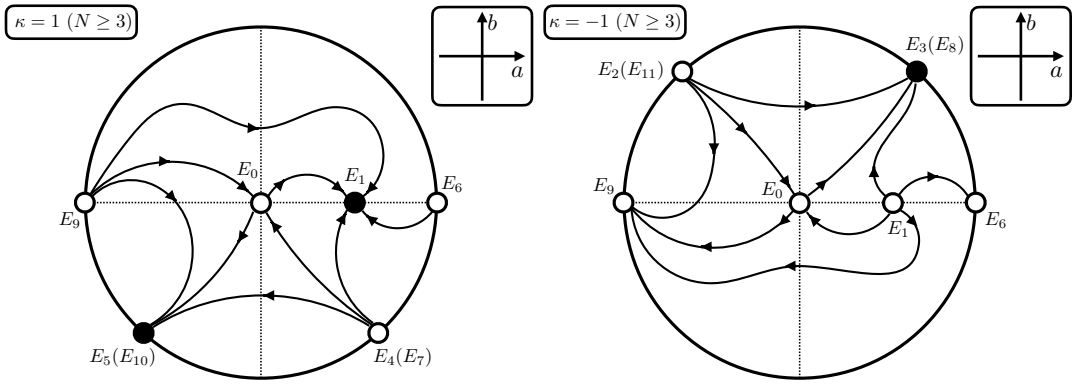

Figure 10.3.1: Schematic pictures of the connecting orbits on the Poincaré-Lyapunov disk in the case that $N \geq 3$, $\kappa = \pm 1$, $\alpha = 1$ and $\beta = 0$.

Remark 10.3.1
In Figure 10.3.1, the circumference corresponds to $\{\|(a,b)\| = +\infty\}$. *Note that for* $\kappa = 1$, *the equilibrium* E_4 *at infinity obtained in the local chart* $\overline{V}_2$ *and the equilibrium* E_7 *at infinity obtained in the local chart* $\overline{U}_1$ *overlap. In Figure 10.3.1, all equilibria at infinity listed in parentheses are the same.*

If we can classify the connecting orbits in the Poincaré-Lyapunov disk for $\kappa = -1$, we can also obtain the $\kappa = 1$ case with the transformation

$$b \mapsto -b, \quad t \mapsto -t.$$

Therefore, it is sufficient to show the existence of connecting orbits for $\kappa = -1$.

In addition,

$$\dot{a}\big|_{a=0} = b, \quad \dot{a}\big|_{b=0} = 0, \quad \dot{b}\Big|_{a=0} = -\kappa(N-4)b, \quad \dot{b}\Big|_{b=0} = (N-2)a(2-a)$$

hold in (10.1.16). That is, the following holds:

- Trajectories departing from a point in region $\{(a,b) \mid a > 0, b > 0\}$ (the first quadrant of the ab-plane) should be toward a point on $\mathcal{W}^s(E_3)$ or $\mathcal{W}^{cs}(E_6)$, or toward region $\{(a,b) \mid a < 0, b > 0\}$ (the second quadrant of the ab-plane), depending on the initial value.

- Trajectories departing from a point in region $\{(a,b) \mid a < 0, b > 0\}$ should be toward a point on $\mathcal{W}^s(E_0)$ or toward region $\{(a,b) \mid a < 0, b < 0\}$, or toward region $\{(a,b) \mid a > 0, b > 0\}$, depending on the initial value.

- Any trajectories departing from points on region $\{(a,b) \mid a < 0, b < 0\}$ should all head for points on $\mathcal{W}^{cs}(E_9)$.

- Trajectories departing from a point in region $\{(a,b) \mid a > 0, b < 0\}$ should be toward a point on $\mathcal{W}^s(E_0)$, or toward region $\{(a,b) \mid a < 0, b < 0\}$, depending on the initial value.

Since (10.1.16) is a two-dimensional system, the Poincaré-Bendixson theorem is effective in showing the existence of connecting orbits that connect equilibria including equilibria at infinity. However, with only the information obtained above in the first quadrant of

the ab-plane, trajectories departing from the points on $\mathcal{W}^u(E_0)$ could be toward points on $\mathcal{W}^s(E_3)$ or $\mathcal{W}^{cs}(E_6)$, or $\{(a,b) \mid a<0, b>0\}$. Since $\mathcal{W}^u(E_0)$ is one-dimensional, we need to know where they are going.

Therefore, the dynamics can be determined by further clarifying the flow of vector fields in the first quadrant of the ab-plane. As a preparation, we derive the asymptotic behavior corresponding to the trajectory attracted to a point on the stable manifold at the equilibrium E_3 at infinity.

Lemma 10.3.2
Assume that $N \geq 3$ and $\kappa = -1$. Then, the solution of (10.1.16) is, if exists, characterized by trajectories whose initial data are on the stable manifold of the equilibrium at infinity E_3 of (10.1.16). The asymptotic behavior of $a(t)$ and $b(t)$ are

$$\begin{cases} a(t) \sim M(t_+ - t)^{-1}, \\ b(t) \sim M(t_+ - t)^{-2}, \end{cases} \quad \text{as} \quad t \to t_+ - 0, \tag{10.3.10}$$

where $0 < t_+ < +\infty$ and $M > 0$ are constants.

Proof. Using the eigenvalues and eigenvectors of the linearized matrix J_3, the solution at the around E_3 on chart $\overline{U}_2$ has the form

$$\begin{cases} \lambda(\tau) = C_1 e^{-\frac{\sqrt{2}}{2}\tau}, \\ x(\tau) = C_1 N e^{-\frac{\sqrt{2}}{2}\tau} + C_2 e^{-\sqrt{2}\tau} + \sqrt{2}, \end{cases}$$

where C_1 and C_2 are constants. Then

$$\frac{dt}{d\tau} = \lambda = C_1 e^{-\frac{\sqrt{2}}{2}\tau}$$

holds. This yields $t(\tau) = C_3 e^{-\frac{\sqrt{2}}{2}\tau} + C_4$. Set

$$t_+ = \lim_{\tau \to +\infty} t(\tau),$$

then we have

$$t_+ = C_5 \int_0^{+\infty} e^{-\frac{\sqrt{2}}{2}\tau}(1 + o(1))\, d\tau < \infty.$$

Therefore, we obtain

$$t_+ - t \sim C_6 e^{-\frac{\sqrt{2}}{2}\tau} \quad \text{as} \quad \tau \to +\infty$$

holds with constants C_j. We then obtain

$$\begin{aligned} a(t) &= \lambda^{-1} x \\ &= \left(C_1 e^{-\frac{\sqrt{2}}{2}\tau}\right)^{-1} \left(C_1 N e^{-\frac{\sqrt{2}}{2}\tau} + C_2 e^{-\sqrt{2}\tau} + \sqrt{2}\right) \\ &\sim C_7 e^{\frac{\sqrt{2}}{2}\tau} \quad \text{as} \quad \tau \to +\infty \\ &\sim M(t_+ - t)^{-1} \quad \text{as} \quad t \to t_+ - 0, \end{aligned}$$

where C_j are constants. Since, the trajectories are lying on $\{a > 0\}$, it follows that the constant $M > 0$ holds. Similarly, the following holds:

$$\begin{aligned} b(t) = \lambda^{-2} &= \left(C_1 e^{-\frac{\sqrt{2}}{2}\tau}\right)^{-2} = C_9 e^{\sqrt{2}\tau} \\ &\sim M(t_+ - t)^{-2} \quad \text{as} \quad t \to t_+ - 0. \end{aligned}$$

Note that the first equation $\dot{a} = b$ of the original equation (10.1.16) is satisfied in the asymptotic sense $\dot{a} \sim b$ as $t \to t_+ - 0$. Therefore, we obtain (10.3.10). This completes the proof of Lemma 10.3.2. □

Using the results of Lemma 10.3.2, the existence of connecting orbits such as those connecting E_0 and E_3 in the case $\kappa = -1$ is shown by Lemma 10.3.3 below.

Lemma 10.3.3
Assume that $N \geq 3$ and $\kappa = -1$. Then, there exists a connecting orbit such that the corresponding function $a(t)$ satisfies the following:

- *$a(t)$ is a continuous function on a semi-infinite interval $(-\infty, t_+]$ and it satisfies the equation* (10.1.16) *on $(-\infty, t_+)$ ($a(t) \in C^2(-\infty, t_+) \cap C^0(-\infty, t_+]$, $-\infty < t_+ < +\infty$).*
- *$a(t)$ has $a(t) > 0$ ($t < t_+$) and satisfies the following:*

$$\lim_{t \to t_+ - 0} a(t) = \lim_{t \to t_+ - 0} \dot{a}(t) = +\infty, \quad \lim_{t \to -\infty} a(t) = \lim_{t \to -\infty} \dot{a}(t) = 0.$$

In other words, there exists a connecting orbit between the points of $\mathcal{W}^u(E_0)$ and the points of $\mathcal{W}^s(E_3)$ on the Poincaré-Lyapunov disk in the case that $\kappa = -1$.

Proof. First, from equation (10.3.10) of Lemma 10.3.2, the maximum existence time t_+ of $a(t)$ is finite, $a(t) > 0$ ($t < t_+$), and also satisfies

$$\lim_{t \to t_+ - 0} a(t) = \lim_{t \to t_+ - 0} \dot{a}(t) = +\infty.$$

Furthermore, by focusing on the trajectories departing from the points on $\mathcal{W}^u(E_0)$, the solution in the neighborhood of E_0 can be expressed using positive eigenvalues and eigenvectors in the unstable direction as follows (see Subsection 10.3.1):

$$\begin{cases} a(t) \sim C_1 e^{(N-2)t}, \\ b(t) \sim C_1 (N-2) e^{(N-2)t}, \end{cases} \qquad \text{as} \quad t \to -\infty.$$

Therefore,

$$\lim_{t \to -\infty} a(t) = \lim_{t \to -\infty} \dot{a}(t) = 0$$

holds.

Next, consider the flow on the line $b = (N-2)a$ on which the eigenvector $(1, N-2)^T$ of E_0 in the unstable direction in the first quadrant of the ab-plane rides. In this case, from

$$\dot{a}\big|_{b=(N-2)a} = b = (N-2)a, \quad \dot{b}\Big|_{b=(N-2)a} = (N-2)^2 a,$$

the trajectory starting from points on $\mathcal{W}^s(E_3)$ is found to go to $\Phi = \{(a, b) \mid b > (N-2)a, a > 0, b > 0\}$ as Φ in the first quadrant. In other words, there is no way to leave this area.

Finally, it is sufficient to show that equilibrium E_3 at infinity exists in this region Φ and that trajectories departing from a point in Φ are toward $\mathcal{W}^s(E_3)$. Then, we take a compact subset $W \subset \Phi$ (such that it contains a point on $\mathcal{W}^s(E_3)$). There is no equilibrium or closed orbit in W. Therefore, by Poincaré-Bendixson theorem, any trajectory starting from a point in W cannot remain in W as t increases. Therefore, any trajectories starting from points in Φ must be toward $\mathcal{W}^s(E_3)$. This means that the equilibrium E_3 at infinity

lies in the region Φ in this first quadrant. Thus, it can be shown that a trajectory starting from points on $\mathcal{W}^u(E_0)$ heads toward $\mathcal{W}^s(E_3)$. This completes the proof of Lemma 10.3.3. □

By the same argument as in Lemma 10.3.3, we can classify all the connected orbits in the Poincaré-Lyapunov disk at $\kappa = -1$. Then, by the transformation

$$b \mapsto -b, \quad t \mapsto -t,$$

we also obtain the case $\kappa = 1$. From the above discussion, we obtain Figure 10.3.1.

We have discussed the cases $\alpha = 1$ and $\beta = 0$. The dynamics at the disks for $\alpha < \beta$ are obtained from (10.1.17) as described above (see Figure 10.3.2). Note that for Figure 10.3.2, the equilibria are numbered at the positions obtained by the symmetry (10.1.17).

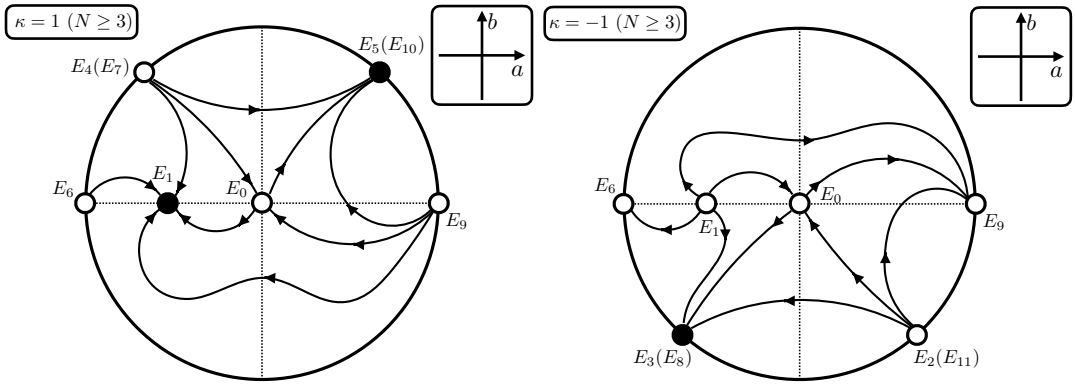

Figure 10.3.2: Schematic pictures of the connecting orbits on the Poincaré-Lyapunov disk in the case that $N \geq 3$, $\kappa = \pm 1$ and $\alpha < \beta$.

10.3.8 Dynamics on the Poincaré-Lyapunov disk of (10.1.16) in the case that $\alpha < \beta$

In this subsection, all the dynamics of (10.1.16) on $\mathbb{R}^2 \cup \{\|(a,b)\| = +\infty\}$ in the case that $\alpha < \beta$. This is obtained from the symmetry of the results obtained in Subsection 10.3.7, but only the results are summarized for the proof of the main results (in particular, the derivation of the asymptotic behavior). All (10.1.16) treated in this section are assumed to be the case when $\alpha < \beta$.

Dynamics near finite equilibria of (10.1.16)

The finite equilibria of (10.1.16) are

$$E_0 : (a,b) = (0,0), \quad E_1 : (a,b) = (-2(\beta - \alpha)^{-1}, 0).$$

The Jacobi matrices at each equilibrium, their eigenvalues and eigenvectors are the same as in Subsection 10.3.1.

Dynamics on the chart $\overline{U}_2$

The type and order of (10.1.16) in $\alpha < \beta$ are the same as those of Lemma 10.3.1. As in Subsection 10.3.3, we introduce coordinates (λ, x) by the formulas

$$a = x/\lambda, \quad b = 1/\lambda^2,$$

and time-rescaling $d\tau/dt = \lambda^{-1}$. Then we have

$$\begin{cases} \lambda_\tau = 2^{-1}\kappa(N-4)\lambda^2 + 2^{-1}\kappa(\alpha-\beta)\lambda x - (N-2)\lambda^3 x + 2^{-1}(N-2)(\alpha-\beta)\lambda^2 x^2, \\ x_\tau = 1 + 2^{-1}\kappa(N-4)\lambda x + 2^{-1}\kappa(\alpha-\beta)x^2 - (N-2)\lambda^2 x^2 + 2^{-1}(N-2)(\alpha-\beta)\lambda x^3. \end{cases} \tag{10.3.11}$$

- If $\kappa = -1$, then there is no equilibrium.
- If $\kappa = 1$, then there exists equilibria

  $$E_4 : (\lambda, x) = (0, -\sqrt{2(\beta-\alpha)^{-1}}), \quad E_5 : (\lambda, x) = (0, \sqrt{2(\beta-\alpha)^{-1}}).$$

  The Jocobian matrices at these equilibria are

  $$E_4 : \begin{pmatrix} 2^{-1}(\beta-\alpha)\sqrt{2(\beta-\alpha)^{-1}} & 0 \\ 2^{-1}N\sqrt{2(\beta-\alpha)^{-1}} & (\beta-\alpha)\sqrt{2(\beta-\alpha)^{-1}} \end{pmatrix},$$
  $$E_5 : \begin{pmatrix} -2^{-1}(\beta-\alpha)\sqrt{2(\beta-\alpha)^{-1}} & 0 \\ -2^{-1}N\sqrt{2(\beta-\alpha)^{-1}} & -(\beta-\alpha)\sqrt{2(\beta-\alpha)^{-1}} \end{pmatrix} = J_5.$$

  Therefore, E_4 is unstable and E_5 is asymptotically stable. The eigenvalues of matrix J_5 are $-2^{-1}(\beta-\alpha)\sqrt{2(\beta-\alpha)^{-1}}$ and $-(\beta-\alpha)\sqrt{2(\beta-\alpha)^{-1}}$. The eigenvectors corresponding to the eigenvalues are $(\beta-\alpha, -N)^T$ and $(0,1)^T$, respectively.

Dynamics on the chart $\overline{V}_2$

The change pf coordinates $a = -x/\lambda$ and $b = -1/\lambda^2$, and time-rescaling $d\tau/dt = \lambda^{-1}$ yield

$$\begin{cases} \lambda_\tau = 2^{-1}\kappa(N-4)\lambda^2 - 2^{-1}\kappa(\alpha-\beta)\lambda x - (N-2)\lambda^3 x - 2^{-1}(N-2)(\alpha-\beta)\lambda^2 x^2, \\ x_\tau = 1 + 2^{-1}\kappa(N-4)\lambda x - 2^{-1}\kappa(\alpha-\beta)x^2 - (N-2)\lambda^2 x^2 - 2^{-1}(N-2)(\alpha-\beta)\lambda x^3. \end{cases} \tag{10.3.12}$$

When $\kappa = 1$, there is no equilibrium, and when $\kappa = -1$, there are two equilibria,

$$E_2 : (\lambda, x) = (0, -\sqrt{2(\beta-\alpha)^{-1}}), \quad E_3 : (\lambda, x) = (0, \sqrt{2(\beta-\alpha)^{-1}}).$$

By deriving the linearized matrices at these equilibria, E_2 is unstable and E_3 is asymptotically stable. The eigenvalues of Jacobian matrix at E_3 are $-2^{-1}(\beta-\alpha)\sqrt{2(\beta-\alpha)^{-1}}$ and $-(\beta-\alpha)\sqrt{2(\beta-\alpha)^{-1}}$. The eigenvectors corresponding to the eigenvalues are $(\beta-\alpha, N)^T$ and $(0,1)^T$, respectively.

Dynamics on the chart $\overline{U}_1$

The change pf coordinates $a = 1/\lambda$ and $b = x/\lambda^2$, and time-rescaling $d\tau/dt = \lambda^{-1}$ yield

$$\begin{cases} \lambda_\tau = -\lambda x, \\ x_\tau = -\kappa(N-4)\lambda x - \kappa(\alpha-\beta)x + 2(N-2)\lambda^2 - (N-2)(\alpha-\beta)\lambda - 2x^2. \end{cases} \tag{10.3.13}$$

If $\kappa = 1$, then the equilibria on $\{\lambda = 0\}$ are

$$E_9 : (\lambda, x) = (0, 0), \quad E_{10} : (\lambda, x) = (0, 2^{-1}(\beta-\alpha)).$$

If $\kappa = -1$, then the equilibria on $\{\lambda = 0\}$ are E_9 and

$$E_{11} : (\lambda, x) = (0, -2^{-1}(\beta-\alpha)).$$

By deriving the linearized matrices at these equilibria, E_9 is not hyperbolic and E_{10} is asymptotically stable, and E_{11} is unstable. The dynamics around E_9 can be understood by the center manifold theorem as in Subsection Subsection 10.3.5. In addition, we can obtain (10.3.7) and (10.3.8).

Dynamics on the chart $\overline{V}_1$

By using the transformations $a = -1/\lambda$ and $b = -x/\lambda^2$, and time-rescaling $d\tau/dt = \lambda^{-1}$, we have

$$\begin{cases} \lambda_\tau = -\lambda x, \\ x_\tau = -\kappa(N-4)\lambda x + \kappa(\alpha-\beta)x + 2(N-2)\lambda^2 + (N-2)(\alpha-\beta)\lambda - 2x^2. \end{cases} \tag{10.3.14}$$

If $\kappa = 1$, then the equilibria on $\{\lambda = 0\}$ are

$$E_6 : (\lambda, x) = (0, 0), \quad E_7 : (\lambda, x) = (0, -2^{-1}(\beta - \alpha)).$$

If $\kappa = -1$, then the equilibria are E_6 and $E_8 : (\lambda, x) = (0, 2^{-1}(\beta - \alpha))$. As before, by finding the linearized matrices at these equilibria, E_7 is unstable, E_8 is asymptotically stable, and E_6 is not hyperbolic. The dynamical system around E_6 can be understood by the center manifold theorem as in Subsection 10.3.5.

10.4 Proof of theorems

In this section, we prove our main results. If the initial data exists within a finite range in the Poincaré-Lyapunov disk, the existence of the solutions follows from the standard theory for the ordinary differential equations. Therefore, we consider the existence of the trajectories that connect equilibria and the detailed dynamics near the equilibria on the Poincaré-Lyapunov disk and their asymptotic behavior. Table 10.1 shows the correspondence between each connecting orbit in the case that $\alpha = 1$ and $\beta = 0$ (see Figure 10.3.1) and the radial symmetric stationary solutions described in the theorem proved below.

Table 10.1: The correspondence between each connecting orbit in Subsection 10.3.7 and the radial symmetric stationary solutions described in the theorem proved below (see also Figure 10.3.1).

Proposition/Theorem	Connecting orbits ($\kappa = 1$)	Connecting orbits ($\kappa = -1$)
Theorem 10.2.1	between E_0 and E_1	between E_1 and E_0
Proposition 10.2.1	between E_4 / E_9 and E_1	between E_1 and E_3 / E_9

Table 10.2 shows the correspondence between each connecting orbit in the case that $\alpha < \beta$ (see Figure 10.3.2) and the radial symmetric stationary solutions described in the theorem proved below.

Table 10.2: The correspondence between each connecting orbit obtained by the proposition and the radial symmetric stationary solutions described in the theorem proved below (see also Figure 10.3.2).

Theorem	Connecting orbits ($\kappa = 1$)	Connecting orbits ($\kappa = -1$)
Theorem 10.2.2 (i)	between E_4 and E_5	between E_2 and E_3
Theorem 10.2.2 (ii)	between E_4 and E_0	between E_0 and E_3
Theorem 10.2.2 (iii)	between E_0 and E_5	between E_2 and E_0

10.4.1 Proof of Theorem 10.2.1

Proof. First, the proof of the existence of the connecting orbit between E_0 and E_1 is obtained in Subsection 10.3.7. Therefore, equation (10.1.5) has the radially symmetric stationary solution which corresponds to the orbit of (10.1.16).

Second, we show that $u(r) > 0$ for $r \in (0, +\infty)$. For $\kappa = -1$, this orbit is in region $\{(a, b) \mid b < (N-2)a\}$ (see Figure 10.3.1). Thus, from (10.1.11), (10.1.12) and (10.1.16), we have

$$u = rw_r + Nw = r^{-2}((N-2)a - b) > 0,$$

which implies that $u(r) > 0$ for $r \in (0, +\infty)$.

Next, we show that

$$\lim_{r\to 0} u(r) = C, \quad \lim_{r\to 0} u'(r) = 0.$$

For $\kappa = -1$, the solution around the equilibrium E_0 is

$$\begin{pmatrix} a(t) \\ b(t) \end{pmatrix} = C_1 e^{(N-2)t} \begin{pmatrix} 1 \\ N-2 \end{pmatrix} + C_2 e^{-2t} \begin{pmatrix} 1 \\ -2 \end{pmatrix}.$$

Here, by focusing on the trajectory from region $\{(a, b) \mid a > 0, b < 0\}$ into the point on $\mathcal{W}^u(E_0)$, i.e., along the eigenvector $(1, -2)^T$ of E_0, the principal terms of the solution are as follows:

$$\begin{cases} a(t) \sim C_2 e^{-2t}, \\ b(t) \sim -2C_2 e^{-2t}, \end{cases} \qquad \text{as} \quad t \to +\infty.$$

Using (10.1.14) for $\kappa = -1$, we obtain

$$\lim_{r\to 0} w(r) = \lim_{r\to 0} r^{-2} a = C_2, \quad \lim_{r\to 0} w'(r) = 0.$$

Therefore, we obtain

$$\lim_{r\to 0} u(r) = \lim_{r\to 0}(rw_r + Nw) = C_2 N, \quad \lim_{r\to 0} u'(r) = \lim_{r\to 0}\{-(N-4)C_2^2 r\} = 0$$

from (10.1.11).

Finally, we shall compute the asymptotic behavior of u for $r \to +\infty$ the trajectory near the equilibrium E_1. The derivation of the asymptotic behavior of u for $r \to +\infty$ is almost the same as in [32, 33, 38], but is reproduced for the reader's convenience. We define

$$\tilde{a} = a - 2, \quad \tilde{b} = b - 0.$$

Then, there are three cases to consider:

(i) Let us consider the case that $N \geq 11$, namely, the matrix J_1 has the real distinct eigenvalues $\sigma_\pm$ (see Subsection 10.3.1). By using the eigenvalues and corresponding eigenvectors of J_1, we then obtain the following behavior:

$$\begin{pmatrix} \tilde{a}(t) \\ \tilde{b}(t) \end{pmatrix} = C_1 \begin{pmatrix} 1 \\ \sigma_- \end{pmatrix} e^{\sigma_- t} + C_2 \begin{pmatrix} 1 \\ \sigma_+ \end{pmatrix} e^{\sigma_+ t}$$

with any constants C_j $(j = 1, 2)$. Therefore, the solution around the equilibrium E_1 is

$$\begin{cases} a(t) = C_1 e^{\sigma_- t} + C_2 e^{\sigma_+ t} + 2, \\ b(t) = C_1 \sigma_- e^{\sigma_- t} + C_2 \sigma_+ e^{\sigma_+ t}. \end{cases}$$

Using $\kappa = 1$ in (10.1.14), we derive the following:

$$w(r) \sim 2r^{-2} \sim 2r^{-2} + r^{-2} + C_1 r^{-2+\sigma_-} + C_2 r^{-2+\sigma_+} \quad \text{as} \quad r \to +\infty.$$

Similarly, we obtain

$$w_r(r) \sim -4r^{-3} \sim -4r^{-3} + (-2+\sigma_-)C_1 r^{-3+\sigma_-} + (-2+\sigma_+)C_2 r^{-3+\sigma_+} \quad \text{as} \quad r \to +\infty.$$

Note that $-2 + \sigma_\pm < 0$ holds. Hence, from the above discussion and (10.1.11), we obtain as follows:

$$\begin{aligned} u(r) &\sim 2(N-2)r^{-2} \\ &\sim 2(N-2)r^{-2} + (N-2+\sigma_-)C_1 r^{-2+\sigma_-} + (N-2+\sigma_+)C_2 r^{-2+\sigma_+} \end{aligned}$$

as $r \to +\infty$. Since C_1 and C_2 are arbitrary constants, it holds that $N - 2 + \sigma_\pm > 0$.

(ii) Consider the case that $N = 10$, namely, the matrix J_1 has a multiple real eigenvalue $\sigma = -2^{-1}(N-2) < 0$. The eigenvector and the generalized eigenvector corresponding to the eigenvalue are $(1, -4)^T$ and $(1, -3)^T$. Therefore, the solution around the equilibrium E_1 is

$$\begin{cases} a(t) = (C_1 t + C_2)e^{-4t} + C_1 e^{-4t} + 2, \\ b(t) = -4(C_1 t + C_2)e^{-4t} - 3C_1 e^{-4t}, \end{cases}$$

where C_j are constants. Using $\kappa = 1$ in (10.1.14), we derive the following:

$$\begin{aligned} &w(r) \sim 2r^{-2} \sim 2r^{-2} + C_1 r^{-6} \log r + (C_1 + C_2)r^{-6} \quad \text{as} \quad r \to +\infty, \\ &w_r(r) \sim -4r^{-3} \sim -4r^{-3} - 6C_1 r^{-7} \log r - 5C_1 r^{-7} - 6C_2 r^{-7} \quad \text{as} \quad r \to +\infty. \end{aligned}$$

Hence, from the above discussion and (10.1.11), we obtain as follows:

$$u(r) \sim 16r^{-2} \sim 16r^{-2} + r^{-6}[4C_1 \log r + 5C_1 + 4C_2] \quad \text{as} \quad r \to +\infty.$$

(iii) Consider the case that $3 \le N \le 9$. The matrix J_1 has the complex eigenvalues

$$\sigma = -\frac{N-2}{2} \pm i\frac{1}{2}\sqrt{|D|}, \quad D = (N-2)(N-10).$$

The eigenvectors corresponding to each eigenvalue are

$$\mathbf{v} = \begin{pmatrix} 1 \\ -2^{-1}(N-2) \end{pmatrix} \pm i \begin{pmatrix} 0 \\ 2^{-1}\sqrt{|D|} \end{pmatrix}.$$

The function $\tilde{a}(t)$ and $\tilde{b}(t)$ are expressed as following:

$$\begin{pmatrix} \tilde{a}(t) \\ \tilde{b}(t) \end{pmatrix} = z(t) \begin{pmatrix} 0 \\ 2^{-1}\sqrt{|D|} \end{pmatrix} + w(t) \begin{pmatrix} 1 \\ -2^{-1}(N-2) \end{pmatrix},$$

where

$$\begin{pmatrix} z(t) \\ w(t) \end{pmatrix} = e^{-\frac{(N-2)}{2}t} \begin{pmatrix} \cos[2^{-1}\sqrt{|D|}t] & -\sin[2^{-1}\sqrt{|D|}t] \\ \sin[2^{-1}\sqrt{|D|}t] & \cos[2^{-1}\sqrt{|D|}t] \end{pmatrix} \begin{pmatrix} z(0) \\ w(0) \end{pmatrix}.$$

Therefore, the solution around the equilibrium E_1 is

$$\begin{cases} a(t) = 2 + e^{-\frac{(N-2)}{2}t}W(t), \\ b(t) = 2^{-1}\sqrt{|D|}e^{-\frac{(N-2)}{2}t}Z(t) - 2^{-1}(N-2)e^{-\frac{(N-2)}{2}t}W(t), \end{cases}$$

where $Z(t)$ and $W(t)$ are

$$\begin{aligned} Z(t) &= z(0)\cos[2^{-1}\sqrt{|D|}t] - w(0)\sin[2^{-1}\sqrt{|D|}t], \\ W(t) &= z(0)\sin[2^{-1}\sqrt{|D|}t] + w(0)\cos[2^{-1}\sqrt{|D|}t]. \end{aligned}$$

Using (10.1.14) for $\kappa = 1$, we obtain from $Z(t)$ and $W(t)$ the following:

$$\begin{aligned} \overline{Z}(r) &= z(0)\cos[2^{-1}\sqrt{|D|}\log r] - w(0)\sin[2^{-1}\sqrt{|D|}\log r], \\ \overline{W}(r) &= z(0)\sin[2^{-1}\sqrt{|D|}\log r] + w(0)\cos[2^{-1}\sqrt{|D|}\log r]. \end{aligned}$$

Therefore, we obtain

$$\begin{aligned} w(r) &\sim 2r^{-2} \\ &\sim 2r^{-2} + r^{-\frac{N+2}{2}}\overline{W} \quad \text{as} \quad r \to +\infty, \\ w_r(r) &\sim -4r^{-3} \\ &\sim -4r^{-3} - 2^{-1}(N+2)r^{-\frac{N+4}{2}}\overline{W} + 2^{-1}\sqrt{|D|}r^{-\frac{N+4}{2}}\overline{Z} \quad \text{as} \quad r \to +\infty. \end{aligned}$$

Hence, from the above discussion and (10.1.11), we obtain as follows:

$$\begin{aligned} u(r) &\sim 2(N-2)r^{-2} \\ &\sim 2(N-2)r^{-2} + 2^{-1}(N-2)r^{-\frac{N+2}{2}}\overline{W} + 2^{-1}\sqrt{|D|}r^{-\frac{N+2}{2}}\overline{Z} \quad \text{as} \quad r \to +\infty. \end{aligned}$$

Therefore, we obtain the asymptotic behavior (10.2.1) and (10.2.2). This completes the proof of Theorem 10.2.1. □

10.4.2 Proof of Proposition 10.2.1

Proof. We show that (10.1.5) corresponding to the cases $\alpha = 1$ and $\beta = 0$ has no sign-changing solution. In ab-plane, when $\kappa = -1$, there exists t_* such that $t_* = -\log r_*$, $r_* \in (0, +\infty)$ and

$$u(r_*) = r_* w_r(r_* + Nw(r_*) = r_*^{-2}\{(N-2)a(t_*) - b(t_*)\}.$$

That is, the trajectory through line $b = (N-2)a$ in the Poincaré-Lyapunov disk corresponds to a sign-changing radially symmetric stationary solution. Two types of trajectories correspond to this: one starting from points on $\mathcal{W}^u(E_1)$ and reaching points on $\mathcal{W}^{cs}(E_9)$, and the other starting from points on $\mathcal{W}^u(E_1)$ and reaching points on $\mathcal{W}^s(E_3)$. Then, passing through this line, $u(r)$ turns from positive to negative due to the increase in t (decrease in r) when $\kappa = -1$.

In addition,

$$u_r(r_*) = r_*^{-3}a(t_*)\{b(t_*) - (N-2)a(t_*)\} = 0$$

holds when passing through this line. Then, $u'(r)$ turns from positive to negative due to the increase in t (decrease in r) when $\kappa = -1$. In the region $\{(a, b) \mid a > 0\}$ for $\kappa = -1$,

we see that $u_r(r)$ turns from negative to positive due to the increase in t (decrease in r) as it passes through this line.

In other words, the signs of $u(r)$ and $u_r(r)$ both reverse when passing through this line, contradicting the shape of the solution. Both of the two types of trajectories described above are consistent in the sense of (10.1.16), but are inconsistent in shape and increase/decrease relation in the sense of the solution of (10.1.5), which claims the non-existence of a sign-changing radially symmetric stationary solution. The same conclusion can be reached for (10.1.6). This completes the proof of Proposition 10.2.1. □

10.4.3 Proof of Theorem 10.2.2

Proof. **(i)** Similar to the proof of Theorem 10.2.1 in Subsection 10.4.1, there exists a family of the functions (which corresponds to a family of the corresponding orbits of E_2 and E_3 in the case that $\alpha < \beta$) defined on the finite interval such that each function $u(r)$ satisfies (10.1.6) on a finite interval (r_-, r_+) $(0 < r_- < r_+ < +\infty)$. In addition, we see that $u(r) > 0$ for $r \in (r_-, r_+)$. Note that it follows from Lemma 10.3.2 and Lemma 10.3.3 that $0 < r_- < r_+ < +\infty$. From the discussion in Subsection 10.4.2, there exists $t_* = \kappa \log r_*$ such that $u_r(r_*) = 0$ since these connecting orbits pass through the line $a = 0$. All that remains is to derive (10.2.3) and (10.2.4).

First, we show (10.2.3). For $\alpha < \beta$, we obtain

$$
\begin{aligned}
&w(r) \sim -K_1 r^{-2}(\log r - \log r_-)^{-1} \quad \text{as} \quad r \to r_- + 0 \\
&w_r(r) \sim 2K_1 r^{-3}(\log r - \log r_-)^{-1} + K_1 r^{-3}(\log r - \log r_-)^{-2} \quad \text{as} \quad r \to r_- + 0
\end{aligned}
$$

from (10.1.14) by the same argument as (10.3.10) in Lemma 10.3.2 (see Appendix B, if necessary). Hence, from these discussion and (10.1.11), we obtain (10.2.3) as follows:

$$
u(r) \sim K_1 r^{-2}(\log r - \log r_-)^{-2}[-(N-2)(\log r - \log r_-) + 1] \quad \text{as} \quad r \to r_- + 0.
$$

Similarly, (10.2.4) and the following are also shown.

$$
\lim_{r \to r_- + 0} u(r) = +\infty, \quad \lim_{r \to r_+ - 0} u(r) = +\infty.
$$

(ii) The existence of functions satisfying equation (10.1.6) and their positivity can be shown in the same way as in the above proof (i). The behavior of the solution for $r \to +\infty$ is shown by the following. For $\kappa = 1$, the solution around the equilibrium E_0 is

$$
\begin{pmatrix} a(t) \\ b(t) \end{pmatrix} = C_1 e^{2t} \begin{pmatrix} -1 \\ -2 \end{pmatrix} + C_2 e^{-(N-2)t} \begin{pmatrix} -1 \\ N-2 \end{pmatrix}.
$$

Here, by focusing on the trajectory from region $\{(a, b) \mid a < 0, b > 0\}$ into the point on $\mathcal{W}^u(E_0)$, i.e., along the eigenvector $(-1, N-2)^T$ of E_0, the principle terms of the solution are as follows:

$$
\begin{cases} a(t) \sim -C_2 e^{-(N-2)t}, \\ b(t) \sim (N-2) C_2 e^{-(N-2)t}, \end{cases} \qquad \text{as} \quad t \to +\infty.
$$

Using (10.1.14) for $\kappa = 1$, we obtain

$$
\lim_{r \to +\infty} w(r) = \lim_{r \to +\infty} (-C_2) r^{-N} = 0, \quad \lim_{r \to +\infty} w'(r) = N C_2 r^{-(N-1)} = 0.
$$

Therefore, we obtain

$$\lim_{r\to+\infty} u(r) = \lim_{r\to+\infty}(rw_r + Nw) = 0, \quad \lim_{r\to+\infty} u_r(r) = 0$$

from (10.1.11).
(iii) The existence of functions satisfying equation (10.1.6) and their positivity can be shown in the same way as in the above proof (i), and by the same process as in Subsection 10.4.1, the following is shown:

$$\lim_{r\to 0} u(r) = C, \quad \lim_{r\to 0} u_r(r) = 0.$$

This completes the proof of Theorem 10.2.2. □

10.5 Discussion

In this chapter, we use dynamical systems theory and geometric approaches to reveal previously unknown aspects of radially symmetric stationary solutions of some chemotaxis equations. The introduction of the transformation of integral (10.1.7) in (10.1.5) and (10.1.6) has made the analysis easier by attributing the problem to scalar equations. This is because it is related to the author's previous works to investigate dynamics at infinity in 2-dimensional ODE (10.1.16). However, a limitation such as (10.1.8) is added to the solution obtained. In this connection, there are connecting orbits in the dynamics at infinity that do not give a conclusion. Some orbits also exist as connecting orbits but cannot be explained with the corresponding solution's shape. This chapter provides a discussion of them.

10.5.1 A connecting orbit between E_1 and E_6 in the case $\alpha = 1$ and $\beta = 0$

For $\alpha = 1$, $\beta = 0$, and $\kappa = -1$, the existence of a connecting orbit between E_1 and E_6 is obtained in Subsection 10.3.7 (see Figure 10.3.1). Therefore, there is a radially symmetric stationary solution of (10.1.5) corresponding to this orbit of (10.1.16).

For $\kappa = -1$, this orbit is in region $\{(a, b) \mid b < (N-2)a\}$ (see Figure 10.3.1). Thus, from (10.1.11), (10.1.12) and (10.1.16), we have

$$u = rw_r + Nw = r^{-2}((N-2)a - b) > 0,$$

which implies that $u(r) > 0$ for $r \in (0, +\infty)$. Note that $E_6 : (a, b) = (+\infty, 0)$ for $\kappa = -1$, and from (10.1.11), (10.1.12), and (10.1.16) we obtain

$$\lim_{r\to 0} u(r) = \lim_{r\to 0}(rw_r + Nw) = \lim_{r\to 0} r^{-2}((N-2)a - b) = +\infty.$$

A singular solution is a solution $u(r)$ satisfying (10.1.5) and

$$\lim_{r\to 0} u(r) = +\infty.$$

We can see that the solution corresponding to the connecting orbit between E_1 and E_6 that we are now discussing is a singular solution. However, it is known that the positive-valued singular solution of (10.1.1) is unique from the uniqueness of the positive-valued singular solution of (10.1.4) derived from (10.1.1) (see [52, 53]).

At first glance, it appears to be a contradiction. In fact, the solution corresponding to the connecting orbit between E_1 and E_6 does not satisfy (10.1.8). The reason for this is explained below.

From (10.3.7) and (10.3.8), the solution near the equilibrium E_6 at infinity is

$$\begin{cases} \lambda(\tau) = [(N-2)\tau + L_1]^{-1}, \\ x(\tau) = (N-2)[(N-2)\tau + L_1]^{-1} \end{cases}$$

if the initial value exists on the central manifold ($\tilde{x} = 0$). Here, L_1 is a constant. Note that $\kappa = -1$ since we examine $r \to 0$. From $\lambda(0) = L_1^{-1} > 0$, we obtain that $L_1 > 0$. Then,

$$\frac{d\tau}{dt} = \lambda^{-1} = (N-2)\tau + L_1$$

holds. This yields

$$\tau(t) = \frac{L_2}{N-2} e^{(N-2)t} - \frac{L_1}{N-2}.$$

Since $L_2 > 0$, this formula shows that $t \to +\infty$ corresponds to $\tau \to +\infty$. Therefore, we have

$$a(t) = \lambda^{-1} = (N-2)\tau + L_1 = L_2 e^{(N-2)t}.$$

Using (10.1.14) for $\kappa = -1$, we obtain

$$w(r) = r^{-2} a \sim L_2 r^{-N} \quad \text{as} \quad r \to 0.$$

Therefore, from $L_2 > 0$, $w(r)$ does not satisfy (10.1.8).

What the above discussion suggests is that for solutions that are non-bounded at the origin, one must investigate whether (10.1.8) is satisfied. This is because the transformation (10.1.7) of the integral is used to investigate radially symmetric stationary solutions.

10.5.2 A connecting orbit between E_0 and E_6 in the case $\alpha < \beta$

Consider the solution corresponding to the connecting orbit between E_0 and E_9 (together, Figure 10.3.2) in the case $\alpha < \beta$. From the same discussion as in Subsection 10.4.1, we see that there exists a corresponding radially symmetric stationary solution $u(r) > 0$ for $r \in (0, +\infty)$ and

$$\lim_{r \to 0} u(r) = +\infty$$

holds. This should be a singular solution, but the same argument as for Subsection 10.5.1 shows that it does not satisfy (10.1.8).

10.5.3 Connecting orbits between E_2 and E_9 in the case $\alpha < \beta$

Finally, in the case $\alpha < \beta$ and $\kappa = -1$ (see Figure 10.3.2), we give a note on the radially symmetric stationary solutions corresponding to the connecting orbits between E_2 and E_9. Note that these orbits connect between E_5 and E_9 for $\kappa = 1$. Focusing on the trajectories entering E_5 for $\kappa = 1$, the asymptotic behavior is (10.2.4). On the other hand, From the same discussion as in Subsection 10.4.1, the corresponding behavior for the trajectories entering E_9 for $\alpha < \beta$ is

$$\lim_{r \to 0} u(r) = +\infty.$$

In other words, there should exist $r_* \in (0, r_+)$ such that $u_r(r_*) = 0$ when considering the shape of the radially symmetric stationary solutions corresponding to the connecting

orbits. However, for r_* to exist, the trajectory must pass through a straight line with either $a = 0$ or $b = (N-2)a$, which is not possible. For the above reasons, the solutions corresponding to the connecting orbits are considered to be meaningless as solutions to the original PDE since the existence of r_*, which should exist with respect to the shape, cannot be claimed.

Chapter 11

On global behavior of a some SIR epidemic model based on the Poincaré compactification

Abstract

It is important to study the global behavior of solutions to systems of ordinary differential equations describing the transmission dynamics of infectious disease. In this chapter, we present a different approach from the Lyapunov function used in most of the study. This approach is based on the Poincaré compactification. We then apply the method to an SIR endemic model as a test case, and discuss its effectiveness and the potential applications of this approach. In addition, we refine the discussion of dynamics near the equilibrium, derive the asymptotic behavior, and mention its relation to the basic reproduction number. This chapter is based on the following published paper ([34]):

> Ichida, Y: On global behavior of a some SIR epidemic model based on the Poincaré compactification, JSIAM Lett., **14** (2022), 65–68.

11.1 Introduction

There have been many studies dealing with systems of ordinary differential equations (for short, ODEs) describing the transmission dynamics of infectious disease. In particular, these fundamental questions are the global behavior of the solution for systems of ODEs, such as the number of infectious and their final state, and the derivation of the basic reproduction number, which plays an important role in understanding this behavior. For details on the basic reproduction number and its derivation, for instance, see [67] and references therein. Let us denote the basic reproduction number by $\mathcal{R}_0$.

In many studies, the Lyapunov function is constructed and discussed in order to investigate the global behavior of the solution. Note that understanding the global behavior of the solution is the same as studying the global stability of the equilibrium. Global stability of an equilibrium is defined as the local asymptotic stability of the equilibrium and the convergence of all solutions of the system of ODE under consideration to the equilibrium. The method of investigating the global stability of equilibria by means of the Lyapunov function is very powerful, but to the best of the author's knowledge, there is no theoretical system that constitutes the Lyapunov function in general (for instance, see [70]). In other words, when investigating the global behavior of solutions to complex systems of ODEs

that incorporate more elements, constructing the Lyapunov function is itself a difficult problem. Therefore, investigating the global behavior of solutions is not an easy work in general.

In this chapter, we present a method using the Poincaré compactification (see Section 1.1) to study the global behavior of solutions. We then apply the method to a mathematical model of infectious disease epidemics described by a system of ODE. Note that this is essentially different from the analysis method using the Lyapunov function. An overview of Poincaré compactification is given in [14], which is one of the compactifications of the phase space (the embedding of $\mathbb{R}^n$ into the unit upper hemisphere of $\mathbb{R}^{n+1}$) (see, e.g. [14, 31, 32, 33, 49, 50]). The most important feature of applying this method is that it allows us to investigate the global behavior of the system of ODEs of interest by revealing all its dynamics including infinity. This method has been used, for instance, in the analysis of the Liénard equation ([14] and references therein), in the classification of phase portraits of ODE systems derived from the Gray-Scotte model ([10]), in the reconsideration of blow-up solutions of systems of ODEs in the view of dynamical systems ([49, 50]), and in the analysis of the behavior of characteristic and typical solutions of certain partial differential equations ([31, 32, 33]). To the best of the author's knowledge, there are no studies of its application to investigate the global behavior of solutions to ODEs related to infectious disease epidemics, such as the susceptible-infectious-recovered (SIR) model. In this chapter, we describe how to apply this method. Using one of the most basic and representative mathematical models of infectious diseases, the SIR model such that it has birth and death terms (e.g., [28]) as a test case, we show that the global behavior of the solution can be studied by this method. It should be emphasized that this method can be used without constructing the Lyapunov function.

Furthermore, by refining the dynamics near the equilibria that are not located at infinity in this model (disease-free equilibria and epidemic equilibria, to be discussed in Subsection 11.2.2), we obtain the asymptotic behavior of the decay of infectious population for $\mathcal{R}_0 < 1$ and $\mathcal{R}_0 = 1$. In particular, this is studied by applying the center manifold theory in the case that $\mathcal{R}_0 = 1$.

This chapter is organized as follows. In Section 11.2, we describe the specific model described above and review the previously known methods for understanding the global behavior of solutions in that model. This is based on the LaSalle's invariance principle with the Lyapunov function. In Section 11.3, we apply the Poincaré compactification and concentrate on showing the effectiveness of this method for the concrete example presented in Section 11.2. Section 11.4 shows the asymptotic behavior. Finally, Section 11.5 is devoted to the conclusions and the possible applications of this method.

11.2 The model as a test case

In this section, we present a model as a test case to verify the effectiveness of the above method based on the Poincaré compactification. Before testing this method, we briefly review known results for the global behavior obtained by using the LaSalle's invariance principle with the Lyapunov function that are known.

11.2.1 The model

In this chapter, the following model is treated as a concrete example (see [63]):

$$\begin{cases} \dot{S} = A - \beta S(t)I(t) - \mu S(t), \\ \dot{I} = \beta S(t)I(t) - qI(t) - \mu I(t), \\ \dot{R} = qI(t) - \mu R(t), \end{cases} \qquad \left(\dot{} = \frac{d}{dt} \right). \tag{11.2.1}$$

The ODE system (11.2.1) is called an SIR model with birth and death terms, and is one of the classical and representative mathematical models for infectious diseases. To be more precise, we modify the Kermack-McKendrick model (for instance, see [55]), which is the most typical SIR model, to introduce the fertility rate A as inputs and the natural mortality rate μ. The model with $A = \mu$ is described, for instance, in [28]. The model (11.2.1) assumes that infection has no effect on births or deaths and that there is no vertical transmission.

$S(t)$ represents the susceptible population, $I(t)$ the infectious population, and $R(t)$ the recovered population, which are non-negative functions. In this model, we impose initial conditions such as $S(0) > 0$, $I(0) > 0$, and $R(0) \geq 0$. The constants A, β, μ, q are positive. Furthermore, in (11.2.1), the first and second equations do not contain any information about $R(t)$. Therefore, it is sufficient to consider the following 2D:

$$\begin{cases} \dot{S} = A - \beta S(t)I(t) - \mu S(t), \\ \dot{I} = \beta S(t)I(t) - qI(t) - \mu I(t), \end{cases} \qquad \left(\dot{} = \frac{d}{dt} \right). \tag{11.2.2}$$

The basic reproduction number for this model is known to be $\mathcal{R}_0 = A\beta/\mu(q+\mu)$.

11.2.2 Known results

Eq. (11.2.2) has the following equilibria:

$$\begin{aligned} &E_0 : (S, I) = \left(A\mu^{-1}, 0 \right), \\ &E_* : \left((q+\mu)\beta^{-1}, \mu\beta^{-1}(\mathcal{R}_0 - 1) \right) =: (S_*, I_*), \end{aligned}$$

where E_0 is the disease-free equilibrium and E_* is the endemic equilibrium. Note that E_* exists only if $\mathcal{R}_0 > 1$. The Jacobian matrices of the vector field (11.2.2) at these equilibria are

$$\begin{aligned} E_0 &: \begin{pmatrix} -\mu & -A\beta/\mu \\ 0 & [A\beta - \mu(q+\mu)]/\mu \end{pmatrix}, \\ E_* &: \begin{pmatrix} -A\beta/(q+\mu) & -(q+\mu) \\ \mu(\mathcal{R}_0 - 1) & 0 \end{pmatrix}. \end{aligned}$$

If $\mathcal{R}_0 < 1$, then E_0 is a sink. If $\mathcal{R}_0 > 1$, then E_0 is a saddle and E_* is asymptotically stable.

According to [63], if $\mathcal{R}_0 > 1$, then E_* is globally asymptotically stable, and if $\mathcal{R}_0 \leq 1$, then E_0 is globally asymptotically stable. When $\mathcal{R}_0 > 1$, we construct the following the Lyapunov function in region Ω, which is shown by LaSalle's invariance principle:

$$V(S, I) = S - S_* - S_* \log \frac{S}{S_*} + I - I_* - I_* \log \frac{I}{I_*}.$$

Here, we set $\Omega = \{(S, I) \mid S > 0,\ I > 0\}$. On the other hand, the case $\mathcal{R}_0 \leq 1$ can be shown similarly by using the following function:

$$V(S, I) = S - A\mu^{-1} - A\mu^{-1}\log(A^{-1}\mu S) + I.$$

Thus, the method using the Lyapunov function does not have a general theory of construction, and in this model we have to construct two functions.

11.2.3 The case $\mathcal{R}_0 = 1$: Application of the center manifold theory

We focus on the Jacobian matrix of the vector field (11.2.2) at E_0 in the case that $\mathcal{R}_0 = 1$. It has the real distinct eigenvalues $-\mu$ and 0. Therefore, the center manifold theory (e.g. [9]) is applicable to study the dynamics of (11.2.2). In [28, 63], there is no discussion of this case.

We set

$$S(t) = A\mu^{-1} + U(t), \quad I(t) = 0 + V(t)$$

and

$$\begin{cases} \dot{U} = -\mu U - A\beta\mu^{-1}V - \beta UV, \\ \dot{V} = \beta UV \end{cases}$$

hold. Note that we are only shifting E_0 to the origin in this transformation.

The eigenvectors correspond to each eigenvalue are

$$\mathbf{v}_1 = \begin{pmatrix} 1 \\ 0 \end{pmatrix}, \quad \mathbf{v}_2 = \begin{pmatrix} -A\beta\mu^{-1} \\ \mu \end{pmatrix}.$$

We set a matrix T as $T = (\mathbf{v}_1, \mathbf{v}_2)$. Then we obtain

$$\begin{aligned} \frac{d}{dt}\begin{pmatrix} U \\ V \end{pmatrix} &= \begin{pmatrix} -\mu & -A\beta\mu^{-1} \\ 0 & 0 \end{pmatrix}\begin{pmatrix} U \\ V \end{pmatrix} + \begin{pmatrix} -\beta UV \\ \beta UV \end{pmatrix} \\ &= T\begin{pmatrix} -\mu & 0 \\ 0 & 0 \end{pmatrix}T^{-1}\begin{pmatrix} U \\ V \end{pmatrix} + \begin{pmatrix} -\beta UV \\ \beta UV \end{pmatrix}. \end{aligned}$$

Let

$$\begin{pmatrix} \tilde{U} \\ \tilde{V} \end{pmatrix} = T^{-1}\begin{pmatrix} U \\ V \end{pmatrix}.$$

We then obtain the following system:

$$\begin{cases} \dot{\tilde{U}} = -\mu\tilde{U} + (A\beta^2\mu^{-1} - \beta\mu)\tilde{U}\tilde{V} + (A\beta^2 - A^2\beta^3\mu^{-2})\tilde{V}^2, \\ \dot{\tilde{V}} = \beta\tilde{U}\tilde{V} - A\beta^2\mu^{-1}\tilde{V}^2. \end{cases}$$

The center manifold theory is applicable to study the dynamics of above system. It implies that there exists a function $h(\tilde{V})$ satisfying

$$h(0) = \frac{dh}{d\tilde{V}}(0) = 0$$

such that the center manifold of the origin for above system is locally represented as $\{(\tilde{U}, \tilde{V}) \mid \tilde{U}(t) = h(\tilde{V}(t))\}$. Differentiating it with respect to t, we have

$$-\mu h + (A\beta^2\mu^{-1} - \beta\mu)h\tilde{V} + (A\beta^2 - A^2\beta^3\mu^{-2})\tilde{V}^2 = \frac{dh}{d\tilde{V}}\left\{\beta h\tilde{V} - A\beta^2\mu^{-1}\tilde{V}^2\right\}. \quad (11.2.3)$$

We assume that h has the form $h(\tilde{V}(t)) = O(\tilde{V}^2)$. Substituting into (11.2.3), we obtain $\tilde{U}(t) = h(\tilde{V}(t)) = A\beta^2\mu^{-1}(1 - A\beta\mu^{-2})\tilde{V}^2 + O(\tilde{V}^3)$. The, by using the transformations in this subsection, we obtain that the approximation of the (graph of) center manifold is

$$\left\{(S, I) \mid S(t) = A\mu^{-1} - A\beta\mu^{-2}I(t) + O(I^2)\right\} \tag{11.2.4}$$

and the dynamics of (11.2.2) near E_0 is topologically equivalent to the dynamics of the following equation:

$$\dot{I} = -A\beta^2\mu^{-2}I^2 + O(I^3). \tag{11.2.5}$$

The above discussion has been made, for instance, in [32, 30].

Here, the dynamics around E_0 is strictly different for $\mathcal{R}_0 < 1$ and $\mathcal{R}_0 = 1$. Note, however, that in the later conclusions on global behavior and in Figure 11.3.1, they are treated together in $\mathcal{R}_0 \leq 1$ since they share the common feature of being attracted to E_0.

11.3 Application of the Poincaré compactification

In this model, we have a two-dimensional system, and we can use the Poincaré-Bendixson theorem (e.g. [70]). That is, if we know that there is no trajectory toward the equilibrium at infinity, we can show the global stability of the equilibrium without constructing the Lyapunov function, since it is attracted to the bounded equilibrium.

11.3.1 Dynamics on the local charts

First, to obtain the dynamics on the chart $\overline{U}_2$, we introduce the coordinates (λ, x) by the formulas

$$S(t) = x(t)/\lambda(t), \quad I(t) = 1/\lambda(t).$$

Then, we have

$$\begin{cases} \dot{\lambda} = -\beta x + (q + \mu)\lambda, \\ \dot{x} = A\lambda - \beta\lambda^{-1}x - \beta\lambda^{-1}x^2 + qx, \end{cases} \qquad \left(\cdot = \frac{d}{dt}\right).$$

By using the time-scale desingularization $d\tau/dt = \lambda^{-1}$, we can obtain

$$\begin{cases} \lambda_\tau = -\beta\lambda x + (q + \mu)\lambda^2, \\ x_\tau = A\lambda^2 - \beta x - \beta x^2 + q\lambda x, \end{cases} \tag{11.3.1}$$

where $\lambda_\tau = d\lambda/d\tau$ and $x_\tau = dx/d\tau$. The equilibrium of the system (11.3.1) on $\{\lambda = 0, x \geq 0\}$ is $E_1 : (\lambda, x) = (0, 0)$. By calculating the Jacobian matrix, we apply the center manifold theory. Therefore, we obtain that the approximation of the (graph of) center manifold is

$$\left\{(\lambda, x) \mid x(\tau) = A\beta^{-1}\lambda^2 + O(\lambda^3)\right\} \tag{11.3.2}$$

and the dynamics of (11.3.1) near E_1 is topologically equivalent to the dynamics of the following equation:

$$\lambda_\tau = (q + \mu)\lambda^2 - A\lambda^3 + O(\lambda^4). \tag{11.3.3}$$

In conclusion, this argues that the trajectories will never go to E_1.

Second, we consider the dynamics on the chart $\overline{U}_1$. From the change of coordinates $S(t) = 1/\lambda(t)$, $I(t) = x(t)/\lambda(t)$, and time-rescaling $d\tau/dt = \lambda^{-1}$, we obtain

$$\begin{cases} \lambda_\tau = -A\lambda^3 + \beta\lambda x + \mu\lambda^2, \\ x_\tau = \beta x - q\lambda x - A\lambda^2 x + \beta x^2. \end{cases} \tag{11.3.4}$$

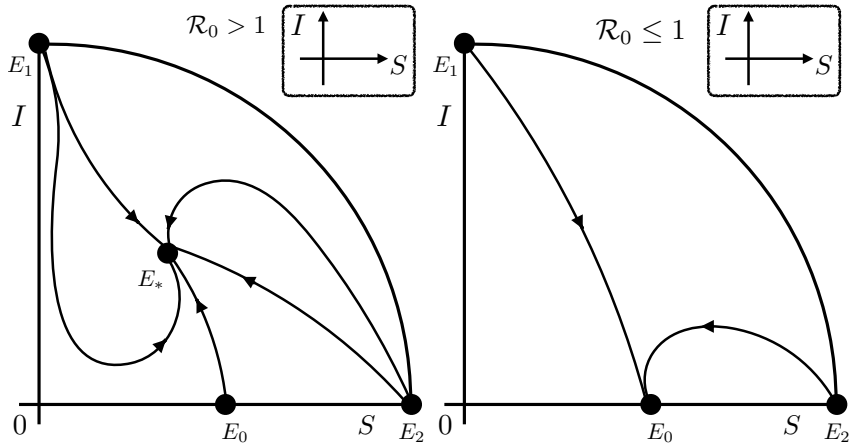

Figure 11.3.1: Schematic pictures of the dynamics on the Poincaré disk for (11.2.2). [Left: Case $\mathcal{R}_0 > 1$.] [Right: Case $\mathcal{R}_0 \leq 1$.] Note that the circumference corresponds to $\{\|(S, I)\| = +\infty\}$.

The equilibrium of the system (11.3.4) on $\{\lambda = 0, x \geq 0\}$ is $E_2 : (\lambda, x) = (0, 0)$. By calculating the Jacobian matrix, we apply the center manifold theory. However, it is not shown explicitly as (11.3.2) and (11.3.3) since the center manifold is not unique. As we can see from the nullcline, we conclude that the trajectories will never go to E_2.

11.3.2 Dynamics on the Poincaré disk

Combining the dynamics on the charts $\overline{U}_j$ $(j = 1, 2)$, we can obtain the dynamics on the Poincaré disk (see Figure 11.3.1).

We explain why the connected trajectories can be represented as shown in Figure 11.3.1 in the both cases $\mathcal{R}_0 > 1$ and $\mathcal{R}_0 \leq 1$. First, by computing $\dot{S}|_{S=0}$, $\dot{S}|_{I=0}$, $\dot{I}|_{S=0}$ and $\dot{I}|_{I=0}$, it is easy to see that both the Poincaré disks are an invariance set. Second, bounded orbits cannot go to infinity by the local dynamics at infinity. Finally, the dynamics on them are determined from the Poincaré-Bendixson theorem (e.g. [70]).

Thus, we can understand the global behavior of the solution to (11.2.2) without constructing the Lyapunov function. This means that the method introduced in Section 1.1 is effective in (11.2.2).

11.4 Asymptotic behavior

In this section, we derive the asymptotic behavior of $I(t)$ as $t \to \infty$ in the case that $\mathcal{R}_0 < 1$ and $\mathcal{R}_0 = 1$, respectively. We can also calculate the asymptotic behavior as $t \to +\infty$ in the case that $\mathcal{R}_0 > 1$. See [32, 33] for similar arguments.

First, from the Jacobian matrix at E_0 in the case that $\mathcal{R}_0 < 1$, the solution $I(t)$ can be approximated as follows

$$I(t) = C_1 e^{[A\beta\mu^{-1} - (q+\mu)]t}(1 + o(1)) = C_1 e^{(q+\mu)(\mathcal{R}_0 - 1)t}(1 + o(1)) \quad \text{as} \quad t \to +\infty.$$

That is, we obtain that $I(t)$ converges exponentially to 0 with $t \to \infty$. Here, C_1 is a positive constant.

Next, we examine the case that $\mathcal{R}_0 = 1$. By considering terms up to the second order in (11.2.5) and solving for $I(t)$, we obtain

$$I(t) = (A\beta^2\mu^{-2}t + C_2)^{-1}.$$

This equation is the asymptotic behavior as $t \to \infty$. Note that from $I(0) > 0$, C_2 is a positive constant.

Although these results are same in that $I \to 0$ is obtained as $t \to +\infty$, the decay is different. Therefore, we can see that the smaller $\mathcal{R}_0$ is than 1, the faster the convergence of $I(t)$ to 0 as $t \to \infty$. This is a result that gives a sense of the importance of making the basic reproduction number $\mathcal{R}_0$ small.

11.5 Concluding remarks

In this chapter, by using the Poincaré compactification, we were able to give another proof for the global stability and boundedness of the equilibrium in (11.2.2). It is expected that this method will be applied to problems for which the global behavior of the solution has not been shown. In this sense, the Poincaré compactification seems to be very convenient. However, this method is not applicable in all cases. To the best of the author's knowledge, local dynamics at infinity can be studied for phase spaces of dimension three or more, but it becomes difficult to immediately prove connecting orbits such as Subsection 11.3.2 since the Poincaré-Bendixson theorem cannot be used. Also, this method is not immediately applicable to non-polynomial vector fields in 2D system (for instance, see [14]). This leads to the question of whether the structure at infinity is properly extracted. According to [49], a vector field satisfying the scaling law of quasi-homogeneous clears the above problem. Solving technical problems and expanding the range of application of this method are future works.

Bibliography

[1] Álvarez, M.J., Ferragut, A., Jarque, X.: A survey on the blow up technique, Internat. J. Bifur. Chaos Appl. Sci. Engrg, **21**, 3108–3118 (2011).

[2] Anada, K., Fukuda, I., Tsutsumi, M.: Regional blow-up and decay of solutions to the initial-boundary value problem for $u_t = uu_{xx} - \gamma(u_x)^2 + ku^2$, Funkcial. Ekvac, **39**, No. 3, 367–387 (1996).

[3] Anada, K., Ishiwata, T.: Asymptotic behavior of blow-up solutions to a degenerate parabolic equation, J. Math-for-Ind. 3C, **2011**, Spec. Issue, 1–8 (2011).

[4] Anada, K., Ishiwata, T.: Blow-up rates of solutions of initial-boundary value problems for a quasi-linear parabolic equation, J. Differential Equations, **262**, 181–271 (2017).

[5] Angenent, S., Velázquez, J.J.L.: Asymptotic shape of cusp singularities in curve shortening, Duke Math. J., **77**, 71–110 (1995).

[6] Biler, P., Zienkiewicz, J.: Blowing up radial solutions in the minimal Keller-Segel chemotaxis model, J. Evol. Equ. **19**, 71–90 (2019).

[7] Bonheure, D., Casteras, J.-B., Foldes, J.: Singular radial solutions for the Keller-Segel equation in high dimension, J. Math. Pures Appl. **134**, 204–254 (2020).

[8] Brunella, M.: Topological equivalence of a plane vector field with its principal part defined through Newton polyhedra, J. Differential Equations, **85**, 338–366 (1990).

[9] Carr, J.: Applications of centre manifold theory, Springer-Verlag, New York-Berlin (1981).

[10] Chen, T., Li, S., Llibre, J.: Phase portraits and bifurcation diagram of the Gray-Scott model, J. Math. Anal. Appl. **496**, No. 2, Article ID 124840, 28 p. (2021).

[11] Childress, S., Percus, J.K.: Nonlinear aspects of chemotaxis, Math. Biosci., **56**, 217–237 (1981).

[12] Corless, R.M., Gonnet, G.H., Hare, D.E.G., Jefferey, D.J., Knuth, D.E.: On the Lambert W function, Adv. Comput. Math, **5**, 329–359 (1996).

[13] Dumortier, F., Herssens, C.: Polynomial Liénard Equations near Infinity, J. Differential Equations, **153**, 1–29 (1999).

[14] Dumortier, F., Llibre, J., Artés, C.J.: Qualitative theory of planar differential systems, Springer-Verlag, Berlin (2006).

[15] Duong, G.K., Zaag, H.: Profile of a touchdown solution to a nonlocal MEMS model, Math. Models Appl. Sci. **29**, 1279–1348 (2019).

[16] Esteve, C., Souplet, P.: No touchdown at points of small permittivity and nontrivial touchdown sets for the MEMS problem, Adv. Differential Equations, **24**, 465–500 (2019).

[17] Flores, G., Mercado, G., Pelesko, J.A., Smyth, N.: Analysis of the dynamics and touchdown in a model of electrostatic MEMS, SIAM J. Appl. Math, **67**, 434–446 (2006).

[18] Folino, R., Lattanzio, C., Mascia, C.: Motion of interfaces for a damped hyperbolic Allen-Cahn equation, Commun. Pure Appl. Anal., **19**, No. 9, 4507–4543 (2020).

[19] Fukunishi, M., Watanabe, T.: Variational approach to MEMS model with fringing field, J. Math. Anal. Appl. **423**, 1262–1283 (2015).

[20] Gage, M., Hamilton, R.S.: The heat equation shrinking convex plane curves, J. Differential Geom., **23**, 69–96 (1986).

[21] Ghergu, M., Miyamoto, Y.: Radial regular and rupture solutions for a pde problem with gradient term and two parameters, Proc. Amer. Math. Soc. **150**, 1697–1709 (2022).

[22] Grayson, M: The heat equation shrinks embedded plane curves to round points, J. Differential Geom., **26**, 285–314 (1987).

[23] Guo, J.-S., Recent developments on a nonlocal problem arising in the micro-electro mechanical system, Tamkang J. Math. **45**, No. 3, 229–241 (2014).

[24] Guo, J.-S., Huang, B.-C.: Hyperbolic quenching problem with damping in the micro-electro mechanical system device, Discrete Contin. Dyn. System. Ser. B, **19**, 419–434 (2014).

[25] Guo, J.-S., Souplet, P.: No touchdown at zero points of the permittivity profile for the MEMS problem, SIAM J. Math. Anal. **47**, No. 1, 614–625 (2015).

[26] Guo, J.-S., Huang, B.-C., Wakasa, T., Wang, C.-J., Yu, C.-Y.: The structure of stationary solutions to a micro-electro mechanical system with fringing field, J. Differential Equations, **269**, 7676–7704 (2020).

[27] Guo, J.-S., Morita, Y., Yotsutani, S.: Self-similar solutions for a quenching problem with spatially dependent nonlinearity, Nonlinear Anal. **147**, 45–62 (2016).

[28] Hethcote, H.W.: Qualitative analyses of communicable disease models, Math. Biosci., **28**, 335–356 (1976).

[29] Hillen, T., Painter, K.J.: A user's guide to PDE models for chemotaxis, J. Math. Biol. **58**, 183–217 (2009).

[30] Ichida, Y., Matsue, K., Sakamoto, T.O.: A refined asymptotic behavior of traveling wave solutions for degenerate nonlinear parabolic equations, JSIAM Lett. **12**, 65–68 (2020).

[31] Ichida, Y., Sakamoto, T.O.: Quasi traveling waves with quenching in a reaction-diffusion equation in the presence of negative powers nonlinearity, Proc. Japan Acad. Ser. A Math Sci. **96**, 1–6 (2020).

[32] Ichida, Y., Sakamoto, T.O.: Traveling wave solutions for degenerate nonlinear parabolic equations, J. Elliptic Parabol. Equ. **6**, 795–832 (2020).

[33] Ichida, Y., Sakamoto, T.O.: Radial symmetric stationary solutions for a MEMS type reaction-diffusion equation with spatially dependent nonlinearity, Jpn. J. Ind. Appl. Math. **38**, 297–322 (2021).

[34] Ichida, Y: On global behavior of a some SIR epidemic model based on the Poincaré compactification, JSIAM Lett. **14**, 65–68 (2022).

[35] Ichida Y., Sakamoto, T.O.: Stationary solutions for a 1D pde problem with gradient term and negative powers nonlinearity, J . Elliptic Parabol. Equ, **8**, 885–918 (2022).

[36] Ichida, Y., Sakamoto, T.O.: Radially symmetric stationary solutions for a MEMS type reaction-diffusion equation with fringing field, Nonlinearity, **36**, 71–109 (2023).

[37] Ichida, Y.: Traveling waves with singularities in a damped hyperbolic MEMS type equation in the presence of negative powers nonlinearity, Electron. J. Differ. Equ, **2023**, 1–20 (2023).

[38] Ichida, Y: Classification of nonnegative traveling wave solutions for the 1D degenerate parabolic equations, Discrete Contin. Dyn. Syst., Ser. B, **28**, 1116–1132 (2023).

[39] Ichida, Y.: Radially symmetric stationary solutions for certain chemotaxis systems in higher dimensions: a geometric approach, Discrete Contin. Dyn. Syst., **43**, 1975–2001 (2023).

[40] Ichida, Y.: A new analysis of finite-time singularities for nonlinear differential equations based on dynamical systems theory, Maser's thesis, Meiji University, 2021.

[41] Johnson, R., Pan, X.B., Yi, Y.F.: Positive solutions of super-critical elliptic equations and asymptotics , Comm. Partial Differential Equations, **18**, 977–1019 (1993).

[42] Joseph, D, Lundgren, T.: Quasilinear Dirichlet problems driven by positive sources, Arch. Ration. Mech. Anal. **49**, 241–269 (1973).

[43] Keller, E.F., Segel, L.A.: Initiation of slime mold aggregation viewed as an instability, J. Theor. Biol., **26**, 399–415 (1970).

[44] Kuehn, C.: Multiple Time Scale Dynamics, Springer, Berlin (2015).

[45] Kuznetsov, Y.A.: Elements of applied bifurcation theory. Third edition, Springer-Verlag, New York (2004).

[46] Low, B.C.: Resitive diffusion of force-fee magnetic fields in a passive medium, Astrophys. J., **181**, 209–226 (1973).

[47] Low, B.C.: Nonlinear classical diffusion in a contained plasma, Phys. Fluids, **25**, 402–407 (1982).

[48] Luca, M., Chavez-Ross, A., Edelstein-Keshet, L., Mogilner, A.: Chemotatic signaling, microglia, and Alzheimer's disease senile plague: Is there a connection? Bull. Math. Biol. **65**, 673–730 (2003).

[49] Matsue, K.: On blow-up solutions of differential equations with Poincaré-type compactificaions, SIAM J. Appl. Dyn. Syst., **17**, 2249–2288 (2018).

[50] Matsue, K.: Geometric treatments and a common mechanism in finite-time singularities for autonomous ODEs, J. Differential Equations, **267**, 7313–7368 (2019).

[51] Matsue, K.: Rigorous numerics of finite-time singularities in dynamical systems - methodology and applications, arXiv:1806.08487.

[52] Mignot, F., Puel, J.-P.: Solution radiale singulière de $-\Delta u = \lambda e^u$. C.R. Acad. Sci. Paris Sér. I Math. **307**, 379–382 (1988).

[53] Miyamoto, Y., Naito, Y.: Fundamental properties and asymptotic shapes of the singular and classical radial solutions for supercritical semilinear elliptic equations, NoDEA Nonlinear Differ. Equ. Appl., **27**, 24 p. (2020).

[54] Miyasita, T.: Global existence and Quenching for a damped hyperbolic MEMS equation with the fringing field, Tamkang J. Math, **48**, 31–47 (2017).

[55] Murray, J.D.: Mathematical biology I: An Introduction, Springer-Verlag, New York, 2002.

[56] Naito, Y., Suzuki, T.: Self-similar solutions to a nonlinear parabolic-elliptic system, Taiwanese J. Math., **8**, 43–55 (2004).

[57] Naito, Y.: Blow-up criteria for the classical Keller-Segel model of chemotaxis in higher dimensions, J. Differ. Equations **297**, 144–174 (2021).

[58] Nanjundiah, V.: Chemotaxis, signal relaying, and aggregation morphology, J. Theor. Biol., **42**, 63–105 (1973).

[59] Pelesko, J., Triolo, A.: Nonlocal problems in MEMS device control, J. Engrg. Math, **41**, 345–366 (2001).

[60] Poincaré, H.: Mémoire sur les courbes définies par une équation différentielle (I), Journal de Mathématiques Pures et Appliquées, **7**, 375–422 (1881).

[61] Poon, C.C.: Blow-up of a degenerate non-linear heat equation, Taiwanese J. Math., **15**, 1201–1225 (2011).

[62] Poon, C.C.: Blowup rate of solutions of a degenerate nonlinear parabolic equation, Discrete Contin. Dyn. Syst. Ser. B, **24**, 5317–5336 (2019).

[63] Saito, Y.: Backward bifurcation caused by treatment capacity in a disease transmission model, Ôyôsûri, bulletin of the JSIAM, **31**, 13–21 (2021). (in Japanese).

[64] Souplet, P., Winkler, M.: Blow-up profile for the parabolic-elliptic Keller-Segel system in dimensions $n \geq 3$, Commun. Math. Phys., **367**, 665–681 (2019).

[65] Tao, Y., Wang, Z-A.: Competing effects of attraction vs. repulsion in chemotaxis, Math. Models Methods Appl. Sci. **23**, 1–36 (2013).

[66] Tello, J.I.: Stability of steady states of the Cauchy problem for the exponential reaction-diffusion equation, J. Math, Anal. Appl. **324**, 381–396 (2006).

[67] van den Driessche, P., Watmough, J.: Reproduction numbers and sub-threshold endemic equilibria for compartmental models of disease transmission, Math. Biosci., **180**, 29–48 (2002).

[68] Wang, Q.: Estimates for the quenching time of a MEMS equation with fringing field, J. Math. Anal. Appl. **405**, 135–147 (2013).

[69] Wei, J., Ye, D.: On MEMS equation with fringing field, Proc. Amer. Math. Soc. **138**, 1693–1699 (2010).

[70] Wiggins, S.: Introduction to Applied Nonlinear Dynamical Systems and Chaos, Springer-Verlag, New York (2003).

[71] Yazaki, S.: Numerical computation of moving plane curves, Kyouritsu Shuppan, Tokyo (2019).